AD-A164 601 SUMMER STUDY PROGRAM IN GEOPHYSICAL FLUID DYNAMICS 1/3
WOODS HOLE OCEANOGRAPH..(U) WOODS HOLE OCEANOGRAPHIC
INSTITUTION MA G VERONIS ET AL. NOV 85 WHOI-85-36
UNCLASSIFIED N00014-82-G-0079 F/G 20/4 NL

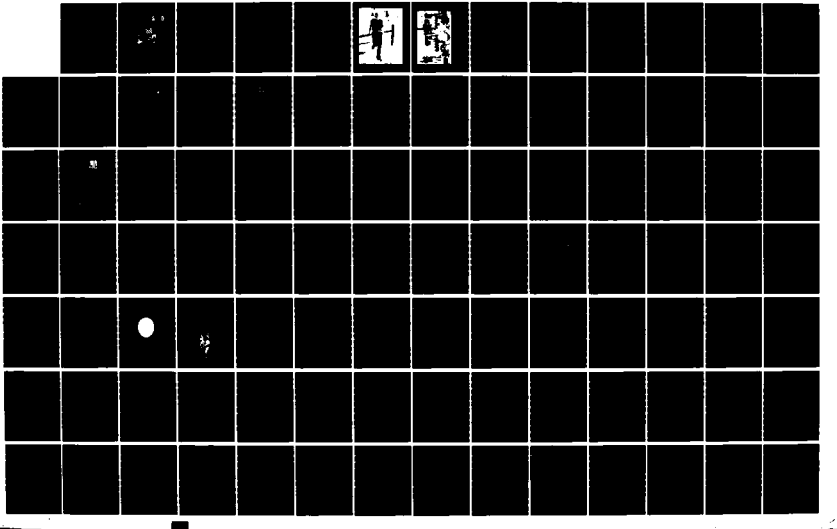

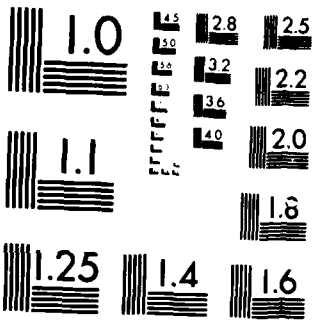

WHOI-85-36
1985

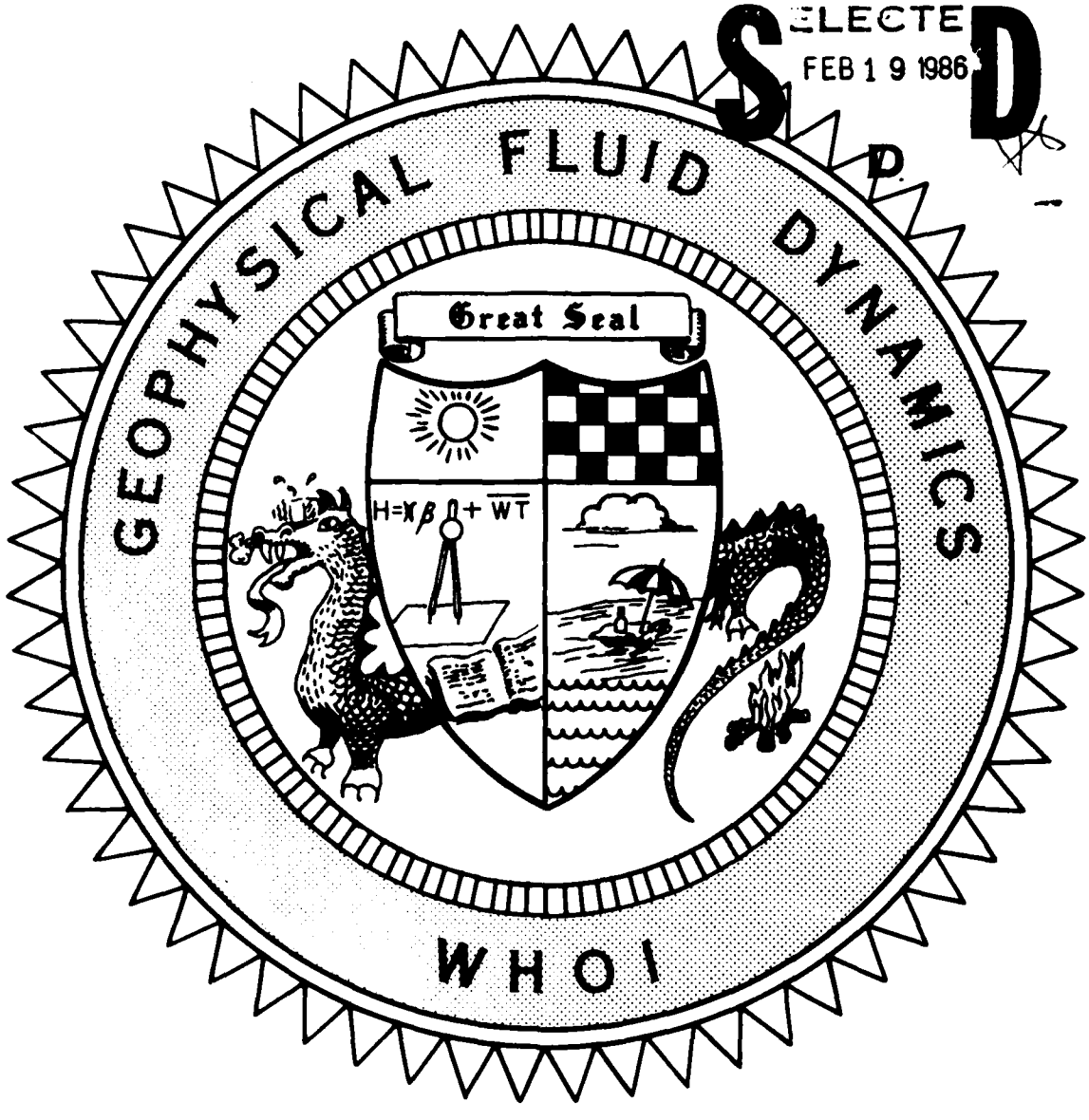

COURSE LECTURES
ABSTRACTS OF SEMINARS
LECTURES OF THE FELLOWS

1985 SUMMER STUDY PROGRAM

in

GEOPHYSICAL FLUID DYNAMICS

at

THE WOODS HOLE OCEANOGRAPHIC INSTITUTION

CHAOS

WHOI-85-36

SUMMER STUDY PROGRAM
in
Geophysical Fluid Dynamics
Woods Hole Oceanographic Institution

CHAOS

by

George Veronis, Director
and
Linda M. Hudon, Editor

Woods Hole Oceanographic Institution
Woods Hole, Massachusetts 02543

November 1985

Technical Report

Prepared for the Office of Naval Research under contract N00014-82-G-0079
and the National Science Foundation under Grants
MCS-82-000450 and DMS-85-04166.

Approval for Distribution:

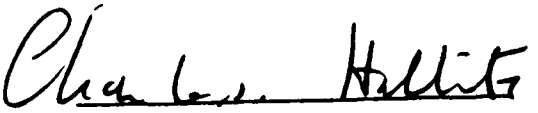

Charles D. Hollister
Dean of Graduate Studies

GEOPHYSICAL FLUID DYNAMICS PROGRAM
June 24 - August 30, 1985

STAFF AND VISITORS

CHILDRESS, Stephen	New York University
COULLET, Pierre H.	Universite de Nice
FARRELL, Brian	Harvard University
FAUVE, Stephan	L'Ecole Normale Superieure, Paris
FLIERL, Glenn	Massachusetts Institute of Technology
FOURNIER, Jean-Daniel	Observatoire de Nice
FRISCH, Uriel	Observatoire de Nice
GOLLUB, Jerry	Haverford College
HOWARD, Louis	Florida State University
LANDAHL, Marten	Massachusetts Institute of Technology
LEBOVITZ, Norman	University of Chicago
LIBCHABER, Albert	University of Chicago
LUNDBERG, Peter	Göteborgs Universitet, Sweden
MALKUS, Willem	Massachusetts Institute of Technology
MOFFATT, Keith	Cambridge University
MOIN, Pariz	NASA-AMES
POMEAU, Yves	L'Ecole Normale Superieure, Paris
PROCACCIA, Itamar	University of Chicago
PUMIR, Alain	Cornell University
SALMON, Rick	Scripps Institution of Oceanography
SAWADA, Yasuji	Tohoku University, Japan
SHRAIMAN, Boris	University of Chicago
SPIEGEL, Edward A.	Columbia University
STERN, Melvin	University of Rhode Island
VERONIS, George	Yale University
WEISS, Nigel	Cambridge University
WHITEHEAD, Jack	Woods Hole Oceanographic Institution
YOUNG, William	Massachusetts Institute of Technology
ZALESKI, Stephane	L'Ecole Normale Superieure, Paris

FELLOWS

BECKER, Janet	Scripps Institution of Oceanography
BRATTKUS, Kirk	Northwestern University
COLLINS, William	University of Chicago
LANDMAN, Michael	California Institute of Technology
MORRELL, William	Yale University
SMITH, Leslie	Massachusetts Institute of Technology
SWIFT, James	University of California, Berkeley

PRINCIPAL LECTURER - EDWARD A. SPIEGEL

Back Row: Worcester, Holyer, Childress, Pomeau, Becker, Spiegel, Kerr, Gollub, Malkus

Middle Row: Morrell, Howard, Collins, Leslie Smith, Veronis, Stern, Hudon

Front Row: Swift, Landman, Brattkus, Salmon, Leonard Smith

Absentees: Coullet, Farrell, Fauve, Flierl, Fournier, Frisch, Lebovitz, Libchaber, Lundberg, Moffatt, Moin, Procaccia, Pumir, Sawada, Shraiman, Weiss, Whitehead, Young, Zaleski

EDITOR'S PREFACE

The explosive growth of dynamical systems theory in the past two decades stems in large part from the realization that it is applicable to many natural phenomena. Indeed, much of the theoretical development has been sparked by numerical and laboratory experiments which exhibit ordered sequences of behavior that call for a general framework of interpretation.

We have been fortunate this summer to have had in residence both pioneers and developers of dynamical systems theory and its applications to fluid mechanics. Several recent texts contain the basic principles that Ed Spiegel used as a springboard for five lectures in which he exposed us to elementary examples of bifurcation and chaos, to symmetry breaking, normal forms and temporal and spatial disorder, as well as to pertinent fluid mechanical and astrophysical phenomena. Yves Pomeau continued the development with an elegant summary of different types of intermittency. Stephan Fauve agreed to write up his impressive seminars on phase instability and turbulence as an extension of the lecture series. Many of the remaining seminars introduced new concepts in the theory, some with specific examples, others via mathematical development, and still others through ways of interpreting the data that emerge from calculations and experiments. As an outstanding example of this, Albert Libchaber has demonstrated the fascinating correspondence between the frequencies observed in one of his recent fluid mechanics experiments and results from number theory relating the Fibonacci series to the golden mean.

This volume contains Spiegel's lectures as interpreted and reported by the fellows, extended abstracts of most of the seminars, and the fellows' reports of their own research activity of the summer. Research projects initiated by the staff during the program will be reported later in scientific journals.

All of us are indebted to Tom Spence of the Oceanography branch of the Office of Naval Research and to Al Thaler of the Applied Mathematics program of the National Science Foundation for arranging financial support of the program. We acknowledge the capable administrative assistance of A. Lawrence Peirson, III, and Dixie Berthel of the Woods Hole Oceanographic Institution. Special thanks go to Linda Hudon, who served as secretary, troubleshooter, coffeemaker, and problem-solver, always with a smiling countenance and exemplary eagerness.

George Veronis

TABLE OF CONTENTS

ABSTRACTS OF SEMINARS

Page

Page

LECTURES OF FELLOWS

GEOPHYSICAL FLUID DYNAMICS

Edward A. Spiegel

LECTURE 1

Pandemonium in Walsh Cottage

The mathematical definition of a dynamical system is a vector field on a manifold

$$\dot{\vec{x}} = d\vec{x}/dt = \vec{f}(\vec{x},t)$$

where $f(\vec{x},t)$ is a vector field (in fluid dynamics, $\vec{f}(\vec{x},t)$ is the Eulerian velocity and x is the Lagrangian coordinate). This equation may produce rich, complicated orbits. Chaos is a fundamental aspect of dynamical systems; the erratic behavior of chaos is reminiscent of turbulence. Though turbulence may be considered to exhibit chaotic behavior, chaos is not the turbulence of vortex dynamics. However, turbulence is probably chaotic.

For an introduction to chaos, here are some recent books

1) Universality in Chaos - Cvitanović
2) Chaos - Hao
3) Deterministic Chaos - Schuster
4) Ordre et chaos, vers une description deterministe de la turbulence - Bergé, Pomeau, Vidal

This summer we will attempt to connect chaos and fluid dynamics.

Bifurcation theory has its roots in astronomy, specifically in the studies of equilibrium figures of rotating, self gravitating bodies. We begin our study of dynamical systems with a qualitative description due to Landau of what happens when a fluid goes unstable. Schematically, his analysis proceeds as follows:

$$U_t = LU + UU + \ldots$$

where L is a linear operator that depends upon the parameters of the problem and UU represents nonlinear terms.

Let $U = A_1 e^{ikx} + A_2 e^{2ikx} + \ldots +$ complex conjugate

The amplitude equations for these modes are, schematically

$$A_1 = \lambda_1 A_1 + A_1 A_2 + \ldots$$

$$A_2 = \lambda_2 A_2 + A_1 A_1 + \ldots$$

$$A_3 = \lambda_3 A_3 + A_1 A_2 + \ldots$$

where $A_i A_j$ are the nonlinear terms that resonantly force A_k $(k=i\pm j)$

and λ_k are the eigenvalues of the linear operator L ordered in the following sense

$$|\mathrm{Re}\ \lambda_1| < |\mathrm{Re}\ \lambda_2| < \ldots < \mathrm{Re}\ \lambda_k.$$

These equations may be likened to the reaction equations of chemical kinetics (A_k represents the chemical concentration of the k^{th} species). The rapidly reacting components go to equilibrium and the slower reacting components move this equilibrium around. This is the idea behind the following.

Now consider the case where mode 1 has just gone unstable; $\mathrm{Re}\lambda_1$, has just crossed from negative to positive with all other $\mathrm{Re}\lambda$'s remaining negative. In this situation, the dynamics are driven by A_1. A_2, A_3 . . . decay quickly to zero if they are not driven. Thus one may approximate (adiabatically)

$$A_2 \sim -A_1^2/\lambda_2$$

and so

$$\dot{A}_1 = (\lambda - |A_1|^2/\lambda_2)\, A_1. \tag{1.1}$$

We see that the modes that A_1 excites modify (or renormalize) its linear growth rate: thus, Landau's equation.

Next, it is instructive to study a physical example from Andronov and Chaikin (1930) of a bead sliding on a rotating loop, which is basically the same as the particle sliding in a hemispherical bowl (see Lamb 1907). This is an analogue to the problem of the equilibrium figures of rotating, self-gravitating bodies (see Lebovitz lecture, this volume).

The nondissipative equation of motion for the system is

$$\ddot{\theta} = -g/a \sin\theta + \Omega^2/2 \sin 2\theta \tag{1.2}$$

Define

$$\omega_o^2 = g/a \quad ; \quad \alpha^2 = \Omega^2/\omega_o^2 \quad ; \quad t' = \omega_o t$$

to obtain

$$\ddot{\theta} = -\sin\theta + \alpha^2/2 \sin 2\theta = -\partial V/\partial\theta \tag{1.3}$$

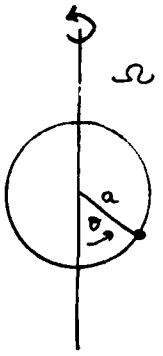

Figure 1

$$V = -[\cos\theta - \alpha^2/4 \cos 2\theta] \tag{1.4}$$

Adding dissipation one obtains

$$\ddot{\theta} = -\mu\dot{\theta} - \partial V/\partial\theta \tag{1.5}$$

Now examine $V(\theta)$

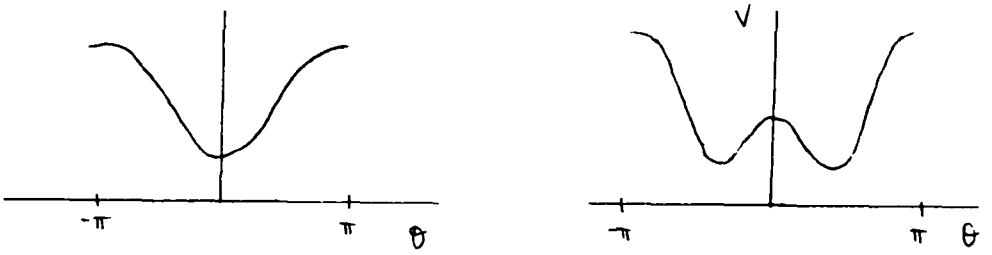

Case I $\alpha^2 < 1$ Case II $\alpha^2 > 1$

There always exist stationary solutions to equation (1.2) at $\theta = 0, \pi$.

$\theta = 0$ is stable for case I while it is unstable for case II

$\theta = \pi$ is always unstable

as $\alpha^2 \uparrow 1$ two new stable stationary solutions become possible with $\theta = \cos^{-1}(1/\alpha^2)$.

The corresponding bifurcation diagram is

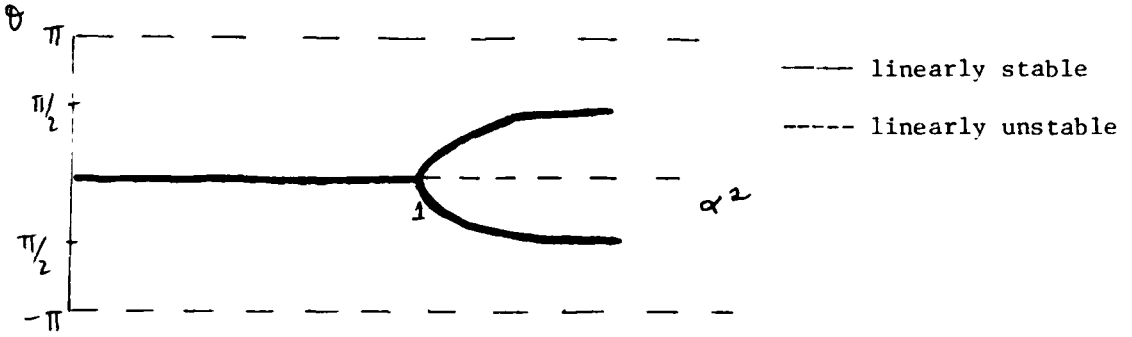

Figure 2

One does not know at which side of the loop the mass will end up once α^2 crosses one. This is exemplified in numerical experiments (Figures 3 and 4).

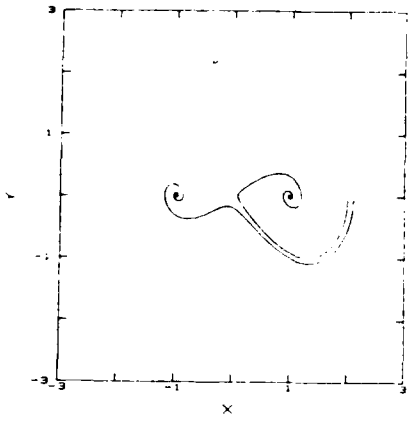

Figure 3: Trajectories in the phase obtained by solving EQ (1.5) with α=1.8 and ν=0.5 for two initial conditions:
(i) X_0=2.0, Y_0=0;
(ii) X_0=2.1, Y_0=0
The orbits diverge near the saddle point at the origin.

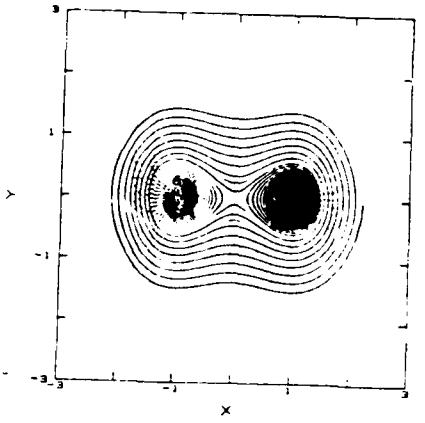

Figure 4: Another pair of trajectories of EQ (1.5) for α=-1.8 and ν=0.2 for

(i) X_0=2.13, Y_0=0;
(ii) X_0=2.20, Y_0=0.

Two closely spaced initial conditions end up at different fixed points. This is a classical analog of the two slit experiment. Though this is a deterministic system, there is still unpredictibility about the end state - this can be called pandemonium. Sustained pandemonium is chaos; therefore, one is interested in examining forced systems. (Figures 3 - 7 from Spiegel, 1985.)

The above-described system may be approximated to leading order by

$$\ddot{x} = -\partial V/\partial x - \nu\dot{x} \tag{1.6}$$

$$V = 1/4\ x^4 - ax^2 \tag{1.7}$$

This approximation yields the same type of pandemonium as the exact expression for V. If one breaks the symmetry of the potential with a forcing term, the behavior of the system may be studied via numerical simulations as presented in Figures 5 and 6 (notice that transients have decayed). The governing equations are (Marzec and Spiegel, 1980; Moore and Spiegel, 1966)

$$\begin{aligned} &\text{i)} && \dot{X} = Y \\ &\text{ii)} && \dot{Y} = -\partial V/\partial X - \nu Y \\ &\text{iii)} && \dot{Z} = -\epsilon\,[Z + bX + cX^3] \\ &\text{iv)} && V = 1/4\ X^4 - 1/2\ aX^2 - ZX \end{aligned} \tag{1.8}$$

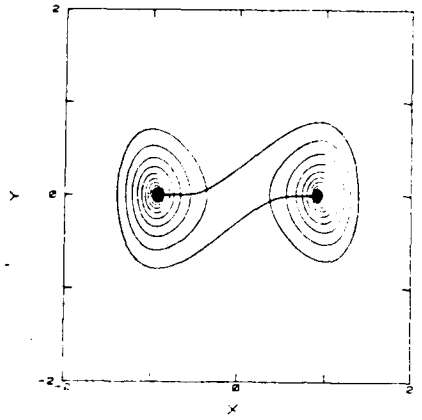

Figure 5: A solution of EQ (1.8) i>iv for: a=.7, v=1, b=1, c=1.2, ε=.02. A projection of the orbit into the X-Y plane is shown. The transients are supressed.

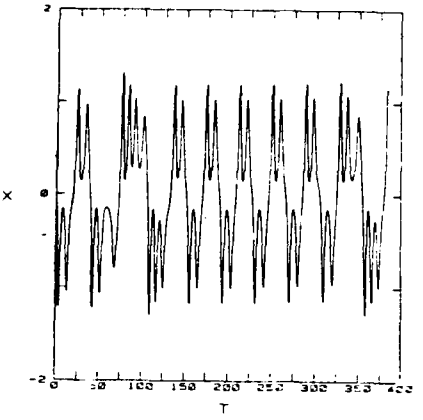

Figure 6: X(t) from (1.8) i>iv for a=.6, b=.9, c=1.1, ε=.1, v=0. For long runs in time, the behavior continues as shown.

Figure 5 shows the projection of the orbit onto the X,Y plane for the indicated parameter values. Though the conditions here are such that one expects to see chaos, this numerical experiment does not detect it. Increasing the damping gives the time series of Figure 6 exemplifying aperiodicity. These parameter values also show sensitive dependence to initial conditions. Often systems like this are also sensitive to numerical error. One may argue that really the system in Figure 6 is periodic and this would be evident if the numerics were better or if the record length of the time series was extended. Computers play an important role in detecting chaos; as with any experimental technique, the results must be interpreted carefully. For this system there is analytic evidence (Arneodo et al. 1985) that chaos does exist.

Various types of solutions of dynamical systems have been discovered. Historically, the discovery of equilibria has been attributed to Cleopatra, periodic solutions to Galileo and perhaps chaos to Poincaré. Today we often think about dynamical systems in terms of Poincaré surfaces of section. Taking a planar cut through phase space, one examines the series of points where trajectories pierce this plane. For a periodic orbit, these trajectories will return to their starting points in the plane. For a chaotic orbit, the motion lies on a strange object, like that in Figure 7.

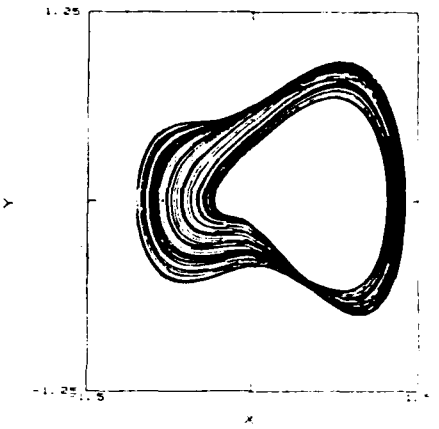

Figure 7: Like Figure 5, a projection of an orbit. This is a strange attractor of EQ (1.8) i > iν for: a=.5, b=1.3, c=1.3, ε=.01, ν=.01. The orbits do not completely cover the surface; they "never" do the same thing twice.

Let us examine how this complicated behavior arises in fluid motions in the warhorse problem of the GFD program, doubly diffusive convection. The physical system is described in Figure 8 and in the following qualitative remarks (Moore and Spiegel, 1966).

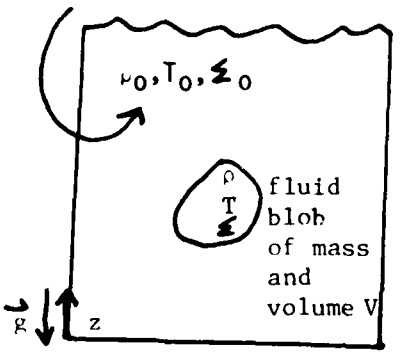

Figure 8

The fluid blob obeys

$$\rho V\ddot{z} = -g(\rho-\rho_0)V - \mu\dot{z} \qquad (1.9)$$

with the equation of state given by

$$\rho = \rho_0[1-\alpha_T(T-T_0)+\alpha_\xi(\xi-\xi_0)] \qquad (1.10)$$

and the temperature and salinity fields obeying

$$\dot{T} = -q_T(T-T_0) + \partial_t T_0(z,t) \qquad (1.11)$$

$$\dot{\xi} = -q_\xi(\xi-\xi_0) + \partial_t \xi_0(z,t) \qquad (1.12)$$

One may approximate, for an almost incompressible fluid:

$$\frac{\rho-\rho_0}{\rho} \approx \frac{\rho-\rho_0}{\rho_0} = -\alpha_T(T-T_0) + \alpha_\xi(\xi-\xi_0) \qquad (1.13)$$

Then one may combine the above equations to obtain

$$\dddot{z} = -\mu\ddot{z} + g(-\alpha_T T_{oz} + \alpha_\xi \xi_{oz})\dot{z} + g(-\alpha_T q_T(T - T_o) + \alpha_\xi q_\xi(\xi - \xi_o)) \quad (1.14)$$

$$= -\mu\ddot{z} + A\dot{z} + B$$

where A and B are prescribed functions of z.

For $A = a + \gamma z^2$

$B = \beta z^3 - \delta z + \lambda$

one may write (1.14) in the form

$$\ddot{z} = az + \gamma z^3/3 - \mu\dot{z} + \lambda$$
$$\dot{\lambda} = (\lambda + \beta z^3 - \delta z) \quad (1.15)$$

and, for $\partial=0$, we obtain the same system as (1.8). Thus one may obtain chaos from this simple model of convection.

For a small stable salinity gradient and the following mean temperature profile (Figure 9), one obtains the behavior of Figure 3. Physically the small damped oscillations of the fluid blobs result from the salinity spring balancing the buoyancy force

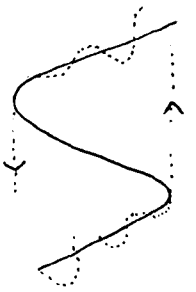

path of fluid blob ----------

mean temp gradient ————

Figure 9

Again examine the system (1.8); for a system that conserves mass the divergence of the flow field (X,Y,Z) gives the rate of change of volume/unit volume of an initial swarm of particles. Here

$$\partial\dot{X}_k/\partial x_k = -\epsilon - \nu$$

and we see that the initial swarm of particles will decay to zero volume. The object of zero volume onto which the representative points contract is called an attractor. The simplest attractor is a fixed point, while a periodic orbit or limit cycle is the next simplest attractor. For a strange (or fractal) attractor, two particles placed close together move apart on the average (see Figure 7).

NOTES SUBMITTED BY
Janet Becker

LECTURE 2

Chaos Comes to Walsh Cottage

A Generic Chaotic System

Any discussion of dynamical systems these days is bound to be riddled with references to "chaotic" behavior. In the search for a workable and concise mathematical definition of the term chaotic, we turn to the Oxford English Dictionary (unabridged) which gives us:

Chaos - A state of utter confusion and disorder; a confused mass.*

Armed with this definition, we continue where we left off last lecture and consider a prototype third order dynamical system that exhibits possible chaotic behavior. If a particle of unit mass is subjected to a slowly varying potential in a system that includes dissipation, the equations of motion become

$$\begin{aligned} \ddot{x} &= -\partial V/\partial x - \nu\dot{x} \\ V &= V(x,\lambda(x,t)) \qquad \varepsilon,\ \nu > 0 \\ \dot{\lambda} &= \varepsilon L(x,t) \end{aligned} \tag{2.1}$$

Under the restriction that λ remains bounded for all time we choose a simple form of L to be $L = -(\lambda + g(x))$. This system is reduced to three coupled, first order equations:

$$\begin{aligned} \dot{x} &= y \\ \dot{y} &= -\partial V/\partial x - \nu y \qquad \varepsilon,\ \nu > 0 \\ \dot{\lambda} &= -\varepsilon(\lambda + q(x)) \end{aligned} \tag{2.2}$$

An important feature of these equations is that the divergence of the velocity field associated with the flow is always negative. A simple calculation reveals that

$$\frac{\partial \dot{x}}{\partial x} + \frac{\partial \dot{y}}{\partial y} + \frac{\partial \dot{\lambda}}{\partial \lambda} = -(\varepsilon + \nu) \tag{2.3}$$

This property guarantees that volumes of initial conditions in phase space will eventually shrink to zero volume. These regions are defined as "attractors" and if these attractors have a cantor set structure in at least one of their dimensions, they are called strange - a term first coined by Ruelle and Takens in 1971.

*The note taker insists that any correspondence of the definition to these lecture notes is purely coincidental.

The potential has yet to be specified so we define it as a polynomial in x with coefficients that depend on λ,

$$V(x,\lambda) = \frac{x^M}{M} + \sum_{k=1}^{M-2} \alpha_k(\lambda) \frac{x^k}{k}$$

As a specific example (see the previous lecture) the system $V = 1/4x^4 - 1/2\delta x^2 + \lambda x$ with $g(x) = ax(x^2 - 1)$ contains the salient features of the thermohaline convection problem which was derived from a normal form calculation. With small modifications these equations result in a general third order differential equation of the form

$$\dddot{x} + \alpha\ddot{x} + (\beta + \gamma x^2)\dot{x} + (\sigma + \mu x^2)x = 0 \qquad (2.5)$$

which incorporates both Van der Pol and cubically nonlinear spring terms.

The figures below represent numerically computed solutions to the system (2.2) with $V(x,\lambda) = 1/4x^4 - 1/2\delta x^2 - \lambda x$ and $g(x) = x(1-x^2)$. The first figure is a projection of the orbit onto the scaled (x,x) plane for $\delta = 0.6202$. The solution is a limit cycle with period two. Figure 2 on the other hand shows a seemingly chaotic solution to the same system with $\delta = 0.625$ (Marzec and Spiegel, 1980).

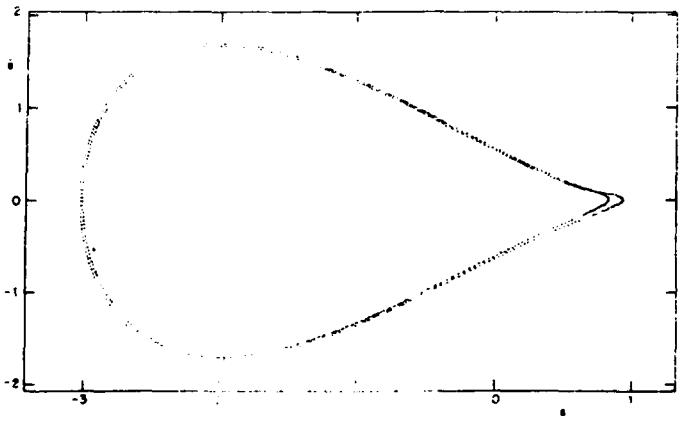

Figure 1: Doubly periodic solution to system (2).

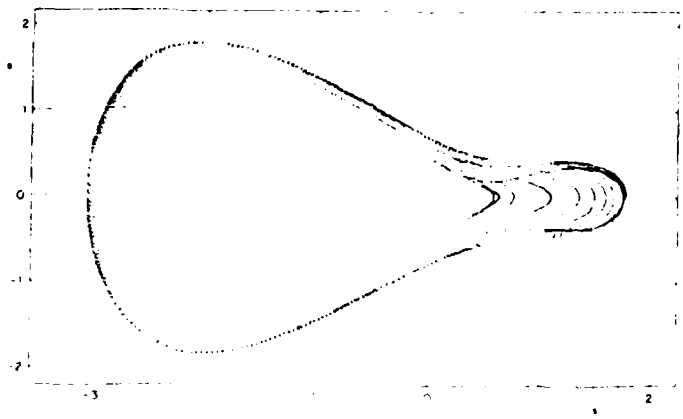

Figure 2: A bicycle seat - the beginnings of a strange attractor.

The question as to whether or not the solution to the system (2.2) with $\delta = 0.625$ is chaotic brings up an important point. The primary evidence suggesting chaotic behavior is purely numerical and the integrations cannot be separated from the inherent numerical errors. We are unsure whether or not the computed orbit is a true reflection of the solution. The argument can be made allowing the possibility that the true solution is periodic of high order periodicity and that the numerical errors are causing the random behavior. We argue that the system is truly chaotic in a direct analogy to the Feigenbaum sequence of period doublings and by examining the structure of the return map.

This generic dynamical system (2.2) is capable of creating any number of systems which exhibit complicated behaviors including the existence of strange attractors. As the order of the polynomial is increased, the behavior of the resulting O.D.E. will become even more complicated as the number of stationary points increase. We also make the observation that the Lorenz equations, the most studied chaotic system, can be cast into this form by choosing $V = 1/4x^4 + 1/2\lambda x^2$, $g = a(x^2 - 1)$ and scaling appropriately.

Poincaré Stroboscopy

A general dynamical system can be written as

$$\dot{\underline{x}} = \underline{F}(\underline{x}, t) \tag{2.6}$$

Systems with periodic forcing are of current interest and the period of the forcing gives a natural measure of time. We will however restrict our considerations to autonomous systems where

$$\dot{\underline{x}} = \underline{F}_r(\underline{x};\underline{a}) \tag{2.7}$$

$$\underline{x}(0) = \underline{a}$$

Here a is the position of the system at zero time and r is some set of bifurcation parameters. We use x_1 (for instance) as a clock for the system, and construct a return map or Poincare section as being the set of all points which cross some plane x_1 = constant in the same sense i.e. from positive values of x_1 to negative values of x_1. We can always translate coordinates so that $x_1 = \pi$ is replaced by the $x_1 = 0$ plane. Several qualitative features of the orbit can be described in terms of its return map.

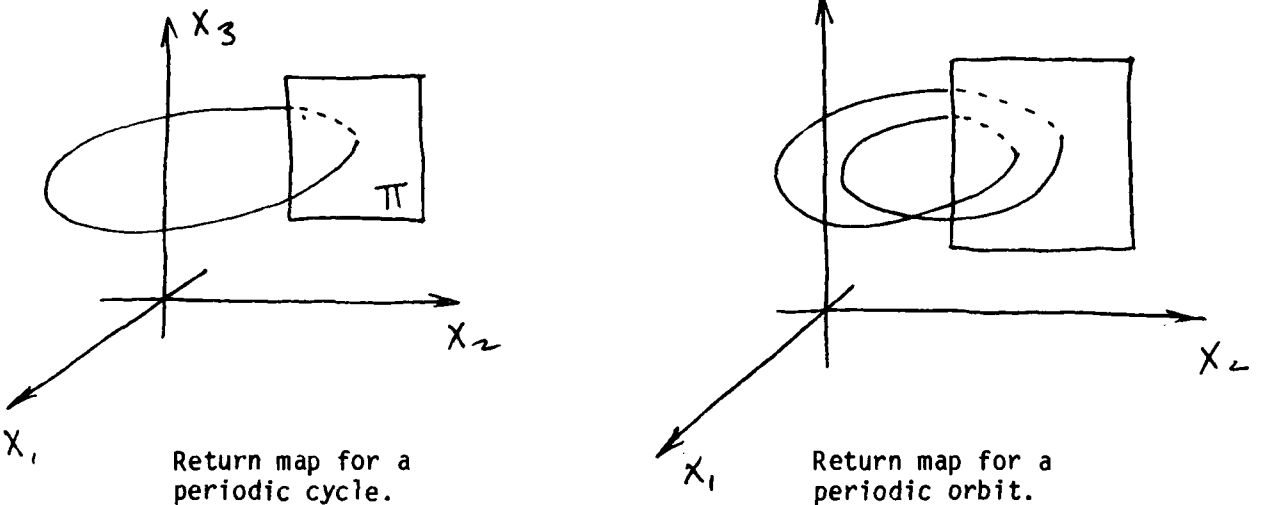

Return map for a periodic cycle.

Return map for a periodic orbit.

Figure 3

For example, a periodic orbit will cross the $x_1 = 0$ plane only a finite number of times before it passes through points previously traversed. The return map can be visualized by imagining that there is a "Poincare Stroboscope" which flashes every time the orbit crosses the $x_1 = 0$ plane positively. By studying the return map we have reduced the dimensionality of the original problem by one and the description of three dimensional orbits has been reduced to a much more tractable study of the two dimensional section.

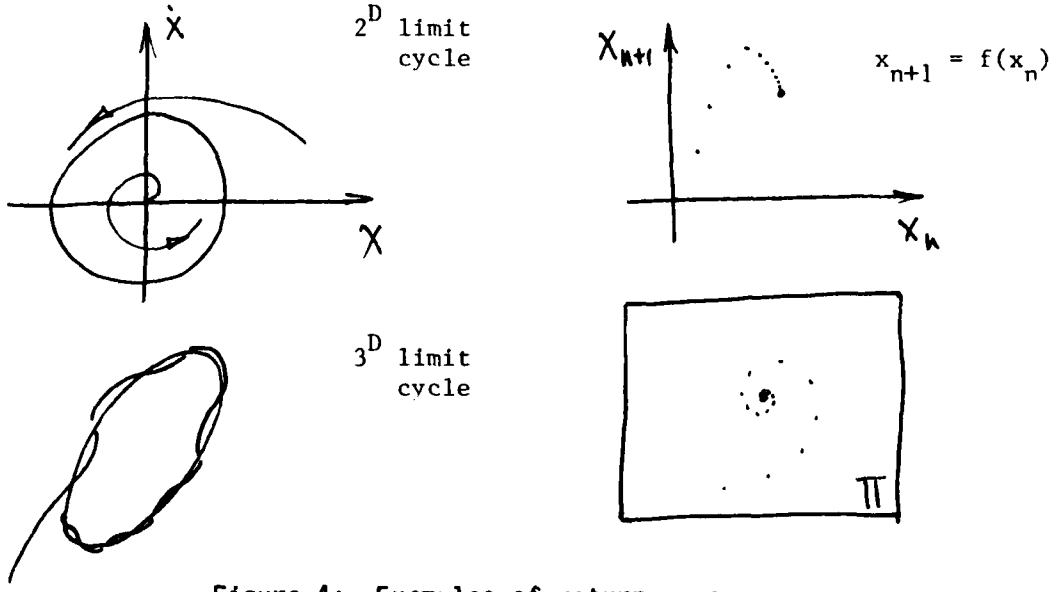

Figure 4: Examples of return maps.

Turning back to the salt oscillator model we can introduce a coordinate transformation and deal with (x, E, λ) space instead of $(x, \dot{x}, \lambda)$ space with the energy, $E = 1/2\dot{x}^2 + V$. The equations of motion become

$$\left.\begin{aligned} \dot{x} &= \pm\sqrt{E - v(x,\lambda)} \\ \dot{E} &= -2v(E - V(x,\lambda)) \\ \dot{\lambda} &= -\varepsilon(\lambda + g(x)) \end{aligned}\right\} \qquad \begin{aligned} V(x,\lambda) &= 1/4\, x^4 - 1/2\, {}_0x^2 \\ &-\lambda x \\ g(x) &= x(1 - x^2) \end{aligned} \tag{2.8}$$

and the return map for the orbits in Figures 2 and 3 (Marzec and Spiegel, 1980) are shown in Figure 5 (B is a scaled λ coordinate).

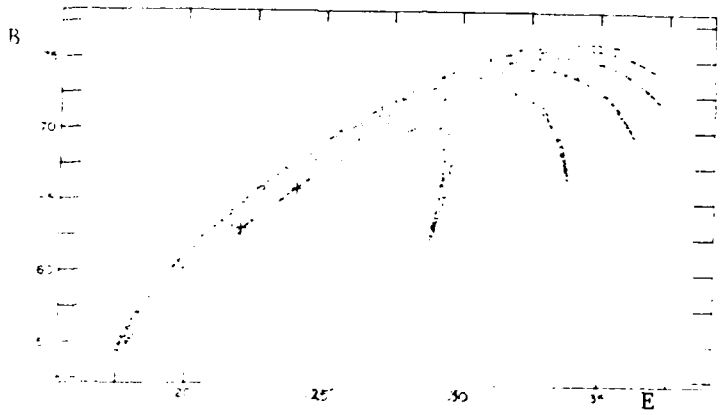

Poincaré Section showing evolution to a two cycle.

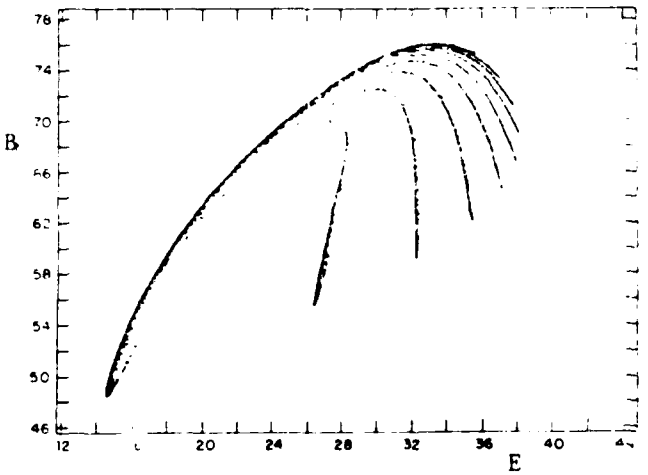

A fully developed (stable) strange attractor.

Figure 5

We can see in the first of these two graphs the "ghost" of an unstable attractor sometimes called a strange invariant set. After spending a considerable time wandering around this set, the system settles down to a two cycle and the return map becomes just two points which are marked by pluses. This metastable chaos can persist for long periods of time and can make it difficult to determine whether or not the system is actually chaotic. The time that the orbit spends on this strange invariant set increases as the bifurcation parameter increases until finally the invariant set becomes stable and the orbit becomes a strange attractor as seen in the second of the two return maps. The attractor has nine leaves which the orbit hits successively, counterclockwise, on each return to $x = 0$. To examine the finer structure of one leaf, we isolate it by defining the distance from the bottom of the leaf on the n^{th} pass through the leaf as a new variable ζ_n. This procedure gives a basically one dimensional map $\zeta_{n+1} = f(\zeta_n)$ which is plotted in Figure 6.

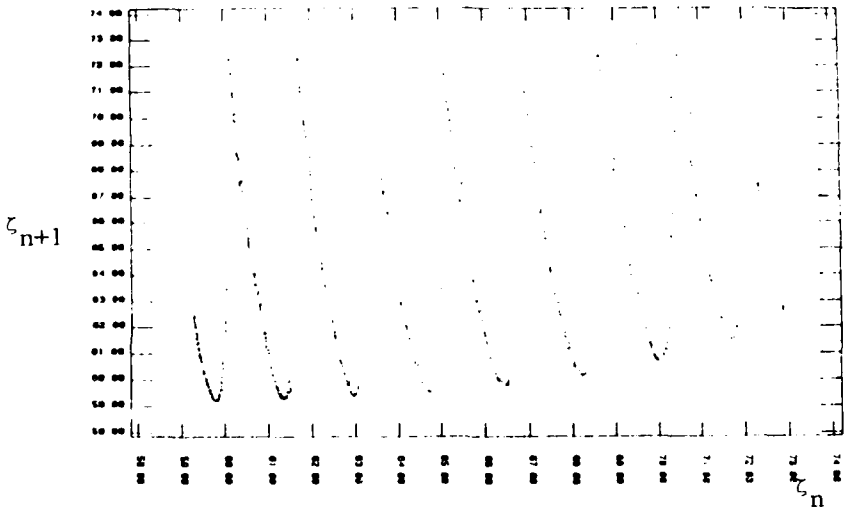

Figure 6

Much simpler algegraic systems also exist that exhibit chaotic behavior. One of the more famous of these is the Hénon map (Hénon 1976), given by:

$$x_{n+1} = 1 - ax_n^2 + y_n$$
$$y_{n+1} = bx_n \qquad (2.9)$$

The mapping's characteristic folding and stretching properties can be exposed by considering the first few iterates of an initial ellipse (Figure 7).

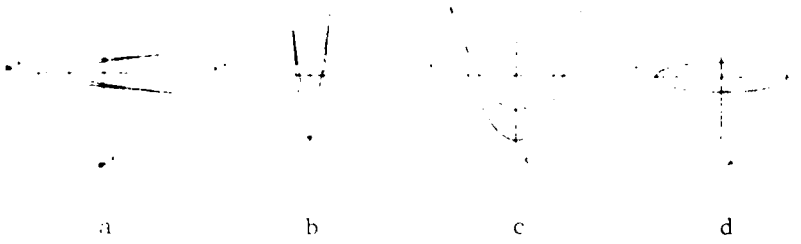

Figure 7 (Hénon, 1976)

After very many iterations the system tends toward its strange attractor which is pictured below. The self similar cantor set structure is revealed by examining the attractor on smaller and smaller length scales. Presumably, if we continue to reduce the size of our microscope we shall see the same structures repeated. This statement has not been proven mathematically but the numerical evidence supports the claim. There are, however, proofs of the existence of strange attractors in other algebraic systems such as the Lozi map.

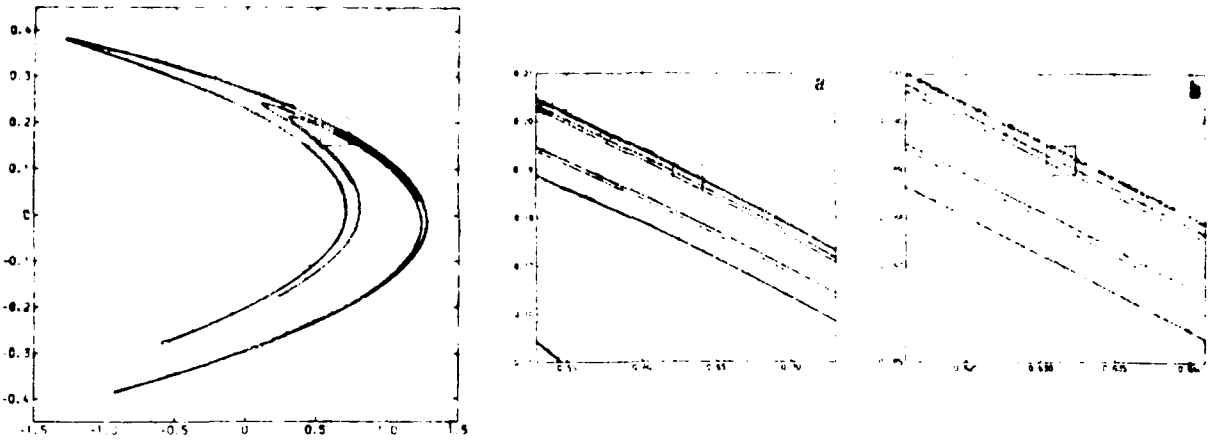

Figure 8: Self similar structure revealed (Hénon, 1976) - each successive frame is the magnification of the box in the previous frame.

One Dimensional Maps

Many times even the higher dimensional Poincaré sections can be reduced to a one dimensional study. Lorenz was able to reduce the dimensionality of the Lorenz system by plotting successive relative maxima of the Z component of the orbits. A similar procedure allowed us to do the same thing for the salt oscillator. In both cases, we reduce the problem to the study of the one dimensional iterated mapping $x_{n+1} = f_r(x_n)$. The mapping $x_{n+1} = f_r(x_n)$ gives the time evolution of the variable x which can be followed by cobwebbing between the curve $x_{n+1} = f_r(x_n)$ and the bisectrix $x_{n+1} = x_n$. This is made clear graphically in the following diagrams.

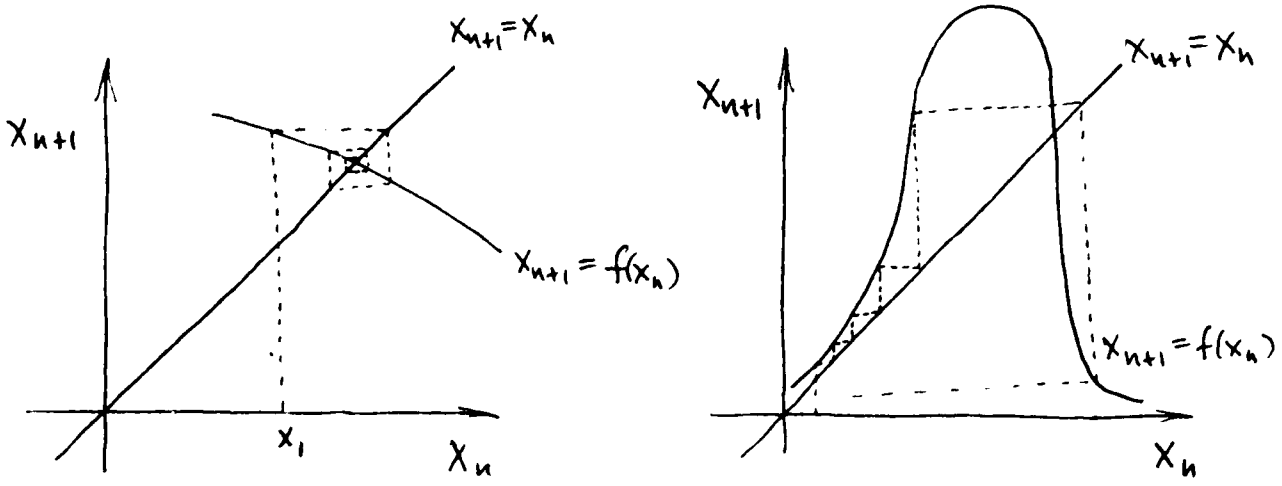

Figure 9

The fixed points of the mapping correspond to interesting points of the return map. If an orbit returns to the same point on the section then it is a periodic orbit of period one. These fixed points are given by $x_0 = f_r(x_0)$ and are the intersections of the function f_r and the bisectrix. The question of the stability of the fixed points is resolved by perturbing the fixed points and asking whether or not the perturbations decay. Let $x_n = x_0 + \zeta_n$; $||\zeta_n|| \ll 1$ for $n < N$. Then

$$x_{n+1} = x_0 + \zeta_{n+1} = f_r(x_0 + \zeta_n) \approx f_r(x_0 + \zeta_n \left.\frac{\partial f_r}{\partial x}\right|_{x_0} + \ldots$$

therefore $\zeta_{n+1} \approx \zeta_n \left(\frac{\partial f_r}{\partial x}\right)_{x_0}$ and $\zeta_n \to 0$ iff $||\left(\frac{\partial f_r}{\partial x}\right)_{x_0}|| < 1$

So the fixed point is stable if $||\partial f_r/\partial x)_{x_0}|| < 1$ and unstable if $||\partial f_r/\partial x)_{x_0}|| > 1$. The consequences of a fixed point going unstable as the parameter r is increased depends on the nature of the map f_r, but Feigenbaum's investigations have shown that there is a universality property for all maps with quadratic maxima and that in some sense all quadratic maps behave the same as r is increased. So we consider a special quadratic mapping - the logistic map $x_{n+1} = 4rx_n(1 - x_n)$.

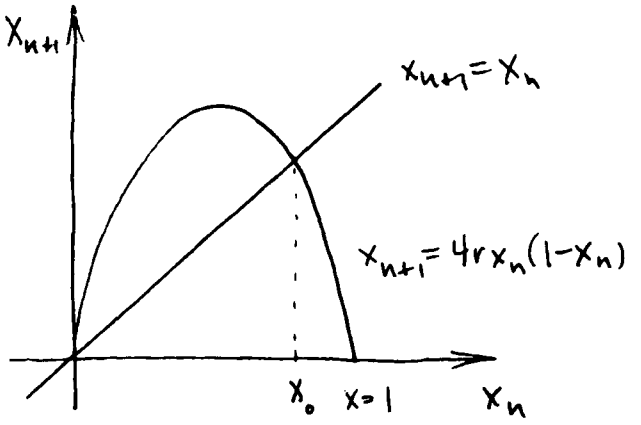

Figure 10

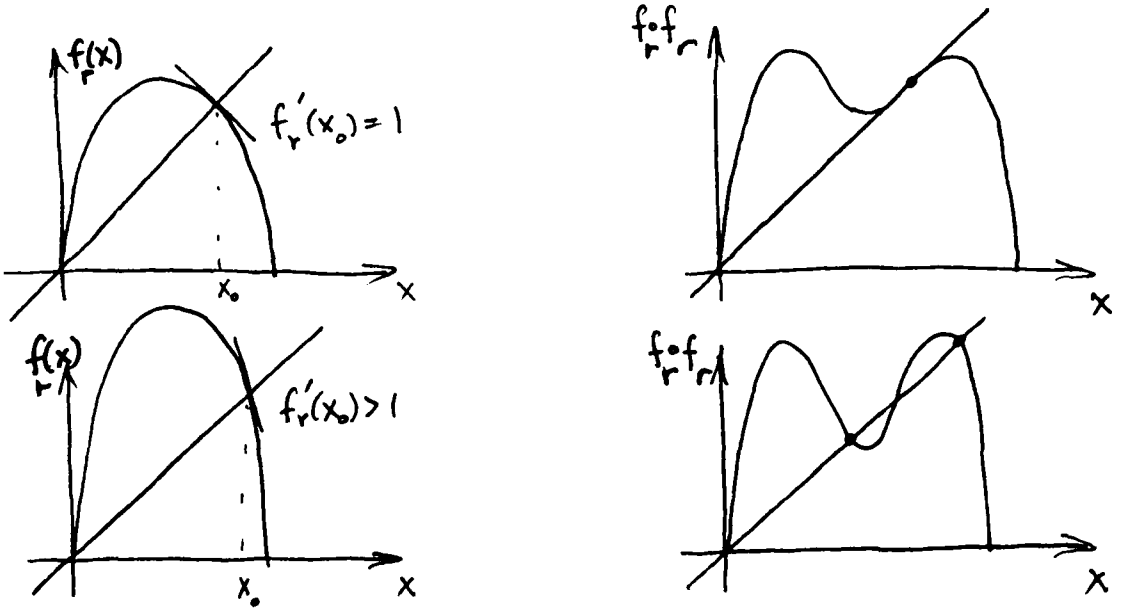

Figure 11

Tne fixed point goes unstable with increasing r when $\left|\left|\left(\frac{\partial f_r}{\partial x}\right)_{x_0}\right|\right| = 1.$
By looking at the second iterate of f we see that the single fixed point becomes unstable by splitting into two fixed points of $f \bullet f$. The fixed points of $f \bullet f$ correspond to a two cycle; the iterates repeat themselves every other iteration. In terms of behavior on the return map this means that the periodic orbit of unit period has now become an orbit of period two hence implying the term period doubling for this bifurcation route. Now as the bifurcation parameter increases further, these two stable fixed points of f(f(x)) will go unstable and form a 4 cycle which corresponds to fixed points of $f^{(4)}(x)$, etc., etc. The process continues forming 2^n cycles at each nth splitting but there is a finite limit point to the series $r_1, r_2, r_3, \ldots$ representing the splitting

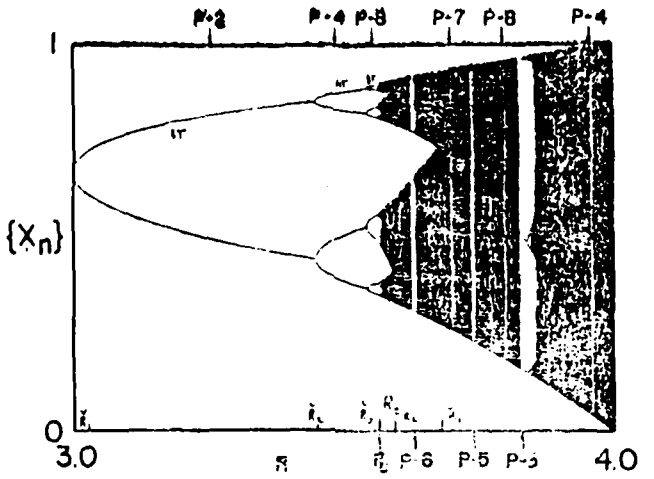

Figure 12: Period Doubling Cascade

Such scenarios would be very limited if they applied only to one dimensional iterated maps, but as we have seen these concepts can sometimes be extended to dynamical systems by way of their return maps. A system similar to the salt oscillator undergoes a sequence of period doublings leading to chaotic orbits (Figure 13) only to pass through the region of chaos into another periodic regime (Arneodo et al., 1985).

$$\dddot{x} + \ddot{x} + 2\dot{x} + ax + x^2 = 0$$

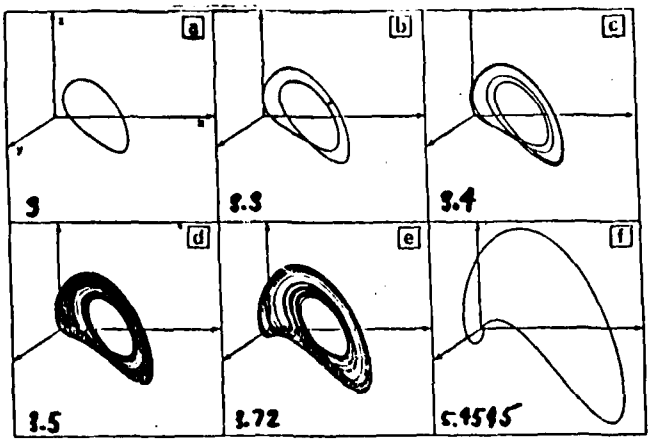

Figure 13

Since the Poincare sections are not always reducible to one dimension, we need to generalize the ideas of fixed points to higher dimensional maps. This proceeds rather straightforwardly in principle and a pictorial representation is given below for a series of fixed point bifurcations in two dimensions. Darkened points have gone unstable. Universality has yet to be set on firm ground in higher dimensional maps but the intuitive picture is clear.

We have seen that there are very complicated behaviors in dynamical systems which can be understood by way of analogy to low dimensional iterated maps. The Feigenbaum route to chaos in one dimensional maps with quadratic maxima is, at least qualitatively, similar to the sequence of period doublings leading to chaos in some dynamical systems. The quantitative connection comes about by observation of the Poincare section which can often be viewed as a one dimensional map. In the figure below we see the skein of stable and unstable manifolds of the periodic orbits that is intimately connected to the occurrence of chaos. A point bouncing around in the last case can do so for quite some time.

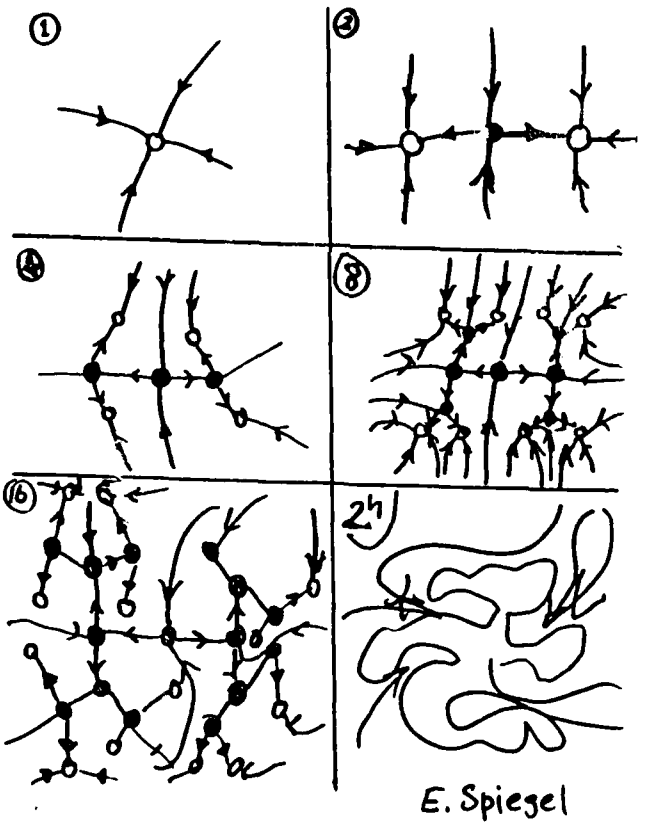

Figure 14

NOTES SUBMITTED BY
Kirk Brattkus

LECTURE 3

Chaos and the Sobriety of Seventeenth Century Astronomers

Experiments in Chaos

The onset of temporal chaos has been observed in a thin convection cell by Gollub and Benson (1980). When the Reynolds number R is adjusted to roughly $R/R_c = 17$, stable Rayleigh-Benard convection rolls form in the cell. These rolls develop oscillatory waves (frequency f_2) transverse to the rolls through a secondary instability described by Busse. Gollub and Benson observe three different routes to aperiodic behavior as they increase R. In one of the transitions, a second oscillation develops with frequency f_1 incommensurate with f_2 so the velocity time-series is quasi-periodic (figure 1). At larger values of R, phase locking occurs when f_2/f_1 approaches 9/4. The velocity spectrum peaks at harmonics of f_1, f_2, and the locking frequency is

$$f_L = f_2/9 = f_1/4.$$

Phase locking persists over a narrow range of R. At the upper end of the range, the spectrum is noisy although most of the power is still concentrated at f_1, f_2, and corresponding harmonics. As $R/R_c \to 70$, the flow becomes chaotic. Four spatial eigenmodes are sufficient to describe the observed initial roll pattern, and the authors suggest that a limited number of modes would prescribe the flow at higher R as well.

Astrophysical Chaos

Low-order systems of amplitude equations can also model variations in solar magnetic activity. During the last 300 years the number of sunspots has varied with an eleven-year period, but the maximum number observed fluctuates in an apparently random way from cycle to cycle (Eddy, 1976; see figure 2).

In the last 8000 years there have also been periods when almost no sunspots appeared, such as the Maunder minimum during the seventeenth century. The combination of nearly regular oscillations with periods of inactivity is qualitatively similar to the chaos observed in simple systems of ODE's. According to a suggestion of Spiegel and Weiss (1980), the spots observed on the surface are due to an instability in the magnetic field below the convective zone. The field is trapped in the boundary between the core, where energy is transported by radiative diffusion, and the outer regions, where convection dominates.

The similarity with thermohaline convection is due to the very slow diffusion of magnetic fields in highly conducting plasmas (Spiegel and Weiss, 1982). However, changes in salt concentration and magnetic field strength have opposite effects on the buoyancy of the surrounding medium. In hydrostatic equilibrium, the magnetic and gas pressures inside a flux tube must balance the gas pressure outside:

$$\rho_i k T_i + B^2/2\pi = \rho_e k T_e$$

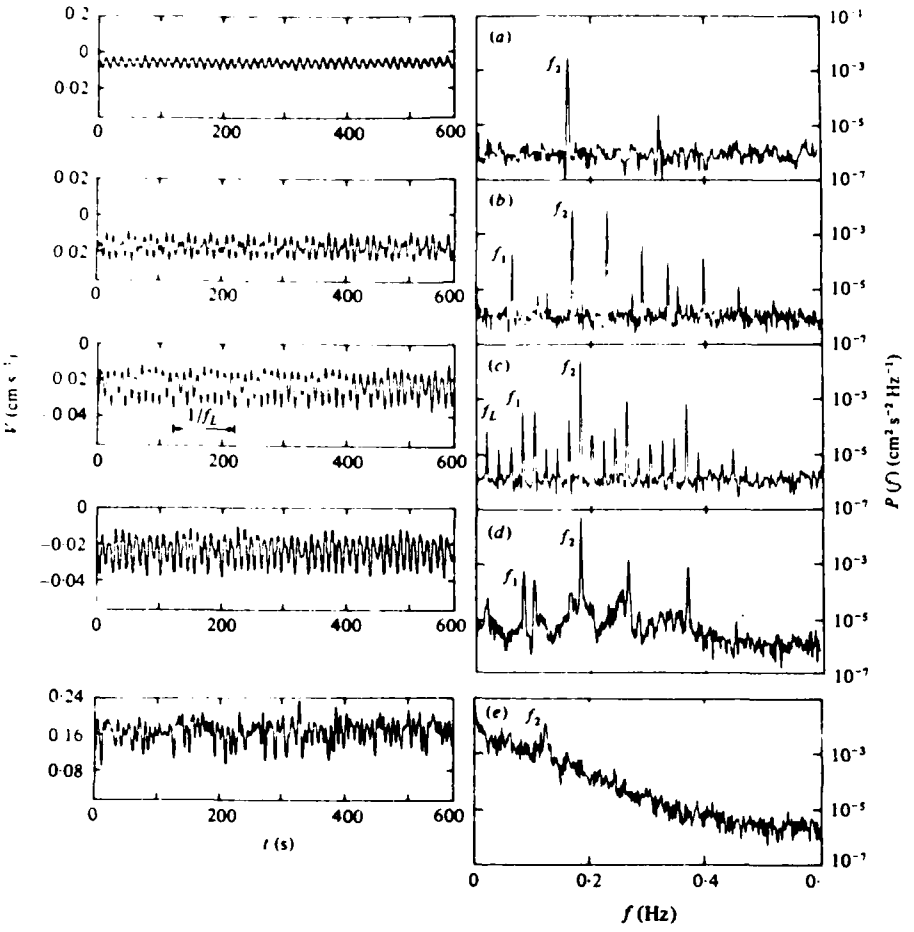

Figure 1: Velocity time-series and power spectra for Gollub and Benson's type I transition to aperiodicity. The sequence is: (a. steady rolls at R/R_c = 31.0; (b. quasi-periodicity when R/R_c = 35.0; (c. phase-locking at R/R_c = 45.2; (d. onset of noise at R/R_c = 46.8; and (e. broadband noise at R_c = 65.4 (Gollub and Benson, 1980).

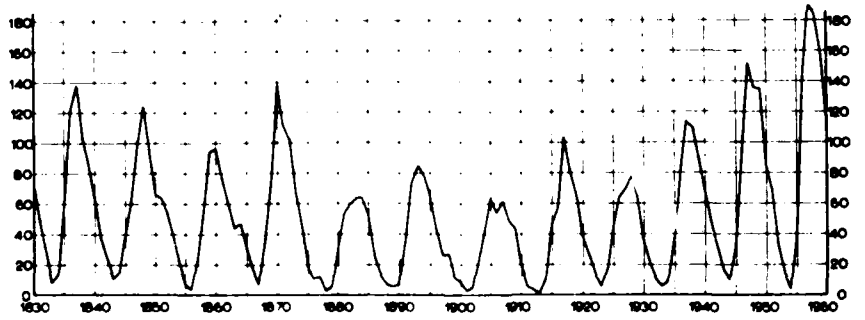

Figure 2: Annual sunspot number from 1830-1960 (adapted from Eddy, 1976).

Because heat diffuses rapidly, $T_e \simeq T_i$ and therefore $\rho_i < \rho_e$. As $|B|$ increases the density contrast grows and the tube becomes more buoyant. In the boundary layer the temperature gradient is stable and the magnetic pressure gradient unstable. Whenever the field grows to roughly 10^4 G., an interchange instability pushes flux tubes up into the convection zone. These tubes then rise to the surface driven by magnetic buoyancy and coallesce to form sunspots.

A model for this mechanism couples the two amplitude equations for the instability (e.g. Childress and Spiegel, 1980) with the Lorenz equations for the convective dynamo process that generates the flux pumped into the layer. An example of such a fifth order system is (Spiegel 1980, 1985):

$$\begin{aligned} \ddot{x} &= -x^3 - 2xy + \lambda x - \epsilon \nu \dot{x} \\ \ddot{y} &= -y^3 - x^2 + \lambda y - \epsilon \nu \dot{y} \\ \dot{\lambda} &= -\epsilon [\lambda + a(x^2 + y^2 - 1] \end{aligned} \tag{3.1}$$

With $x = 0$ these equations reduce to the Lorenz system and resemble the pair of ODE's describing the bead on the rotating wire hoop (Lecture #1). In a large region of parameter space equation (3.1) produces the aperiodic and intermittent behavior like that of solar activity (figure 3); there are, however, significant differences in detail.

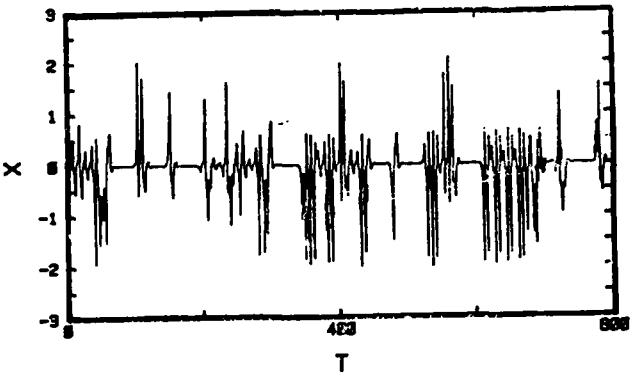

Figure 3: Amplitude vs. time for a numerical solution of equation (3.1) (Spiegel, 1980).

Spiegel and Wolf have analyzed a century of sunspot counts using delay coordinates. The analysis suggests that the solar cycle falls on an attractor; Wolf's algorithms imply that this attractor has a dimension less than five. This suggests that a simple fifth order system like (3.1) may be a useful model for certain features of the solar atmosphere.

Fractal Dimensions in Fluids

In fully developed turbulence regions of laminar and turbulent flow are intermixed, displaying a kind of spatial intermittency. Kolmogorov's theory models this intermittency by predicting the number of eddies N_ℓ of size ℓ present at equilibrium. After a characteristic eddy rotation time $t_\ell = \ell/v_\ell$ an eddy in this model splits into n vortices of size $\ell/2$. Therefore N_ℓ evolves by (Kida, 1982)

$$\dot{N}_\ell = -N_\ell/\tau_\ell + n N_{2\ell}/\tau_{2\ell}$$

To prevent kinetic energy from accumulating at some wavenumber, the energy flux/unit mass must be equal at each scale in the inertial-range cascade. This implies $\tau_\ell \sim \ell^{2/3}$. Once the flow has equilibrated, the number of eddies stops changing. Setting $dN_\ell/dt = 0$ and $n = 2^3$ gives

$$N_\ell \ell^{2/3} = 2^3 N_{2\ell}(2\ell)^{-2/3}$$

The solution is $N \sim \ell^{-7/3}$. This remark of Procaccia and Spiegel implies that eddies are not space-filling.

The resulting eddy configuration becomes more sparse at smaller scales since the volume occupied by the eddies of size ℓ varies as

$$V_\ell = N_\ell \ell^3 = \ell^{2/3}$$

Although this scaling behavior does not agree with numerical experiments, it does illustrate the notion of a fractal set. Magnifying ordinary objects of integer dimension D and characteristic length ℓ_0 by a factor ℓ/ℓ_0 yields a new set containing $(\ell/\ell_0)^D$ of the original objects. For example, a cube magnified by 2 contains 2^3 cubes with sides ℓ_0. The dimension can therefore be defined by

$$D = [\ln(V_\ell/V_{\ell_0})]/[\ln(\ell/\ell_0)] \qquad (3.2)$$

where V is the volume at the different scales.

Cantor dust is an example of a set for which D is not an integer. The dust is constructed on the unit interval by an iterative procedure. At each step, all the segments of the interval which have not been deleted are divided into thirds and the middle third is removed:

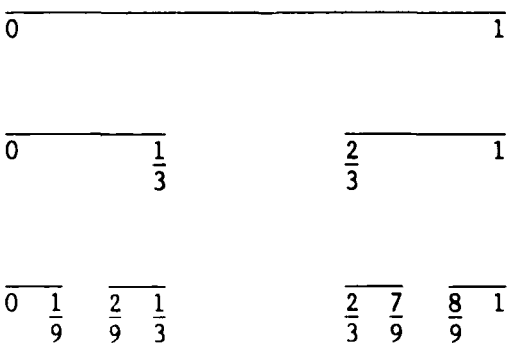

The resulting set is self-similar. Magnifying a section of the set by 3 gives 2 copies of the section and therefore D = ln 2/ln 3. For the Kolmogorov model, the volume resulting from rescaling an eddy with $V_0 = \ell_0^3$ by ℓ/ℓ_0 is

$$V_{2\ell_0} = \frac{N_{\ell_0}/2}{N_{\ell_0}} \ell_0^3$$

which implies D = 7/3.

Numerical experiments on a wide class of self-similar sets including Cantor dust have periodic ripples superimposed on the scaling law implied by equation (3.2) (Smith, Fournier and Spiegel, in preparation):

$$\ln N = -D \ln\ell + \Psi(\ln\ell)$$

The function Ψ has a period $\ln \alpha$ where α is the magnification factor. The oscillations arise from the lacunarity of the set; two sets with the same dimension can have different distributions of empty volume. ß-model turbulence may also display these oscillations since the passive fluid regions in the model do not cascade.

Transient Chaos

The salt oscillator described by

$$\ddot{x} = x^3 - \delta x + \lambda = -\partial_x V$$

$$\dot{\lambda} = -\ [\lambda + ax(x^2 - 1)]$$

exhibits transient phase space trajectory for values of δ for which there is no strange attractor. The transient Poincare section looks like the strange attractor for δ in the chaotic range (Marzec and Spiegel, 1980; Spiegel, 1978; see figures 4 and 5). The numerical experiments were run with $\epsilon = 10^{-3}$ and a = 1. For $\delta < .619$, the system has a simple limit cycle. At δ = 0.61919 there is a period doubling bifurcation followed by a succession of further doubling bifurcations as δ is increased. For $\delta > 0.622$ the system is aperiodic. Between $0.62 \lesssim \delta < 0.622$ the trajectory spends a long time tracing out what appears to be a strange attractor before settling onto the limit cycle.

This behavior may be understood by examing two catastrophe sets in the problem. It is convenient for studying the motion to define new variables

$$E = 3(1/2\ \dot{x}^2 + V)/\delta^2$$

$$B = -(3/\delta^3)^{1/2}\ \lambda$$

$$s = (3/\delta)^{1/2}\ x$$

where E is proportional to the total energy and B represents the buoyancy. A Poincare section in the E-B plane eliminates the rapid oscillations along the s dimension. The potential V has one or two minima for B greater or less than 2/3, respectively. The point B = 2/3 therefore corresponds to the catastrophe set of V:

$$\partial_x V = 0$$

$$\partial^2_x V = 0$$

In the range $0.62 \leq \delta < 0.622$ the value of B repeatedly passes through 2/3. Qualitatively, this results in a trajectory composed of two kinds of motion: a) the system is loosely bound by the quartic character of the potential, and b) the system is tightly bound momentarily in one of the two minima. The transition from b) → a) results in large oscillations in s, while the transition from a) → b) occurs as oscillations are damped out and the system is trapped in one of the minima.

The transition to one of the minima can depend very sensitively on the values of s and s when it occurs. In particular, infinitesimal perturbations about the state $\dot{x} = \ddot{x} = 0$ or equivalently

$$E = 3V/\delta^2$$
$$\partial_x V = 0 \qquad (3.3)$$

will result in selection of one of the two minima. This divergence of nearly adjacent points in phase space is characteristic of strange attractors. The conditions (3.3) specify the catastrophe set of the "super-potential"

$$V = 1/5\ x^5 - 4(\delta/6\ x^3 + \lambda/2\ x^2) - 4/3\ E\delta^2 x \qquad (3.4)$$

This set is plotted on the Poincare section for $\delta = 0.625$ (figure 6). The trajectory crosses the set repeatedly. For $0.62 < \delta < 0.622$ the points corresponding to a limit cycle fall close to the catastrophe set, but for $\delta < 0.61$ the cycle does not lie near the set. The appearance of the leafy transient trajectory is therefore connected with the approach of the cycle to the set. As δ approaches 0.622, the amplitude of the attracting limit cycle decreases but the system is still in state a) At $\delta = 0.622$, the limit cycle loses stability to the strange attractor just when the amplitude is small enough to permit transition to b).

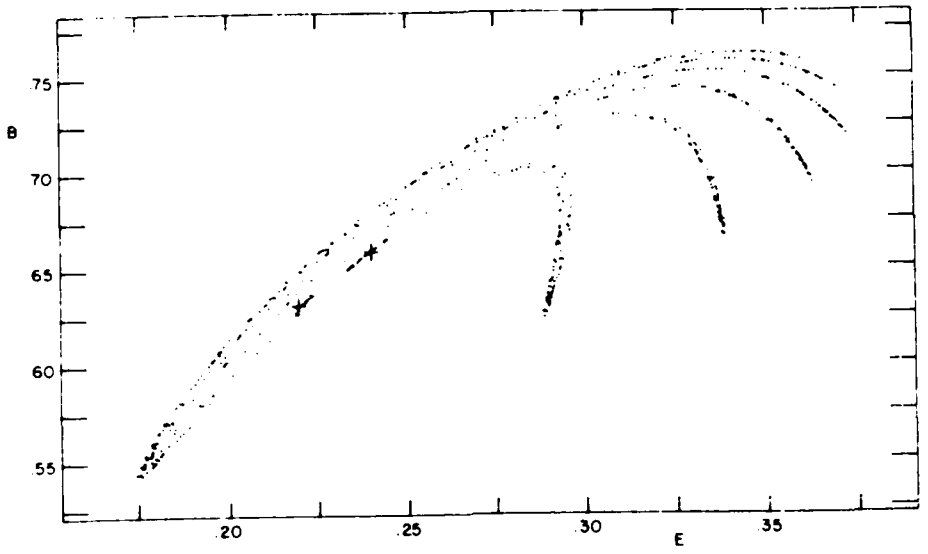

Figure 4: The Poincaré section s = 0 in (E, B, s) space for a value of δ between 0.62 and 0.622. The crosses are the limit cycle and the dots are the transients (Marzec and Spiegel, 1980).

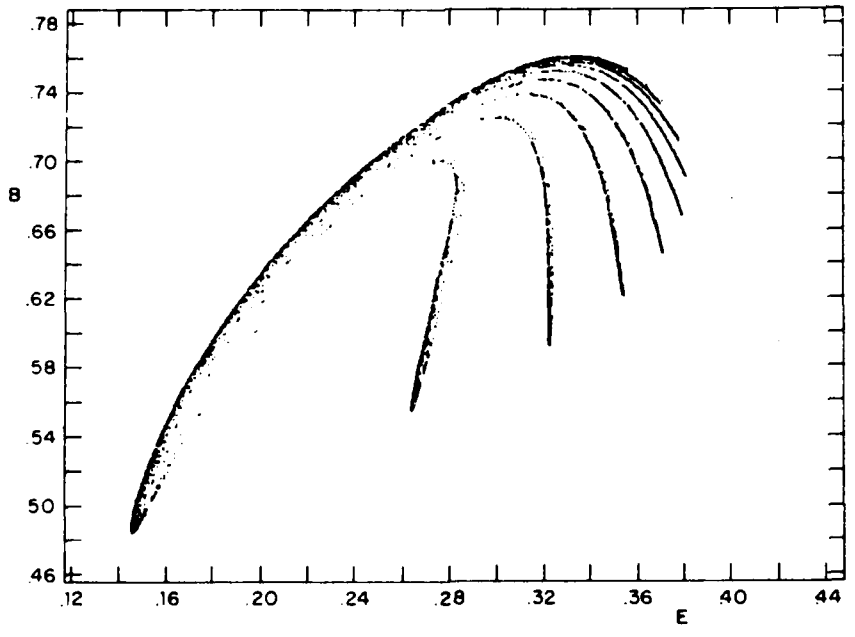

Figure 5: The section s = 0 for δ = 0.625. The dots lie on the strange attractor.

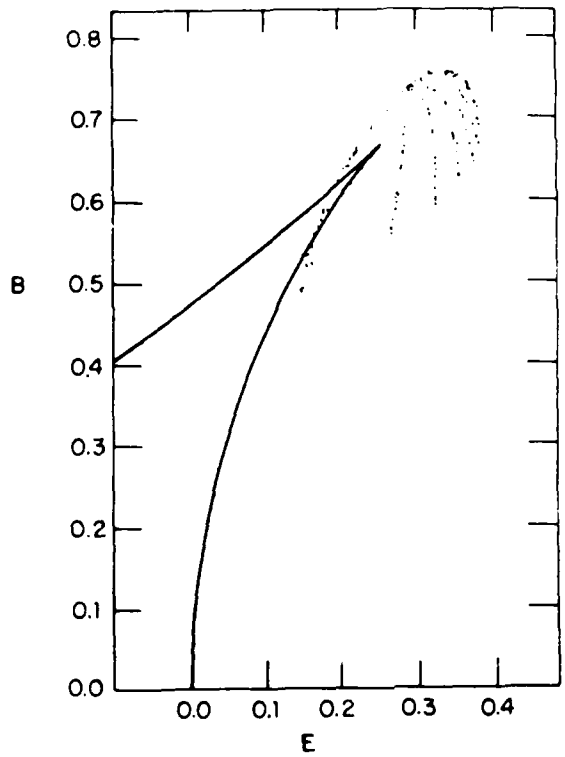

Figure 6: The intersection of the catastroph set (equation 3.4) with the E-B plane (solid line) and the Poincare se tion of the strange attractor for $\delta = 0.625$ (dots).

NOTES SUBMITTED BY
William Collins

LECTURE 4

Normal Forms for Amplitude Equations

Introduction

The derivation of amplitude equations describing the onset of instabilities in a physical system is a common method of reducing the problem to one in which there are relatively few degrees of freedom. In this way one can capture the essential dynamics near criticallity and understand the nonlinear instability mechanism. It is therefore useful to develop a method of deriving amplitude equations and to classify them according to their basic types. This is the nature of normal form theory, which we outline below.

In particular, the resulting amplitude equations may describe a chaotic system in time. It is thus possible to find chaos arbitrarily close to criticality in certain fluid problems, because the normal form equations that are derived are at least of third order. We are therefore interested in developing normal form theory in the case of multiple instabilities where several competing modes lose stability simultaneously.

Equations of Motion

The example we refer to sporadically comes from rotating thermohaline convection. Rotating parallel plates contain a layer of Boussinesq fluid heated from below. The fluid's properties are defined by its velocity, temperature and salinity. See Figure 1.

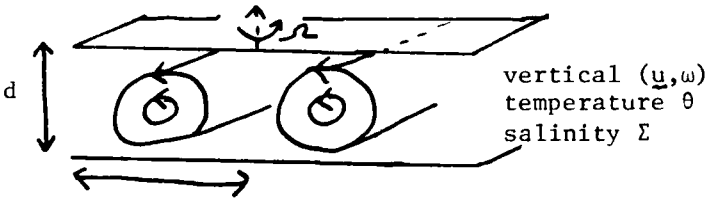

$\frac{\pi d}{\kappa}$ = horizontal length scale

Figure 1: Triple convection

Let the velocity of the fluid be $\underset{\sim}{u} = (\underset{\sim}{v},w)$ where $\underset{\sim}{v}$ is the horizontal velocity vector and w the vertical component of velocity. Incompressibility implies

$$\nabla \cdot \underset{\sim}{v} = -\partial_z \omega \qquad \text{where} \qquad \nabla = (\partial_x, \partial_y)^T. \tag{4.1}$$

The vorticity component in the z-direction is given by

$$\zeta = \hat{\underset{\sim}{z}} \cdot (\nabla \wedge \underset{\sim}{v}) \tag{4.2}$$

We have two equations and four unknowns specifying the velocity field - we will choose ω and ζ as the velocity variables.

The equations of motion are derived from the continuity equation and Navier-Stokes equations. These are coupled by buoyancy effects with the heat equation for the temperature θ and the equation for the salinity ξ. We only note here that these equations are in the general form

$$\partial_t \mathcal{L} U = \mathcal{M} U + \mathcal{N}(U) \tag{4.3}$$

where in our example the field variable $U = U(\underline{x},t)$ is given by $U = (\omega, \rho, \theta, \xi)^T$. $\mathcal{L}$ and $\mathcal{M}$ are linear differential operators, $\mathcal{N}$ is strictly nonlinear differential operator and these operators depend on the vector λ whose components are the control parameters in the problem. In the convection problem λ includes the rotation rate and thermal and saline Rayleigh numbers, for instance.

Implicit in equation (4.3) are the boundary conditions, which are often chosen to be mathematically convenient ones. We now approach the problem of deriving amplitude equations valid near a point of a linear instability. We do this not by the more established methods of multiple timescales, but by describing the methods of deriving normal form equations.

The Associated Linear Problem

We consider the linear part of equation (4.3)

$$\partial_t \mathcal{L} U = \mathcal{M} U \tag{4.}$$

As the only time appears only in the operator ∂_t, solutions $U(x,t)$ are separable, so we write

$$U = e^{st}\, \Phi(x,y,z) \tag{4.5}$$

which, when substituted into (4.4) gives

$$(\mathcal{M} - s\mathcal{L})\, \Phi = 0 \tag{4.6}$$

This is an eigenvalue problem for s, yielding the characteristic value equation

$$\mathcal{F}(s;\, \lambda,\, \underline{k}) = 0 \tag{4.7}$$

where the vector $\underline{k}$ is related to the spatial structure of the solution.

In the triple convection example the vertical scale separates out so

$$\Phi\,(x,y,z) = f(x,y)\, W(z) \tag{4.8}$$

and one finds that the horizontal spatial variation is governed by the Helmholtz equation

$$\nabla^2 f + k^2 f = 0. \tag{4.9}$$

where k is the inverse horizontal scale of the convection calls. In this case the solutions to (4.9) may be nontrivial if we do not assume simple geometry with periodic rolls (as is usually done, of course). The question that the solutions of (4.9) may be related to nonperiodic tilings of the plane is an interesting one and may be worthy of further investigation. In any case given k, another eigenvalue problem appears for W yielding an equation of type (4.7).

We now discuss the type of instability mechanisms to which we restrict our attention. In the usual convection problem as we change a single parameter, there is a primary instability to convective rolls followed by a secondary instability to a Busse oscillation. See Figures 2 and 3.

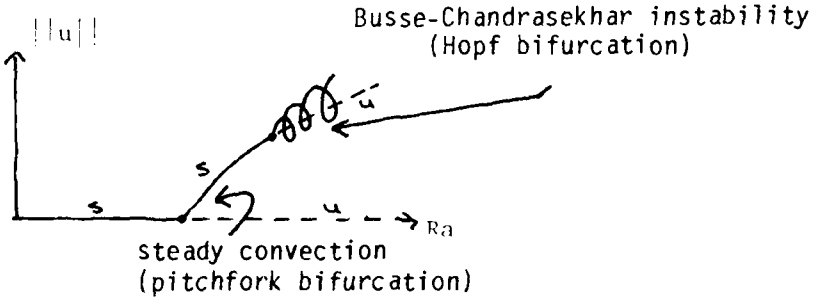

Figure 2: Usual instability scenario for convection

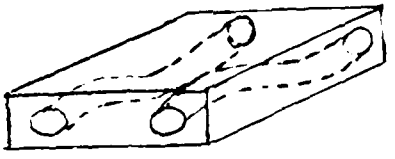

Figure 3: Busse oscillations in convective rolls

We are interested however in tuning a set of parameters to a value where several bifurcation points coalesce. In this way we can bring together a number n of linear and nonlinear instabilities to a single point on what is called the "critical surface" in λ-space; the philosophy being that we can learn more about the problem if we expand in a neighborhood of the most singular place in parameter space. We thus get n eigenvalues which pass through the imaginary axis in the s-plane at $\lambda = \lambda_0$, as in Figure 4.

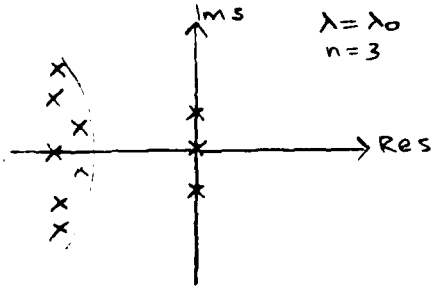

Figure 4: Eigenvalue scenario

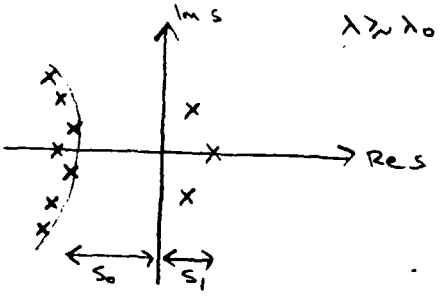

Figure 5

The assumptions are that the remainder of the spectrum remains bounded (and discrete for ease of presentation) away from the imaginary axis for some range of "near" λ. The amplitude equations will of course be valid only within some neighborhood of λ_0. The underlying small parameter defining "near" in parameter space is

$$\varepsilon = |s_1| \; / \; |s_0| \tag{4.10}$$

where s_1 and s_0 are defined as in Figure 5. The modes governed by eigenvalues with $|Re s| < |s_1|$ are called the "slow" modes (ϕ). Those with $Re\, s < s_0$ are called the fast modes (f) because their dynamics are primarily controlled by the slow modes as we shall see (Haken, 1977 calls them "slave" modes). The assumptions made on the spectrum will in general occur in dissipative systems where the spectrum crossing the imaginary axis is not continuous. This will not occur say in an "open" system such as convection in a box of infinite extent. Our description can be modified to take this into account, though the formalism for this is not rigorous. These problems have been handled by singular perturbation techniques in the past; see for instance the work of Segel (1969) or Newell and Whitehead (1969) for the convection problem. In Hamiltonian systems where all the eigenvalues are pure imaginary a different formulation can be used which we do not discuss here.

Nonlinear Theory

We now expand the solution to the original problem (4.3) in the eigenfunctions from linear theory corresponding to the eigenvalues s

$$U(\underset{\sim}{x},t) = \sum_{i=1}^{n} \alpha_i(t)\, \phi_i(\underset{\sim}{x}) + \sum_{i=1}^{\infty} \beta_i(t) f_i(\underset{\sim}{x}). \tag{4.11}$$

If, when $\lambda = \lambda_0$, there is a multiple eigenvalue $\bar{s}$ on the imaginary axis, it is possible that the number of eigenfunctions of equation (4.4) for $s = \bar{s}$ is less than the multiplicity of $\bar{s}$. In this case we must use generalized eigenfunctions for the ϕ_i, defined

$$\mathcal{M}\phi_i = \mathcal{L}(M_{ij}\phi_j) \tag{4.12}$$

where M is a matrix that can be put into Jordan canonical form if desired.

We now substitute the expansion (4.11) into the full equation (4.3). Using onthogonality properties of the eigenfunctions, we will get a set of ordinary differential equations

$$\begin{aligned} \dot{\alpha} &= M\alpha + F(\alpha,\beta) \\ \dot{\beta} &= K\beta + G(\alpha,\beta) \end{aligned} \tag{4.13}$$

where α and β are vectors with components α_i and β_i respectively, and F and G are strictly nonlinear.

To a first approximation, we would say β decays exponentially to zero. Setting $\beta \equiv 0$ in (4.13) gives the usual Galerkin approximation. Alternatively, the eigenvalues of $\mathbb{K}$ are strictly negative so that $\mathbb{K}$ is invertible - hence we can write

$$\beta = \mathbb{K}^{-1}(\dot{\beta} - \mathcal{G}(\alpha,\beta)). \tag{4.14}$$

This lends itself to a solution by successive approximations, namely

$$\beta_{j+1} = \mathbb{K}^{-1}(\dot{\beta}_j - \mathcal{G}(\alpha,\beta_j)) \tag{4.15}$$

with $\beta_0 = 0$. We thus get an approximate solution for β which we write as

$$\beta \cong \mathbb{B}(\alpha) \tag{4.16}$$

For instance, after one iteration (4.13) becomes

$$\dot{\alpha} = \mathbb{M}\alpha + F(\alpha, -\mathbb{K}^{-1}\mathcal{G}(\alpha,0)) \tag{4.17}$$

which is the adiabatic approximation and would give the usual Landau amplitude equations as discussed in Lecture 1.

We therefore have a formulation that reduces the dynamics to an n-dimensional system of amplitude equations

$$\begin{aligned} \dot{\alpha} &= \mathbb{M}\alpha + F(\alpha, \mathbb{B}(\alpha)) \\ &= \mathbb{M}\alpha + \Gamma(\alpha). \end{aligned} \tag{4.18}$$

Normal Forms

Performing the above formal steps to derive equation (4.18) for a given physical system may be difficult or tedious. However, one can decide from the linear stability mechanism what the structure of the above equations will be. The reduction of (4.18) to a standard equation is called *normal form theory* (Arnold, 1983).

Consider the schematic diagram in α-β amplitude space in Figure 6.

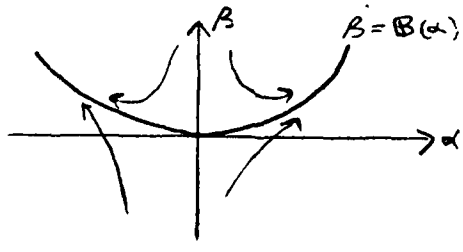

Figure 6: The Center Manifold

After a transient period ~ $1/|s_0|$ the motion lies for $\lambda = \lambda_0$ on what is called to center manifold, defined by $\beta = \mathbb{B}(\alpha)$. But α is not the "natural" coordinate of this manifold. We thus seek a transformation on that will ultimately simplify (4.18) into a normal form. We write

$$a = A + \Psi(A) \tag{4.19}$$

where Ψ is a strictly nonlinear function of the n-vector A. The normal form equations will be of the form

$$\dot{A} = \mathbb{M} A + g(A) \tag{4.20}$$

where g is a "nicer" function than Γ in equation (4.18). Substituting (4.19) and (4.20) into (4.18) gives an equation for Ψ

$$\mathcal{L}_{\mathbb{M}}\Psi = \Gamma(A + \Psi(A)) - g(A) \cdot (I + \delta_A \Psi) \tag{4.21}$$

where Ψ is operated upon linearly by

$$\mathcal{L}_{\mathbb{M}} = \mathbb{M} A \delta_A - \mathbb{M} \tag{4.22}$$

which can be interpreted as a convective derivative of dimension n in A-space.

A perturbative method for the solution of (4.21) is based on expanding the nonlinear functions Γ, g and Ψ in a Taylor series in the components of A. On collecting terms of degree D in (4.21), we are left with a sequence of linear problems to solve. Since there is a solvability condition to be imposed, a restriction on the choice of g results. Given the relevant scalar product on the space of polynomials in the components of A, we must find the adjoint null vectors $z^{(i)}$ such that

$$\mathcal{L}^{+}_{\mathbb{M}} z^{(i)} = 0. \tag{4.23}$$

The solvability condition is then

$$(z^{(i)}, \Gamma(A + \Psi(A)) - g(A)(I + \delta_A \Psi)) = 0. \tag{4.24}$$

We would consequently choose as simple a g as possible for equation (4.20) under this solvability constraint.

In theory then, we have found the normal form of the amplitude equations. Our analysis however has only given the amplitude equations on the critical surface at $\lambda = \lambda_0$. To know what is happening near λ_0, it is a matter of writing all the quantities depending on λ perturbatively in $\lambda - \lambda_0$ to obtain the more general normal form equations. Often this may be done approximately "by inspection" by just perturbing the linear terms of (4.20) only and leaving the nonlinear terms the same. Alternatively we can do the whole analysis above without assuming $\lambda = \lambda_0$, though often the calculation would become impractical.

In this way the dynamics near criticallity has been reduced to a study of ordinary differential equations. In the triple convection problem, we are left with a set of three first order o.d.e.'s. By studying Poincare maps and using other techniques outlined in the first three lectures, it has been demonstrated that chaos is exhibited arbitrarily close to the critical point when a particular triple instability occurs. For this case the result of Shil'nikov is applicable and gives a sufficient condition for chaos (see Lecture 5).

NOTES SUBMITTED BY
Michael Landman

LECTURE 5

Spatial Disorder in Large Systems

To motivate the study of competing instabilities, consider thermohaline convection in the "diffusive" regime, where heat is destabilizing and salt is stabilizing. We can choose the stability parameters to be M and Γ (the Melvin and George numbers, respectively). These numbers are both linear combinations of ΔT and ΔS, defined so that the steady state (Landau) bifurcation is at $\Gamma_0 = 27\pi^4/4$ and the oscillatory (Hopf) bifurcation is at $M_0 = 27\pi^4/4$, $\Gamma > \Gamma_0$. At $M = M_0$, $\Gamma = \Gamma_0$ there is a double bifurcation. The underlying linear problem gives a characteristic equation for the eigenvalues s:

$$\mathcal{M}_\lambda \Phi = s\Phi \Rightarrow F(s,\lambda; k)$$

where λ stands for the parameters of the problem and k is the horizontal wavenumber.

At the multiple bifurcation in thermohaline convection, the characteristic equation is

$$F(s, \lambda_0, k) = s^2 R(s, \lambda_0, k)$$

where R is the remainder. At a more general multiple bifurcation one finds

$$F(s, \lambda_0, k) = s^\ell (s^2 + \omega_1^2)\,(s^2 + \omega_2^2) \ldots R(s, \lambda_0 k).$$

The critical polynomial (Coullet and Spiegel, 1983) is defined for λ in the neighborhood of λ_0, by

$$P(s, \lambda, k) = \frac{F(s,\lambda,k)}{R(0,\lambda_0, k)} .$$

In the thermohaline problem the critical polynomial is

$$P(s,\lambda,k) = s^2 + \mu s + \nu,$$

where μ and ν are the two components of λ,

$$\mu = M - M_0$$

$$\nu = \Gamma - \Gamma_0 .$$

Note that when $\mu = 0$, the eigenvalues are $s = \pm\sqrt{-\nu}$ (Hopf) and when $\nu = 0$ one of the eigenvalues is zero (Landau).

The matrix $\mathbb{M}_\lambda$ which acts on the slow modes, defined in equation (4.12) in Lecture 4, is

$$\mathbb{M}_\lambda = \begin{pmatrix} 0 & 1 \\ -\nu & -\mu \end{pmatrix}, \quad \mathbb{M}_{\lambda_0} = \begin{pmatrix} 0 & 1 \\ 0 & 0 \end{pmatrix}$$

In the μ, ν parameter plane below the sign of the eigenvalues are indicated, and three sample paths are shown.

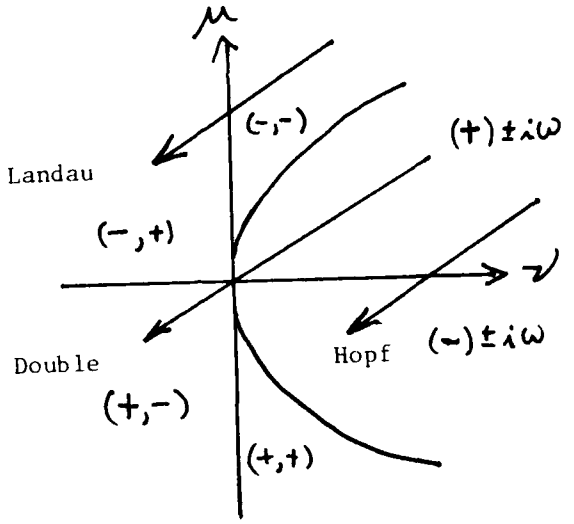

The three paths indicate how the parameters μ and ν might change as the experimentalist turns a single knob on the apparatus, keeping all other knobs fixed. If a second knob is set just right, the path goes through the double bifurcation at $\mu = \nu = 0$. This is called double because the experimentalist must fiddle with two knobs to find it, and fiddling with a third knob (such as the Prandtl number) won't make a big difference.

The nonlinear evolution of the system is described by the amplitude equation, which can be put into normal form. Recall the setup. The nonlinear problem is

$$\partial_t \mathcal{U} = \mathcal{M}_\lambda \mathcal{U} + \mathcal{N}(\mathcal{U}) \tag{5.1}$$

The critical or slow modes Ψ satisfy

$$\mathcal{M}_\lambda \Psi = \mathbb{M}_\lambda \Psi$$

where

$$\det(\mathbb{M}_\lambda - sI) = P(s,\lambda,k)$$

Now we will rederive the normal form a la Bogoliubov (Coullet and Spiegel, 1983; note equivalence to the Stuart-Watson method when operators are diagonalizable).

We make the anzatz

$$\mathcal{U}(x, t) = V(x, A)$$

$$\dot{A} = \mathbb{M}_\lambda A + g(A).$$

This anzatz turns (5.1) into

$$\mathcal{L}_\lambda V = \mathcal{N}(V) - g \odot \partial_A V, \tag{5.2}$$

where

$$\begin{aligned} \mathcal{L}_\lambda &= (\mathbb{M}_\lambda A) \odot \partial_A - \mathcal{M}_\lambda \\ &= (\mathbb{M})_{ij} A_j \partial_A - \mathcal{M}_\lambda. \end{aligned} \tag{5.3}$$

In what follows, it is helpful to keep in mind the special case where $\mathbb{M}_{\lambda 0} = 0$ (Landau bifurcation), and $\mathcal{L}_{\lambda_0} = -\mathcal{M}_{\lambda 0}$.

Now expand g and V by Taylor expansion in the variables $A = (A_1, \ldots, A_k)$, and let V_n and g_n be the (as yet unknown) terms of degree n. We know that g_1 is zero by definition. We demand that V_1 satisfies

$$\mathcal{L}_\lambda V_1 = 0$$

$$\Rightarrow \quad (\mathbb{M}_\lambda A) \odot \partial_A V_1 = \mathcal{M}_\lambda V_1$$

In other words, V_1 spans the generalized eigenspace of $\mathcal{M}_\lambda$ which has the same eigenvalues as those of $\mathbb{M}_\lambda$. Now we can proceed order by order in the Taylor expansion of (5.2):

$$V_n = I_n(N_{n-1}, V_{n-2}, \ldots, V_1, g_{n-1}, \ldots g_2) - g_n \odot \partial_A V_1 \tag{5.4}$$

where I_n are known terms, and V_n and g_n are to be found. This equation (5.4) for V_n cannot always be solved: We will choose g_n to be as simple as possible, consistent with the solvability conditions:

$$\langle V_1^+ | I_n \rangle = \langle V_1^+ | g_n \odot \partial_A V_1 \rangle,$$

where V_1^+ is any vector in the null space of the adjoint operator of $\mathcal{L}_\lambda$:

$$\mathcal{L}_\lambda^+ V_1^+ = 0.$$

An inner product in the space of V_n's is needed. Define

$$\langle f(x) A_1^{\ell_1} A_2^{\ell_2} \ldots | g(x) A_1^{m_1} A_2^{m_2} \ldots \rangle = \langle f(x) | g(x) \rangle \, \delta_{\ell_1 m_1} \, \delta_{\ell_2 m_2} \cdots$$

where the first term is some inner product on normal function space.

The solvability condition can be interpreted as follows: g_n is the projection of the nonlinear terms I_n onto the critical modes V_1. Note the similarily of this method to the Lindstedt method used by Malkus and Veronis (1958) in Benard convection, where $\mathbb{M}_{\lambda_0} = 0$.

The Bogdanov Normal Form

The normal form for the bifurcation when the linear matrix is $\begin{pmatrix} 0 & 1 \\ 0 & 0 \end{pmatrix}$, and there is no symmetry, is

$$\ddot{A} + (\mu - \alpha A)\dot{A} + (\gamma - \beta A)A = 0. \tag{5.5}$$

(It is assumed that α and β are order 1, and μ and ν are small. In the thermohaline example, $\alpha = 0$ and $\beta = 0$, due to the $A \rightarrow -A$ symmetry and one must include the cubic terms.) A complete analysis of the normal form (5.5) will not be given here (see Arneodo et al., 1985).

In the control parameter space there is a Hopf bifurcation (H) at ($\mu = 0$, $\nu > 0$) and a saddle loop bifurcation (SL) at $\nu > 0$, $\mu = (6\alpha/7\beta)\nu$.

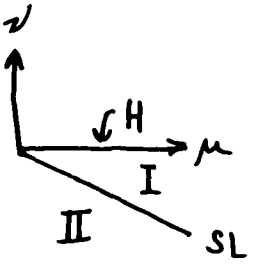

In region I, there is a stable limit cycle. The phase portrait and time series are drawn below:

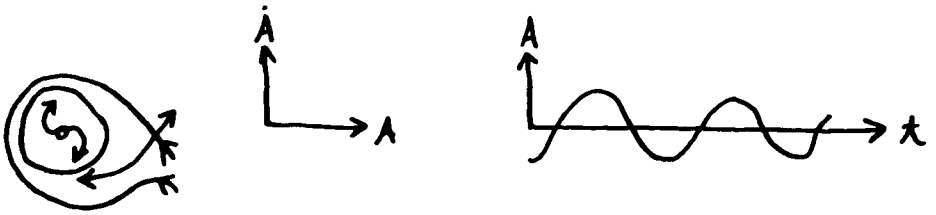

At the SL boundary between regions I and II, the period of the limit cycle has increased to infinity, and the phase portrait is

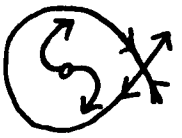

(In region II almost all trajectories escape to infinity.)

Just before the saddle loop (in region I), the time series shows "periodic intermittency," or relaxation oscillations.

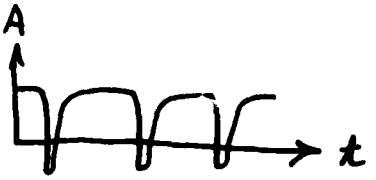

By tuning the parameters μ and ν, can be made to the relaxation oscillation occur as close as you want to the onset of instability (Arneodo et al., 1985). This is unusual because relaxation oscillators are usually seen at large amplitude.

When there are three competing instabilities (which can occur in triple convection), it is possible to tune the three parameters so that chaos occurs as close as desired to the initial instability.

Asymptotic Analysis

Asymptotic analysis yields amplitude equations which are simpler than the full normal form. In the case of three instabilities, the asymptotic equations are chaotic

Asymptotic analysis on the normal form for two competing instabilities (5.5) gives the scaling

$$A = \varepsilon A', \quad d/dt = \sqrt{\varepsilon}\, d/dt', \quad \mu = \sqrt{\varepsilon}\, \hat{\mu}, \quad \nu = \varepsilon\hat{\nu}$$

This is chosen to preserve the linear dynamics at leading order. When we drop the primes, the equation becomes

$$\ddot{A} = \hat{\mu}\dot{A} + \hat{\nu}A - \beta A^2 = \sqrt{\varepsilon}\ \alpha A\dot{A}$$

When the right hand side is neglected, $A > 0$ if the friction μ is positive, and A blows up if the friction is negative. When the scaling is $\mu = \varepsilon\mu$ the leading order asymptotics is

$$\ddot{A} + \nu A - \beta A^2 = 0.$$

The above equation is conservative, and the dynamics are qualitatively different from those of the full system. The normal form method doesn't have this difficulty.

Three Competing Instabilities

In the case of three competing instabilities, the asymptotic analysis which preserves the linear terms,

$$L = \begin{pmatrix} 0 & 1 & 0 \\ 0 & 0 & 1 \\ -\mu_0 & -\mu_1 & -\mu_2 \end{pmatrix}$$

is

$$\dddot{A} + \mu_2\ddot{A} + \mu_1 A + \mu_0 A = \pm A^n, \tag{5.6}$$

where $n = 2$ if no $A \rightarrow -A$ symmetry is imposed, and $n = 3$ with the symmetry (as for fluids). This asymptotic equation (5.6) contains interesting behavior - including chaos. The full normal form treatment would presumably yield qualitatively similar behavior, but is much more difficult.

Consider the case $n = 2$ in the asymptotic equation. There are two stationary solutions ($\dot{A} = \tilde{A} = 0$), at $A = 0$, and $A = \mu_0$. (The $\pm$ sign in (5.6) can be made a plus sign.) Numerical experiments (Arneodo et al. 1985) reveal the sequence of events pictured below.

In figure (a), the fixed point at the origin is an unstable saddle focus, and the other fixed point is stable. As some parameter is changed the stable fixed point undergoes a Hopf bifurcation, leading to the stable limit cycle shown in figure (b). As the parameter is increased further, there is a homoclinic connection (figure (c)). At this homoclinic connection a single trajectory approaches the origin as t approaches both positive and negative infinity.

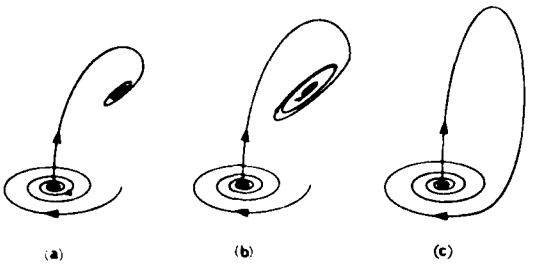

A cascade of period doubling bifurcations, leading to chaos is observed between figures (b) and (c). This chaos is related to the homoclinic orbit of saddle-focus type, using the ideas of Shil'nikov (1968) and others (see, for instance Arneodo et al., 1985).

The analysis of the behavior near a homoclinic orbit is separated into two regimes: 1) the flow near the fixed point, where adjacent trajectories are sheared and wrapped up, and 2) the flow away from the fixed point which brings the unstable manifold back to the origin, but which is otherwise well behaved.

Near the saddle focus at the origin, we can choose coordinates so that the ODE system is

$$\dot{x} = -\alpha x + \omega y + \ldots$$

$$\dot{y} = -\alpha y - \omega x + \ldots$$

$$\dot{z} = \beta z \ldots$$

The Poincaré map for the flow near the homoclinic orbit is the composition of two maps - describing the local and global flow mentioned earlier. There are two surfaces of section: P^0 is a patch of the plane $y = 0$, and P^1 is a patch of $z = h$. Both of these surfaces are pierced by the homoclinic orbit as shown in the figure below.

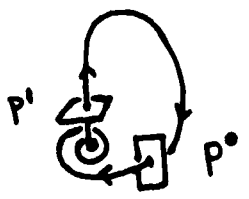

For ease of analysis, we will assume that the linearization is exact near the origin. This can be arranged by a (nonanalytic) change of coordinates using Hartman's theorem. Then the mapping from $(x_0, z_0) \in P^0$ to the polar coordinates $(\rho, \theta) \in P^1$ is

$$\rho = x_0 \, (z_0/h)^{\alpha/\beta} \quad , \quad \theta = \omega/\beta \, \ln(z_0/h)$$

A line of constant x_0, with $z_0 > 0$ wraps around the z axis in a logarithmic spiral:

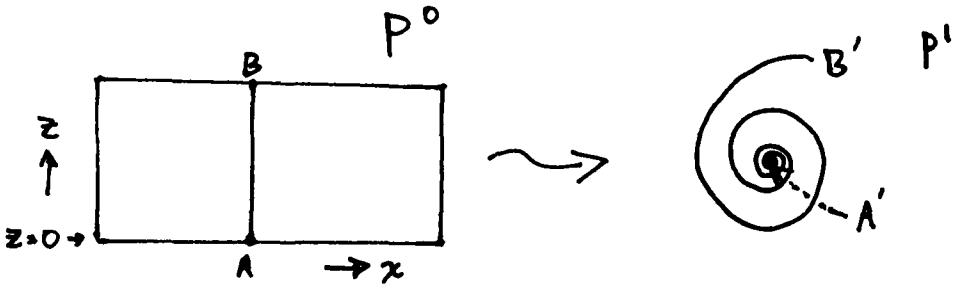

The map from P^1 back to P^0 is constrained by the fact that there is a homoclinic orbit. In other words $\rho = 0$ on P^1 must return to somewhere on the line $z = 0$ in P^0 when there is a homoclinic orbit. As some parameter is changed, we assume that the unstable manifold of the origin returns at $z > 0$ (figure (a)), $z = 0$ (figure (b)) and then $z < 0$ (figure (c)).

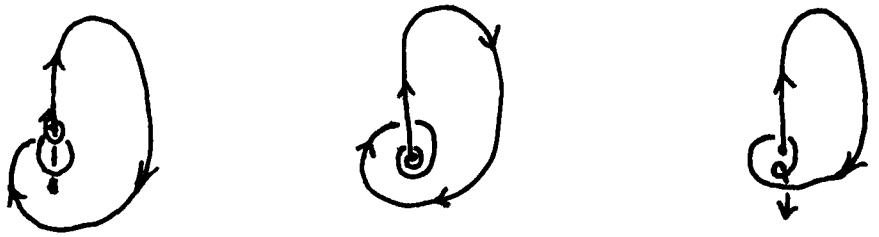

(a) (b) (c)

It is of course difficult to calculate when this homoclinic orbit occurs without the aid of a computer; this makes the analysis of the original asymptotic form (5.6) difficult.

We will assume that the map from P^1 to $(x_1, z_1) \in P^0$ takes the form

$$x_1 = \rho\cos(\theta + \varphi) + \tilde{x}$$

$$z_1 = \rho\sin(\theta + \varphi) + \tilde{z}$$

where $\tilde{x}$, $\tilde{z}$ and φ are constants ($|\tilde{z}| << 1$). More general mappings, including shear and contraction or expansion, do not affect the results when z is small enough (i.e. close enough to the homoclinic orbit).

The composition of the two maps gives the return map from P^0 back to itself:

$$x_1 = x_0\,(z_0/h)^{\delta}\cos[\xi \ln(z_0/h) + \varphi] + \tilde{x}$$
$$z_1 = x_0\,(z_0/h)^{\delta}\sin[\xi \ln(z_0/h) + \varphi] + \tilde{z} \qquad (5.7)$$

where the two parameters

$$\delta = \alpha/\beta \quad , \quad \xi = \omega/\beta$$

characterize the linear dynamics near the origin. The return map for a strip with x ~ constant is drawn below.

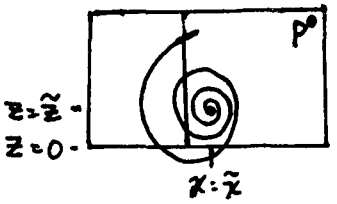

The mapping 7 can be rescaled to yield

$$X' = 1 + bXZ^{\delta}\cos[\xi \ln(Z) + \Phi]$$
$$Z' = c + XZ^{\delta}\sin[\xi \ln(Z) + \Phi]$$

where $b = (h/\tilde{x})^{\delta/(\delta-1)}$ and the other scalings are found in Arneodo et al. 1985. Under the assumption b = 0, we always have X = 1, and this map reduces to a one dimensional map:

$$Z' = c + Z^{\delta}\sin[\xi \ln(Z) + \Phi] \qquad (5.8)$$

At the homoclinic orbit, c = 0. Thus c may be thought of as the control parameter. The figures below, from Arneodo et al. 1985, show the behavior of the 1-D map (5.8) for various parameter values.

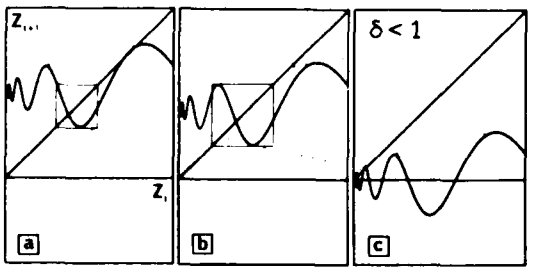

Graph of the unidimensional map ( ) for parameter values satisfying condition (6.13): $\delta = 0.5$, $\xi = 5$, $\Phi = 2.7177$; a) $c = 5.2$; b) $c = 4.128$; c) $c = 0$. In a) and b) the squares isolate regions in the variable Z that are invariant under (6.19). Scales: $(Z_i)_{min} = 0$, $(Z_i)_{max} = 10.25$, $(Z_{i+1})_{min} = -5.125$, $(Z_{i+1})_{max} = 10.25$

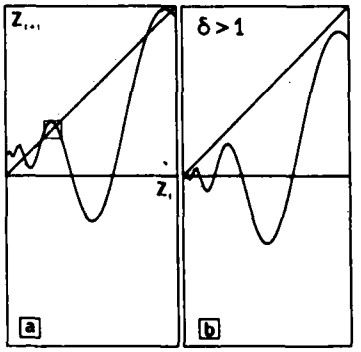

Graph of the unidimensional map ( ) for parameter values that do not satisfy condition (6.13): $\delta = 1.2$, $\xi = 5$, $\Phi = -2.7177$; a) $c = 0.1$; b) $c = 0$. The square in a) defines an invariant region where (6.19) produces, as in fig. 10a, a single-humped mapping. Scales: $(Z_i)_{min} = 0$, $(Z_i)_{max} = 0.75$, $(Z_{i+1})_{min} = -0.75$, $(Z_{i+1})_{max} = 0.75$

In the $\delta < 1$ case there is an infinite number of unstable fixed points (periodic orbits of the ODE) at $c = 0$. As c decreases to zero from above there is a cascade of period doubling bifurcations leading to chaos as each one of the valleys on the graph of Z' vs Z pushes through the diagonal. Figure b above shows the graph as one of the valleys completes its "universal sequence." The dynamics in the box are equivalent to $x \rightarrow 4x(1-x)$. Therefore there is a cascade of cascades of period doublings, each leading to chaos as c decreases to zero.

Unfortunately this chaos is difficult to observe, because if any Z_n is negative, the mapping stops. This is because the trajectory of the ODE has returned below x-y plane and shoots down the negative z axis to infinity.

For $\delta > 1$ there is only one fixed point near the origin for $c > 0$ and this is always stable. For larger c, there is chaos which is outside of the realm of validity of the analysis, yet which is easier to detect than the subtle chaos of the $\delta > 1$ case.

Spatial-temporal Chaos

The radial motion of gasses at the surface of the sun can be measured by Doppler shift, and a time series of the "five minute" oscillations looks chaotic.

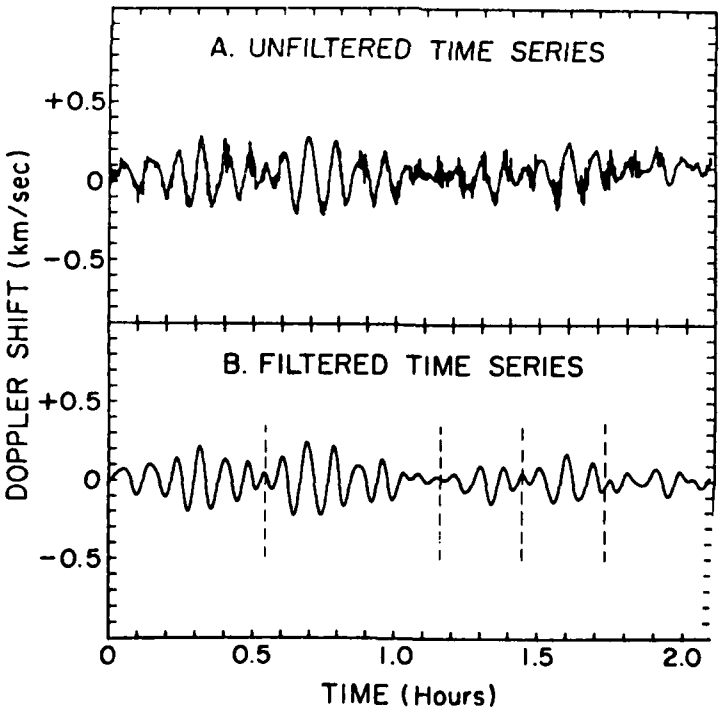

Typical Velocity Curve for Individual Oscillation (from White and Cha 1973).

One can cook up a system of ODEs which exhibit chaotic oscillations, but this model must be wrong because it assumes that the spatial structure is regular. A superposition of time series taken at adjacent positions shows that there are packets of waves propagating erratically.

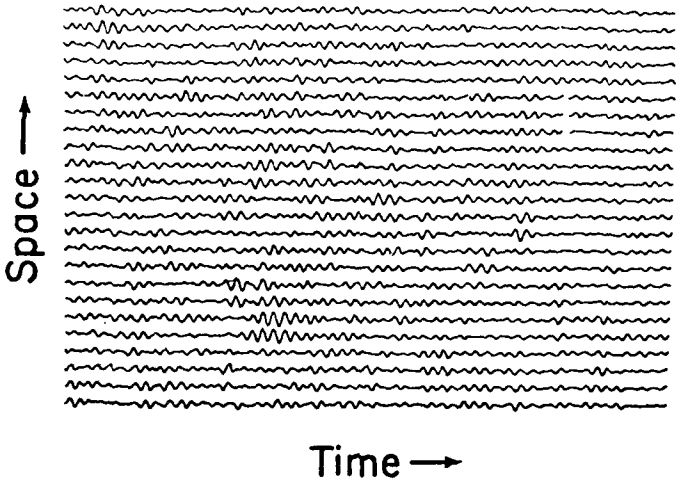

Velocity vs time at different positions along a line. Adjacent points are 1.8 Mm apart (Stein and Leibacher, 1974).

In order to describe these spatial structures, we want to allow a continuum of wavenumbers. In the previous examples the patterns were assumed to be periodic and we obtain an ODE for the discrete amplitudes in k-space. In the following, an integro-differential equation is derived for the continuum of amplitudes (Coullet and Spiegel, in preparation).

The vertical velocity W and temperature difference θ can be written

$$W(\underset{\sim}{x},z,t) = \int W_{\underset{\sim}{k}}(z,t)\, e^{i\underset{\sim}{k}\cdot\underset{\sim}{x}} d\underset{\sim}{k}$$

$$\theta(\underset{\sim}{x},z,t) = \int \theta_{\underset{\sim}{k}}(z,t)\, e^{i\underset{\sim}{k}\cdot\underset{\sim}{x}} d\underset{\sim}{k}$$

$$\mathcal{V}_{\underset{\sim}{k}} \equiv \begin{pmatrix} W_{\underset{\sim}{k}} \\ \theta_{\underset{\sim}{k}} \end{pmatrix}$$

where $\underset{\sim}{k}$ and $\underset{\sim}{x}$ are vectors in the horizontal plane. The convection equations can be written in k-space as

$$\partial_t \mathcal{V}_k = \mathcal{M}_{\underset{\sim}{k}} \mathcal{V}_{\underset{\sim}{k}} + \mathcal{N}_{\underset{\sim}{k}}(\mathcal{V}_q)$$

where

$$\mathcal{N}_{\underset{\sim}{k}}(\mathcal{V}_q) = \iint d\underset{\sim}{p}\, d\underset{\sim}{q}\, \delta(\underset{\sim}{k}-\underset{\sim}{p}-\underset{\sim}{q})\, \mathcal{N}^{(2)}(\mathcal{V}_{\underset{\sim}{p}}, \mathcal{V}_{\underset{\sim}{q}}; \underset{\sim}{p},\underset{\sim}{q}) + \ldots$$

At the onset of stationary convection, the linear equation for the critical amplitude is

$$\dot{A}_{\underset{\sim}{k}} = (R-R_c)A_{\underset{\sim}{k}} - (|\underset{\sim}{k}|^2 - k_c^2)^2 A_{\underset{\sim}{k}} \equiv \sigma_{\underset{\sim}{k}} A_{\underset{\sim}{k}}$$

The Boyolioubov anzatz in this case is

$$\mathcal{V}_{\underset{\sim}{k}}(z,t) = \mathcal{V}_{\underset{\sim}{k}}(z, \{A_q\})$$

where

$$\dot{A}_{\underset{\sim}{k}} = \sigma_{\underset{\sim}{k}} A_{\underset{\sim}{k}} + \Gamma_{\underset{\sim}{k}}(\{A_{\underset{\sim}{q}}\})$$

Here the curly brackets represent functionals. Plugging the anzatz into the equation yields

$$\mathcal{L}\mathcal{V}_{\underset{\sim}{k}} = \mathcal{N}_k(\{A_{\underset{\sim}{q}}\}) - \int d\underset{\sim}{q}\, \Gamma_{\underset{\sim}{q}} - (\{A_{\underset{\sim}{p}}\})\ \delta\mathcal{V}_{\underset{\sim}{k}}/\delta A_{\underset{\sim}{q}}$$

where

$$\mathcal{L} = \int d\underset{\sim}{q}\, \sigma_{\underset{\sim}{q}} A_q\ \delta/\delta A_q - \mathcal{M}_k$$

(Note the similarity of these equations to equations (5.2) and (5.3).)

This formalism is not supported by the center manifold theorem, and there are problems if the amplitude does not decay sufficiently fast as k leaves the circle of critical k vectors. Nevertheless, this can be Thought of as "the physicists center manifold" technique.

Modulation Theory

An alternative approach to the k-space treatment is modulation theory. Here a slowly varying function of space and time modulate the critical disturbance.

The modulation function is written as a function of the slow space variable $X = \varepsilon x$. Here the fields are written as (supressing z dependence)

$$\Psi(x,t) = \psi(X,t)e^{ik_o x} + c.c.$$

This leads to the Newell-Whitehead-Segel equation (in one horizontal spatial dimension)

$$\partial_t \psi = \varepsilon\psi + \psi_{xx} - \psi^3$$

When there is an oscillatory instability, we have

$$\Psi(x,t) = \psi(X,T)e^{ik_o x - \omega_o t} + \psi(X,T)e^{ik_o x + \omega_o t} + c.c.$$

where $T = \varepsilon t$ is a slow time. Here ψ is the amplitude of the right-going wave and ψ is the amplitude of the left-going wave. Modulation theory gives (after suitable scaling - see Bretherton and Spiegel, 1983)

$$\begin{aligned} \psi_T + \psi_X &= \varepsilon\left[\psi + (1 + i\mu)\psi_{xx} + \alpha\psi|\psi|^2 + \beta\psi|\tilde{\psi}|^2\right] \\ \tilde{\psi}_T - \tilde{\psi}_X &= \varepsilon\left[\tilde{\psi} + (1 + i\mu)\tilde{\psi}_{xx} + \bar{\alpha}\tilde{\psi}|\tilde{\psi}|^2 + \bar{\beta}\tilde{\psi}|\psi|^2\right] \end{aligned} \qquad (5.9)$$

where μ is real and α, β are complex. From the left hand side of the above equations, we see that wave packets move to the left or right with group velocity 1 in this scaling.

It turns out that $Re(\alpha) = 0$ for thermohaline convection with free boundaries and fixed salt and temperature on top and bottom. This term, if it is present, renormalizes the growth rate of a pure traveling wave; if $\tilde{\psi} = 0$ and $\psi_X = 0$, then equation (5.9) implies

$$|\psi|^2_T = \epsilon((\psi|^2 + Re(\alpha)(\psi|^4$$

As a consequence of $Re(\alpha) = 0$, the pure travelling waves grow exponentially until fifth order terms in the amplitude equation become important, or until there are modulational instabilities of the spatially uniform state. We will consider these modulational instabilities, assuming $\tilde{\psi} = 0$ [which is okay provided $Re(\beta) < 0$]. By changing coordinates to ξ and τ, where

$$\xi = X-T, \ \tau = \epsilon T \rightarrow \partial_T = -\partial_\xi + \epsilon\partial_\tau, \ \partial_X = \partial_\xi$$

We get, on scaling $Im(\alpha)$ to 1,

$$\partial_\tau\psi = \psi + (1 + i\mu)\psi_{\xi\xi} + i\psi|\psi|^2 \qquad (5.10)$$

This is a special case of the complex Landau-Ginzberg equation: the real part of the cubic term is "accidentally" zero.

In the case where μ is large, ψ can be rescaled to yield the nonlinear Schroedinger equation in the limit of small ϵ.

$$i\partial_\tau\psi = i(\mu/\epsilon)\psi_{\xi\xi} - \psi|\psi|^2 + i\epsilon\ \psi + \psi$$

(Here μ/ϵ is assumed to be order 1). When $\epsilon = 0$ these equations have a soliton solution

$$\psi = A\,\mathrm{sech}(\xi - V\tau)$$

For ϵ small, the amplitude and velocity are functions of a slow time $\epsilon\tau$.

$$\dot{A} = 2A(1 - V^2) - 2/3\ A^3$$

$$\dot{V} = -4/3\ A^2\ V$$

This is a dull dynamical system the solitons either die away ($A \rightarrow 0$) or come to rest ($A \rightarrow 3$, $V \rightarrow 0$). As shown below, a soliton moves a finite distance and stops.

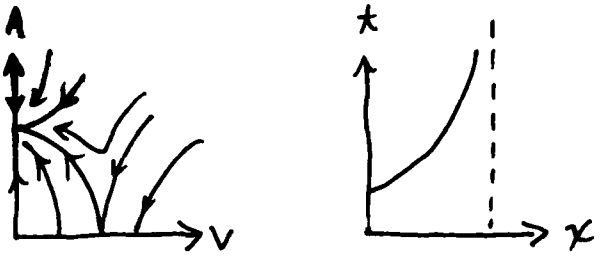

In numerical experiments with $\varepsilon \neq 0$, however, a single soliton seems to split into two, and the interaction of many solitons leads to intermittency in both space and time. The following figure, from Bretherton and Spiegel (1983), shows the evolution of equation (5.10) started with a small amount of white noise. Remember that this is just the modulation of the wave packet, seen in a reference frame moving with the group velocity. These results bear a resemblance to the observations of the solar five minute observations.

Finally, we mention another application of the asymptotic equation (6). One can do a WKB analysis on the Landau-Ginzberg equation by assuming

$$\psi(x,t) = R(x,t)\, e^{i\varphi(x,t)}$$

and eliminating R variations adiabatically. The result is the Burger's equation, but the diffusion constant can be positive or negative. For a negative diffusion constant, we must add a stabilizing term with 4 spatial derivatives. This leads to the Kuramoto-Sivashinski equation for $U = \varphi_x$:

$$U_t + UU_x + U_{xx} + U_{xxxx} = 0.$$

If we assume a solution of the form

$$U = f(x - ct)$$

and integrate the equations once, we get

$$f''' + f' - cf + 1/2\, f^2 = 0.$$

This is a special case of the asymptotic equation (5.6) for 3 competing instabilities. In the present case, there is no f" term, so the equation is Liouvillian (i.e. volumes are preserved.) This equation has been studied by Spiegel and Fournier (in preparation), where it was found numerically that the trajectories were on a torus in the initial value problem:

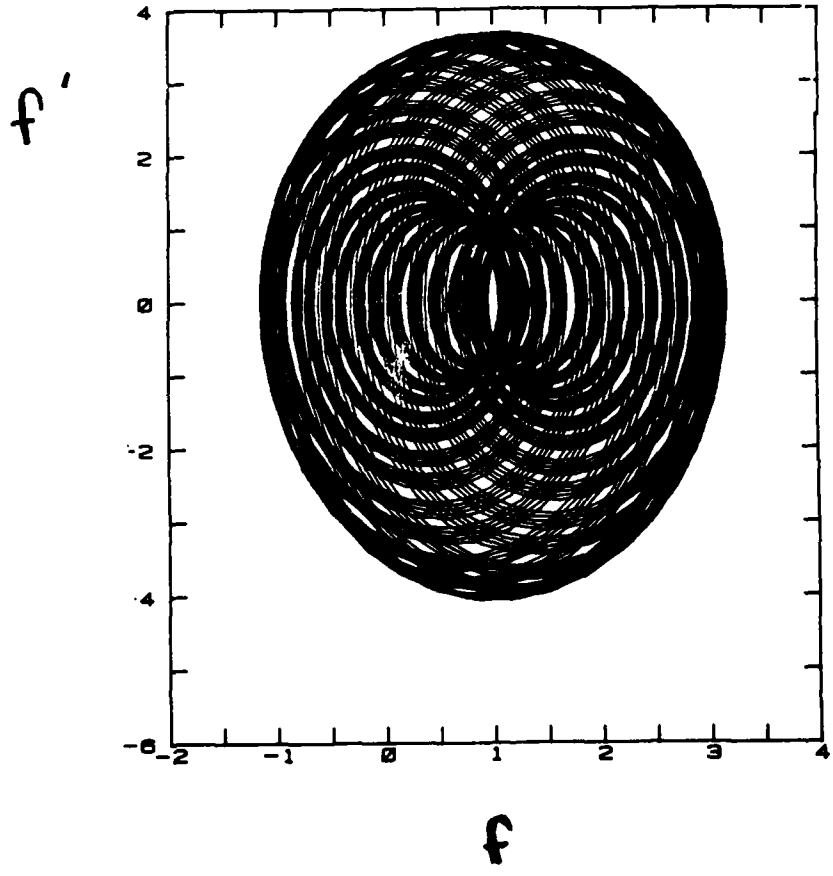

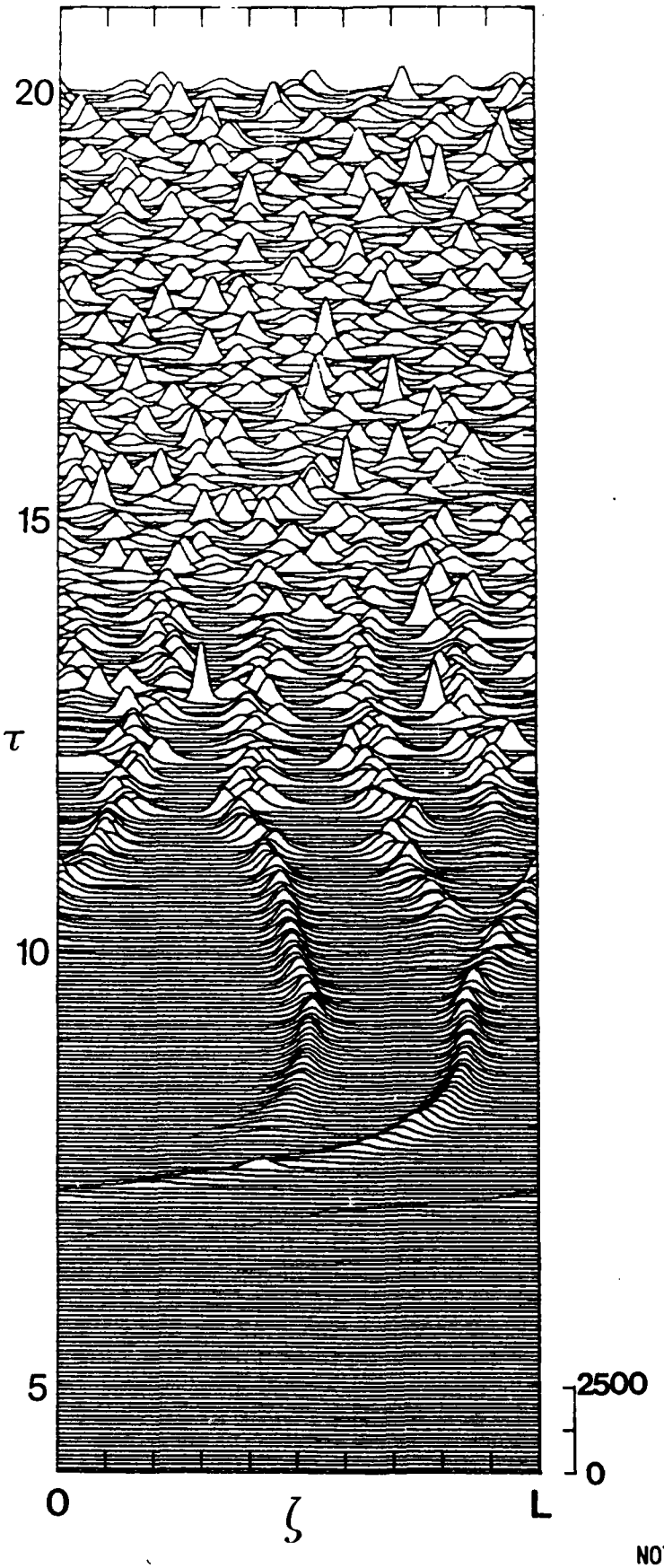

NOTES SUBMITTED BY
James W. Swift

REFERENCES

Arneodo, A., P.H. Coullet and E.A. Spiegel, 1985. The Dynamics of Triple Convection, Geophys. Astrophys. Fluid Dynamics 31, 1-48.

Arneodo, A., P.H. Coullet, E.A. Spiegel and C. Tresser, 1985. Asymptotic Chaos, Physica 14D, 327-347.

Arnold, V.I., 1983. Geometrical Methods in the Theory of O.D.E.'s, Springer-Verlag, Grundlagen der mathematiseten Wissenschaften 250.

Beckers, J.M. and R.C. Canfield, 1976. Physique des Mouvement dans les Atmospheres stellaires, ISBN 2-222-01923-0 (CNRS).

Bretherton, C.S. and E.A. Spiegel, 1983. Intermittency through Modulational Instability, Physics Letters 96A, no. 3, 152-156.

Childress, S. and E.A. Spiegel, 1980. Variations of the Solar Constant, S. Sofia, ed., NASA Conference Publication 2191, 273-292.

Coullet, P.H. and E.A. Spiegel, 1983. Amplitude Equations for Systems with Competing Instabilities, SIAM J. Applied Math. 43, #4, 776-821.

Crutchfield, J., J.D. Farmer and B.A. Huberman, 1982. Phys. Reports 92, 45.

Eddy, J., 1976. The Maunder Minimum, Science 192, 1189-1202.

Gollub, J.P. and S.V. Benson, 1980. Many routes to turbulent convection, J. Fluid Mech. 160, 449-470.

Haken, H., 1977. Synergetics. An Introduction: Nonequilibrium Phase Transitions in Physics, Chemistry and Biology. Springer-Verlag.

Henon, M., 1976. Comm. Math. Phys. 50, 69-77.

Kida, S., 1980. Statistics of active regions in the beta-mode of turbulence, Prog. T. Phys. 67, 1630-1632.

Lorenz, E.N., 1963. J. Appl. Sci. 20, 130-141.

Malkus, W.V.R. and G. Veronis, 1958. Finite Amplitude Cellular Convection, J. Fluid Mech., vol. 4, 225-260.

Marzec, C.J. and E.A. Spiegel, 1980. Ordinary differential equations with strange attractors, SIAM J. Appl. Math. 38, 403-421.

Moore, D.W. and E.A. Spiegel, 1966. Astrophys. J. 143, 871-887.

Newell, A.C. and J.A. Whitehead, 1969. J. Fluid Mech. 38, 279-303.

Ruelle, D. and F. Takens, 1971. Comm. Math. Phys. 20, 167-192.

Segel, L.A., 1969. J. Fluid Mech. 38, 203-224.

Shil'nikov, L.P., 1968. On the Generation of Perioic Motion from Trajectories Doubly Asymptotic to an Equilibrium State of Saddle Type, Math. U.S.S.R. Sbornik 6, 427-438.

Smith, L., J.-D. Fournier and E.A. Spiegel, 1985. Lacunarity and Intermittency in Fluid Turbulence, preprint.

Spiegel, E.A., 1980. N.Y. Acad. Sci. 357, 305-312.

_____, 1982. Magnetic buoyancy and the Boussinesq approximations, Geo. Astro. Fluid Mech. 22, 219-234.

_____, 1985. Cosmic Arrythmias, Preprint #A68, Columbia Uni. Dept. of Astronomy and Astrophysics.

Spiegel, E.A. and N.O. Weiss, 1980. Magnetic activity and variations in solar luminosity, Nature 287, 616-617.

Stein, R.F. and J. Leibacher, 1985. Ann. Rev. Astr. and Astrophys. 12, 407-435.

ABSTRACTS OF SEMINARS

Intermittency

Yves Pomeau

I. Intermittency in maps and ODE

Transitions to turbulence in ordinary differential equations (ODE) and maps is known to occur (with codimension 1 in the parameter space) in four different ways.

1) Through a "first order" or subcritical transition. This happens for instance in the Lorenz system where fixed points lose their stability to give place to a chaotic attractor to which they do not belong. Within the framework of codimension 1 approach, one cannot control this behavior, although something can be done in codimension 2 (see lectures of E. Spiegel at this GFD conference).

2) For the time being, they are three registered "second order" or supercritical (in a loose sense) routes from a regular behavior to a chaotic one. They are listed below with some comments.

2i) The Ruelle-Takens-Newhouse route: It describes what happens when a new periodic motion appears on the top of a time dependent dynamics with a finite number (3 or 4) of independent frequencies. Under rather special hypothesis (depending on the number of base frequencies), one may prove that adding a new frequency to a quasiperiodic regime with 3 or 4 frequencies leads a chaotic behavior on a strange attractor. However, the detailed analysis of this kind of transition meets awkward difficulties related to small denominators in every expansion that can be made, and so the final word is not yet said.

2ii) The period doubling: This is covered in E. Spiegel's lecture (same volume) and is also well explained in the book by Collet and Eckmann (1980).

2iii) The intermittent transition: This transition may occur when a limit cycle loses its stability, through a subcritical bifurcation. The gross phenomenology is always the same: for a value of the control parameter R (that can be, for instance, the Rayleigh number in convection experiments) less than a critical R_c, one observes regular (and thus stable) oscillations, lasting forever. For R a slightly higher than R_c, the same regular oscillations persist most of the time, but are sometimes interrupted by large bursts. These bursts are followed by a relaminarization, i.e. by a return to seemingly regular oscillations, then interrupted by a new large burst, and so on. As R gets close to R_c, the mean time interval between consecutive bursts increases indefinitely, although their amplitude does not change significantly. Inside this picture, some variations take place, and they can be explained by considering the various possible subcritical instabilities of a limit cycle.

Let M be the (real) Floquet matrix describing the first return map linearized around a closed trajectory. This one goes from linearly stable to linearly unstable whenever this Floquet matrix gets one (or more) eigenvalue - with a modulus larger than 1. This may happen in three different

fashions, because the root of the secular equation $|M - \lambda I| = 0$ (λ = eigenvalue of the Floquet matrix, $|\cdot|$ = determinant of $\cdot$, I unit matrix) may go out of the unit circle either through (+1) (type I intermittency), through (-1) (type III intermittency) or through two complex conjugates eigenvalues (type II intermittency).

Paul Manneville and I (1980) discussed theoretically type I intermittency that has a rather simple picture. This splits in two parts: first one has to describe the vicinity of the fixed point, where the seemingly periodic (or "laminar") phase of the motion takes place, then one has to explain how the bursts can end into a new laminar phase (this is the "relaminarization process" in a terminology freely adapted from fully developed turbulence theory).

It is worth noticing at this point that, in type I intermittency, the bursting regime can be chaotic, quasiperiodic or even periodic, depending on the specific situation one is considering. This constrasts with types II and III, where the bursting regime is generically chaotic. This bursting regime is periodic or quasiperiodic when it occurs at ends of periodicity windows (in the parameter space) for circle diffeomorphisms, i.e. first return maps for flow on a T^2 torus. In 1d maps with a single maximum, as the quadratic map $X \to 1 - Ax^2$, $0 < A < 2$, $-1 < x < +1$, the periodicity window of stable generic periods (= not obtained by period doubling), ends on one side (as A increases) by period doubling and on the other side by type I intermittency. Again, this intermittency may correspond either to a chaotic or to a periodic behavior, as the fine structure of the quadratic map has (Collet and Eckmann 1980) an overwhelming complexity nearby the first occurrence of a new generic stable period in the parameter space.

In any case, the mean interval between two bursts increases as $(R-R_c)^{-1/2}$ when the control parameter R tends to R_c, not staying in the intermittent regime. Many predictions of this theory have been checked experimentally in Rayleigh Bénard (R.B.) convection (Bergé et al. 1980) and in chemical oscillations (Pomeau et al. 1980). In this last case, it was even possible to exhibit a detailed first return map, in complete agreement with theory.

The phenomenology of type III intermittency is very similar to the previous one. Here, the basic mechanism is a subcritical period doubling. Nonlinear effects, instead of keeping the weakly unstable subharmonic fluctuations at a low level near the bifurcation, tend instead to increase their amplitude in a "catastrophic" manner. Accordingly, during laminar periods, one can observe slowly growing subharmonic fluctuations. They manifest themselves as an amplitude difference between consecutive oscillation maxima. The relaminarization process is less obvious than in type I intermittency. It relies upon the fact that a slightly beyond the instability threshold, attraction toward the periodic trajectory along its stable manifold is still efficient and that a point wandering in phase space has still a good chance to land nearby this stable manifold. When this happens, this point will come next to the closed trajectory before to feel the weak instability along the unstable manifold. All this has been checked (Dubois et al. 1983) experimentally in great details in a high-quality R.B. experiment by the Bergé group in Saclay, although at my knowledge no ODE has yet been found with this sort of behavior. One of the

outcomes of the theory is that, near the threshold, the mean duration between two bursts diverges as $(R-R_c)^{-1}$ near R_c. Exactly at threshold ($R=R_c$), there is still an intermittent regime (although for type I intermittency, the limit cycle still exists at threshold). This regime is really intermittent in the sense of mathematicians. The probability distribution for the duration t of a long laminar period is as $t^{-3/2}$ as $t \to \infty$. Although this probability law has a finite total weight, the mean duration between two bursts diverges. So, as long as is the observation time T, there will be during this time a laminar period of approximately the same length. If one plots the turbulent bursts on the real line, the set of points drawn in this way will have the fractal dimension 1/2. Another way of telling the same thing is to notice that, during a long observation period T, the number of turbulent bursts will be of order $T^{1/2}$ C, and the coefficient C keeps fluctuating with a relative amplitude of order 1 as $T \to \infty$.

Type II intermittency has never been observed as far as I know, either in numerical simulations of ODE or in real life experiments. N. Weiss (private communication), however, pointed out to me that there is some hope to observe this particular transition in PDE-simulation of convection with internal heating.

II. Extended intermittency

Looking at the recent work of Kaneko on string of maps and at previous studies of Paul Manneville on the PDE $Y_t+YY_x = [\epsilon - (\partial^2_{x2} + 1)^2]Y$, for $\epsilon \simeq 0.4$, I've been laid to consider the possibility that intermittency might be also relevant for the transition to turbulence in extended systems.

Let us consider, as Kaneko did, a string of 1d maps, each one being some local oscillator near an intermittent transition. Let us turn on furthermore some coupling parameter between neighboring "oscillators." One may believe that, once an oscillator has jumped into a bursting regime, it will change the working point of its neighbors, and make them jumping to a bursting regime too (this is the "contamination" process), because these oscillators are nearby a subcritical instability and are thus unstable against finite amplitude fluctuations.

Consider now a 2d parameter space where the coordinates are the nearest-neighbors coupling strength and $(R - R_c)$, as measured for each individual oscillator. There is, in this parameter space a special point, $R = R_c$, and zero coupling, where one certainly has extended intermittency. By continuity one may guess that a continuous line can be drawn from this special point (the "origin") such that there is a transition across it from globally stable oscillations to sustained chaos, this chaos being intermittent for control parameters just on the transition line. Moreover, it is likely that the transition remains of 2d order (in the terminology of equilibrium statistical physics) at least nearby the origin. If this is true, a natural question appears: what is the universality class (if there is any) of this transition ? I conjecture that this could be the one of directed animals. This problem has been analytically solved in 2d for a square lattice by J.P. Nadal et al. (1982), thanks to a clever "Bethe Ansatz," although some questions remain unsolved. Following earlier suggestions (1982), the time direction should be the dimension along which the animal grows, so that a linear (1d) string at the intermittent transition

would correspond to the 2d directed animal of Nadal et al. (1982). This conjecture may be justified as follows.

Once an oscillator of the string begins to burst, it will either trigger the bursting of neighbors or settle back to the regular oscillatories before it contaminates its neighbors. This is reminiscent of the rules needed for growing a directed animal: from a point on the animal that would correspond to a bursting oscillator, one may either grow links in the forward direction (and so have bursting neighbors), or stop building the animal from this point. The "critical animal" is reached for a well definite ratio of the probability of dying or of contaminating the neighbors. Indeed, as usual for critical phenomena, the universality class should be relevant as far as the scaling properties (≃ the critical exponents) of each individual realization within the class are concerned, although the short range structure depends on the details of each realization.

A possible (?) realization of this extended intermittency could be sought in R.B. thermal correction, where the gross structure would be held by differential heating to avoid slow phase turbulence. In that case, the short time scale would be of the order of a rotation period in a roll.

REFERENCES

Berge, P., M. Dubois, P. Manneville and Y. Pomeau, 1980. J. de Phys. Lett., 41, L347.

Collet, P. and J.P. Eckmann, 1980. "Iterated maps on the interval as dynamical systems," Birkhauser, Boston.

Dubois, M., M.A. Rubio and P. Berge, 1983. Phys. Rev. Lett. L51, 1446 and 2345.

Nadal, J.P., B. Derrida and J. Vannimenus, 1982. J. de Phys. 43, 1561 and V. Hakim and J.P. Nadal, 1983, J. of Phys. A16, L213.

Pomeau, Y., P. Manneville, 1980. Comm. Math. Phys. 74, 189.

Pomeau, Y., J.C. Roux, A. Rossi, S. Bachelart and C. Vidal, 1981. J. Phys. Lett. 42, L271.

Pomeau, Y., 1982. J. of Phys. 43, 859.

Large Scale Instabilities of Cellular Flows

Stephan Fauve

INTRODUCTION

In past years the unpredictability of turbulent flows has been understood in the framework of dynamical system theory, and the words "chaos" or "weak turbulence" are commonly used to describe flows with temporal erratic behaviors, but "simple" spatial structures. Such situations exist in laboratory experiments, where the spatial degrees of freedom can be quenched by the boundary conditions. An important question to investigate is whether and how dynamical system theory can be extended to the study of situations that involve many degrees of freedom, associated with the different spatial scales that interact in a turbulent flow.

As a first step in that direction, we will consider how the elementary bifurcations that lead to cellular flows are modified when spatial degrees of freedom are taken into account; we will show that marginal modes result from the broken symmetries at the bifurcation and can lead to large scale instabilities of the cellular flow.

The first part of the talk concerns well-known large scale instabilities in fluid dynamics, presented with the formalism of phasedynamics. The second part consists of recent results obtained in collaboration with P. Coullet and E. Tirapegui.

1. EXAMPLES OF LARGE SCALE INSTABILITIES

1.1 Collective modes of stationary cellular flows

In many nonlinear dissipative systems driven far from equilibrium by an external homogeneous forcing, there is a transition from a uniform state to one varying periodically in space. The widely studied example is the Rayleigh-Benard instability, which occurs in a horizontal layer of fluid heated from below; when the temperature difference across the layer exceeds a critical value ΔT_c, the buoyancy force overcomes the dissipative effects of viscous shear and thermal conduction, and the motionless state spontaneously breaks up into convective cells. When the temperature is fixed at the boundaries, the buoyancy effects cannot drive the motion on large scales compared to the height of the layer, and small scale motions are inhibited by the dissipative effects; thus the instability occurs at a finite wavenumber k_c, and the growth rate of the unstable modes of wavenumber $k \simeq k_c$ reads

$$n(k) = \mu - \xi_0 (k^2 - k_c^2)^2 + o[(k^2 - k_c^2)^3] \qquad (1)$$

where μ measures the distance from criticality ($\mu \propto \Delta T - \Delta T_c$).

A simple one-dimensional model that mimics this instability is (Swift and Hohenberg 1979)

$$u_t = [\mu - (\nabla^2 + k_c^2)^2]\, u - u^3 \qquad (2)$$

The instability first occurs for $\mu = 0$, with a finite critical wavenumber k_c. For $\mu > 0$ there exists a band of unstable modes around k_c (see Figure 1).

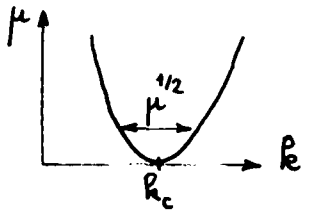

Figure 1: Neutral stability curve

The concept of wave packet can be used to take into account the interaction between these modes in the post bifurcation stage (see for instance, Newell 1974); we write

$$u(x,t) = A(X,T)\exp i k_c x + cc + \mathcal{V} \qquad (3)$$

where $A(X,T)$ is the slowly varying envelope (in X and T) of the roll pattern of wave number k_c, and we look for an evolution equation for A in the form

$$A_T = f(A, A_x, A_{xx}, \ldots) \qquad (4)$$

The main assumption is that, in the vicinity of the bifurcation, the critical modes vary on a time scale much slower than the one of the other modes, and thus contain all the information about the asymptotic time dependence of u near the instability onset. We next assume that $\mathcal{V}$ and f can be expanded in Taylor series in A, A_x, A_{xx}, ..., and get from (2), (3), and (4) a set of linear inhomogeneous equations by identifying the terms at each order A, A_x, A^2, AA_x, ... Solvability conditions then give the evolution equation (4). The form of this equation can be found by symmetry arguments:

-Translational invariance in space implies that if $u(x)$ is a solution of (2), $u(x + \varphi)$ is also a solution; from (3), this implies the invariance of the evolution equation under the transformation

$$A \to A \exp i k_c \varphi.$$

Therefore the only possible nonlinear term, up to the third order in A is, $|A|^2 A$.

-Space reflection invariance implies the invariance of the evolution equation under the transformation

$$X \to -X, \quad A \to \bar{A}, \quad \bar{A} \to A.$$

Therefore the coefficient of $|A|^2 A$ should be real. The linear part of the amplitude equation can be obtained by the Fourier transformation of equation (1). The amplitude equation thus reads at leading order

$$A_T = \mu A + A_{xx} + \epsilon |A|^2 A \qquad \epsilon = \pm 1 \qquad (5)$$

where we have simplified the coefficients by appropriate scalings of amplitude and space. A similar equation has been obtained for the convection problem by Newell and Whitehead (1969) and Segel (1969).

a) The Eckhaus instability (1965)

We consider the evolution equation (5) for a supercritical bifurcation ($\epsilon = -1$). The solutions of the form

$$A_o(X) = Q \exp iqX,\ Q^2 = \mu - q^2,\ |q| < \mu^{1/2} \tag{6}$$

represent perfectly periodic patterns of wavenumber $k_c + q$. To study their stability, we write

$$A(X,T) = A_o(X) + a(X,T) \exp iqX, \tag{7}$$

and find from (5)

$$a_T = -2Q^2 Re(a) + 2iq\, a_X + a_{XX} - Q[a^2 + 2|a|^2] - |a|^2 a \tag{8}$$

Writing

$$a = R + i\varphi \tag{9}$$

we get from (8)

$$R_T = -2Q^2 R - 2q\varphi_X + R_{XX} + \ldots \tag{10.a}$$

$$\varphi_T = 2q\, R_X + \varphi_{XX} + \ldots \tag{10.b}$$

Equations (10) read in Fourier space

$$s \begin{pmatrix} \tilde{R}_k \\ \tilde{\varphi}_k \end{pmatrix} = \begin{pmatrix} -2Q^2 - k^2 & -2iqk \\ 2iqk & -k^2 \end{pmatrix} \begin{pmatrix} \tilde{R}_k \\ \tilde{\varphi}_k \end{pmatrix}$$

The eigenvalues are given by

$$s_\pm(k) = -(Q^2 + k^2) \pm (Q^4 + 4q^2k^2)^{1/2}$$

In the long wavelength limit ($k \to 0$), we have

$$s_-(k) = -2Q^2 + O(k^2)$$

The corresponding mode is damped; it is an amplitude mode,

$$s_+(k) = -k^2\left(1 - \frac{2q^2}{Q^2}\right) - \frac{2q^4}{Q^6} k^4 + O(k^6) \tag{11}$$

This second eigenvalue vanishes in the long wavelength limit. This is due to the translational invariance of the problem. Indeed, adding a perturbation $a = i\varphi$ in (7) corresponds for small φ to the transformation

$$qX \to qX + (\varphi/Q) \tag{12}$$

in the solution (6), and therefore to a global phase shift of the pattern.

In the complex plane, this corresponds to a displacement along the circle of radius $|A_o| = Q$ (see Figure 2)

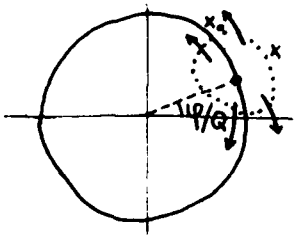

Figure 2

Thus the translational symmetry implies that the phase of the periodic structure is a mode with a vanishing growth rate in the long wavelength limit. We thus expect that this mode can be easily destabilized. We see from (11) that this indeed occurs for $Q^2 = 2q^2$ or $\mu = 3q^2$.

This is the Eckhaus instability that limits the range of stable wavenumbers around k_c (see Figure 3).

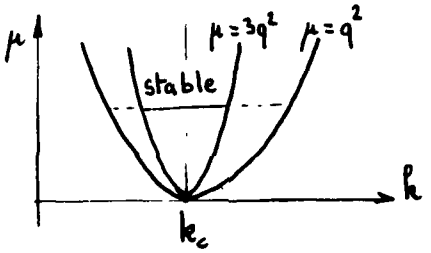

Figure 3: The Eckhaus instability

The mechanism of this instability can be understood as follows: let us consider an initial condition shown in Figure 2; the dotted line represents a perturbation of a homogeneous solution A_o, with R and φ varying periodically in space. The first term of the righthandside of (10.a) tends to contract the dotted circle along the circle of radius Q ($R \to 0$), but an antagonistic effect is generated by the term $2qR_x$ in (10.b), that consists of a stretching which tends to spread the phase along the circle of radius Q (arrows in Figure 2). When q is large enough, this effect becomes important, and the phase instability occurs. In the long wavelength limit, R is damped on a fast timescale compared to the one of φ, which is nearly marginal. Therefore R follows adiabatically the gradients of the phase, and can be eliminated from equations (10) to get an evolution equation for the phase. Its linear part is the Fourier transform of (11)

$$\varphi_T = (1 - 2(q^2/Q^2))\varphi_{xx} - 2(q^4/Q^6)\varphi_{xxxx} + \ldots .$$

The form of the nonlinear terms can be determined by symmetry considerations. The translational invariance in space implies the invariance of the phase equation under the transformation

$$\varphi \to \varphi + C \qquad (C = \text{constant})$$

Therefore φ cannot appear explicitly in the phase equation, and the leading order term is φ_x^2. However, this term is also forbidden because of the reflection symmetry which implies the invariance of the phase equation under the transformation

$$X \to -X, \quad \varphi \to -\varphi$$

We thus get at leading order an equation of the form

$$\varphi_T = D(\mu, q)\, \varphi_{xx} - K \varphi_{xxxx} + g\, \varphi_x \varphi_{xx} \tag{13}$$

We next notice that $\varphi = hX$ is a particular solution of (13); from (12) and (6) we see that it represents an homogeneous solution of wavenumber $q + h/Q$. Its linear stability is governed by the dispersion relation

$$s = -D(q + h/Q)k^2 + O(k^4) \tag{14}$$

We can also compute s by linearization of (13) near $\varphi = hX$; we have

$$s = -[D(q) + hg]k^2 + O(k^4) \tag{15}$$

We get from (14) and (15)

$$g = 1/Q \quad \partial D/\partial q$$

This implies, as noted by Kuramoto (1983), that the nonlinearity in the phase equation is associated with local changes in the phase diffusion coefficient.

The nonlinear term in (13) does not saturate the instability as we can see by computing the amplitude equation for an unstable mode of wavenumber k_o; we write

$$\varphi(X,T) = A(T)e^{ik_o x} + cc$$

This mode is marginally stable if

$$L \cdot \varphi \equiv D_o \varphi_{xx} - K \varphi_{xxxx} = 0$$

or

$$D_o = -K k_o^2$$

We consider the weakly unstable regime $D \lesssim D_o$, and expand

$$D = D_o - \varepsilon D_1 - \varepsilon^2 D_2 \ldots$$

$$\varphi = \varepsilon \varphi^{(1)} + \varepsilon^2 \varphi^{(2)} + \ldots$$

We choose the time scale $\partial_T = \varepsilon^2 \partial_\tau$ in order to have nonlinear and time dependent terms at the same order in the equation for A. At order ε, we find the linear problem, and

$$\varphi^{(1)} = A(\tau)e^{ik_o x} + c.c.$$

At order ε^2, we get

$$\mathcal{L}.\varphi^{(2)} = - D_1 k_0^2 \mathcal{A} \exp ik_0x - ig k_0^3 \mathcal{A}^2 \exp 2ik_0x + c.c.$$

and the solvability condition implies $D_1 = 0$. The amplitude equation is obtained at order ε^3

$$\mathcal{L}.\varphi^{(3)} = \left\{ - D_2 k_0^2 \mathcal{A} + \mathcal{A}_\tau - g^2 \frac{k_0^2}{6k} \mathcal{A}^2 \bar{\mathcal{A}} \right\} \exp ik_0x + cc$$

+ nonresonant terms

The solvability condition gives

$$\mathcal{A}_\tau = D_2 k_0^2 \mathcal{A} + g^2 \frac{k_0^2}{6k} |\mathcal{A}|^2 \mathcal{A}$$

and the Eckhaus instability is thus subcritical in this long wavelength limit. Moreover we can write the evolution equation (13) under the form of a conservation equation

$$\varphi_T = \partial_X \left\{ D\varphi_X - \kappa \varphi_{XXX} + \frac{g}{2} \varphi_X^2 \right\}$$

and see that the spatial average of φ is a conserved quantity for periodic boundary conditions along the X axis. Therefore an unstable periodic pattern cannot evolve to a stable one, by continuously changing its wavelength. Thus, in the unstable regime, changes in wavelength occur by nucleation or annihilation of a pair of rolls; so the instability does not saturate at large wavelength, and therefore the description of the unstable regime should incorporate the fast modes that we have eliminated.

b) The zig-zag instability

We consider now the dynamics of the torsion modes of the roll pattern described by (6), and look for long wavelength perturbations of the phase along the Y axis (see Figure 4).

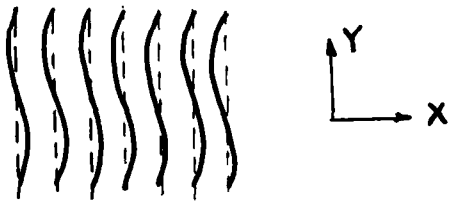

Figure 4: Zig-zag instability

We have thus to consider solutions of (2) under the form

$$u(x,y,t) = A(X,Y,T)\, e^{ik_c x} + cc \qquad (16)$$

We have, as in section 1.a, a family of stationary solutions for A

$$A_o(X) = Q\, e^{iqX} , \quad Q^2 = \mu - q^2 , \quad q^2 < \mu \qquad (17)$$

We consider perturbations of the form

$$A(X,Y,T) = A_o(X) + a(Y,T)\, e^{iqX} \tag{18}$$

with

$$a(Y,T) = R + i\varphi \tag{19}$$

The form of the nonlinear evolution equation for φ can be determined by the following symmetry arguments:

-invariance under the transformation

$\varphi \to \varphi + C$ (translational invariance)

-invariance under the two transformations

$X \to -X, \quad \varphi \to -\varphi$

$Y \to -Y$ (space reflection symmetry)

We have thus at leading order

$$\varphi_T = D_\perp \varphi_{YY} - K_\perp \varphi_{YYYY} + g_\perp (\varphi^3_Y)_Y \tag{20}$$

$D_\perp$ and $K_\perp$ are given by the linear stability analysis; $g_\perp$ can be computed as follows: we first notice that

$$\varphi = hY$$

is a particular solution of (20). We see from (16), (18) and (19) that for h small, it corresponds to a slight rotation of the roll pattern, of angle

$$\frac{h}{Q(k_c + q)} \approx \frac{h}{Qk_c}$$

The rotated pattern has a modified wavenumber

$$(k_c+q)\left(1+\frac{h^2}{2Q^2k_c^2}\right) \simeq k_c + q + \frac{h^2}{2Q^2k_c}$$

and

$$g_\perp = \frac{1}{6k_cQ^2}\frac{\partial D_\perp}{\partial q}$$

The zig-zag instability occurs for decreasing $D_\perp$, when $D_\perp$ vanishes. The nonlinear term renormalizes the diffusivity which becomes $D_\perp + 3g_\perp\varphi^2_Y$, and saturates the instability if $g_\perp > 0$. This can be checked by computing the amplitude equaton for an unstable mode

$$\varphi(Y,T) = \mathcal{A}(\tau)\, e^{ik_cY} + cc$$

We get

$$\mathcal{A}_\tau = D_\perp^{(2)}k_c^2\mathcal{A} - 3g_\perp{}^4|\mathcal{A}|^2\mathcal{A}$$

Consequently the zig-zag instability can be supercritical. In that case, the evolution equation (20) for the phase also describes the unstable regime. The subcriticality of the Eckhaus instability thus appears as a singular behavior of one-dimensional cellular structures.

c) Phasedynamics of two-dimensional patterns

Hydrodynamic instabities also generate two-dimensional patterns that consist of squares (convection between top and bottom boundaries of low thermal conductivity), or hexagons (Marangoni instability). The phase-dynamics of these patterns involve two coupled phases, φ and ψ, associated with the broken translational invariances along the X and the Y axis. Symmetry arguments are less easy to use than for one-dimensional patterns, but, still, they constrain the form of the evolution equations for the phases.

1.2 Spatial desynchronization of a limit cycle

We consider in this section a dissipative dynamical system, driven far from equilibrium by a constant external constraint. We model the transition from a static state to a time periodic regime, with the normal form for the Hopf bifurcation. This has been done by Ortovela and Ross (1973) to describe the behavior of oscillatory chemical reactions.

In the vicinity of the bifurcation, the growth rate of the marginal modes of wavenumber k is

$$\eta(k) = \mu - \xi_0 k^2 + i(\omega + \omega_1 k + \omega_2 k^2) + O(k^3) \qquad (21)$$

The instability occurs first for $\mu = 0$, for increasing μ, and consists of a temporal oscillation at frequency ω. In the vicinity of the bifurcation we look for $\underline{U}$ under the form

$$\underline{U}(x,t) = [A(X,T) \exp i\omega t + c.c.] + \underline{U}^0 \qquad (22)$$

where $\underline{U}$ stands for the set of concentrations that describe the chemical reaction. The linear part of the evolution equation for A is the Fourier transform of (21), and the form of the nonlinear terms is determined by symmetry arguments, i.e. translational invariance in time, that implies the invariance of the amplitude equation under the transformation

$$A \to A \exp i\theta$$

We have thus at leading order

$$A_T = (\mu + i\omega)A + \omega_1 A_X + (\xi_0 - i\omega_2)A_{XX} \pm \gamma|A|^2 A$$

We can eliminate the terms $i\omega A$ and $\omega_1 A_X$ with the transformations $A \to A \exp(-\omega T)$ and $X \to X + \omega_1 T$, $T \to T$. With appropriate scalings of amplitude and space, we get in the supercritical case

$$A_T = \mu A + (1 + i\alpha) A_{XX} - (1 + i\beta)|A|^2 A \qquad (23)$$

Equation (23) has a family of solutions

$$A_o(T) = P\, e^{i\Omega T} \qquad P^2 = \mu, \quad \Omega = -\beta\mu \tag{24}$$

that represent temporal oscillations at frequency $\omega - \beta\mu$, homogeneous in space. We study the stability of these solutions with respect to inhomogeneous perturbations; we write

$$A(X,T) = A_o(T) + a(X,T) \exp i\Omega T \tag{25}$$

and we get from (23) and (24)

$$a_T = -2Q^2(1+i\beta)\mathrm{Re}(a) + (1+i\alpha)a_{xx} - (1+i\beta)\left[Q(a^2+2|a|^2)+|a|^2 a\right] \tag{26}$$

We write

$$a = R + i\theta \tag{27}$$

and consider the linear part of (26). The eigenvalues are given by

$$s_{\pm}(k) = -(Q^2+k^2) \pm \left[(Q^2+k^2)^2 - 2Q^2k^2(1+\alpha\beta) - (1+\alpha^2)k^4\right]^{1/2}$$

There is one amplitude mode that corresponds to $s_- < 0$, and is damped. The other eigenvalue is

$$s_+(k) = -k^2(1+\alpha\beta) - \alpha^2(1+\beta^2)k^4/2Q^2 + O(k^6) \tag{28}$$

The persistent zero eigenvalue $s_+(0) = 0$ reflects translational invariance in time. The phase modes that correspond to the dispersion relation (28), lead to an instability when $1 + \alpha\beta$ vanishes. This corresponds to a spatial desynchronization of the homogeneous state described by (24). The linear part of the evolution equation for the phase in the long wavelength limit is given by the Fourier transform of (28). Symmetry considerations (translational invariance in time) constrain the form of the nonlinear terms. We have thus at leading order an evolution equation of the form

$$\theta_T = D\theta_{xx} - K\theta_{xxxx} + g\theta_x^2 \tag{29}$$

We can compute g on noting that (23) has a family of travelling wave solutions

$$A_p = P_p \exp i(\Omega_p T - pX) \tag{30}$$

with

$$P_p^2 = \mu - p^2, \qquad \Omega_p = -(\alpha-\beta)p^2 - \beta\mu$$

We next look for a phase equation under the form

$$\theta_T = c\theta_x + D\theta_{xx} + g\theta_x^2 + \ldots \tag{31}$$

which has the particular solution $\theta = aT - rX$ if

$$a = -cr + gr^2 + \ldots \tag{32}$$

We notice from (22), (27) and (30) that this solution corresponds to a travelling wave of frequency $\omega - (\alpha-\beta)p^2 - \beta\mu + a/P$ and of wavenumber $p + r/P$. Therefore we have

$$\Omega_p(p + r/P) = \Omega_p(p) + a/Pp \tag{33}$$

We get from (32) and (33)

$$c = -\partial\Omega_p/\partial p \; ; \quad g = (1/2Pp) \cdot (\partial^2\Omega_p/\partial p^2)$$

For $p = 0$, we find

$$c = 0; \qquad g = (\beta-\alpha)/P$$

In order to determine the effect of the nonlinear term in (29) we consider a weakly unstable mode

$$\theta(X, T) = A(\tau)\, e^{ik_0 x} + cc, \quad D_0 = -\kappa k^2$$

and we look for the evolution equation for $\mathcal{A}$. We thus expand θ and D

$$\theta = \varepsilon\theta^{(1)} + \varepsilon^2\theta^{(2)} + \ldots$$

$$D = D_0 + \varepsilon D_1 + \varepsilon^2 D_2 + \ldots$$

and solve (29) at each order in ε. At order ε we have to take into account a mode, constant in space, that is marginal and forced by $\mathcal{A}$ through nonlinear interactions. Thus, we take

$$\theta^{(1)} = \mathcal{A}(\tau)\exp ik_0 x + cc + B(\tau)$$

The solvability condition at order ε^2 determines the evolution equation for $\mathcal{B}$

$$B_{\tau 1} = 2gk_0^2|\mathcal{A}|^2 \tag{34}$$

At order ε^3, we find the evolution equation for $\mathcal{A}$

$$A_{\tau 2} = D_2 k^2 \mathcal{A} - (g^2/3K)\,|\mathcal{A}|^2\mathcal{A} \tag{35}$$

In the unstable regime ($D_2 > 0$) we get

$$A^2 = 3KD_2k_0^2/g^2 \tag{36.a}$$

$$B = 6KD_2k_0^4\, t/g \tag{36.b}$$

Equation (36.b) shows that a change in the oscillation frequency occurs because of the phase instability. Equation (29) has been derived by Kuramoto and Tsuzuki (1976). The phase instability is saturated by the nonlinear term in (29), and therefore this equation governs the long wavelength dynamics of the temporal phase, even in the weakly unstable regime.

2. PHASEDYNAMICS IN THE VICINITY OF CODIMENSION-TWO SINGULARITIES

In this section, we consider cellular flows generated by instabilities that simultaneously break several symmetries. Since different phase modes are associated with each broken symmetry, we expect the possibility of different large scale instabilities, and richer phasedynamics due to their interaction.

2.1 Large scale instability of nonlinear standing waves

Hydrodynamic instabilities often lead to time dependent cellular patterns. The Couette-Taylor flow between counter-rotating cylinders (Di Prima and Grannick, 1971) or thermal convection in the presence of a salinity gradient (Bretherton and Spiegel, 1983), can undergo a Hopf bifurcation, with critical modes of finite spatial wavenumber thus the flow consists of a periodic pattern in space, with oscillatory behavior in time. Depending on the coefficients of the nonlinear terms in the amplitude equations, one may get at the onset of instability, either propagating waves, or standing waves (Demay and Iooss, 1984).

Let us consider a standing wave solution of the form

$$u(x,t) = v(x + ct,\ x - ct) \tag{37}$$

Due to the translational invariance of the problem in space and time, there exists a family of solutions of the form

$$u(x + \phi,\ t + \theta) = v(x + ct + \psi_+,\ x - ct + \psi_-)$$

obtained by constant phase shifts in space and time. We have

$$u(x + \phi,\ t + \theta) = u(x,t) + \phi\ \partial_x u + \theta \partial_x u + \ \ldots\ .$$

Thus ϕ and θ are the phases associated with the neutral modes $\partial u/\partial x$ and $\partial u/\partial t$, due to translational invariances in space and time. For spatially homogeneous phase perturbations, we have

$$\partial_t \begin{pmatrix} \phi \\ \theta \end{pmatrix} = \begin{pmatrix} 0 & 0 \\ 0 & 0 \end{pmatrix} \begin{pmatrix} \phi \\ \theta \end{pmatrix} \tag{38}$$

Equation (38) represents a singularity with two zero eigenvalues associated with the two translational modes. For ϕ and θ slowly varying in space, we assume that a gradient expansion of the lefthandside of (38) exists, and write the higher order terms (i.e. more differentiated in x), using symmetry arguments:

-translational invariances in space and time, which imply that ϕ and θ appear in the phase equations only through their x-derivatives.

-space reflection invariance, which implies the invariance of the phase equations under the transformation

$$x \to -x,\ \phi \to -\phi,\ \theta \to \theta$$

Thus we get

$$\phi_t = a_1\theta_x + a_2\phi_{xx} + \ldots + g\phi_x\theta_x + \ldots \tag{39.a}$$

$$\theta_t = b_1\phi_x + b_2\theta_{xx} + \ldots + g_1\phi^2 + g_2\theta_x^2 + \ldots \tag{39.b}$$

The linear part of (39) reads in Fourier space

$$s\begin{pmatrix}\tilde{\phi}\\ \tilde{\theta}\end{pmatrix} = \begin{pmatrix}-a_2k^2+\ldots & i(a_1k+\ldots)\\ i(b_1k+\ldots) & -b_2k^2+\ldots\end{pmatrix}\begin{pmatrix}\tilde{\phi}\\ \tilde{\theta}\end{pmatrix}$$

The dispersion relation is at leading order

$$s^2 + s(a_2 + b_2)k^2 + a_1b_1k^2 = O(k^4)$$

A stationary instability occurs for $a_1b_1 = 0$, and the standing wave pattern undergoes a Hopf bifurcation for $a_2+b_2 = 0$, with $a_1b_1 > 0$. If $a_2+b_2 > 0$ and $a_1b_1 > 0$, the pattern is stable in the limit $k \to 0$, but can be unstable with respect to small but finite wavenumber perturbations, if one of the coefficients in the dispersion relation vanishes when higher order terms in k are taken into account (Coullet, Fauve and Tirapegui, 1985). In this case the phase instability occurs at a finite wavelength, and if nonlinearly saturated, leads to a periodic pattern on a larger scale than the initial standing wave pattern. The new pattern can itself undergo a phase instability; one could thus describe a cascade mechanism toward large scales.

2.2 Propagative phasedynamics for systems with Galilean invariance

In fluid dynamics, the equations of transport of mass, momentum and heat, are Galilean invariant. Therefore it is interesting to consider the corresponding phase modes, and thus to investgate the phasedynamics for a cellular pattern generated by an instability, in a system with translational and Galilean invariances.

Let us consider as a simple model, a one-dimensional velocity field u(x,t), governed by an equation of the form

$$\partial_t U = L\cdot U + N(U) \qquad (40)$$

where L is a liear operator, and N(u) represents nonlinear terms. We consider a cellular pattern, described by a velocity field $u_o(x)$, periodic in x. Its stability with respect to a perturbation v(x,t), is studied by linearizing (40) in v about u_o. We get

$$\partial_t v = L\cdot v + DN_{u_o}\cdot v = \mathcal{L}\cdot V \qquad (41)$$

We next consider that, due to translational and Galilean invariances

$$u_o(x+\phi) = u_o(x) + \phi\,\partial_x u_o + \ldots \qquad (42.a)$$

$$u_o(x+\psi t) - \psi = u_o(x) + \psi t\,\partial_x u_o - \psi + \ldots \qquad (42.b)$$

are also solutions of (40). From (42.a) and (41) we get

$$\mathcal{L}\cdot\partial_x u_o = 0 \qquad (43)$$

which shows that $\partial_x u_o$ is the neutral mode associated with the translational invariance in space. Equation (41) with

$$v(x,t) = +\psi t\partial_x u_o - \psi$$

gives

$$\mathcal{L}\cdot(-1) = \partial_x u_o \qquad (44)$$

ϕ and ψ are thus the two phases associated with translational and Galilean invariances; the corresponding generalized eigenvectors are $\partial_x u_o$ and $-I$.

We consider long wavelength phase perturbations, and we write

$$v(x,t) = \phi(x,t)\ \partial_x u_o - \psi(x,t) + \vartheta$$

where ϑ stands for corrections perpendicular to the generalized eigenspace. For ϕ and ψ homogeneous in space, we get from equations (41), (43) and (44)

$$\partial_t \begin{pmatrix} \phi \\ \psi \end{pmatrix} = \begin{pmatrix} 0 & 1 \\ 0 & 0 \end{pmatrix} \begin{pmatrix} \phi \\ \psi \end{pmatrix} \qquad (45)$$

The linear coupling between the phase modes ϕ and ψ can be understood as follows: the advection of the pattern at a constant speed ψ, leads to a spatial phase ϕ that increases linearly in time. Equation (45) represents a codimension-two singularity. Two control parameters are usually necessary to reach such a situation, which arises "naturally" here because of the structure of the Galilee group. This makes the phasedynamics second order in time, and one could expect oscillatory behavior.

We next assume that ϕ_t and ψ_t can be expanded in gradients of ϕ and ψ, and determine higher order terms with symmetry arguments:

-translational and Galilean invariances imply the invariance of the phase equations under the transformations

$$\phi \to \phi + c$$

and

$$\phi \to \phi + ct \quad ; \psi \to \psi + c$$

-the space reflection symmetry implies the invariance of the phase equations under the transformation

$$x \to -x \ ; \quad \phi \to -\phi; \ \psi \to -\psi.$$

Consequently the form of the phase equations is

$$\phi_t = \psi$$
$$\psi_t = a\phi_{xx} + b\psi_{xx} + \ldots + g_1\phi_x\phi_{xx} + g_2\phi_x\psi_{xx} + g_3\phi_{xx}\psi_x$$

(the highest order terms in (46.a) can always be eliminated by change of variable).

The linear part of (46) gives the dispersion relation

$$s^2 + bk^2\, s + ak^2 = O(k^4).$$

In the limit $k \to 0$ we get a pair of damped propagative modes, with a propagation speed $\sqrt{a}$, if a and b are positive. A stationary instability occurs when a vanishes, and a Hopf bifurcation occurs when $b = 0$, with

$a > 0$; this corresponds to an oscillatory instability of the stationary pattern associated with the velocity field $u_o(x)$. The oscillatory instability of convection rolls, predicted by Busse (1972), is a similar type of instability; in his analysis, the top and bottom boundaries are assumed stress-free, and the system is thus Galilean invariant in the horizontal plane. An important difference with our model is that the longitudinal mode governed by (49) does not exist for the convection problem because of the incompressiblity condition. The coupling between the two phases requires a two-dimensional pattern, and the oscillatory instability of convection rolls consists of standing or propagating waves along the axis of the rolls, i.e. a torsion mode of the roll pattern. When the top and bottom boundaries are rigid instead of stress-free, the Galilean invariance is broken. However, the interaction between the damped Galilean mode and the translational neutral mode, still leads to the oscillatory instability, which occurs with a finite wavelength, instead of an infinite one, and for a higher Rayleigh number than in the stress-free case (Clever and Busse, 1974; Bolton, Busse and Clever, 1985).

CONCLUSION

Long wavelength modes are very general features of cellular flow patterns, which occur in nonlinear dissipative systems, driven externally with a homogeneous and constant forcing. These modes are analogous to Goldstone modes of condensed-matter physics, and can be traced back to continuous broken symmetries. They describe the long wavelength perturbations of a periodic structure through its slowly varying phase. The phase dynamics are governed by prototypical evolution equations; their form depends on the broken symmetries, and the short range structure of the flow only affects the value of the coefficients in the phase equations.

We have shown here, with the help of this phase formalism, how to take into account long wavelength spatial modes, in the description of the dynamics which occurs in the vicinity of elementary bifurcations. The next step is to use the same formalism, in order to determine how the transition scenarios to chaos, via one or several bifurcations, are modified when spatial degrees of freedom are taken into account.

Acknowledgements: I wish to thank E. Spiegel and E. Bolton for their comments on this manuscript.

REFERENCES

Bolton, E.W., F.H. Busse and R.M. Clever, 1985, preprint.

Bretherton, C.S. and E.A. Spiegel, 1983. Phys. Lett. 96A, 152-156.

Busse, F.H., 1972. J. Fluid Mech. 52, 97-112.

Clever, R.M. and F.H. Busse, 1974. J. Fluid Mech. 65, 625-645.

Coullet, P.H. and S. Fauve, 1985. Macroscopic Modelling of Turbulent Flows and Mixtures, Springer Verlag.

Coullet, P.H., S. Fauve and E. Tirapegui, 1985. J. Phys. Lett. 46, in press.

Demay, Y. and G. Iooss, 1985. J. de Mecanique, in press.

Di Prima, R.C. and R.N. Grannick, 1971. IUTAM Symp. on Instabilities of Continuous Systems, H. Leipholz ed., Springer Verlag.

Eckhaus, W., 1965. Studies in nonlinear stability theory, Springer Verlag.

Kuramoto, Y., 1984. Prog. Theor. Phys. 71, 1182-1196.

Kuramoto, Y. and T. Tsuzuki, 1976. Prog. Theor. Phys. 55, 356-369.

Newell, A.C., 1974. Lectures in Applied Math. 15, 157-163.

Ortovela, P. and J. Ross, 1973. J. Chemical Phys. 58, 5673-5680.

Swift, J. and P.C. Hohenberg, 1979. Phys. Rev. A15, 319-328.

Commensurate-Incommensurate Transition in Hydrodynamical Flows

Pierre Coullet

Many dynamical systems exhibit a transition from a periodic solution to a quasiperiodic one. Particularly interesting are the cases corresponding to the so-called strong resonances (Arnold, 1977). A controllable situation in which these resonances can be studied occurs when one periodically modulates a system near the threshold of an oscillatory instability (Gambaudo, 1985). These resonances lead to a rich variety of phenomena including periodic or locked states, quasiperiodic and chaotic states. One-dimensional pattern-forming transitions bear obvious analogy with Hopf bifurcations. In this paper we consider the effect of a spatial forcing, near the threshold of such a transition. As in the temporal case the notion of weak and strong resonances naturally appears.

The appearance of a one-dimensional periodic pattern is described by the equation (Newell and Whitehead, 1969; Segel, 1969)

$$A_t = \mu A - |A|^2 A + A_{xx} \tag{1}$$

where A represents the slowly varying amplitude of the almost marginal mode. A typical scalar quantity, for example the temperature in a convection experiment reads at the leading order

$$T = A e^{ik_0 x} + \bar{A} e^{-ik_0 x} + \ldots \tag{2}$$

where k_0 is the optimal wave-number of the instability. The invariance of (1) under the transformation

$$A \rightarrow A e^{i\Sigma} \tag{3}$$

reflects the translational invariance of the physical system

$$X \rightarrow x + \Phi \tag{4}$$

where $\Phi = \Sigma / k_0$.

Under the presence of an external periodic modulation the system is no longer invariant under this group of transformations.

We first consider a periodic forcing in resonance with the optimal wave-length of structure. More precisely let k_e be the wave-vector of the external modulation, then $m k_e = n k_0$. Using equation (2) the invariance of the system under the restricted group of transformation

$$x \rightarrow x + 2\pi/k_e \, N \tag{5}$$

implies that the amplitude equation has to be unchanged under the transformation

$$A \rightarrow A e^{i\, 2\pi/n}. \tag{6}$$

At the leading order it leads to the amplitude equation

$$A_t = \mu A + \alpha \bar{A}^{n-1} - |A|^2 A + A_{xx} \qquad (7)$$

where α is proportional to ϵ^m, and ϵ is the strength of the external forcing. We first consider homogeneous solutions $A = Re^{i\theta}$ of equation (7). The equation for the phase reads

$$R\theta_t = -\alpha R^{n-1} \sin n\theta. \qquad (8)$$

Stationary solutions are then given by

$$\theta = \eta \pi/n. \qquad (9)$$

They represent states which are locked by respect to the external forcing. As far one is only interested by the properties of the amplitude near threshold, for small forcing, strong effects do occur for $n \leq 4$ only. These cases correspond to strong resonances. Let Q be the real amplitude of the steady homogeneous solution of (7). The bifurcation diagrams (Kelly and Pal, 1978) can be easily deduced from the following equation for Q.

$$\mu Q + (-1)^{\eta} Q^{n-2} - Q^3 = 0 \qquad (10)$$

In the case n=1 one gets an imperfect bifurcation.
In the case n=2 one has a shift in the parameter value at which the transition takes place.
In the case n=3 one has a subcritical bifurcation.
In the case n=4 only the Landau prefactor is affected by the presence of the periodic modulation.

Such effects are likely to be observed in experiments.

One purpose of this paper is to show that the Amplitude Theory allows to take account of recent experimental results by M. Lowe and J.E. Gollub (1985). Namely they observed soliton-like behavior in quantitative agreement with the solutions of the time-independent sine-gordon equation. We next show that, when one takes into account the detuning or misfit between the two periodicities, the problem can be reduced to a "first order in time sine-gordon equation."

In the almost resonant case, we let $nk_e = n(k_0+q)$ with $q << k_0$. Then the correct amplitude equation becomes

$$A_t = \mu A + \alpha \bar{A}^{n-1} e^{iqnx} - |A|^2 A + A_{xx} \qquad (11)$$

It is useful to note for the following that equation (11) has a gradiant structure, that is

$$A_t = -\delta V/\delta \bar{A} \qquad (12)$$

where

$$V = \int dx [-\mu |A|^2 - \alpha/n \, (\bar{A}^n e^{iqnx} + A^n e^{-iqnx}) + 1/2 |A|^4 + |A_x|^2] \qquad (13)$$

and $\delta/\delta\bar{A}$ denotes the functional derivative by respect to $\bar{A}$. Equation (11) also reads

$$R_t = \mu R + \alpha R^{n-1}\cos n(\theta - qx) - R^3 + R_{xx} - \theta_x^2 R \tag{15}$$

$$R\theta_t = -\alpha R^{n-1}\sin n(\theta - qx) + R\theta_{xx} + 2R_x\theta_x \tag{16}$$

where $A=Re^{i\theta}$. The stationary solutions of these equations, with a constant amplitude Q, are given by

$$\theta = qx + \eta\pi/n \tag{15a}$$

and

$$(\mu - q^2)Q + (-1)^{\eta}\alpha Q^{n-1} - Q^3 = 0 \tag{15b}$$

The odd η's correspond to states which are unstable with respect to phase perturbations. The stability of the solution with η even leads to two types of modes: the amplitude modes and the phase modes. In the range of parameter μ and q implicitly defined by

$$2P^2 >> n\alpha Q^{n-2} \tag{16}$$

where

$$-2P^2 = \mu - q^2 + \alpha(n-1)Q^{n-2} - 3Q^2 \tag{17}$$

is the growth rate of homogeneous perturbation of the amplitude, while $-n\alpha Q^{n-2}$ is associated with the phase, the amplitude modes adiabatically follow the phase fluctuations in such a way that our problem reduces itself to a phase equation

$$\partial_t\theta = -V \sin n(\theta - qx) + D\theta_{xx}, \tag{18}$$

where $V = \alpha Q^{n-2}$ and $D = 1 - 2q/P^2$ generalize the Eckaus phase diffusion constant. Using the phase variable $\Phi = \theta - qx$, equation (18) also reads

$$\partial_t\Phi = -V \sin(n\Phi) + D\Phi_{xx} = -\delta H/\delta\Phi \tag{19}$$

where

$$H = \int dx\left(-\frac{V}{n}\cos(n\Phi) + \frac{1}{2}D\Phi_x^2 - q\Phi_x\right) \tag{20}$$

The functional H turns out to be the potential energy of the continuous version of the Frankel-Kontorova model (Kontorova and Frankel, 1938) for Commensurate-Incommensurate transition in equilibrium systems. This model has been extensively studied in the literature (Pokrovsky and Talapo', 1983). Let us review here its simplest aspects. For q small enough (or V large enough) the second term in (20) dominates and the locked states are favored. For q large enough (or V small enough) the second term dominates the free energy favoring the optimal wave-vector of the periodic pattern. A transition occurs when

$$|q| > q_c = 4/\pi\sqrt{VD/n} \tag{21}$$

The minima of (20) are solution of the pendulum equation

$$D\Phi_{xx} - V \sin(n\Phi) = 0. \tag{22}$$

When $|q| < q_c$ the absolute minima of (20) are given by the unstable equilibrium solutions of the pendulum

$$\Phi = 2\pi/n. \tag{23}$$

When $|q| > q_c$ the absolute minima are given be the rotating solutions of the pendulum equation.
When $|q| = q_c$ both the unstable equilibrium stationary solutions of the pendulum and the separatrix also called one-soliton solution

$$\Phi_s(x) = \frac{4}{n} \tan^{-1}(\exp\sqrt{\frac{nV}{D}}\, x \tag{24}$$

are the absolute minima of the Liapunov functional.

Thus the locked state becomes metastable with respect to wall formation. When q increases one gets a periodic array of such walls also called in the jargon of Commensurate-Incommensurate transition discommensurations.

We now discuss some pathology associated with our model. The incommensurate domain is described in terms of a periodic array of solitons with spacing ℓ. When $|q|$ increases (19) and (20) predict a continuous variation of this spacing which, for $|q|$ close to q_c, is given by

$$\ell \sim -\log(|q| - q_c). \tag{25}$$

One then finds that there exist no locking between the soliton array and the underlaying periodic structure. In a generic situation such lockings are expected to occur when $\ell\, k_e/2\pi$ is a rational number. The same pathology exists for the continuous version of the Frankel-Kontorova model. In that case the origin of the problem is readily found in the limit process since one replaces a problem which possesses a discrete translational symmetry by a problem which is invariant by respect to any translation. When one comes back to the discrete version of this model higher locking states are recover. In the same way equation (19) is invariant under arbitrary space translations while the initial problem is not. The problem is nevertheless of a quite different nature since there is no discrete theory associated in this case. It actually lies in the derivation of the amplitude equation itself. As first pointed by Pomeau (1984) the amplitude theory misses important effects due to the coupling between the large scale behavior and the periodic pattern. Although, at any arbitrary order in the amplitude expansion, such a coupling cannot be catched it is a generic feature of the initial problem. Technically it is associated with the lack of convergence of the amplitude expansion. In the spirit of normal form theory (Guckenheimer and Holmes, 1984) one can model this effect in writing the amplitude equation only up to a finite order and keep a residual term which explicitly depends on the rapid space scale.

$$A_t = \mu A + \alpha \bar{A}^{n-1} e^{inqx} - |A|^2 A + R(A,\bar{A},x) \tag{26}$$

Tracing back the approximations needed to get the phase equation, (19) becomes

$$\partial_t \Phi = -V \sin(n\Phi) + D\Phi_{xx} + S(\Phi,x). \tag{27}$$

The stationary solutions of this equation correspond to the solutions of the pendulum problem in the presence of a small periodic modulation. This dynamical system presents a rich variety of different types of solutions: periodic solutions, quasiperiodic solutions, cantor set and chaotic solutions. All these solutions are potential candidates to be absolute minima of the associated Liapunov functional. The Poincaré map technique is the natural way to study such a problem. We thus recover a discrete model which is the analogous of the initial Frankel-Kontorova model. Aubry (1983) studied the discrete version of the Frankel-Kontorova model and was able to show that its ground states hae the form

$$\mu_n = n\rho + \alpha + f(n\rho + \alpha) \tag{28}$$

where ρ is the so-called rotation number and is associated, in our case, with the ratio between the soliton spacing and the external wavelength, and α is a phase. The function f is periodic with the period of the underlaying lattice. This result rules out the possibility for a chaotic trajectory of the Frankel-Kontorova map to be a ground state of the Frankel-Kontorova free energy. Actually Aubry proved it for a more general class of problems including some continous problems similar to the one considered here. The function f does not need to be analytical. If it is not the ground state it is a well ordered cantor set. There exits a transition when one follows a path in parameter space on which the rotation number is kept fixed at an irrational value. This transition, known after Aubry as the transition by breaking of analyticity, is likely to be observed in a macroscopic experiment as the one performed by M. Lowe and J.E. Gollub (1985). Actually there is already some evidence in their experiment for the existence of quasiperiodic nonanalytic states (Lowe, Gollub and Lubensky, priv. comm.).

In a previous paper by Lowe, Gollub and Lubensky (1983) experimental results on the existence of two-dimensional incommensurate phases have been reported. The work described there mainly differs from the one corresponding to the theoretical model discussed below by the fact they considered a less anisotropic fluid. In a recent work in collaboration with P. Huerre we studied the effects of two dimensional perturbation on the Commensurate-Incommensurate transition. Basically one has to do the following replacement in equation (19)

$$\partial^2/\partial x^2 \rightarrow [(\partial/\partial x) - i(\partial^2/\partial y^2)]^2 + \gamma\, \partial^2/\partial y^2 \tag{29}$$

where γ is a measure of the anisotropy of the system. A similar analysis to the one presented above leads to the Liapunov functional

$$H = \int dx\, (-V/n \cos n\Phi/n + 1/2\, D\Phi_x^2 + 1/2\, D_\perp \Phi_y^2 - q\Phi_x) \tag{30}$$

where

$$D_\perp = q + \gamma \tag{31}$$

represents the phase diffusion coefficient (Pomeau and Manneville, 1979) transverse to the structure. One then has for negative detuning parameter q a competition between Commensurate-Incommensurate transition and the

zig-zag instability. Hence for isotropic systems as a Rayleigh-Benard experiment the Commensurate-Incommensurate transition will only occur for positive detuning. Computation of the ground state when the diffusion constant is slightly negative is in progress. Similar results have been independently obtained by Lubensky (unpublished).

REFERENCES

Arnold, V.I., 1977. Geometrical Methods in the Theory of Ordinary Differential Equations, Springer Verlag.

Aubry, S., 1983. J. Physique 44, 147.

Gambaudo, J.M., 1985. J. Diff. Eq. 57, 172.

Guckenheimer, J. and P. Holmes, 1984. Nonlinear Oscillations, Dynamical Systems, and Bifurcations of Vector Fields, Springer Verlag.

Kelly, R.E. and D. Pal, 1978. J. Fluid Mech. 86, 433. Parts of these results have been already found in the case of Rayleigh-Benard convection submitted to a spatially periodic thermal perturbation.

Kontorova, T.A. and Ya. I. Frenkel, 1938. Zh. Fksp. Teor. Fiz. 75, 1151.

Lowe, M. and J.E. Gollub, 1985. Phys. Rev. A31, 3893.

Lowe, M., J.E. Gollub and T. Lubensky, 1983. Phys. Rev. Lett. 51, 786.

Lowe, M., J.E. Gollub and T. Lubensky, private communication.

Lubensky, T., unpublished.

Newell, A.C. and J.A. Whitehead, 1969. J. Fluid Mech. 38, 279.

Pokrovsky, V.L. and A.L. Talapov, 1983. Theory of Incommensurate Crystals, Harwood Academic Publishers (see for example).

Pomeau, Y., 1984. Nonadiabatic Phenomena in Cellular Structures, in Cellular Structures in Instabilities, Springer Verlag, 210, 207.

Pomeau, Y. and P. Manneville, 1979. J. Phys. Lettres 40, 609.

Segel, L.A., 1969. J. Fluid Mech. 38, 203.

The Topology of Chaos

by H.K. Moffatt

1. Let D be a domain in R^3 with smooth boundary ∂D, and let $\underset{\sim}{F}(\underset{\sim}{x})$ be a smooth (C^1) solenoidal vector field in D satisfying

$$\underset{\sim}{n} \cdot \underset{\sim}{F} = 0 \quad \text{on } \partial D \tag{1}$$

We consider the dynamical system

$$d\underset{\sim}{x}/dt = \underset{\sim}{F}(\underset{\sim}{x}) \tag{2}$$

where trajectories are the flow lines (or '$\underset{\sim}{F}$-lines') of the field $\underset{\sim}{F}(\underset{\sim}{x})$.

Let π be a Poincaré section of D (Figure 1) and consider the $\underset{\sim}{F}$-line passing through a point P_0 of π.

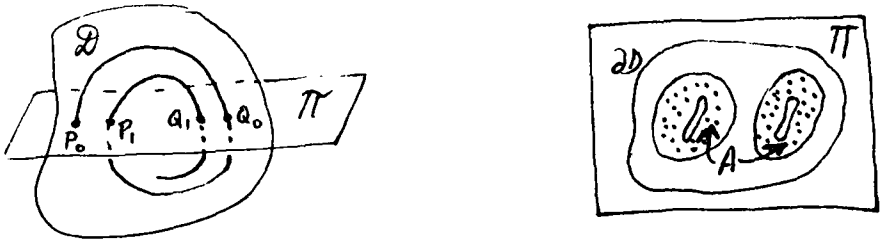

Figure 1

Let the successive intersections of this $\underset{\sim}{F}$-line with π be the set $S = \{P_0, Q_0, \text{---} P_j, Q_j, \text{---}\}$. If the $\underset{\sim}{F}$-line is closed, then S is finite; if the $\underset{\sim}{F}$-line covers a surface Σ, then S consists of all points of the closed curves in which Σ intersects π; and if $\underset{\sim}{F}$ is ergodic in a subdomain D_1 of D, then S consists of all points of the intersection of D_1 with π; this may be an area A of π bounded internally and externally, as illustrated in Figure 1.

2. Suppose now that we wish to consider fields $\underset{\sim}{F}_t(\underset{\sim}{x})$, dependent on some parameter t, which are "topologically accessible" from $\underset{\sim}{F}(\underset{\sim}{x})$ in the sense that the field lines of $\underset{\sim}{F}_t$ may be be obtained by some 'fluid' distortion of the $\underset{\sim}{F}$-lines; by a fluid distortion, we mean one which can be achieved by a smooth velocity field $\underset{\sim}{v}(\underset{\sim}{x},t)$ $(0 < t < \infty)$ for which the 'dissipation integral'

$$\int_0^\infty dt \int_D (\partial v_i/\partial x_j)^2 dV \tag{3}$$

is finite. Under this flow field, a particle initially at $\underset{\sim}{x}$ moves to $\underset{\sim}{X}(\underset{\sim}{x},t)$ where

$$\partial \underset{\sim}{X}/\partial t = \underset{\sim}{v}(\underset{\sim}{X},t), \quad \underset{\sim}{X}(\underset{\sim}{x},0) = \underset{\sim}{x}, \tag{4}$$

for $t > 0$. We shall restrict attention to incompressible distortions ($\nabla\cdot\underset{\sim}{v} = 0$, $||\partial\underset{\sim}{X}/\partial\underset{\sim}{x}|| = 1$) satisfying $\underset{\sim}{v}\cdot\underset{\sim}{n} = 0$ on ∂D. For any finite t, $\underset{\sim}{X}(\underset{\sim}{x}, t)$ is continuous, and the mapping $\underset{\sim}{x} \to \underset{\sim}{X}(\underset{\sim}{x},t)$ is a homeomorphism; discontinuities may however develop as $t \to \infty$.

Topological accessibility is guaranteed by the following procedure: Let $\underset{\sim}{B}(\underset{\sim}{x},t)$ (which we shall refer to as 'magnetic field') satisfy the frozen field equation

$$\partial\underset{\sim}{B}/\partial t = \text{curl}\ (\underset{\sim}{v}\wedge\underset{\sim}{B}), \tag{5}$$

and let $\underset{\sim}{B}(\underset{\sim}{x},0) = \underset{\sim}{F}(\underset{\sim}{x})$. Equation (5) guarantees that $\nabla B = 0$ and $n\cdot B = 0$ on ∂D for all $t > 0$. It also guarantees that all linkages and knots of $\underset{\sim}{B}$-lines are conserved. A particular consequence of (5) is that the 'magnetic helicity' which is one (very incomplete) measure of $\underset{\sim}{B}$-line linkages, is invariant; but the equation in fact captures the invariance of the complete topological structure of $\underset{\sim}{B}$, whatever that may be. We identify $\underset{\sim}{F}_t(\underset{\sim}{x})$ with $\underset{\sim}{B}(\underset{\sim}{x},t)$.

We want to consider particular velocity fields $\underset{\sim}{v}$ which lead to as much 'untangling' of the initial field $\underset{\sim}{F}(\underset{\sim}{x})$ as possible (without violating the topology). To this end, suppose that $\underset{\sim}{v}$ satisfies the dynamical equation

$$\partial\underset{\sim}{v}/\partial t + \underset{\sim}{v}\cdot\nabla\underset{\sim}{v} = -\nabla p + (\nabla\wedge\underset{\sim}{B})\wedge\underset{\sim}{B} + \nu\nabla^2\underset{\sim}{v}, \tag{6}$$

with $\underset{\sim}{v}(\underset{\sim}{x},0) = 0$. Then (5) and (6) may be combined to provide an energy equation

$$d/dt\ (M(t) + K(t)) = -\Phi(t), \tag{7}$$

where

$$M(t) = 1/2\int\underset{\sim}{B}^2 dV, \quad K(t) = 1/2\int\underset{\sim}{v}^2 dV, \tag{8}$$

and

$$\Phi(t) = \nu\int(\partial v_i/\partial x_j)^2 dV. \tag{9}$$

The energy then decreases monotonically for so long as $\underset{\sim}{v} \not\equiv 0$, and a steady state is reached if and when $\underset{\sim}{v} \equiv 0$ in D. At this stage, (6) becomes

$$(\nabla\wedge\underset{\sim}{B})\wedge\underset{\sim}{B} = \nabla p, \tag{10}$$

i.e. $\underset{\sim}{B}$ is a 'magnetostatic equilibrium'. In this equilibrium B may include tangential discontinuities (consequencies of possible noncontinuity of the asymptotic mapping $\underset{\sim}{x} \to \underset{\sim}{X}$ as $t \to \infty$).

If the topology of the initial field $\underset{\sim}{B}(\underset{\sim}{x},0) = \underset{\sim}{F}(\underset{\sim}{x})$ is nontrivial, then the magnetic energy has a positive lower bound, associated with this topology. This is essentially because the volume of each flux tube is conserved under incompressible flow, and two linked flux tubes cannot therefore shrink indefinitely without mutual interference. Equally, if $\underset{\sim}{F}(\underset{\sim}{x})$ is ergodic in a subdomain D_1, then this ergodicity which is essentially a topological property, is conserved, so that if $D_1 \to \hat{D}_1$ under the limit mapping $\underset{\sim}{x} \to \underset{\sim}{X}(\underset{\sim}{x})$, then the volume of D_1 is equal to the volume of $\hat{D}_1$, and the limit magnetostatic field $\underset{\sim}{B}(\underset{\sim}{x})$ is ergodic in $\hat{D}_1$ (Figure 2).

This has a very interesting consequence, since a magnetostatic field that is ergodic in $\hat{D}_1$ must satisfy the equation

$$\nabla \wedge \underset{\sim}{B} = \alpha_1 \underset{\sim}{B} \quad \text{in } \hat{D}_1 \tag{11}$$

for some constant α_1 (Arnold 1965). The boundary of the domain $\hat{D}_1$ (both external and internal) may be quite complex, but the simple character of the equation (11) contains important information about the structure of $\underset{\sim}{B}$ and hence about the structure of the initial field $\underset{\sim}{F}$. Evidently the relaxed field $\underset{\sim}{B}$ is one of maximal helicity

$$\frac{(\nabla \wedge \underset{\sim}{B})\cdot\underset{\sim}{B}}{|\underset{\sim}{B}|\,|\nabla\wedge\underset{\sim}{B}|} = \pm 1 \qquad \text{according as } \alpha_1 \gtrless 0 \tag{12}$$

If $\underset{\sim}{F}(\nabla\wedge\underset{\sim}{F})$ is positive in some parts of D_1 and negative in others, this indicates that right-handed twist can always be compensated and cancelled by left-handed twist in the 'untangling' or relaxation process, very much in accord with intuitive experience gained in the untangling of a tangled skein of wool whose two ends are permanently knotted together.

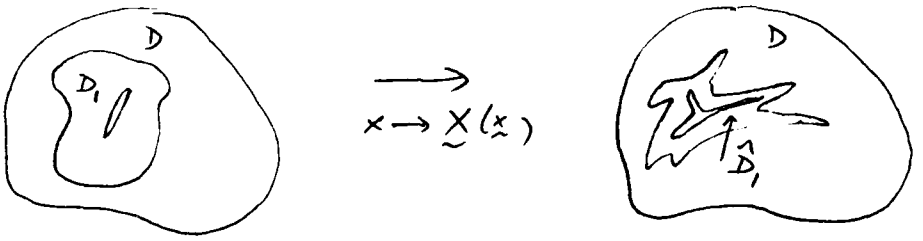

Figure 2

3. The above argument, which is developed in detail in Moffatt (1985), implies the existence of at least one magnetostatic equilibrium for any arbitrarily prescribed topology - e.g. if a field $\underset{\sim}{B}_0(\underset{\sim}{x})$ is given in which flux tubes are linked and knotted in a complex manner, we may assert the existence of a field $\underset{\sim}{B}^\varepsilon(\underset{\sim}{x})$ (which may have tangential discontinuities imbedded within it) whose field lines may be obtained by distortion of the field lines of $\underset{\sim}{B}_0(\underset{\sim}{x})$.

The well-known analogy between magnetostatic equilibria and Euler flows (i.e. steady solutions of the Euler equations for an inviscid incompressible fluid) then implies the existence of an equally rich variety of such flows which may be regarded as the fixed points in the function space in which unsteady solutions of the Euler equations evolve. These flows are characterized by 'ergodic blobs' within which $\underset{\sim}{\omega} = \alpha\underset{\sim}{u}$ with α constant, the streamlines being space-filling throughout each blob, and surfaces separating the blobs on which vortex sheets may be located. The fixed points are likely to be unstable, in view of the Kelvin-Helmholz instability to which such vortex sheets are known to be subject.

This description provides an attractive scenario for the possible structure of turbulent flow. The ergodic blobs then fulfill the role of 'coherent structures,' which persist simply because $\underset{\sim}{u} \wedge \underset{\sim}{\omega} \approx 0$ in such blobs so that energy cascade to small scales does not occur. This cascade occurs through the Kelvin-Helmholz instability of the vortex sheets, which leads to double-spiral structures of well-documented type. It is tempting to speculate (Moffatt 1984) that it is the structure of these spiral singularities, distributed randomly throughout the fluid, which determines the $k^{-5/3}$ energy spectrum in the inertial range.

REFERENCES

Arnold, V., 1985. C.R. Acad. Sci. Paris, 261, 17-20.

Moffatt, H.K., 1984. Proc. IUTAM Symp. on Turbulence and Chaotic Phenomena in Fluids (ed. T. Tatsumi), 223-230, Elsevier.

Moffatt, H.K., 1985. Magnetostatic equilibria and analogous Euler flows of arbitrarily complex topology. J. Fluid Mech. (to appear).

Homoclinic Orbits and Chaos

Colin Sparrow

Introduction

This abstract is to introduce, briefly, some results about homoclinic orbits in finite-dimensional differential equations, and to explain why they may be interesting. For detailed results and analysis readers will be referred to published papers.

Homoclinic Orbits

A homoclinic orbit in a flow is a trajectory which tends, in both forwards and backwards time, towards the same stationary (or equilibrium) point. The stationary point is necessarily a saddle. Figure 1 shows two examples. More generally we may think about heteroclinic loops which are a series of trajectories (forming a loop) tending in forwards time to one stationary point and in backwards time to another. Figure 2 shows two examples. Homoclinic orbits in flows are not to be confused with homoclinic points in diffeomorphisms (return maps). In the absence of very special restrictions on the systems under consideration, homoclinic orbits and heteroclinic loops will be sensitive to parameter changes; they exist for certain parameter values but will disappear for slight changes of the parameters. Thus, they are not easily observed in physical problems, but I shall argue that their existence has implications for the behavior over wide ranges of parameter values and hence that they are physically important.

Two Generalizations and Some Justification

Mathematicians have realized that the behaviors commonly described as "chaotic" are extremely complicated and that rigorous descriptions of the dynamics of so-called "chaotic attractors" are, in general, not available at present. As an example, the kind of chaos seen after period-doubling in systems of more than one dimension is believed, by most mathematicians and for some parameter values, to actually contain infinitely many stable periodic orbits (most if not all of which will have ridiculously large periods and be practically unobservable), and, by all mathematicians and for many parameter values (possibly almost all?), to have a finite (nonzero) number of stable periodic orbits. On the other hand, physicists and fluid dynamicists have become interested in various measurable, quantitative properties of chaotic flows (dimension, Lyapounov exponents etc.) which may be used to compare models with experiments, regardless of the fact that the limits used to define these quantities will frequently not even exist in a rigorous mathematical sense. There is room between these two extreme approaches for another approach which is both theoretical and experimental (in the sense of numerical experiements on a computer), which concentrates on objects which are simple intuitively and mathematically, but which goes some way towards increasing understanding of the way in which chaotic behavior arises in useful model equations. The objects referred to here are periodic orbits, and the connection with homoclinic orbits is that occurrence of a homoclinic orbit can be shown, in various different cases, to produce or destroy one or more periodic orbits as a parameter changes. Figure 3 illustrates the production of a periodic

orbit in a two-dimensional flow with a homoclinic orbit as a parameter changes. Two cases are shown, depending on the ratio of the eigenvalues at the stationary point; it is typical that in one case a stable orbit is produced and that in the other case an unstable orbit is produced. Justification for concentration on periodic orbits can be found in the following remarks:

1) Whatever the detailed structure of so-called chaotic attractors, most of them are densely packed with periodic orbits, albeit unstable ones. In some cases a knowledge of the periodic orbits involved will completely determine the structure of the attractor (e.g. the geometric Lorenz strange attractors of Guckenheimer & Williams), and in other cases they may almost do so.

2) Periodic orbits are easy objects to do numerical experiments with; reasonably low period orbits can be located numerically using standard techniques independent of whether they are stable or not, and can be followed as parameters change.

3) The types of bifurcations which create or destroy individual periodic orbits are well understood and small in number. In dissipative systems without symmetries these are Hopf bifurcation, saddle-node (or tangent) bifurcation, period-doubling bifurcation and homoclinic (or heteroclinic) bifurcation. See the bibliography for references.

4) Sensible physical models often have the property that the behavior is analytically accessible for small and large values of a parameter. Thus, for example, one may know that there are no periodic orbits for small parameter values and (for instance in the Lorenz equations) one periodic orbit at large parameter values. In some systems it may be possible to learn much about the behavior merely by doing some bookkeeping on the orbits and bifurcations known to occur. In the Lorenz case it is almost certain that a rigorous argument could be constructed which proved the occurrence of a homoclinic orbit as the only possible method of producing the large parameter orbit and then (because of the symmetry of these equations) this has further implications for the occurrence of complicated (and possibly chaotic) behaviors at intermediate parameter values.

5) Because homoclinic orbits depend on the behavior of the unstable manifold of the stationary point, and because this must vary continuously (for finite times) as a parameter is changed continuously, it is frequently possible to deduce the existence of other homoclinic orbits once one knows the existence of one. This argument adds force to point 4) above.

Caveats

It is sensible to point out that the approaches described above (like most others) do not, separately or together, yield a coherent (or universal) theory or classification of chaotic systems. Certainly it is true that certain groups of ODE's (e.g. Rossler's equations, certain piecewise linear systems and Spiegel's asymptotic chaos equations) all can be understood in terms of a single mechanism; a periodic orbit is produced in a Hopf bifurcation at one stationary point, grows until it disappears in a homoclinic bifurcation at the other stationary point, and

the chaotic behavior observed depends on intermediate developments which can, more or less, be understood by only looking at the homoclinic bifurcation. This suggests a tentative classification scheme which depends on the number of stationary points, the eigenvalues there, and the possible topological restrictions (if any) on homoclinic and heteroclinic loops which can occur in the system. However, this scheme has the distinct (and for some purposes overwhelming) disadvantages that it is difficult if not impossible to predict qualitative or quantitative properties of the observed flows at particular parameter values; the type of arguments used are likely to suggest, for example, that each of the two orbits will be stable in some parameter range, but not to say which will be stable first.

Details

There are no details. The bibliography is arranged so as to guide newcomers through the literature in a sensible way, and little attempt has been made to either be complete or give proper precedence to workers who wrote the first (but possibly the most incomprehensible) paper on any given subject.

REFERENCES

Papers in the Spirit of this Abstract

1. Glendinning, P. and C. Sparrow, 1984. "Local and global behavior near homoclinic orbits," J. Stat Phys. 35, 645-697. This paper concentrates on homoclinic orbits as shown in Fig. 1(b).

2. Sparrow, C., 1982. "The Lorenz equations: Bifurcations, chaos and strange attractors," Appl. Math. Sci. 41, Springer-Verlag. Contains a lot of detail about the Lorenz equations, in particular an analysis of a symmetric three-dimensional version of the orbit occurring in Fig. 1(a) which gives rise to a very complicated "strange" invariant set.

Original papers by Sil'nikov

3. Sil'nikov, L.P., 1965. Sov. Math. Dokl. 6, 163-166.

4. Sil'nikov, L.P., 1970. Math. USSR Sbornik. 10, 91-102.

   And other papers in the same journals. Hard to understand and using a different technique to analyze the behavior near to homoclinic orbits. This other technique is explained in an appendix to a preprint by Howard and Krishnamurti, and in a recent paper by Gaspard in J. Stat. Phys.

Further results and examples involving homoclinic orbits

(a) Local results in various special cases (symmetries, etc.)

5. Gaspard, P., 1983. "Generation of a Countable Set of Homoclinic Flows through Bifurcation," Phys. L. 97A, 1-4.

6. Gaspard, P., R. Kapral and G. Nicolis, 1984. "Bifurcation phenomena near homoclinic systems: A two parameter analysis," J. Stat. Phys. 35, 697-727.

7. Glendinning, P., 1984. "Bifurcations near Homoclinic Orbits with symmetry," Phys. L. 103A(4), 163-166.

8. Tresser, C., 1983. "A theorem of Sil'nikov in $C^{1,1}$," C.R. Acad. Sci. (Paris) Serie I, 296, 729-732.

9. Tresser, C., 1984. "About some theorems by L.P. Sil'nikov," Ann. de. l'I.H.P. 40, 441-461.

(b) Papers containing studies of particular sets of equations and discussing their behavior in relation to homoclinic orbits.

10. Evans, J. N. Fenichel and J. Feroe, 1983. "Double impulse solutions of a nerve axon equation," SIAM J. Appl. Math. 42(2), 235-246 and the paper by Feroe which follows this in the same issue.

11. Gaspard, P. and G. Nicolis, 1983. "What can we learn from Homoclinic Orbits in Chaotic Dynamics?" J. Stat. Phys., 31, 499-518. This paper looks at Rossler's equations.

Papers with relevance to fluid dynamics, etc. and homoclinic orbits

12. Arneodo, A., P. Coullet, E. Spiegel and C. Tresser, 1985. "Asymptotic chaos," Physica 14D, 327-347, as described in Spiegel's lectures and (in preprint form) the inspiration for paper 1 above.

13. Knobloch, E. and N.O. Weiss, 1983. "Bifurcations in a Model of Magnetoconvection," Physica 9D, 379-407.

14. Bernoff, A., 1984. "Heteroclinic and Homoclinic Orbits in a Model of Magnetoconvection," Preprint, DAMTP, Cambridge.

15. Knobloch, E., D. Moore, J. Toomre and N.O. Weiss, 1983. "Transitions to Chaos in Two-dimensional Double-diffusive Convection," Preprint, DAMTP (for the full version) and Nature 303, 663-667, (1983) for a shorter version.

16. A preprint by L. Howard and R. Krishnamurti.

Forthcoming papers

17. Fowler, A. and C. Sparrow, "Bifocal homoclinic orbits," a study of the 4-d case with two complex pairs of eigenvalues at the stationary point.

18. Glendinning, P. and C. Sparrow, 1985. 'T-points: A codimension two heteroclinic bifurcation,' an analysis of the situation shown in Fig. 2(b), inspired by numerical work (and some misleading statements) in Alfsen, K. and J. Froyland, 1985, "Systematics of the Lorenz model at $\sigma = 10$," Physica Scripta 31, 15-20.

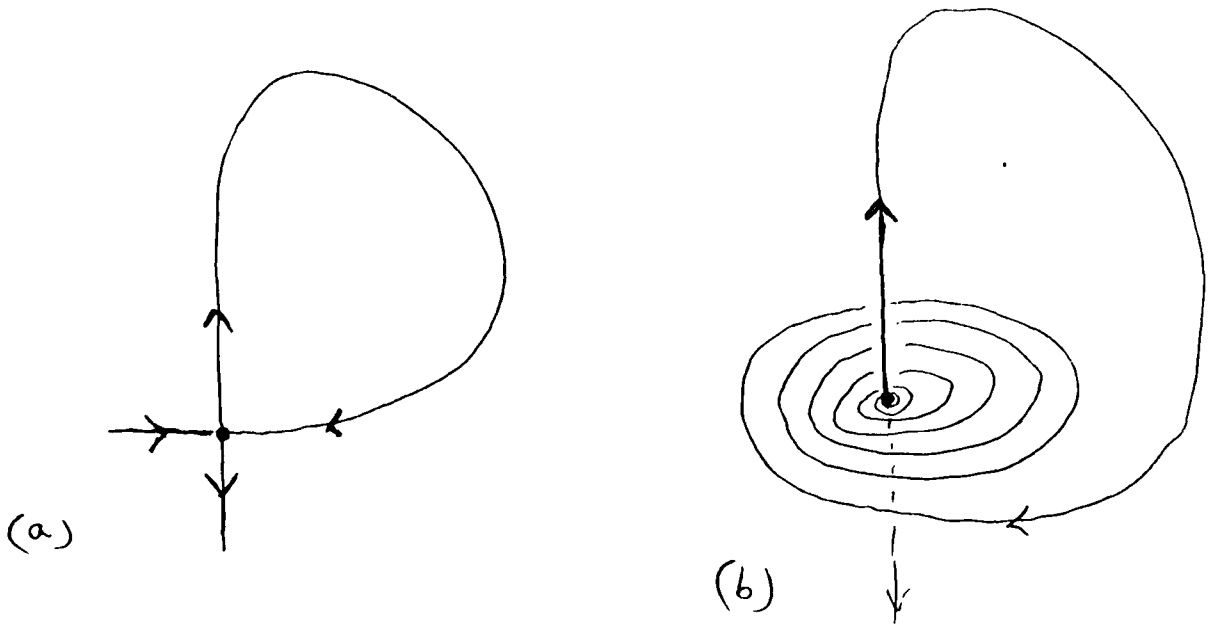

Figure 1
Homoclinic orbits.
(a) Two real eigenvalues (possible in 2 dimensions).
(b) One real eigenvalue and a complex pair (needs 3 dimensions).

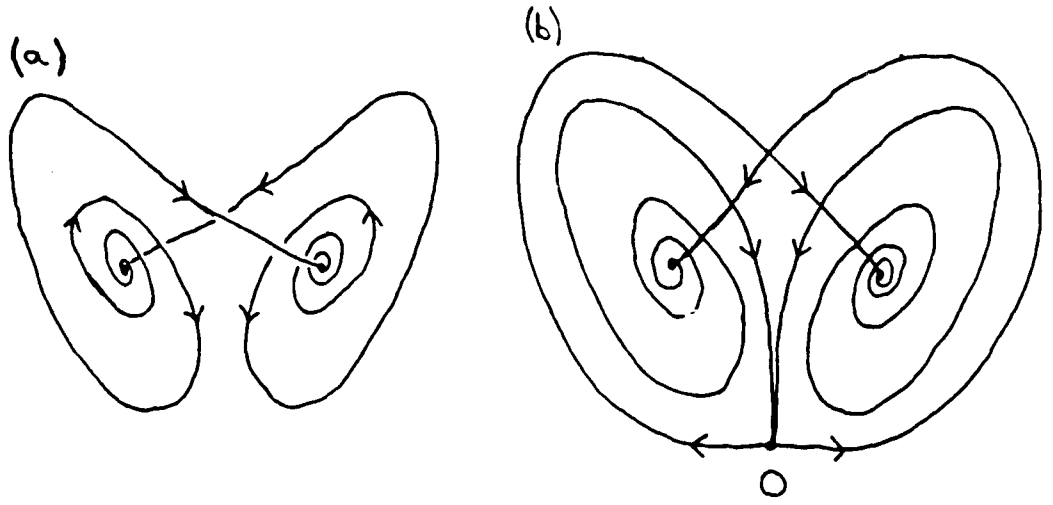

Figure 2
Heteroclinic loops (which occur in the Lorenz equations)
(a) Between two stationary points.
(b) Between three stationary points.

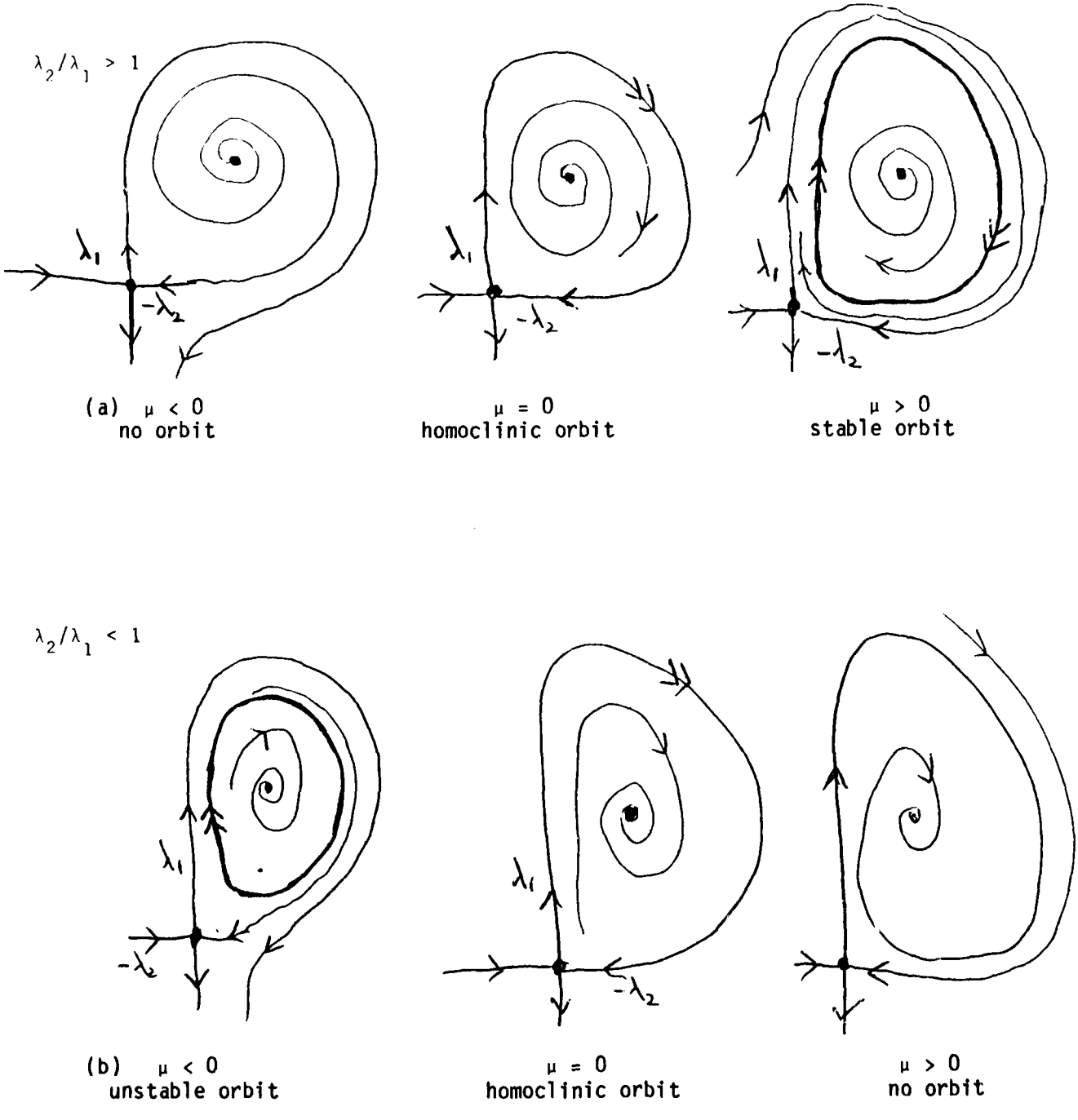

Figure 3
Phase diagrams for a two-dimensional flow with three parameter values, $\mu < 0$, $\mu = 0$ (when we have a homoclinic orbit), and $\mu > 0$. In (a) we have $\lambda_2/\lambda_1 > 1$ and a stable orbit exists in $\mu > 0$. In (b) $\lambda_2/\lambda_1 < 1$ and an unstable orbit exists in $\mu < 0$.

AD-A164 601 SUMMER STUDY PROGRAM IN GEOPHYSICAL FLUID DYNAMICS 2/3
WOODS HOLE OCEANOGRAPH..(U) WOODS HOLE OCEANOGRAPHIC
INSTITUTION MA G VERONIS ET AL. NOV 85 WHOI-85-36
UNCLASSIFIED N00014-82-G-0079 F/G 20/4 NL

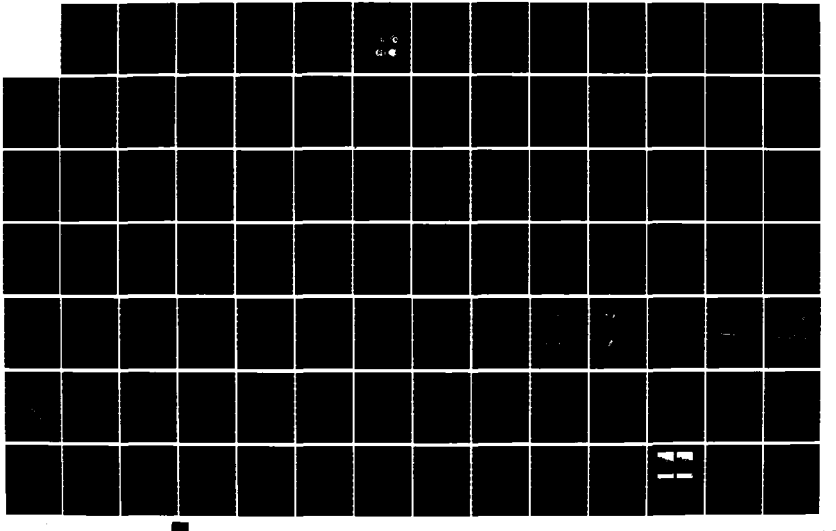

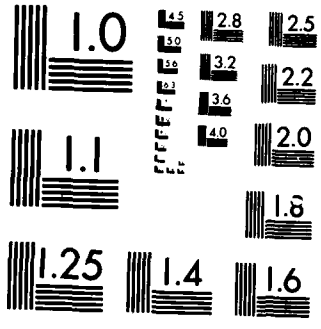

MICROCOPY RESOLUTION TEST CHART
NATIONAL BUREAU OF STANDARDS-1963-A

Chaos in Double-Diffusive Convection

Nigel Weiss

The aim of this talk is to illustrate the general principles enunciated in Spiegel's lectures by detailed discussion of a specific problem; thermohaline convection can be regarded as the 'problem of the house' and is an obvious choice. In studying any self-excited oscillator we should first locate the bifurcation that leads to (overstable) oscillatory motion and then explore the nonlinear regime. If chaos is found we need to discover how the transition from periodic to aperiodic behavior takes place and also to identify the mechanism responsible for the appearance of chaos.

Consider a layer of fluid heated uniformly from below with an imposed gradient in concentration of some solute such that the mean density decreases upwards. If the layer is perturbed the fluid will oscillate and may be overstable if the ratio, τ, of solutal to thermal diffusivity is small (Stern 1960). Two-dimensional convection in a Boussinesq fluid is governed by the equations

$$\frac{1}{\sigma}\left[\partial_t \nabla^2\Psi + \frac{\partial(\Psi, \nabla^2\Psi)}{\partial(x,z)}\right] = R_T \partial_x \Theta - R_S \partial_x \Sigma + \nabla^4\Psi ,$$

$$\partial_t \Theta + \frac{\partial(\Psi, \Theta)}{\partial(x,z)} = \partial_x \Psi + \nabla^2\Theta ,$$

$$\partial_t \Sigma + \frac{\partial(\Psi, \Sigma)}{\partial(x,z)} = \partial_x \Psi + \tau \nabla^2\Sigma .$$

Here Ψ, Θ, Σ are the stream function and perturbations in temperature and solute concentration, R_T, R_S are the thermal and solutal Rayleigh numbers and σ is the Prandtl number. For a cell of normalized width λ, with free boundary conditions, we define modified Rayleigh numbers $r_T = R_T/R_0$ and $r_S = R_S/R_0$, where $R_0 = \pi^4(1 + \lambda^2)^3/\lambda^4$. Then the growth rate, s, of linear perturbations satisfies the dispersion relation

$$s^3 + (1 + \sigma + \tau)s^2 + [\sigma + \tau + \sigma\tau + \sigma(r_S - r_T)]s + \sigma(r_S - \tau r_T) = 0$$

(Stern 1960; Veronis 1965; Baines and Gill 1969). There is a stationary bifurcation at $r_T^{(e)} = 1 + r_S/\tau$ and an oscillatory (Hopf) bifurcation at $r_T^{(o)} = 1 + \tau(1 + \sigma + \tau)/\sigma + (\sigma + \tau)r_S/(\sigma + 1)$, provided that $\tau < 1$ and $r_S > r_S^c = \tau^2(1 + \sigma)/\sigma(1 - \tau)$: a pair of complex conjugate eigenvalues cross the imaginary axis at $r_T^{(o)}$ and subsequently merge on the real axis; thereafter, one real eigenvalue increases while the other decreases and passes through the origin at $r_T^{(e)} > r_T^{(o)}$. It can be confirmed that the (unstable) branches of steady solutions bifurcate from $r_T^{(e)}$ in the direction of decreasing r_T (Veronis 1965).

The behavior of nonlinear oscillations can be investigated by unfolding the degenerate bifurcation of codimension two that occurs when $r_S = r_S^c$. (This is an example of the Bogdanov-Arnold normal form that was discussed by Spiegel.) Knobloch and Proctor (1981) showed that for r_S

slightly greater than r_S^c the oscillatory branch terminated on the unstable steady branch, with a heteroclinic orbit linking the symmetrical pair of saddle-points corresponding to the unstable steady solutions. To proceed further requires numerical experiments, which have been carried out over the years by Veronis (1968), Huppert and Moore (1976) and Moore et al. (1983; Knobloch et al. 1985).

For moderate values of R_S, the period of the oscillations increases along the oscillatory branch, rising rapidly towards the end. This is consistent with the presence of a heteroclinic orbit at R_T^c (say). The steady branch apparently bends backwards and regains stability, so that all trajectories are attracted to one or other of a symmetrical pair of foci for $R_T > R_T^c$. Thus phase portraits for R_T just less than, equal to and just greater than R_T^c are as sketched in Figure 1.

For larger values of R_S there is a transition from periodic to chaotic behavior before the end of the oscillatory branch (Huppert and Moore 1976). With care the route to chaos can be identified. For $R_S = 10^4$, $\tau = 0.316$, $\lambda = \sqrt{2}$ and $\sigma = 1$ the first bifurcation is from symmetrical to asymmetrical oscillations, as shown in Figure 2. Here limit cycles are projected on to the $\bar{u}$ - N_S plane, where $\bar{u}$ is the mean horizontal velocity at the base of the cell and the solutal Nusselt number N_S is a dimensionless measure of the solute flux. In Figure 2(a), for $R_T = 8600$, the oscillation is exactly symmetrical and N_S takes the same values for clockwise and counterclockwise motion; when $R_T = 10{,}000$, as in Figure 2(b), the limit cycle is asymmetrical. By $R_T = 10{,}150$ motion is chaotic. Order is, however, restored: at $R_T = 10{,}325$ there is an orbit of period 4, followed by period 2, an asymmetrical orbit and a symmetrical orbit of period 1 when $R_T = 10{,}500$. As we shall see, this bubble structure is a characteristic feature of the transition to chaos.

The route to chaos follows a period-doubling cascade (which has to be preceded by a bifurcation to asymmetry). Beyond the accumulation point the oscillations are typically aperiodic, though periodic windows can be found. Then there is a reversed cascade, with bifurcations at which the period is halved, after which periodic behavior is restored. Beyond this point behavior becomes more complicated, as shown schematically in Figure 3. For $R_T > 10{,}500$ there is an abrupt transition to a second oscillatory branch, presumably connected to the first by saddle-node bifurcations at $R_T = 10{,}500$ and 10,300. This branch has more elaborate orbits, with their own period-doubling cascade leading to chaos as before. Within the chaotic region windows based on a symmetrical cycle of period 3 can be located. Once again there is a reversed cascade and at least two complete bubbles can be identified. Probably there are many successive (and co-existing) branches before oscillatory solutions disappear at $R_T \sim 11{,}060$. Figure 4 illustrates some of the behavior in this region by showing trajectories in the E - $\dot{E}$ phase plane, where E is the mean square velocity over a cell. In Figure 4(a), for $R_T = 10{,}450$, there is an asymmetrical cycle of period 1; Figure 4(b), for R_T, shows a semiperiodic solution, with a trajectory that wanders within a tube enclosing an unstable periodic orbit (note that trajectories are represented by dots plotted after every timestep). In Figure 4(c), for $R_T = 10{,}500$, the trajectory explores more of phase space and is no longer asymmetrical but Figure 4(d), for $R_T = 10{,}510$, shows a symmetrical cycle of period 3. Finally, Figures 4(e) and (f), for $R_T = 10{,}625$ and 10,900, show the increasing complexity of chaotic motion near the end of the oscillatory branch.

How can this behavior be explained? The simplest approach is to consider a truncated fifth-order system of ordinary differential equations, introduced by Veronis (1965). This system can be obtained by modified perturbation theory, and has the same linear and second-order properties as the partial differential equations. Although there is no formal justification for relying on the truncated model away from bifurcation points, it can be used to explain the behavior of the two-dimensional system from which it was derived (DaCosta et al. 1981). For parameters similar to those used above, the fifth-order model also yields a period-doubling cascade, and bubbles can also be observed (Knobloch and Weiss 1981). More important, the unstable steady branch cas be found analytically and its stability can be investigated. It turns out that as the heteroclinic orbit moves away from the bifurcation point, two negative real eigenvalues merge to form a complex conjugate pair. Thus the saddle-points become saddle-foci, with eigenvalues that satisfy Shilnikov's criterion (see Sparrow's lecture below). Chaos is therefore to be expected. Moreover, the approach to heteroclinicity has now been studied in some detail (Glendinning and Sparrow 1984, Arneodo et al. 1985). It is known that there are many coexisting oscillatory branches, with increasing period as the orbit winds more and more times around the nonstable singular points, and that there are period-doubling cascades producing bubbles on alternate branches. This behavior has been found for the analogous fifth-order system in magnetoconvection (Bernoff 1985). The qualitative similarity between these predictions and the results of the numerical experiments suggests that the same mechanism operates for partial differential equations too.

Of course the bifurcation problems described here are only found for low order systems. If constraints of symmetry were relaxed and three-dimensional perturbations were admitted, much more intricate behavior would occur. Nevertheless, this problem provides a nice demonstration of the use of truncated models to explain complicated dynamics. The appearance of chaos was first predicted on the basis of a third-order model concocted by Moore and Spiegel (1966; Baker et al. 1971; Marzec and Spiegel 1980) and similar behavior is exhibited by the fifth-order system described above. For $\tau \ll 1$, Proctor and I have shown that this system reduces to a third-order variant of the Lorenz equations, which can be written in the form

$$\dot{x} = \sigma(\mu x - \nu y),$$

$$\dot{y} = -y + x(1 - z),$$

$$\dot{z} = b(-z + xy),$$

where $b = 4\lambda^2/(1 + \lambda^2)$ and μ, ν are parameters related to r_T and r_S respectively. This system can be recast to resemble an oscillator with a time-dependent potential, so that

$$\ddot{x} = -\partial V/\partial x - \kappa \dot{x}$$

where $V = 1/2\lambda x^2 + 1/4\ x^4$ and $\dot{\lambda} = -b[\lambda + a(x^2 - x^2)]$. Unfortunately, I know only one way of checking whether such low order models faithfully describe the appearance of chaos in the original problem, and that is to solve the partial differential equations themselves.

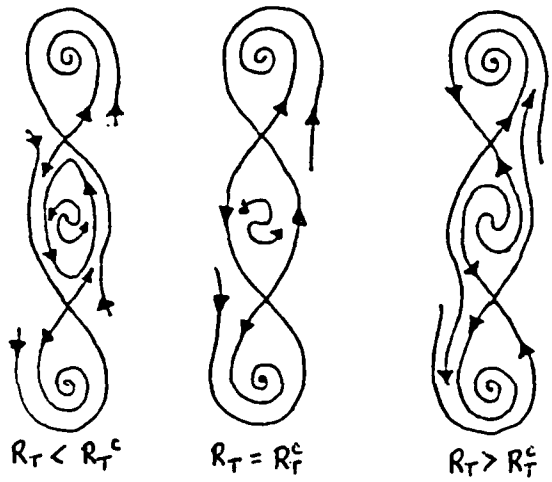

Figure 1

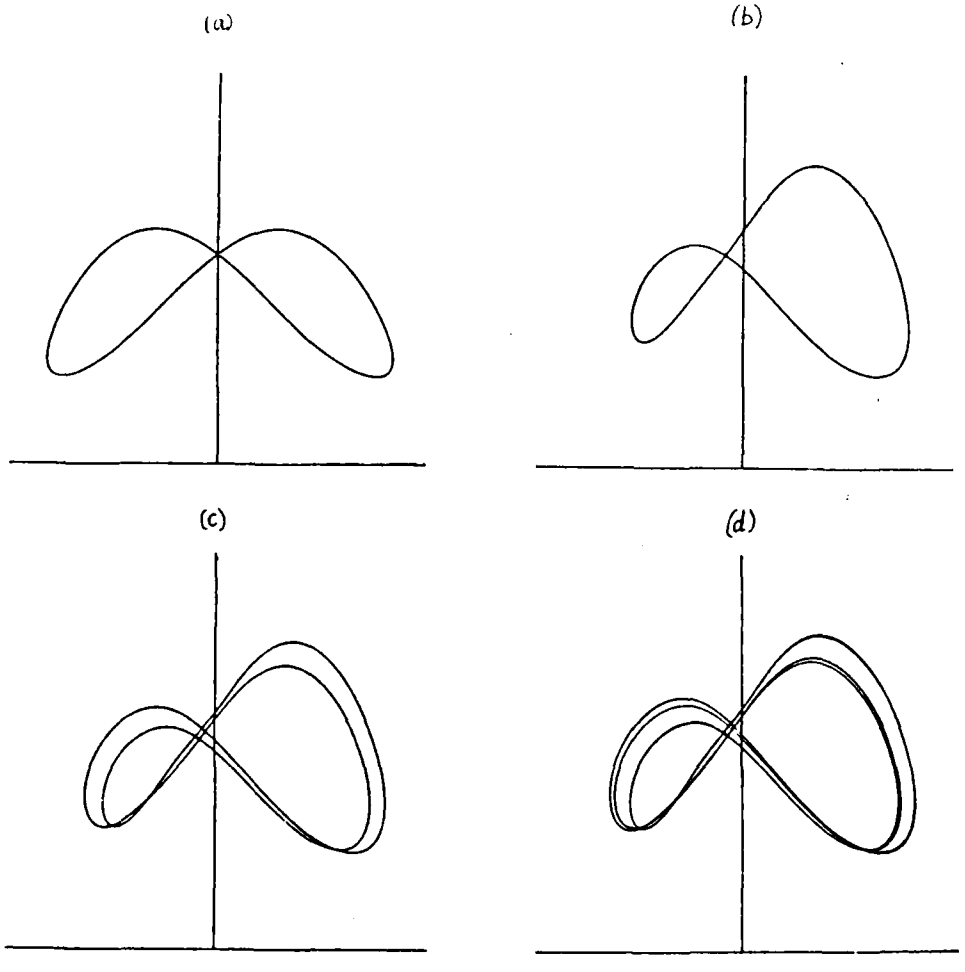

Figure 2

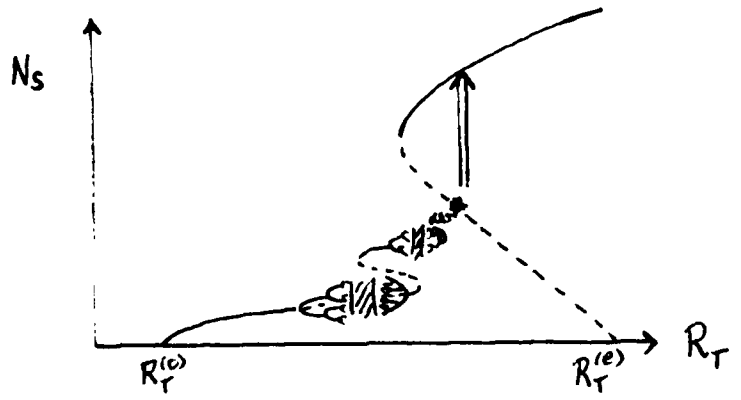

Figure 3

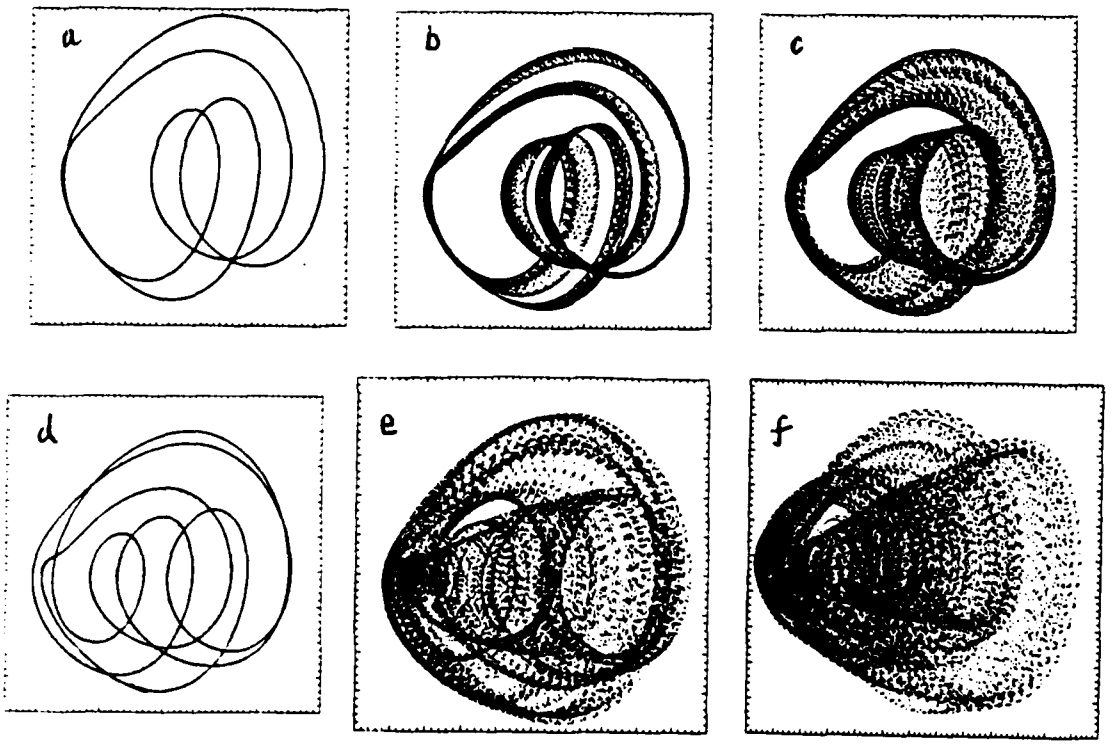

Figure 4

REFERENCES

Arneodo, A., P.H. Coullet, E.A. Spiegel and C. Tresser, 1985. Physica 14D, 327-347.

Baines, P.G. and A.E. Gill, 1969. J. Fluid Mech. 37, 289-306.

Baker, N.H., D.W. Moore and E.A. Spiegel, 1971. Q.J. Mech. Appl. Math. 24, 391-422.

Bernoff, A., 1985. Physica D (submitted).

DaCosta, L.N., E. Knobloch and N.O. Weiss, 1981. J. Fluid Mech. 109, 25-43.

Glendinning, P.A. and C.T. Sparrow, 1984. J. Stat. Phys. 35, 645-696.

Huppert, H.E. and D.R. Moore, 1976. J. Fluid Mech. 78, 821-854.

Knobloch, E., D.R. Moore, J. Toomre and N.O. Weiss. J. Fluid Mech. (submitted).

Knobloch, E. and M.R.E. Proctor, 1981. J. Fluid Mech. 108, 291-316.

Knobloch, E. and N.O. Weiss, 1981. Phys. Lett. 85A, 127-130.

Marzec, C.J. and E.A. Spiegel, 1980. SIAM J. Appl. Math. 38, 403-421.

Moore, D.R., J. Toomre, E. Knobloch and N.O. Weiss, 1983. Nature 303, 663-667.

Moore, D.W. and E.A. Spiegel, 1966. Astrophys. J. 143, 871-887.

Stern, M.E., 1960. Tellus 12, 172-175.

Veronis, G., 1965. J. Marine Res. 23, 1-17.

Veronis, G., 1968. J. Fluid Mech. 34, 315-336.

The Breakdown of Steady Convection

Nigel Weiss

This talk will be concerned with systems where an initial pitchfork bifurcation leads to steady convection and a secondary Hopf bifurcation introduces time-dependent behavior, followed by chaos. I shall try to emphasize spatial rather than temporal structures and, in particular, I shall focus on bifurcations that lead to changes in the pattern of convection. Here we can distinguish between soft transitions (eg. loss of symmetry) and discontinuous changes. The latter include changes of cell size in constrained systems, which are typically associated with complicated time-dependent behavior.

The simplest examples occur in two-dimensional Bénard convection, the problem from which the Lorenz equations were originally derived. In the Lorenz system there is a supercritical pitchfork bifurcation at $r = 1$, giving states of steady convection which eventually undergo a subcritical Hopf bifurcation (eg. Sparrow 1982). However, the strange attractor disappears when higher order approximations are used (Veronis 1966; Curry 1978). Reliable numerical solutions of the partial differential equations show a supercritical Hopf bifurcation at $r \approx 90$, followed by quasi-periodic behavior for $290 \lesssim r \lesssim 800$, but there is no evidence of chaos (Moore and Weiss 1973; Curry et al. 1984). The oscillations are related to the appearance of hot and cold blobs circulating with the flow and similar behavior has been found in laboratory experiments. In what follows I shall try to isolate this particular effect and to understand how such obvious physical behavior relates to the mathematical constraints in a dissipative dynamical system.

Let us consider the geophysically motivated problem of convection driven by internal heating. Dan McKenzie, Dan Moore, Tom Lennie and I have studied the simplest case, of two-dimensional motion in a Boussinesq fluid with infinite Prandtl number, assuming rigid upper and lower boundaries, with no heat flux at the bottom and a fixed temperature at the top. The governing equations are

$$\nabla^4 \psi = -g\alpha/\nu \quad \partial T/\partial x,$$

$$\partial T/\partial t = -\underline{u} \cdot \nabla T + \epsilon + \kappa \nabla^2 T,$$

where T is the temperature and the velocity $\underline{u} = (-\partial\psi/\partial z, 0, \partial\psi/\partial x)$; ϵ is the rate of thermometric heating per unit volume and other symbols have their usual meanings. We consider convection in a box of depth d and width λd, characterized by a Rayleigh number

$$R = g\alpha\epsilon d^5/\kappa^2\nu$$

and a Nusselt number $N = \epsilon d^2/2\kappa\Delta T$, where ΔT is the mean temperature difference across the layer. Then linear theory predicts a pitchfork bifurcation at $R = 2772$, with a critical cell width $\lambda = 1.195$ (Roberts 1967). Thirlby (1970) carried out two- and three-dimensional numerical exponents for a fluid with a finite Prandtl number $\sigma = 6.8$ [for comparison

with laboratory experiments using water which was electrolytically heated (Tritton and Zarraga 1967)]. Further computations (with σ infinite but assuming free boundaries) were done by McKenzie et al. (1974). The two-dimensional results show the effect of asymmetrical boundary conditions: motion is dominated by a thermal boundary layer at the top which forms a cold sinking plume at one side of the cell. The boundary layer thickness scales as $R^{-1/5}$ and ΔT scales as $R^{4/5}$, so the local Rayleigh number in the boundary layer varies as $R^{1/5}$. Hence the boundary layer should become unstable for sufficiently large R. If the flow is forced to be two-dimensional, cold blobs form at the top and are swept into the sinking sheet; if three-dimensional motion is allowed, cold plumes sink at the centers of hexagonal cells. The two-dimensional computations show a transition from steady convection to time-dependent behavior, followed by splitting into several cells, as the Rayleigh number is increased.

We have investigated these transitions in some detail. For $\lambda = 1$ there is a supercritical Hopf bifurcation at $R \approx 2{\cdot}3 \times 10^5$, leading to vacillation about the unstable states corresponding to steady convection. Figure 1 shows isotherms at equally spaced intervals during a periodic oscillation for $R = 3 \times 10^5$. Two blobs are formed and circulate around the cell, so the period of the oscillation is half the turnover time. One might expect that the first bifurcation would destroy this symmetry. In fact, a second Hopf bifurcation occurs at $R \approx 3.05 \times 10^5$ producing quasi-periodic motion. The period of modulation increases until there is a homoclinic bifurcation at $R \approx 3{\cdot}093 \times 10^5$, followed by an immediate transition to chaos. This is consistent with the behavior expected for a strong resonance with eigenvalues close to -1 (Arnold 1983); apparently the branch of period-doubling orbits undergoes a cascade of bifurcations leading to chaos before it regains stability.

When $\lambda = 1{\cdot}5$ the first Hopf bifurcation is followed by a period-doubling cascade that leads to chaos by $R = 1{\cdot}2 \times 10^5$. Within the chaotic regime there are periodic windows, where behavior can be understood as a resonance involving the circulating blobs. Fig. 2 shows part of such a periodic solution for $R = 1{\cdot}6 \times 10^5$. As R is increased, some blobs break off the upper boundary before they are swept into the corner and eventually, when $R \approx 1{\cdot}4 \times 10^6$, the cell splits in two, though motion remains time-dependent. Calculations with $\lambda = 0{\cdot}5$ confirm that narrower cells remain stable at least up to $R = 10^6$ but if two or three such cells are placed together in a box the solutions become time-dependent at a lower Rayleigh number.

The mechanism responsible for this chaotic behavior can only be conjectured. As R is increased the favored cell-width decreases but the number of cells in a box has to change discontinuously. Larger cells undergo Hopf bifurcations and the periodic oscillations increase in amplitude until they lose stability. The unstable orbit probably becomes homoclinic, so generating chaos. As the Rayleigh number is increased, more and more horizontal scales of motion are excited. We conjecture that their basins of attraction are separated by saddle points and that they become unstable, shedding limit cycles which collide with these saddles producing a rich variety of chaotic behavior.

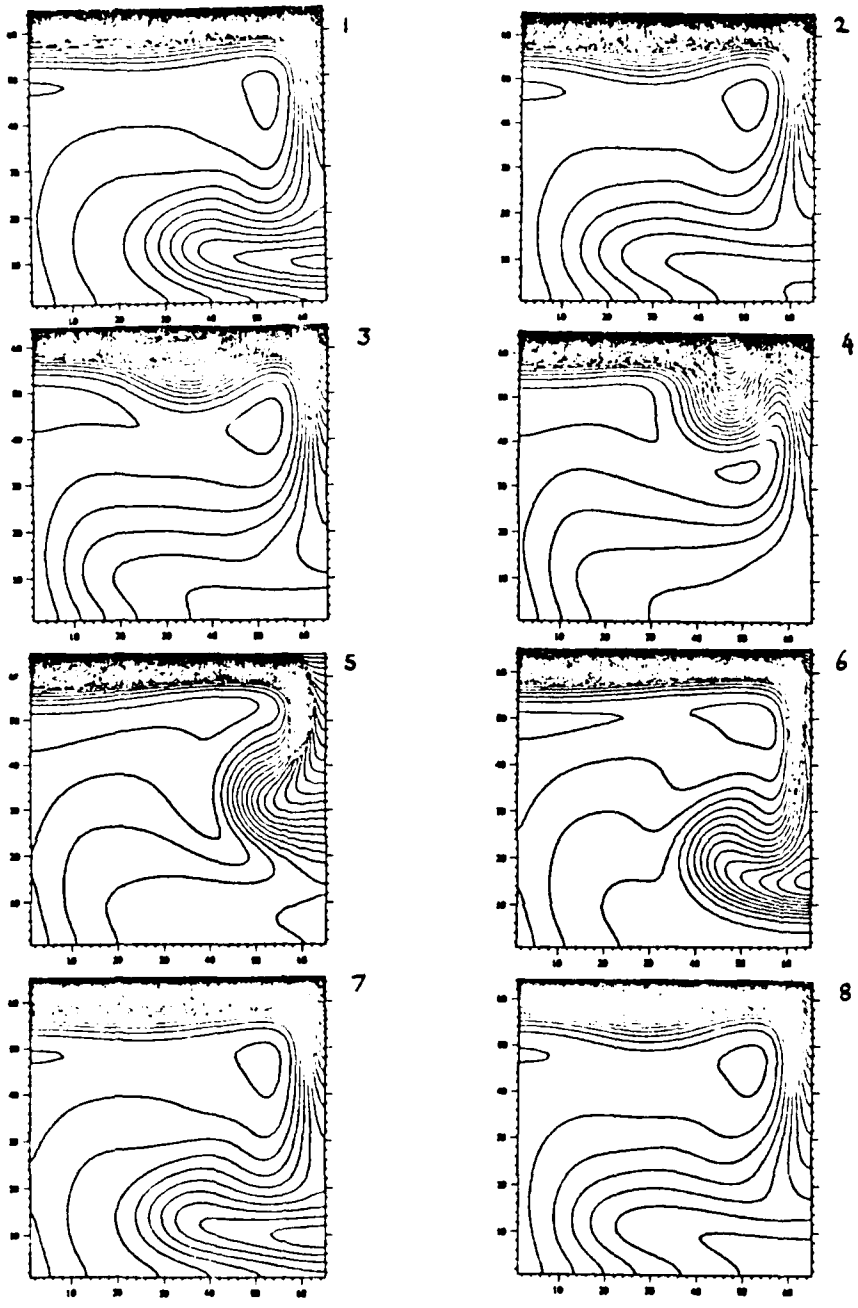

Figure 1
Isotherms for $R = 3 \times 10^5$, $\lambda = 1$

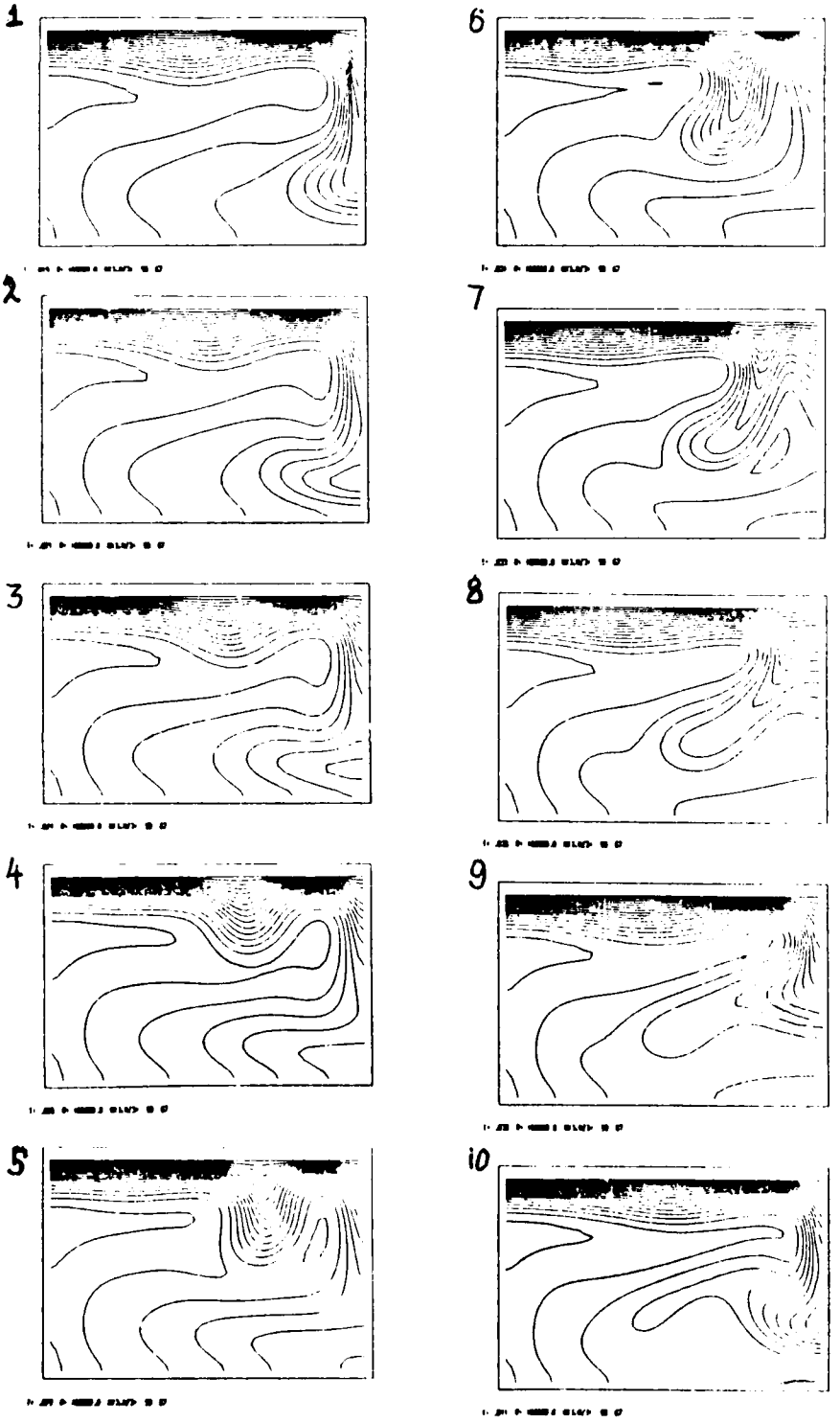

Figure 2
Isotherms for $R = 1{\cdot}6 \times 10^5$, $\lambda = 1{\cdot}5$

REFERENCES

Arnold, V.I., 1983. Geometrical methods in the theory of ordinary differential equations. Springer, Berlin.

Curry, J.H., 1978. Commun. Math. Phys. 60, 193-204.

Curry, J.H., J.R. Herring, J. Loncaric and S.A. Orszag, 1984. J. Fluid Mech. 147, 1-38.

McKenzie, D.P., J.M. Roberts and N.O. Weiss, 1974. J. Fluid Mech. 62, 465-538.

Moore, D.R. and N.O. Weiss, 1973. J. Fluid Mech. 58, 289-312.

Roberts, P.H., 1967. J. Fluid Mech. 30, 33-49.

Sparrow, C.T., 1982. The Lorenz equations: bifurcations, chaos and strange attractors. Springer, New York.

Thirlby, R., 1970. J. Fluid Mech. 44, 673-693.

Tritton, D.J. and M.N. Zarraga, 1967. J. Fluid Mech. 30, 21-31.

Veronis, G., 1966. J. Fluid Mech. 26, 49-68.

Bifurcation to Chaos and Dimensionality of Attractors in an Extended Rayleigh-Bénard Convection System

Y. Sawada

The spatial and temporal bifurcation to chaos and dimensionality of strange attractors in Rayleigh-Bénard convection are studied in an extended rectangular container with aspect ratios 15.0 and 1.0. With increasing Rayleigh number, spatial localized oscillatory states, quasi-periodic states, and then chaotic states were observed. The chaotic state was characterized by the localized attractors whose dimension is small just above the onset of chaos and by the coexistence of different dimensional attractors.

The Fission Theory of Binary Stars

Norman R. Lebovitz

A physical context simulating an early stage of stellar evolution is assumed, wherein the star is in a steady state hydrodynamically but not thermodynamically, so that the figure is losing energy on a slow timescale (T_c) and compensating by contracting slowly. It is assumed that the star is endowed with angular momentum, and the object of the mathematical problem is to follow the evolution of such a self-gravitating, rotating fluid mass as it slowly loses energy.

The history of the subject is reviewed (cf. Lyttleton 1953), including a description of the Maclaurin and Jacobi ellipsoids, of secular and dynamical instability, and of certain notions - and problems - in the theory of instability, bifurcation, and passage through bifurcation in rotating dynamical systems. The focus on bifurcation from the Jacobi family via a certain third-harmonics deformation of the free surface is discussed, along with the apparent impasse in which the theory was left in virtue of the discoveries of Lyapunov (who found that the bifurcating family was unstable) and Cartan (who found that the Jacobi family was dynamically rather than secularly unstable beyond the third-harmonics point of bifurcation).

Recently Eriguchi, Hachisu and Sugimoto (1982) have shown that the fourth-harmonics point of bifurcation is intriguing from the standpoint of fission. However, it is not accessible via an evolutionary trajectory under classical assumptions, because such a trajectory would first encounter a dynamical instability to third harmonics disturbances.

I have reformulated the problems of the evolution, stability, and bifurcation of ellipsoidal masses in the context of inviscid, compressible fluid dynamics (Lebovitz 1981). In this context, evolutionary trajectories are very different from those of the classical (viscous, incompressible) theory. In this revised context, the fluid mass first encounters the fourth-harmonics instability. The shape of the deformed figure and the behavior of the bifurcating branch reveal the favorable features found by Eriguchi et al. (1982), i.e., the deformed figure is pinched in the middle, and the bifurcation is transcritical, so that there is necessarily a stable branch (Lebovitz 1984, 1985).

These results would seem to restore to the subject the picture proposed a century ago for the formation of a binary figure via fission. The differences from the older theory are (1) the newer version is inviscid and (2) the relevant instability belongs to the fourth ellipsoidal harmonics rather than the third.

REFERENCES

Eriguchi, Y, I. Hachisu and D. Sugimoto, 1982. Progr. Theor. Phys. 67, 1068.

Lebovitz, N.R., 1981. Proc. Roy. Soc. London A 375, 249.

Lebovitz, N.R., 1984. Astroph. J. 284, 364.

Lebovitz, N.R., 1985. Unpublished.

Lyttleton, R.A., 1953. The Stability of Rotating Liquid Masses (Cambridge: Cambridge University Press).

Approximations Based on the Hamiltonian Structure of Fluid Dynamics

Rick Salmon

Approximation methods which exploit the underlying Hamiltonian structure of the general fluid equations enjoy two important advantages over more conventional methods. First, when approximations based upon a scaling analysis are applied directly to the fluid Lagrangian, then the resulting equations of motion automatically preserve analogues of all the exact conservation laws, provided only that some care is taken not to disturb the corresponding symmetry properties of the Hamiltonian. Second, because the approximations also have Hamiltonian structure, there exist canonical coordinates in which the approximate equations take their simplest mathematical form.

Two examples illustrate these ideas. In the first example, the Lagrangian for a shallow homogeneous layer of rotating fluid is iterated once about the zero-Rossby-number limit of purely geostrophic motion. The resulting dynamics exactly conserve a 'geostrophic' approximation to the total energy and the potential vorticity on particles. In canonical form, these dynamics generalize the 'semi-geostrophic' equations of meteorology to the important case of a spatially-varying rotation rate.

In the second example, the general Lagrangian for a homogeneous fluid with a free surface is iterated once about the dispersionless limit of a very shallow layer to obtain dynamical equations which are equivalent to those derived by Green and Naghdi (1976) by other methods. The Green-Naghdi equations conserve a form of potential vorticity, which when set initially to zero, permits a reduction to a form of the Boussinesq equations obtained previously by Whitham. A further reduction yields the Lagrangian for the KdV equation.

REFERENCES

Green, A.E. and P.M. Naghdi, 1976. A derivation of equations for wave propagation in water of variable depth. J. Fluid Mech., 78, 237-246.

Miles, J. and R. Salmon. Weakly dispersive, nonlinear gravity waves. J. Fluid Mech. (in press).

Salmon, R., 1985. New equations for nearly geostrophic flow. J. Fluid Mech., 153, 461-477.

Vortex Dynamics and Cascade Theory

Stephen Childress

The elements of the kinematical connections between a velocity field $u(x,t)$ and a vorticity field $\omega(x,t)$ were reviewed. The dynamical statement appropriate to Euler's equations, that the flow lines of ω are material lines of the field u implies the well-known differential equation for ω. The essential nonlocal properties of the vorticity field are summarized in Kelvin's theorem, and the geometry of vorticity derives from the application of this theorem to matarial lines.

Efforts to understand the geometry of small-scale features in fully-developed turbulence have recently focused on the possible role of coherent structures in the energy cascade. Early attempts to give a physical description of a turbulent field utilized ensembles of vortex filaments, sheets, Hill's vortices, and, more recently, vortons (Aksman et al. 1985). Relatively little attention has been paid, however, to the study of nonsingular structures, even in the steady case. Fraenkel (1970) has treated steady vortex rings, and his methods reveal the essential matching that can be exploited to treat slender rings of arbitrary core structure. Since two-dimensional rotational flow and axisymmetric rings are two limiting cases of a one-parameter family of helical rotational flows, it would be of interest to develop matched expansions for slender helical vortex structures, analogous to related calculations in plasma physics.

In this connection, two kinds of "nearly two-dimensional" Euler flows were introduced. The flows of type I include a "stretched" version of the Taylor-Green problem. Those of type II are of the form, in the large, of a vortex filament. In the small, the core of the vortex is a quasi-steady two-dimensional rotational flow. The simplest example of a type II flow is a slender vortex tube whose core is a nested family of simple closed streamlines. These two flows differ in the manner in which the three-dimensionality affects local two-dimensional dynamics.

If the initial-value problem for the Navier-Stokes equations is considered at an enormous Reynolds number ($\sim 10^{12}$), the vortical structures associated with the energy cascade would be revealed in a near inviscid setting, even if a geometrical cascade in the local Reynolds number was involved. The possible role of finite-time singularities in the creation of such a cascade is not obvious. Two extreme views are that (1) singularity structure determines the inertial-range spectrum, and (2) singularities occur (in the inviscid limit) on all scales and (e.g.) initiate steps of the cascade. The finite rate of dissipation of energy in the inviscid limit is believed to be associated with dissipation on a fractal set, although there are no fully dynamical models for this process.

Recent attempts to construct deterministic cascade models were reviewed. Details were given concerning the vortex-tube model of Tennekes (1968), the beta-model (Frisch et al. 1978), the gamma-model (Childress 1984). An example of a model which does not invoke a formal hierarchy of distinct steps is the strained spiral vortex model of Lundgren (1982). These examples suggest that a sensible attack on inertial-range modeling will involve kinematics of vorticity, but also

maintaining a certain number of the invariants of the inviscid flow, including volume, energy, circulation, and topological knottedness. It is important to realize, however, that it is not clear how the topology responds to finite but arbitrarily small viscosity.

An extreme dynamical viewpoint, invoked in the gamma model, is that the cascade can be divided into two-dimensional rotational flow and axial straining of slender vortices ("2 + 1" dynamics). In this picture, each cascade step involves a two-dimensional event, producing structures which are then stretched. If all the two-dimensional are assembled, the assumption is that the resulting dynamics is indistinguishable from two-dimensional turbulence. The model then establishes a connection between the three-dimensional inertial range spectrum and the spectrum of the two-dimensional enstrophy cascade. In particular, intermittency occurs simultaneously in both. The two spectral exponents are related by

$$e_2 = \frac{3e_3 - 1}{3 - e_3}, \quad E(k) \sim k^{-e_n} \tag{1}$$

A simple setting in which to investigate the onset of cascading to small scales is the nearly two-dimensional Taylor-Green problem, wherein the axial wavelength of the initial cells is large compared to cell diameter. An averaging method can be used to study the evolution of the quasi-two-dimensional Bernoulli function H and circulation Γ as functions of streamfunction ψ and slow variables ζ, τ. For the Taylor-Green initial condition the streamline pattern is a simple nested family, and the following equations result:

(A = area within a streamline)

$$DA_\psi + (v_\psi + w_\zeta)A_\psi = 0, \; D = \partial_\tau + v\partial_\psi + w\partial_\zeta, \tag{2a}$$

$$A_\psi \, Dw = \Gamma_\zeta - A_\psi H_\zeta, \tag{2b}$$

$$\Gamma_\psi - A_\psi \, H_\psi = 0, \tag{2c}$$

$$D\Gamma = 0. \tag{2d}$$

Here an "equation or state" relating Γ and A must be supplied by analysis of the elliptic problem $\nabla^2\psi = H_\psi(\psi)$. We have thus replaced an incompressible 3-D problem by an effective (and "shallow") compressible 2-D problem. The system (2) can be analyzed near a plane of symmetry and preliminary numerical calculations indicate that there is finite-time breakdown of the near two-dimensionality.

REFERENCES

Aksman, M.J., et al., 1985. Phys. Rev. Lett. 54, 2410.

Childress, S., 1984. Geophys. Astrophys. Fluid Dynamics 29, 29.

Fraenkel, L.E., 1970. Proc. Roy. Soc. Lond. A. 316, 29.

Frisch, U., et al., 1978. J. Fluid Mech. 87, 719.

Lundgren, T.S., 1982. Phys. Fluids 25, 2193.

Tennekes, H., 1968. Phys. Fluids 11, 669.

A Thermal Relaxation Oscillator

Peter Lundberg

A problem not uncommonly encountered within chemical engineering practice is that of the behavior of a fluid confined to a system of well-mixed and connected reservoirs. This is known as a C*-problem (from Continuously Stirred Tank Reactor) and is well adapted for an analysis in terms of dynamical systems theory. The use of this type of approach for the study of oceanographical problems was pioneered by Stommel (1961).

Here we shall consider two well-mixed closed vessels of equal height H and of volumes V_1 and V_2, connected by tubes at their upper and lower ends. The vessels contain a fluid of kinematic viscosity ν and with a quadratic density maximum as evidenced by the equation of state,

$$\rho = \rho_0(1 - \alpha T^{*2})$$

where ρ is the density, T^* the temperature and α the coefficient of thermal expansion. The thermal forcing of the system is accomplished by immersing the vessels containing fluid of temperatures T_1^* and T_2^* respectively in baths of constant temperatures T_1^{ex} and T_2^{ex}. Hereby Newtonian heat fluxes governed by the external thermal exchange coefficient κ_e can take place. The vessels also interact directly with one another by a diffusive heat flux through a common wall controlled by the internal thermal exchange coefficient κ_i. A density difference between the fluid in the two vessels will give rise to a flow, assumed to obey the law of Hagen-Poiseulle, through the connecting tubes of lengths $\ell/2$ and radii r.

The nondimensionalized ordinary differential equations governing the evolution in time of the temperatures T_1 and T_2 assume the following form:

$$dT_1/dt = Ra|T_2^2 - T_1^2|(T_2 - T_1)/\delta + (\theta/(1-\theta) - T_1)/(\delta Pe) + \kappa(T_2 - T_1)/(\delta Pe)$$

$$dT_2/dt = -Ra|T_2^2 - T_1^2|(T_2 - T_1) + (1/(1-\theta) - T_2)/Pe - \kappa(T_2 - T_1)/Pe$$

Here $Ra = \pi\alpha r^4 \tau\, gH(\Delta T)^2/8\nu\ell V_2$, $Pe = V_2/\tau\kappa_e$, $\theta = T^{ex}/T^{ex}$, $\delta = V_1/V_2$ and $\kappa = \kappa_i/\kappa_e$. All temperatures have been scaled with $\Delta T = T_2^{ex} - T_1^{ex}$ and τ is the relaxation time-scale of the system. Note that the direction of the flow through the connecting tubes has no significance, hence the nonanalytical right-hand sides of the governing equations.

From a thermodynamical standpoint it is not surprising that it can be shown that the solutions to these equations are globally stable. If it furthermore can be demonstrated that the critical points (T_1^c, T_2^c) of the system are unstable, the theorem of Bendixson implies that a periodic solution in the form of a limit cycle in the T_1T_2-phaseplane must ensue. When calculating the critical points it can be shown a posteriori that the condition $T_2^{c2} - T_1^{c2} > 0$ is equivalent to $\theta^2 < 1$. By allowing the volume ratio δ to range over the entire real positive axis the variables can always be defined so as to make $\theta^2 < 1$ why we limit our attention to this case.

For a small enough neighborhood of (T_1^c, T_2^c) the governing equations become analytical in which case a linear stability analysis of the stationary solution is quite straightforward. From the resulting second-degree algebraic equation criteria for the neutral stability of (T_1^c, T_2^c) in terms of a critical Rayleigh number $Ra^c(Pe, \delta, \theta, \kappa)$ can be established. The critical point proves to be stable for small as well as large values of Ra, whereas it is unstable for an intermediate range of the Rayleigh number. An analysis furthermore demonstrates that for increasing values of Ra, the transitions from a stable to an unstable and back to a stable critical point take the form of sub- and supercritically unstable regular and inverse Hopf bifurcations.

An oscillatory solution to the problem in the form of a limit cycle in the phase-plane is shown below.

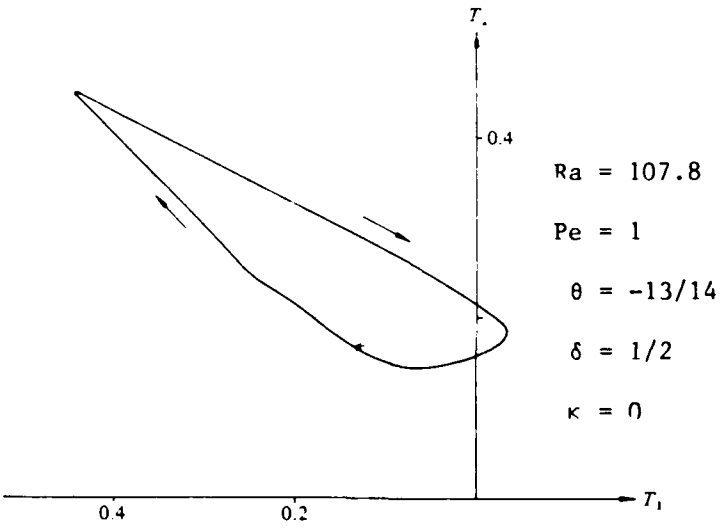

Since this representation does not do justice to the time evolution of the solutions, a more conventional graph of the same oscillation is also shown.

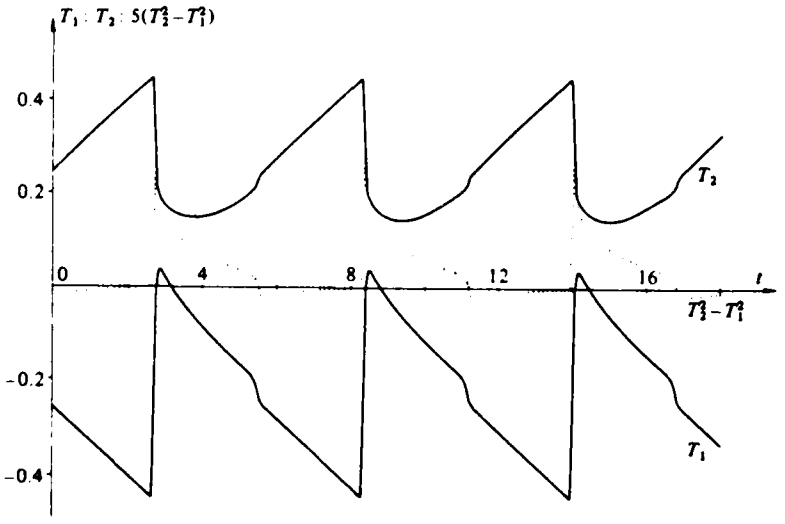

The relaxation character of the oscillation is particularly evident in the latter figure. Loosely speaking, the system alternates in a characteristic jerky manner between two almost hydrostatically balanced states, $T_1 \approx T_2$ and $T_1 \approx -T_2$. (This behavior is even more pronounced for stronger thermal forcing, i.e. larger values of Ra.)

It is important to underline that this is an essentially nonlinear oscillation in that a linear dependence of the density upon temperature only can be associated with a state of steady convection, corresponding in the case presently under consideration to a stable critical point. The unstable orbits associated with the Hopf bifurcations only serve as to extend the range of Ra over which oscillatory behavior of the system is encountered, provided that the initial values of (T_1, T_2) are chosen such that they do not lie within these unstable orbits.

It is finally of interest to point out that in the asymptotic limit of $\delta \to 0$ we have a typical example of a discontinuous oscillation in a second-order system (Andronov, Vitt and Khaiken 1966). In this case the limit cycle can be regarded as primarily constituted by motion of the phase-point along the stable parts of the slow manifold. When instability sets in, the system responds by a rapid jump to a stable branch of the manifold. For the problem presently under consideration the slow manifold looks as follows:

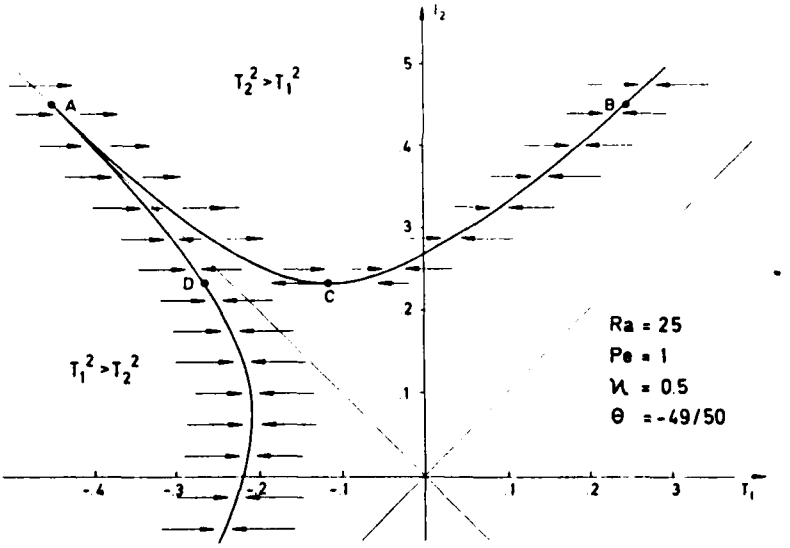

Here the cusp-like shape of the manifold is due to the nonanalyticity of the governing equations. Once the point A has been reached a fast jump to B (parallel with the T_1-axis since we are dealing with the limiting case of δ approaching zero) takes place. Hereafter follows a slow motion towards the point C, where stability once again is lost and D is reached by a jump, and so on. The analysis can, however, be improved in that the effects of a finite value of δ can be incorporated (albeit in a rudimentary manner) without taking recourse to the somewhat extreme measure of constructing matched asymptotic solutions to the problem. The above discussed jumps can be regarded as almost adiabatic, thus permitting a determination of the initial positions of the phase-point on the stable parts of the manifold making use of heat conservation. An invariance property of this type (which sadly enough most relaxation oscillators lack) is known as a Mandelstam condition (Minorsky 1962).

The results outlined here represent an extension of previous work by Lundberg and Rahm (1984).

REFERENCES

Andronov, A.A., E.A. Vitt and S.E. Khaiken, 1966. Theory of Oscillators. Pergamon Press: Oxford.

Lundberg, P. and L. Rahm, 1984. A nonlinear convective system with oscillatory behavior for certain parameter regimes. J. Fluid Mech. 139, 237.

Minorsky, N., 1962. Nonlinear Oscillations. Van Nostrand: New York.

Stommel, H., 1961. Thermohaline convection with two stable regimes of flow. Deep-Sea Res. 13, 224.

Turbulence, Chaos et Génération de Champ Magnétique

Uriel Frisch

L'évolution d'un champ magnétique $\underline{B}(\underline{r},t)$ dans un milieu conducteur animé d'un mouvement $\underline{u}(\underline{r})$ est régi par l'équation d'induction

$$\partial_t \underline{B} = \underline{\nabla}(\underline{u} \wedge \underline{B}) + 1/R_m \nabla^2 \underline{B}, \qquad (1)$$

où R_m est le nombre de Reynolds magnétique (le champ de vitesse $\underline{u}$ étant supposé convenablement adimensionné). Pour $R_m = \infty$ (milieu infiniment conducteur) l'évolution du champ magnétique est la même que celle d'une paire de particules fluides infiniment voisines. Le mouvement des particules fluides est contrôlé par le système dynamique

$$d\underline{r}/dt = \underline{u}(\underline{r}) \qquad \underline{r}(t=0) = \underline{a} \qquad (2)$$

qui est conservatif si $\nabla \cdot \underline{u} = 0$ (ce que l'on suppose). Si ce système est non-intégrable et présente du chaos, la matrice Jacobienne $\partial r_i/\partial a_j$ croît en général exponentiellement en temps et le champ magnétique aussi. Cet argument (dû à Arnold, Zeldovich, Ruzmaikin et Sokolov, 1981) montre qu'il peut y avoir une relation entre le chaos Lagrangien (c'est-à-dire le comportement chaotique des particules fluides) et l'effet dynamo (c'est-à-dire l'amplification d'une semence de champ magnétique par un écoulement conducteur). Bien entendu, la présence d'un terme de diffusion Joule ne permet pas de conclure lorsque R_m est grand mais fini: le chaos Lagrangien favorise aussi l'entortillement du champ magnetique en des configurations où une trés faible diffusion Joule peut suffire à supprimer le champ magnetique par reconnexion des lignes de force.

Pour savoir à quoi s'en tenir nous avons procédé à des expériences numériques en intégrant l'équation de diffusion. Les détails de ce travail sont décrits dans Galloway et Frisch (1984, 1985).

L'écoulement choisi a une structure eulerienne très simple stationnaire

$$\underline{u} = (A \sin z + \cos y,\ B \sin x + A \cos z,\ C \sin y + B \cos x). \qquad (3)$$

Cet écoulement, appelé ABC (A pour Arnold, B pour Beltrami et C pour Childress) a aussi fait l'objet d'une étude détaillée (Dombre, Frisch, Greene, Hénon, Mehr et Soward, 1985). Lorsqu'aucun des trois paramètres A, B et C n'est nul, les lignes de courant (identiques aux trajectoires des particules fluides) présentent la structure habituelle dans les systèmes conservatifs à deux degrés de liberté, c'est-à-dire un mélange de surfaces de KAM et de zônes chaotiques.

Des résultats numériques sur l'effet dynamo dû aux ecoulements ABC ont été obtenus pour des R_m jusqu'à 450 et divers choix des paramètres A, B et C. Pour A=B=C=1 l'effet dynamo se manifeste dans au moins deux fenêtres en R_m. La première s'étend de $\simeq$ 8 a $\simeq$ 18 et la seconde au-delà de $\simeq$ 27. Certaines symétries présentes dans l'écoulement de base sont préservées dans la fenêtre inférieure mais brisées dans la fenêtre supérieure. Le mode magnétique croissant le plus vite présente des

structures très intermittentes en forme de cigares coincidant avec les zônes chaotiques de l'écoulement. Lorsqu'un des coefficients A, B ou C s'annule, l'écoulement de base cesse d'être chaotique mais l'effet dynamo persiste (au moins jusqu'à $R_m = 1500$); dans ce cas le taux de croissance du champ magnétique atteint un maximum vers $R_m = 300$ puis semble décroître vers zéro ce qui est le comportement approprié pour une dynamo lente. Dans le cas général où l'écoulement de base est chaotique, il n'a pas encore été possible de trancher en faveur de l'existence ou non d'une dynamo rapide (c'est-à-dire dont le taux de croissance reste supérieur à un nombre positif quand $R_m \to \infty$).

REFERENCES

Arnold, V.I., Ya.B. Zeldovich, A.A. Ruzmaikin et D.D. Sokolov, 1981. Zh. Eksp. Teor. Fiz. 81, 2052; Sov. Phys. JETP 54, 1083.

Dombre, T., U. Frisch, J.M. Greene, M. Hénon, A. Mehr et A.M. Soward, 1985. "Chaotic Streamlines and Lagrangian Turbulence: The ABC Flows," prepublication Observatoire de Nice, à paraître au J. Fluid Mech.

Galloway, D.J. et U. Frisch, 1984. Geophys. Astrophys. Fluid Dynamics 29, 13.

Galloway, D.J. et U. Frisch, 1985. "Dynamo Action in a Family of Flows with Chaotic Streamlines," prépublication Max-Planck Institut für Astrophysik, Garching, soumis à Geophys. Astrophys. Fluid Dynamics.

Application of Pole Decomposition to an Equation Governing the Dynamics of Wrinkled Flame Fronts

Uriel Frisch

The Sivashinsky integral equation governing certain hydrodynamical instabilities of one-dimensional flame fronts reads:

$$\partial_t u + u\partial_x u = \Lambda u + \partial_x^2 u. \tag{1}$$

Λ is a linear singular integral operator defined conveniently in terms of the spatial Fourier transform:

$$u(t, x) = \int_{-\infty}^{+\infty} e^{ikx}\, u(t, k)\, dk \tag{2}$$

by

$$\Lambda : u(t, k) \to |k|\, u(t, k). \tag{3}$$

This equation is a special case of Lee and Chen's nonlinear plasma models (1982); as such it has a polar decomposition: equation (1) admits solution of the form

$$u(t,x) = -2\nu \sum_{\alpha=1}^{2N} \frac{1}{x - z_\alpha(t)} \tag{4}$$

The z_α's are 2N poles in the complex plane (coming in c.c pairs) moving according to the laws of polar motion ($\alpha = 1, 2, \ldots, 2N$):

$$\dot{z}_\alpha = -2\nu \sum_{\beta \neq \alpha} \frac{1}{z_\alpha - z_\beta} - i \, \text{sign} \, [\mathcal{I}(z)] \qquad (5)$$

where $\mathcal{I}$ denotes the imaginary part. When 2π spatial periodicity is assumed equations (4) and (5) are modified by summation over the periodic images into expressions involving cot $[(x - z_\alpha)/2]$ (4') and cot $[(z_\alpha - z_\beta)/2]$(5') instead of $1/(x - z_\alpha)$ and $1/(z_\alpha - z_\beta)$.

Study of the effects of binary interactions indicates that there is a tendency for alignments of poles parallel to the imaginary axis. The dynamics of 2N poles on such a "vertical" line has been investigated, both in the nonperiodic and periodic cases. It is shown analytically that a unique stable steady state is reached. The equilibrium positions of the poles can be calculated numerically. When N is large the equilibrium positions of poles condense into a continuous distribution which may be determined analytically by asymptotic methods. The corresponding solution in physical space has a wrinkle with a log-structure.

The pole decomposition of the Sivashinsky equation is at the root of its simple behavior reported by various numerical integrations (Michelson and Sivashinsky, 1977; Pumir, 1985). The pole decompositon also predicts that the wrinkles do not have a true cusp structure but are slightly rounded over a distance δ which scales like the inverse of the logarithm of the number of linearly unstable modes. δ is actually the distance from the real axis of the innermost pole; it is also the resolution that must be used in direct numerical simulations of (1).

Details of this work may be found in Thual et al., 1985.

REFERENCES

Lee, Y.C. and H.H. Chen, 1982. Phys. Scr. (Sweden) T2, 41.

Michelson, D.M. and G.I. Sivashinsky, 1977. Acta Astronaut. 4, 1207.

Pumir, A., 1985. Phys. Rev. A31, 543.

Thual, O., U. Frisch and M. Hénon, 1985. J. Phys. 46, 1485.

The Saffman-Taylor Problem: Viscous Fingering

Boris Shraiman

This talk reviews some of the recent work on the Saffman-Taylor problem: the problem of the flow of two viscous fluids in a Hele Shaw cell. Apart from its direct experimental relevance this problem is representative of the broader class of problems dealing with the evolution of interfaces in two dimensions. It is also of interest for the study of cascade into large length scales. We restrict attention to the steady finger flows and review the "pattern selection" problem: the determination of the finger velocity (or width) as a function of the control parameter. This problem was resolved by McLean and Saffman (1981) and Vanden-Broeck (1983) who showed that in the presence of the surface tension only a discrete number of steady state solutions exist. Another issue concerns the stability of the finger solutions. Contrary to the earlier calculations, the fingers appear to be linearly stable for all values of the control parameter (Kessler and Levin, 1985; Bensimon, 1985). At the same time the fingers are unstable w.r.t. finite amplitude perturbations (DeGregoria, 1985; Bensimon, 1985). Both the "selection" and the stability results are in agreement with "Monte-Carlo" numerical simulations of S. Liang (1985) and experiments of Tabeling and Libchaber (to appear).

The second part of the talk addresses the "pole dynamics" method of studying the dynamics of the interface in the absence of surface tension. In that case it is possible (for a large class of initial conditions) to reduce the evolution equation for the interface to a set of ordinary differential equations governing the motion of the critical points of the conformal mapping that maps the interface onto some standard contour (Shraiman and Bensimon, 1984). This method allows to follow the initial instability of the interface (the Mullins-Sekerka instability) into the nonlinear regime and show that many initial conditions lead to singularities in finite time (see last reference). The singularity in this case is the 2/3 power cusp in the interface.

REFERENCES

Bensimon, D., L. Kadanoff, S. Liang, B. Shraiman and C. Tang, Univ. of Chicago, to appear.

Bensimon, D., 1985. Univ. of Chicago (preprint).

DeGregoria, A.J., L.W. Schwartz, 1985. Exxon Research Lab. (preprint).

Kessler, D., H. Levin, 1985. Schlumberger-Doll Research Lab. (preprint).

Liang, S., 1985. Univ. of Chicago (preprint).

McLean, J.W. and P.G. Saffman, 1981. J. Fluid Mech. 102, 455.

Saffman, P.G. and G.I. Taylor, 1958. Proc. Roy. Soc. Lond. A245, 312.

Shraiman, B. and D. Bensimon, 1984. Phys. Rev. A30, 2840.

Tabeling, P. and A. Libchaber, Univ. of Chicago, to appear.

Vanden-Broeck, J.M., 1983. Phys. Fluids 26, 2033.

Such finite time singularities were also investigated by a number of authors: G. Meyer, "Numerical Treatment of Free Boundary Value Problem," ed. J. Albrecht (Birkhauser, Basel, 1982); S.D. Howison, SIAM, J. Appl. Math., to appear and references therein.

Report on the Arcata Conference:* Bifurcations with O(2) Symmetry

James W. Swift

"Multiparameter Bifurcation Theory" was the subject of the conference, but actually half the talks were about bifurcations with O(2) symmetry. This symmetry of the circle results when periodic boundary conditions are imposed. The simplest nontrivial example is Hopf bifurcation, where traveling and standing wave solutions bifurcate from the origin simultaneously. The nonlinear selection between traveling and standing waves is entirely analogous to the selection between roll and square planforms in stationary convection: If both solutions are supercritical the one with larger amplitude is stable.

Some of the talks at the conference were discussed, including three talks about Taylor-Couette flow in counter-rotating cylinders.

*AMS-IMS-SIAM Joint Summer Research Conference in the Mathematical Sciences (July 14-21, 1985). Martin Golubitsky and John Guckenheimer, co-chairmen.

3-D Vortex Dynamics and Singularities of the Fluid Equations

Alain Pumir

The question of singularities in the evolution of the fluid equations is addressed. Although the Navier-Stokes equations are used in many practical applications, it has not been proven so far that singularities do not appear at a finite time, even without any external forces. Only some upper bounds on the dimension of the set on which the singularities exist are known.

Physically, the evolution of the fluid is investigated by following the motion of a vortex tube. In the Euler equations, the circulation is a conserved quantity, according to the Kelvin and Helmholtz theorems. The velocity created by several tubes of vorticity can be shown to be given by a Biot-Savart like formula, at least as a low order result of an asymptotic expansion. The effect of finite-size of the core-size of each tube is accounted for by an appropriate cut-off in the integrals. Moreover the volume of space where the vorticity is concentrated is conserved.

Previous numerical simulations of this model (Siggia 1985) have revealed that two anti-parallel filaments spontaneously tend to get tightly paired, and that the resulting 'curve' then stretches very fast. Due to both volume and circulation conservation, a very strong increase of the vorticity follows.

We have shown numerically (Siggia and Pumir, preprint) that the vorticity in this model blows-up as $1/(t_0 - t)$. Several other numerical and analytical studies allowed us to understand better this ultimate stretching process. However, the relevance of our model, even for the Euler equations is not completely straightforward, since the assumptions leading to the 'Biot-Savart' formula are barely valid during the late stages of the stretching process. One has to worry about the structure of the core-size since in the ultimate stage of the blow-up, the two filaments get closer and closer. It is possible to model more carefully the core structure by representing each filament by a bundle of filaments. With this new way of modeling the vortex tubes we have shown that the blow-up process is not too dramatically modified. Though the cores may be severely distorted (the tubes are no longer cylindrical, but rather elliptical), the law of increase of the vorticity is still valid.

On the phenomenological grounds, the viscosity in the Navier-Stokes equation induces a diffusion of the vorticity, which tends to increase the cross section a of the tube:

$$da/dt = \upsilon$$

On the other hand, the stretching tends to decrease this cross sectional area of the tube, proportionally to the circulation Γ:

$$da/dt = - \Gamma$$

up to some logarithms.

This suggests that the viscosity is barely able to overcome the stretching as soon as the dimensionless ratio (Γ/υ) is large enough. The existence of a finite time singularity in the Navier-Stokes equations thus depends on some logarithmic behavior, that is probably hard to understand. If the solutions we are interested in are stable enough, with respect to both viscous and core deformation effects they provide a physical mechanism to explain the strong intermittency observed experimentally in the boundary layers, in turbulent shear flows.

REFERENCES

Siggia, E.D., 1985. Collapse and amplification of a vortex filaments, Phys. Fluids 28, 794.

Siggia, E.D. and A. Pumir. Incipient singularities in the Navier-Stokes equation (preprint).

A Session on Singularities

Interfaces in the Complex: Condensation of Poles in Burger's Equation

Jean-Daniel Fournier

Localized waves which are solutions of integrable one dimensional partial differential equations of fluid dynamics have in many cases been interpreted as the trace in real space of singular phenomena occurring in the complex (spatial) domain. This is the case for solutions of Korteweg de Vries and quasi-shocks of Burger's equation at small finite viscosity (Choodnowsky and Choodnowsky 1979; Meiss 1980), the analytic continuation of which has poles. The dynamics of those waves is governed by the motion of the set of singular points. The integrability of this motion has received much attention specifically in the case of a finite number of poles (Calogero 1978; Choodnowsky and Choodnowsky 1979; Meiss 1980). For 'generic' initial conditions one may expect an infinite number of poles sitting on lines 'above' the wave, in the complex plane. When the distance between two successive poles tends to zero, these Stokes' lines become sort of interfaces in the complex plane; they support a density of poles and form boundaries which may result in distinct analytic continuations of the solution.

Hereafter we concentrate on this condensation process in the time dependent Burger's equation in the zero viscosity limit with a paradigmatic initial condition; we report some of the results obtained in collaboration with Bessis (1984). Similiar results obtained in an asymptotic and numerical study of the stationary case of Sivashinsky's equation have been reported by Thual et al. (1985).

With the exception of t_*, where the curvature undergoes a sudden change, the Stokes' lines present a cusp-like form, with a power law shape (see for similar results Shraiman and Bensimon 1984; Pomeau 1985). At t_* one of these cusps meets its complex conjugate, forming a cubic pre-shock in the real and creating a boundary between the left and right hand side half complex planes. The subsequent scenario in the complex provides a simple interpretation of the inviscid behavior in the real. In particular,

(i) the amplitude of the shock: the shock appears at t_* with a zero amplitude, grows while it absorbs its neighborhood and eventually decays to zero with the dissipation, which does not vanish as the viscosity goes to zero, becoming the dominant effect. This is summarized in the evolution in time of the density of poles on the cusp (parallel to the imaginary axis)

$$\rho(iy,t) \underset{y \to 0}{\simeq} -i(2\pi)^{-1}\,(t-t_*)^{1/2}\,t^{-3/2}\,t^{-1/2}$$

(ii) the Burger's fluid and the gas of free particles: one can go smoothly from the left to the right hand side of the shock if one uses a multivalued velocity distribution which is locally a solution of Burger's equation and describes a gas of free particles retaining their initial velocity; of course this system differs from Burger's fluid after t_*. But a similar smooth transition can be obtained as a path in the complex; the left and right solutions are analytic continuations of each other if one uses the complete three-sheeted Riemann surface of the problem and not only the complex plane.

REFERENCES

Bessis, D. and J.-D. Fournier, 1984. J. Phys. Lett. (Paris) 45, L. 833.

Calogero, F., 1978. Nuovo Cimento B43, 177.

Choodnowsky, D.V. and G.V. Choodnowsky, 1979. Nuovo Cimento 40B, 339.

Meiss, J., 1980. Rational Solutions to Partial Differential Equations, GFD. Proceedings, W.H.O.I. Tech. Rep.-80-53, p. 225.

Pomeau, Y., 1985. GFD lecture during same session.

Shraiman, B. and D. Bensimon, 1984. Phys. Rev. A Rap. Comm. A30, 5, 2850.

Thual, O., U. Frisch and M. Henon, 1985. Application of Pole Decomposition to an Equation Governing the Dynamics of Wrinkled Flame Fronts, preprint, CNRM Toulouse; and lecture at GFD by U. Frisch.

Turbulent Viscosity: Short lecture on some efforts in recent years to make a justified use of a century old idea

Jean-Daniel Fournier

We first give a short phenomenological and experimental description of developed turbulence. A useful and old picture is to consider it as a state of matter with modified transport coefficients. These are no longer produced by molecular processes but are the result of small scale turbulence acting on large scale motion. In numerical schemes and statistical theories, however, such ideas have often been used in situatons with a continuum of locally (in Fourier space) interacting scales. Then they can hardly be justified and their success is likely to rely more on dimensional analysis than on the physics involked. As an example, we recall Heisenberg's 'derivation' of the Kolmogorov scaling law for the inertial range. So far such models have been somewhat rigorously justified in mainly two types of situations:

(i) a clear scale separation between 'large' and 'small' scale. This provides a small parameter which can be used in two-time type analysis;

(ii) a continuum of scales but with the nonlinear dynamics dominated by the nonlocal (in Fourier space) effects. The iterative procedure of the Renormalization Group (RG) then allows one to deal with the resulting scaling laws.

We illustrate (i) in reporting the phenomenological discussion of the dynamics of atmospheric turbulence with a spectral gap proposed by Pouquet et al. (1983). Point (ii) gives an opportunity to explain the RG in the context of statistical fluid dynamics (Forster et al. 1977; Fournier 1982). The scaling of the turbulent transport coefficients (see e.g.

Fournier, Sulem and Pouquet 1982 for M.H.D.) and in some cases the amplitude of the prefactor (Fournier and Frisch 1983) are obtained within an ϵ-expansion; this enables one to discuss the physics of flows studied with this technique. The nonlocality of the nonlinear interactions (Kraichnan 1982) and the absence of large distance correlations (Fournier and Frisch 1983) in the small scale dynamics are probably the main assumption. As well as for other 'statistical theories' of turbulence, this is likely to exclude any treatement of coherent structures, at least within the current state of the technique.

REFERENCES

Forster, D., D.R. Nelson and M. Stephen, 1977. Phys. Rev. A16, 732.

Fournier, J.-D., 1982. Le Calcul de la Viscosite Turbulente par une Methode de Groupe de Renormalisation Infra-Rouge, Technical Note, Observatoire de Nice.

Fournier, J.-D., P.-L. Sulem and A. Pouquet, 1982. J. of Phys. A15, 1393.

Fournier, J.-D. and U. Frisch, 1983. Phys. Rev. A28, 1000.

Kraichnan, R.M., 1982. Phys. Rev. A25, 3281.

Pouquet, A., U. Frisch, J.P. Chollet, 1983. Phys. Fluids 26, 877.

A less technical lecture but similar in spirit was given by the same author at the Astrophysics Spring School in Goutelas, France, April 1983 and appeared (in French) in the Proceedings, ed. by M. Auvergne and A. Baglin, published by S.F.S.A. Observatoire de Paris-Meudon.

Large Scale Instabilities of Cellular Flows

Melvin Stern

The temporal evolution of large amplitude quasi-geostrophic disturbances in a piecewise uniform potential vorticity flow is elucidated by numerical solutions of the "contour dynamical" equations. Lateral wave-breaking occurs when the intial disturbance amplitude exceeds a certain value, and at later times tongues of the lower vorticity fluid are engulfed or entrained into the higher vorticity shear flow. The effect appears to be important for the evolution of "shingles" observed between the coastal water and the cyclonic side of the Gulf Stream. The effect may also be an important phase in initiating the mixing process at the perimeter of an eddy embedded in another water mass.

Supercritical and Subcritical Flows in Coastal Hydraulics

Roger Hughes

Consider a coastal current flowing in the opposite direction to that in which a long first mode shelf wave usually propagates. Clearly, the current can either sweep such a shelf wave along with it (i.e., the current is of supercritical type) or the wave can propagate against the current (i.e., the current is of subcritical type). Modelling of an unstratified coastal system shows that one current of each type may exist for a given distribution between potential vorticity (or alternatively Bernoulli head) and flux streamfunction. Thus as in the classical theory of open channel flow, a current with a specified structural form may be considered to have an unrealized alternative conjugate structural form. As both the potential vorticity and streamfunction are conserved following an element of the flow under steady frictionless conditions, irregularities in the coastline or bottom topography may cause a transormation of the current structure to its conjugate as the flow proceeds downstream.

Further modelling shows that stratification does not destroy the conjugate behavior described above. At large flows, stratification enables a similar conjugate behavior based on internal Kelvin waves to develop from the shelf wave supercritical structural form of the current. Such conjugate behavior was noted by Gill and Schumann (1979). Conjugate behavior based on higher mode shelf waves may also be found. Such behavior develops from within the first mode shelf wave subcritical structural form of the current.

Let us consider in detail the conjugate behavior associated with the first mode shelf wave. Under exceptional circumstances, the two conjugate structural forms become indistinguishable. We refer to such conditions as critical. It may be shown that eastern boundary flows are apt to develop critical conditions as they move towards the equator. Thus although exceptional, such conditions could conceivably be found in the California Current, for instancae. Interestingly, a current of a high mode shelf wave conjugate type develops first mode shelf wave ciritical conditions with flow reversals in the far field as is observed at times in the outer reaches of the California Current. Of course, wind and friction may be expected to modify the inevitability of this conclusion.

It may be shown that a topographically induced disturbance within a subcritical flow contains lee waves. However, no such lee waves are found in the response within a supercritical flow. Despite this major difference in the form of the disturbance, the disturbance is weak for both types of current unless conditions are near critical. Under such near critical conditions, topographic irregularities have a strong influence on the flow as observed to occur within the California Current.

Consideration of a finite amplitude theory designed to represent the strong response at conditions of near criticality shows the possibility of large off-shelf excursions of the flow possibly indicative of the squirts found by Mooers and Robinson (1984). The theory has been used to study flow along a sinusoidally varying coastline. For realistic parameters a wavelength doubling of the response is possible. Thus by

Feigenbaum's (1980) scenario a spatial chaos might be expected. A spatial chaos would manifest itself as a temporal chaos indicative of the turbulent nature of the California Current. Interestingly, the Reynolds' stresses associated with such behavior are of the correct form to move the flow away from critical conditions. Thus a balance is predicted between the influences of both equatorward movement and eddies on the dynamics of an eastern boundary current.

The California Current has many characteristics of a near critical flow. However, observations of shelf waves in the region indicate that the current has little effect on such waves. Fortunately for the present theory Davis (1985) has noted that there appears to be a much slower propagation within the California Current. Consideration of the structure of the California Current suggests that the level of no motion (i.e., critical level to topographically induced waves) isolates the California Current from the surrounding poleward flow. Some evidence for this idea may be found in observations of a weak stratification at the base of the California Current as required by the isolation mechanism recently suggested by Smith (1985) for atmospheric meso-scale flows.

REFERENCES

Davis, R.E., 1985. Drifter Observations of Coastal Surface Currents During CODE: The Statistical and Dynamical Views. J. Geoph. Res. 90, 4756-4772.

Feigenbaum, M.J., 1980. Universal Behavior in Nonlinear Systems. Los Alamos Science 1, 4-27.

Gill, A.E. and E.H. Schumann, 1979. Topographically Induced Changes in the Structure of an Inertial Coastal Jet: Application to the Agalhas Current. J. Phy. Oceanog. 9, 975-991.

Mooers, C.N.K. and A.R. Robinson, 1984. Turbulent Jets and Eddies in the California Current and Inferred Cross-Shore Transports. Science 223, 51-53.

Smith, R.B., 1985. On Severe Downslope Winds, J. Atmos. Sci., accepted.

Chaos in Surface Waves: Theory in Spiegel's Wake

Itamar Procaccia

We considered an experiment conducted by Ciliberto and Gollub on the transition to chaos in the dynamics of surface waves on the free surface of a fluid contained in a cylinder that is oscillated vertically. This experiment has been picked as a case model for understanding the appearance of low dimensional chaos in systems with infinite degrees of freedom. The hydrodynamic description of the system was used as a starting point for the derivation of low dimensional ODE's that pertain to the onset of chaos. The Center Manifold Theorem and Normal Form Theory were used very much in the foot steps of Coullet and Spiegel to obtain the minimal nonlinear model. The results of the theoretical treatment rationalize the observed phenomena in considerable detail.

Theory of Strange Sets with Applications to Almost Everything

Itamar Procaccia

In this lecture we reviewed theory for the characterization of Chaotic Dynamics via invariants like dimension and entropy. The discussion was focussed on properties of fractal measures. Such measures call for a spectrum of generalized dimensions for their complete characterization. These dimensions were introduced and applied to strange attractors. The definition of generalized dimensions was used as a springboard for an analysis of fractal measures via their singularities. It was argued that quite generally one can consider fractal measures as interwoven sets of singularities of varying strengths, such that each type of singularity lives on a fractal set. A formalism to unfathom this complexity was presented and applied to diffusion limited aggregation, and to important sets from dynamical system theory.

Double-diffusive Interleaving

Judith Y. Holyer

At ocean fronts there are commonly density compensating horizontal gradients of heat and salt. The presence of these horizontal gradients can lead to the formation of layers that propagate almost horizontally. It is believed that the layers are driven by a double-diffusive instability that acquires energy from the horizontal heat and salt gradients. The intrusions can exist in regions where both heat and salt are stably stratified in the vertical and they have been observed in the ocean by Joyce, Zenk and Toole (1978) and Gregg and McKenzie (1979) amongst others.

Holyer (1983) has investigated this instability theoretically and has shown that even when both vertical gradients are stable the system is unstable, and interleaving regions grow. Kerr and Holyer (1985) have extended this model to include the effects of rotation. These two papers describe the initial instability that occurs by molecular processes. The theory predicts that hot, salty intrusions sink. As the interleaving develops Holyer (1983) shows how alternating salt-finger and diffusive interfaces appear. When this occurs heat and salt will no longer be transported by molecular processes. It is possible to control whether a finger interface or a diffusive interface appears first by altering the vertical gradients. This affects the slope of the intrusion.

This seminar gave a review of interleaving and also reported on some experiments that were performed at Bristol University with the intention of finding out how the layering depended on the vertical gradients of the two components. Previous laboratory experiments by Ruddick and Turner (1979) did not investigate this and assumed that the layering depended only on the vertical density gradient and not which component the gradient was made from. It has been stated that intrusions must slope so that hot, salty water rises. We show laboratory experiments where the opposite occurs and hot, salty intrusions sink. Schmitt and Georgi (1982) appear to have oceanic evidence of an intrusion that slopes in this sense. Oceanographers should be aware that double-diffusively driven intrusions can slope in either sense.

REFERENCES

Gregg, M.C. and J.H. McKenzie, 1979. Thermohaline intrusions lie across isopycnals. Nature 280, 310-311.

Holyer, J.Y., 1983. Double-diffusive interleaving due to horizontal gradients. J. Fluid Mech. 137, 347-362.

Joyce, T.M., W. Zenk and J.M. Toole, 1978. The anatomy of the Antartic Polar Front in the Drake Passage. J. Geo. Res. 83, 6093-6113.

Kerr, O.K. and J.Y. Holyer, 1985. The effect of rotation on double-diffusive interleaving. Accepted by J. Fluid Mech.

Ruddick, B.R. and J.S. Turner, 1979. The vertical length-scale of double-diffusive intrusions. Deep Sea Res. 26A, 903-913.

Schmitt, R.W. and P.J. Georgi, 1982. Finestructure and microstructure in the North Atlantic Current. J. Mar. Res. (Supplement) 40, 659-705.

Instability of Vortices

Glenn Flierl

The equations for linearized perturbations on an f plane circular vortex with piecewise constant potential vorticity can be derived very simply using the contour dynamics approach. If we consider a two layer quasi-geostrophic model with each layer having constant potential vorticity in the regions $0 \le r < 1$, $1 < r < b$ (Figure 1) in the basic state, the perturbation streamfunction can be expressed in terms of the interface perturbations by

$$\nabla^2\psi^{(1)} + \frac{\gamma^2}{1+\delta}\left(\psi^{(2)}-\psi^{(1)}\right) = -\bar{Q}_r^{(1)}\eta = -\left(q_b^{(1)}-q_1^{(1)}\right)\eta_1^{(1)}\delta(r-1) + q_b^{(1)}\eta_b^{(1)}\delta(r-b) \quad (1)$$

$$\nabla^2\psi^{(2)} + \frac{\gamma^2\delta}{1+\delta}\left(\psi^{(1)}-\psi^{(2)}\right) = -\bar{Q}_r^{(2)}\eta = -\left(q_b^{(2)}-q_2^{(2)}\right)\eta_1^{(2)}\delta(r-1) + q_b^{(2)}\eta_b^{(2)}\delta(r-b)$$

Here $\delta = H_1/H_2$ is the ratio of the layer depths and $\gamma = L/R_d$ is the ratio of the inner core radius to the deformation radius. The q's are the constant potential vorticity values in the various regions. The equations for the evolution of the interfaces determine the growth rates: if we let $\eta_j^{(i)} = \eta_j^{(i)}\exp[im(\theta - \Omega t)]$ we find

$$\begin{aligned}\left(\bar{V}_1^{(i)}-\Omega\right)\eta_1^{(i)} &= \psi^{(i)}(1)\\ \left(\frac{\bar{V}_b^{(i)}}{b}-\Omega\right)\eta_b^{(i)} &= \frac{1}{b}\psi^{(i)}(b)\end{aligned} \quad (2)$$

The linear form of equation set (1) allows us to write

$$\begin{pmatrix}\psi^{(1)}(1)\\ \psi^{(1)}(b)/b\\ \psi^{(2)}(1)\\ \psi^{(2)}(b)/b\end{pmatrix} = \underset{\approx}{M}\begin{pmatrix}\eta_1^{(1)}\\ \eta_b^{(1)}\\ \eta_1^{(2)}\\ \eta_b^{(2)}\end{pmatrix}$$

and (2) becomes a standard eigenvalue equation for Ω with the eigenvector defining the perturbed interface structures. Analyzing various cases, we find

(1) For barotropic vortices:

(a) Barotropic perturbations:
When $q_b > q_1 > 0$, the high azimuthral modes enter first.
The elliptical ($m = 2$) and squeezing mode ($m = 1$) are stable.
When $q_b < 0 < q_1$, the elliptical mode becomes unstable first as the parameter b decreases. When the eddy is isolated ($V = 0$ for $r > b$), the critical size is $b = 2$, $q_b = -1/4\ q_1$.

(b) Baroclinic perturbations:

When the eddy has a size on the order of the deformation radius ($\gamma \sim 1$), baroclinic squeezing mode perturbations (m = 1) can grow more rapidly than the barotropic perturbations and may be unstable even when all the barotropic modes are stable.

(2) For isolated baroclinic vortices, with V = 0 when r > b:

(a) When $\gamma \lesssim 1$, the instability occurs only for small enough outer radius b. It resembles the barotropic instability above.

(b) When $\gamma \gg 1$ (large eddies compared to the deformation radius), only one mode is unstable but its growth rate is insensitive to b. This is basically a baroclinic instability of the inner vortex.

In addition, the steady state weakly nonlinear structures have been studied for the barotropic vortices. The equations for a steadily rotating shape were solved by expansion in the amplitude of the deviation from the circular form. We attempted to determine the rate of rotation of the structure Ω as a function of the amplitude

$$\Omega(A \mid m, b, q_b/q_1) = \Omega_o + A^2\Omega_1$$

For isolated eddies with $q_b/q_1 < 0$, we find that finite amplitude solutions exist only in the linearly stable regime. Thus the Ω's look like the sketch (Figure 2). This suggests that nonlinear interactions will not lead to equilibration of the unstable vortex.(For solutions $q_b/q_1 > 1$ our results are less complete but suggest that finite amplitude solutions may exist in the unstable range, so that it is reasonable to think of a small perturbation growing and equilibrating [in the presence of dissipation] or vacillating around this finite amplitude state.) Numerical experiments confirm that the elliptical mode perturbation indeed does not equilibrate but instead the vortex breaks into two dipoles (Figure 3). We suspect that in many cases, the unstable perturbations will not equilibrate until some vorticity contours have overturned and broken. In this sense, the amplitude is not likely to be everywhere "small."

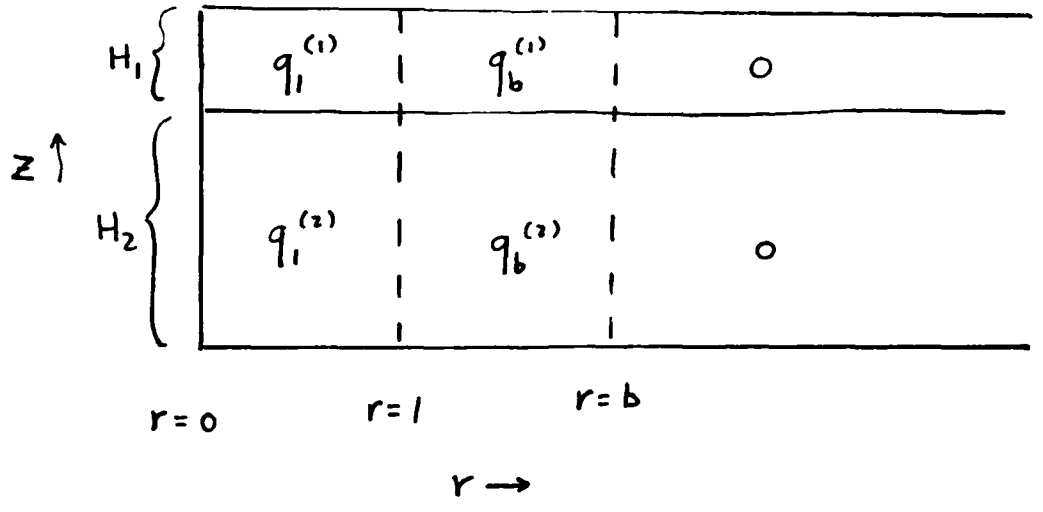

Figure 1: Potential vorticity distribution in the basic state vortex.

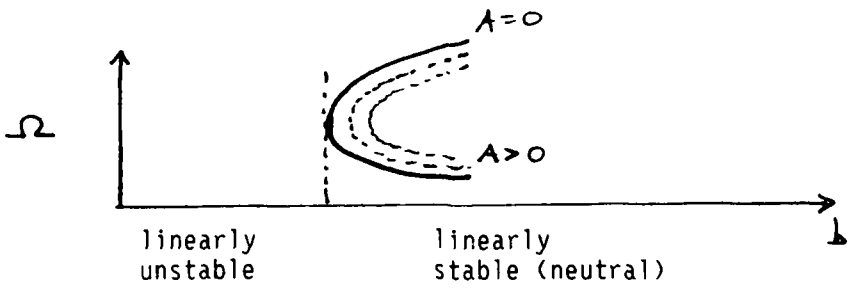

Figure 2: Sketch of dependence of Ω upon the outer radius b and the perturbation amplitude A.

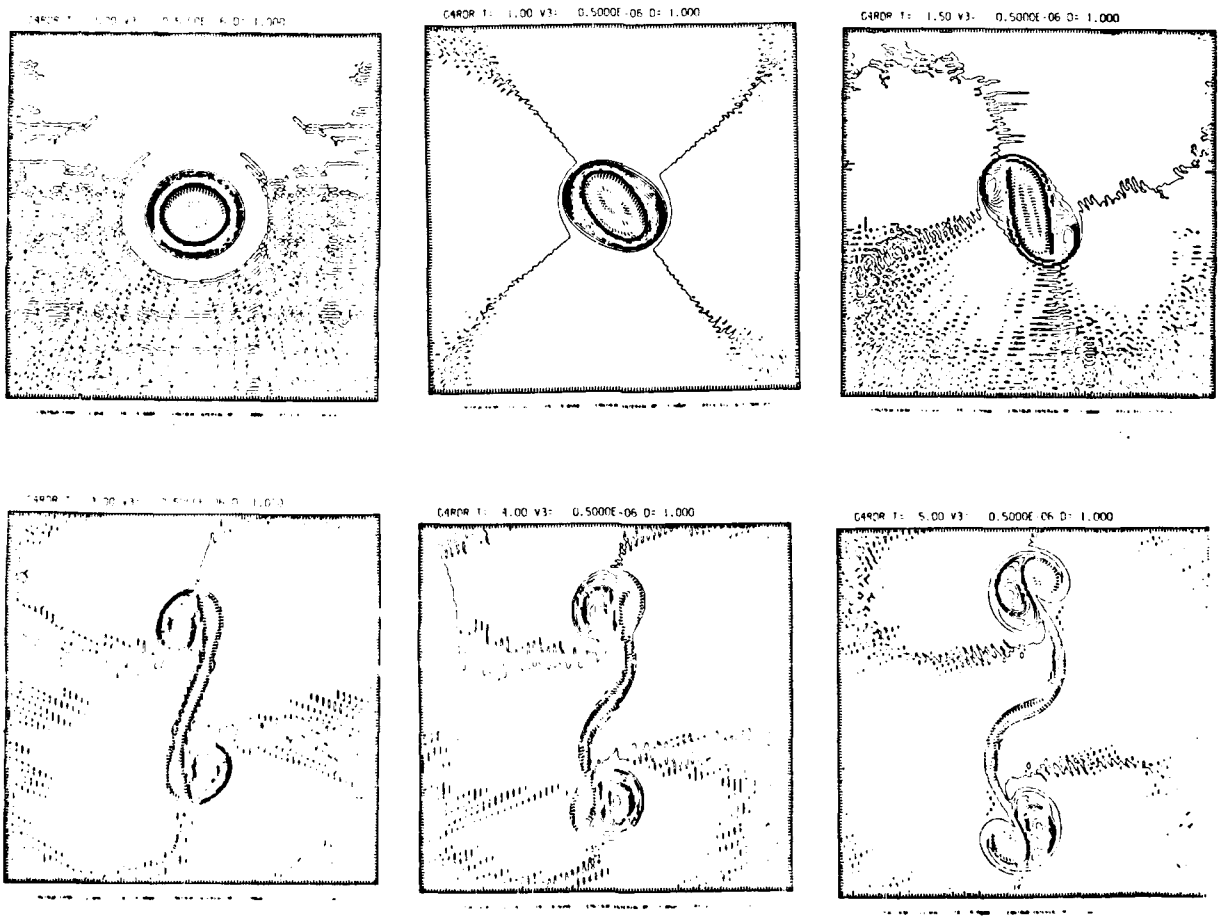

Figure 3: Breakup of an unstable vortex to yield two dipoles. Vorticity maps are shown at various times.

Nonlinear Pattern Formation From Instabilities

J. P. Gollub

When a periodic spatial structure arises from an instability, there are generally many possible structures (a continuum of wavevectors, for example). However, various processes constrict the set of patterns that can actually be realized experimentally as stationary states. These include secondary instabilities such as the Eckhaus instability, external periodic forcing, and pattern selection by boundaries and defects. These phenomena are illustrated by various recent experiments performed in our group at Haverford College and The University of Pennsylvania.

1. The Eckhaus Instability

The Eckhaus instability is a general mechanism of pattern selection for any translationally invariant system where a normal bifurcation produces a spatially periodic structure in one space direction. The linear stability curve and the boundary of the Eckhaus secondary instability are tangent at the minimum. The instability leads to slow spatial modulations of the phase and amplitude of the roll pattern, the nucleation or elimination of roll pairs, and eventually a new pattern with a wavenumber closer to the critical value. This phenomenon is difficult to observe, both because it is often masked by other secondary instabilities, and because of boundary effects. We have performed the first direct observations (Lowe and Gollub, 1985a) of the space and time evolution of the Eckhaus instability, using electrohydrodynamic convection to obtain a sample containing at least 150 rolls. By controlling the initial wavenumber of the roll pattern and the layer depth, we are able to make precise measurements of the stability boundaries and the time evolution of various spatial Fourier components of the pattern. The stability curve and the wavenumber of the secondary flow are consistent with predictions based on an amplitude equation, an expansion in powers and derivatives of a slowly varying field. The late stages of the evolution suggest the need for further theoretical studies. The experiments document the complexity of the convective instability, which arises from the fact that (at least) two stability curves are joined together at the onset. Thus, there are two competing instabilities, one for the amplitude of the rolls, and another primarily for the phase.

2. Pattern Selection By Spatial Forcing

If the translational invariance of the system is broken by an external spatially periodic perturbation, the nature of the stable patterns can be dramatically changed. In fact, a great variety of novel states can be produces (Lowe and Gollub, 1985b; Lowe, Gollub and Lubensky, 1983), including: commensurate phases in which the hydrodynamic flow is "phase-locked" to the perturbation; incommensurate states containing soliton-like discommensurations that are the spatial analog of quasiperiodicity; and complex structures that contain an apparently random array of defects. These are all stable configurations of the flow in the presence of external forcing. They demonstrate the intricacy of the process of pattern selection.

3. Pattern Selection by Boundaries and Defects: Minimization

The patterns produced by Rayleigh-Bénard convection in a laterally large layer do not approximate the straight parallel rolls envisioned by linear stability theory. Rather, the patterns are textured and contain defects. The actual patterns that are produced are a compromise between boundary effects that favor perpendicular alignment of the rolls, and bulk effects that favor reductions in both curvature and wavenumber variations by eliminating defects. We have studied the competition between these various processes quantitatively by using digital processing of shadowgraph images (Heutmaker, Fraenkel and Gollub, 1985). It is possible to characterize the patterns by a wavevector field q(r) that contains the local information about spacings and orientations. Using this field, we have been able to test a two dimensional model of pattern formation known as the Swift-Hohenberg model. This model has the interesting property that the evolution minimizes a Lyapunov functional that can be expressed in terms of the wavevector field. We find that the model provides a pretty good description of the process of pattern evolution for a range of Rayleigh numbers beyond the immediate vicinity of the threshold, but below $R = 3R_c$. This implies that convective patterns behave much like elastic media that minimize a combination of certain elastic energies.

4. Chaos near the Juncture of Two Stability Curves

We close by briefly pointing out that studies of pattern formation may eventually provide some insight into the problem of chaotic motion in fluids. An example where this may be possible occurs in a study of parametrically forced surface waves in a cylindrical container (Ciliberto and Gollub, 1984 and 1985). Different modes of surface oscillation (with different spatial symmetries) occur as the driving amplitude and driving frequency are varied. We find that in some cases two stability curves (for two different modes) can cross. Near the intersection, which is a co-dimension two bifurcation, chaotic flows are found. The behavior of the system near the intersection is in good agreement with a simple nonlinear model based on two coupled forced (and damped) Mathieu oscillators.

Acknowledgement: The work summarized here was supported by NSF grants SM-8310933 and DMR-3216718. I am indebted to the collaborators listed in the references.

REFERENCES

Cilliberto, S. and J.P. Gollub, 1985. "Chaotic Mode Competition in Parametrically Forced Surface Waves," J. Fluid Mech., to appear; Phys. Rev. Lett. 52, 922 (1984).

Heutmaker, M.S., P.N. Fraenkel, and J.P. Gollub, 1985. "Convection Patterns: Time Evolution of the Wavevector Field," Phys. Rev. Lett. 54, 1369.

Lowe, Mary and J.P. Gollub, 1985a. "Pattern Selection Near the Onset of Convection: The Eckhaus Instability," to appear.

Lowe, Mary and J.P. Gollub, 1985b. "Solitons and the Commensurate-Incommensurate Transition in a convection Nematic Fluid," Phys. Rev. A 31, 3893; M. Lowe, J.P. Gollub and T.C. Lubensky, 1983. Phys. Rev. Lett. 51, 786.

Salt Fingers in a Hele Shaw Cell: Experiment and Theory

George Veronis

The Hele Shaw cell was made up of two glass plates of dimensions 50 x 30 cm and separated by a 1 mm gap. A salt solution of density 1.02 g/cm^3 occupied the lower half of the cell initially. The upper half had a sugar solution of density 1.01 g/cm^3. A barrier between the two fluids was withdrawn at time, t = 0, to start the experiment. The Hele Shaw cell makes it possible to follow individual salt fingers as they grow from thin, short features to relatively wide (compared to the gap width) fingers. A series of photographs recorded the evolution.

As the salt finger zone occupying the region between the two reservoirs becomes longer, the stabilizing salt gradient becomes weaker and the width of the fingers must grow. Wider fingers appear to be generated near, and penetrate in from, the outer edges of the finger zone where the mean gradients are weaker. There is smaller scale structure where these penetrating descending and ascending fingers "collide" and adjust so that they form a pattern of up- and down-going fingers.

When the Hele Shaw cell is inclined at the angle, θ, with the horizontal, the effect of gravity is reduced to g $\sin\theta$. Since the width of the fingers is proportional to $g^{-1/2}$, the preferred width of the fingers is increased. Thus, it was possible to generate a pattern of salt fingers of one size at one value of θ and then to alter θ abruptly so that a new finger size is preferred. When θ is increased from some small value, a wide cell becomes unstable to a disturbance inclined at about 45° to the horizontal and a thin interface region between ascending and descending cells takes the shape of a fern leaf pattern. The ends of the fern leaves turn toward the vertical to create intermediate cells. When θ is decreased, wider cells penetrate in from the outer regions of the salt finger zone in a manner reminiscent of evolving fingers.

The linear stability analysis of a pattern of fingers periodic in the horizontal and independent of the vertical coordinate was based on Floquet theory. The fern-leaf pattern of unstable modes for wide cells emerges from the analysis. The stability analysis for cells of arbitrary horizontal scale is still underway.

Howard (1984) gave a preliminary report on a model of steady fingers of finite height driven by a vertical difference (rather than a vertical gradient) of the destabilizing component. The analysis assumes that the diffusivity of the destabilizing component is much smaller than that of the stabilizing component. The lowest order solution assumes vertically infinite fingers. When the correction due to the small diffusivity is incorporated, fingers of finite length can be analyzed. The same analysis for flow in a Hele Shaw cell is somewhat simpler and has been carried out. Fingers that maximize the buoyancy flux have a horizontal scale that is approximately twice the width of a buoyancy boundary layer at lowest order. The analysis for the diffusive correction is valid provided that the ratio of the diffusivities is not greater than about 0.07. Therefore, the model is valid for the heat-salt systems but is not appropriate for the salt-sugar experiment.

Acknowledgement: The experiments were carried out together with John Taylor in Canberra.

REFERENCE

Howard, L.N., 1984. "The Salt Finger Zone," GFD Proceedings, WHOI-84-44, 85-89.

High Reynolds Number Taylor-Couette Turbulence

Willem V.R. Malkus

This extended abstract contains an outline of summer progress on a quantitative theory for the averaged properties of fully turbulent shear flow. The zeroth-order step in the "decoupled-mean" theory (Malkus, 1983) is applied to Taylor-Couette turbulence and compared to the Townsend-Smith 1983 data. The mean boundary layer found in that data at Reynolds numbers of 100,000 is not logarithmic, but varies as the one-third power of distance from the boundary. This observation is in keeping with the Monin-Obukhov similarity theory for buoyancy layers (M. Claussen, 1984). Claussen and I have planned to apply the quantitative and more mechanistic absolute marginal stability theory to the entire mean circulation profile for swirling flow. The zeroth step described here is to find a circulation profile which is absolutely stable to all possible disturbances, but just barely so. The absolute stability condition for Taylor-Couette flow (D.D. Josephs, 1976) parametrically abuts the linear instability condition for narrow-gap flows. The inviscid limit of these stability requirements is the Rayleigh discriminant

$$\Phi = -(1/r^3)(\partial\Gamma^2/\partial r) = -2\Omega[\Omega + (\partial V/\partial r)]$$

where r is the radius and $\Gamma = Vr = \Omega r^2$ is the circulation, and where Φ must be less than zero to assure stability. For swirling flow with an axial velocity W(r), one can apply the Rayleigh discriminant for local helical disturbances inclined at an angle α, where

$$\tan\alpha = (\partial W/\partial r)/(\partial V/\partial r)$$

to the plane containing the vectors $\underline{V}$, and rediscover the Liebovich-Stewartson instability condition

$$-(\partial\Gamma/\partial r - \partial\Gamma/r)\ [(\partial\Gamma/\partial r - 2\Gamma/r)\,\partial\Gamma/\partial r + r^2(\partial W/\partial r)^2\ ] \equiv \mathcal{L} \geq 0$$

This, then, should be the inviscid measure of absolute stability for all flows in which $\partial W/\partial r < \partial V/\partial r$. For $\partial W/\partial r > 10\,\partial V/\partial r$ one expects that Poiseuille-like shear instabities may dominate the flow. A passing observation is that the critical Richardson number is

$$R_i \equiv -\frac{1}{r^3}\frac{\partial\Gamma^2}{\partial r}\Big/\left(\frac{\partial W}{\partial r}\right)^2 = 1$$

for these three dimensional flows, when $\partial\Gamma/\partial r \ll \Gamma/r$.

For buoyancy driven flows instability can be marginally assured if

$$\mathcal{L} \equiv I^*I, \qquad I = \sum_{k=0}^{k_o} I_k e^{ik\varphi}$$

where k_o measures the just unstable viscously controlled scale of the

boundary layer, and where $0 \leq \varphi \leq 2\pi$ across the gap.. The rigid boundary conditions on the mean field require that

$$0 = \Sigma k^2 I_k^* \Sigma I_k + \Sigma k^2 I_k \Sigma I_k^* - 2\Sigma k I_k \Sigma k I_k^*$$

A first estimate for the I_k leading to optimum stability are those that lead to maximum angular momentum flux. For narrow-gap flows these are found to be

$$I_k = (15/13k_o)^{1/2} [1 - 6(k/k_o) + 4(k/k_o)^2].$$

Numerical solution of the cubic equation for $\partial\Gamma/\partial r \equiv \Gamma'$,

$$-(\Gamma' - 2\Gamma/r)[(\Gamma' - 2\Gamma/r)\Gamma' + r^2W'^2] = I^*I$$

and integration to determine $\Gamma(r, k_o)$ provides a qualitative field, containing a one-third law and an interior region of reverse Γ' as does the Townsend data.

More exciting is the quantitative step to determine $k_o(R)$ from the absolute stability intergral. First estimates indicate a value well within a factor of two of the data. Certainly another iteration towards the correct theoretical value will be made this fall. To date then, the results support the proposal that fully turbulent flow is 'adjacent' to a polycritical surface in phase space whose dimensions increase as the square root of the Reynold's number.

REFERENCES

Claussen, M., 1984. Surface Layer Similarity in Circular Couette Flow, J. Fluid Mech. 144, 123.

Joseph, D.D., 1976. Stability of Fluid Motions I, Springer-Verlag, Berlin.

Leibovich, S. and K. Stewartson, 1983. A Sufficient Condition for the Instability of Columnar Vortices, J. Fluid Mech. 126, 335.

Malkus, W.V.R., 1983. The Amplitude of Turbulent Shear Flow, PAGEOPH Vol. 121, 391.

Smith, G.P. and A.A. Townsend, 1983. Turbulent Couette Flow between Concentric Cylinders at Large Taylor Number, J. Fluid Mech. 123, 187.

Transition and Turbulence in Fluid Flows and Low-Dimensional Chaos

K.R. Sreenivasan

Recent studies of the dynamics of low-dimensional nonlinear systems with chaotic solutions have produced very interesting and profound results with several implications in many disciplines dealing wth nonlinear equations. However, the interest of fluid dynamicists in these studies stems primarily from the expectation that they will help us understand better the onset as well as dynamics of turbulence in fluid flows. At this time, much of this expectation remains untested, and many unanswered a priori questions exist, especially in 'open' or unconfined fluid flows. The work described in the talk was aimed at filling some of this gap.

Measurements made in the wake of a circular cylinder, chiefly in the Reynolds number range of about 30-10^4, were analyzed to show aspects of similarity with low-dimensional chaotic dynamical systems. In particular, it is shown that the initial stages of transition to turbulence were characterized by narrow windows of chaos interspersed between regions of order. The route to the first appearance of chaos was shown to be much like the envisaged by Ruelle and Takens (Reulle and Takens, 1971); with further increase in Reynolds number, chaos disappears and a return to three-frequency quasiperiodicity occurs. This is followed in turn by the reappearance of chaos, a return to multifrequency quasiperiodicity, reappearance of chaos, and so on; we have observed several alternations between order and chaos below a Reynolds number of about 200, and suspect that even more exist in the higher Reynolds region. Each window of chaos is associated with a near-discontinuity in the vortex shedding frequency and the rotation number, as well as a dip in the amplitude of the vortex shedding mode. It was further shown that the dimension of the attractor constructed using time delays from the measured velocity signals was truly representative of the number of degrees of freedom in the ordered states interspersed between windows of chaos; within the windows of chaos, the attractor was shown to be characterized by a positive Lyapunov exponent and frational dimension varying between 2.6 and 6. Our measurements and dimension calculations (whose reliability or dimension values exceeding about 8 - 10 is questionable) suggest that the dimension is no more than about 20, even at a moderately high Reynolds number of 10^4.

In the talk, most of these measurements were interpreted in terms of the physical events occuring in the flow.

REFERENCE

Ruelle, D. and F. Takens, 1971. Commun. Math. Phys. 20, 167.

An Experiment on the Transition from Quasiperiodicity to Chaos

A. Libchaber

The experiment is a Rayleigh Benard one, the fluid mercury, in a small aspect ratio cell with two rolls (Libchaber, Laroche and Fauve, 1983).

Existence of quasiperiodic states results from two different oscillating states in the fluid. One is the natural oscillatory instability present for low Prandtl fluids above the onset of convection (Busse, 1978). The second one is imposed externally on the flow velocity field by an electromagnetic excitation which creates an oscillating vertical vorticity (Siggia and Zippelius, 1981). With such a state, by sweeping the frequency and amplitude of the forced oscillation, one can plot the Arnold tongues describing the various phase locked states in an amplitude versus winding number Ω ($\Omega = f_1/f_2$) plot (Stavans, Heslot and Libchaber, 1985).

Figure 1 shows some of the large tongues which follow the Farey construction (Jensen, Bak and Bohr, 1984). The inserts of figure 1 show locking states associated with Fibonocci approximants of the Golden and Silver mean (Shenker, 1982), $\Omega = \sqrt{5}-1/2$ and $\Omega = \sqrt{2} - 1$. From the experiment the following measurements have been performed:

-For the Arnold tongues we have measured the fractal dimension of the devil staircase at the critical line $D \cong 0.85$.

-For the irrational route to chaos at the golden mean we have measured the dimension of the attractor at the chaotic point $D \cong 1$.

-For $\Omega = \sqrt{5}-1/2$ and $\Omega = \sqrt{2}-1$ we have measured the two critical exponents δ and α.

The agreement between this experiment and a circle map model is good. There is by now no theory relating the fluid equations, in the small aspect ratio case, to a circle map iteration scheme.

REFERENCES

Busse, F.H., 1978. Rep. Prog. Phys. 41, 1929.

Jensen, M.H., P. Bak and T. Bohr, 1984. Phys. Rev. A30, 1960.

Libchaber, A., C. Laroche and S. Fauve, 1983. Physica 7D, 73.

Shenker, S.J., 1982. Physica 5D, 405.

Siggia, E.D. and A. Zippelius, 1981. Phys. Rev. Lett. 47, 835.

Stavans, J., F. Heslot and A. Libchaber, 1985. Phys. Rev. Lett.

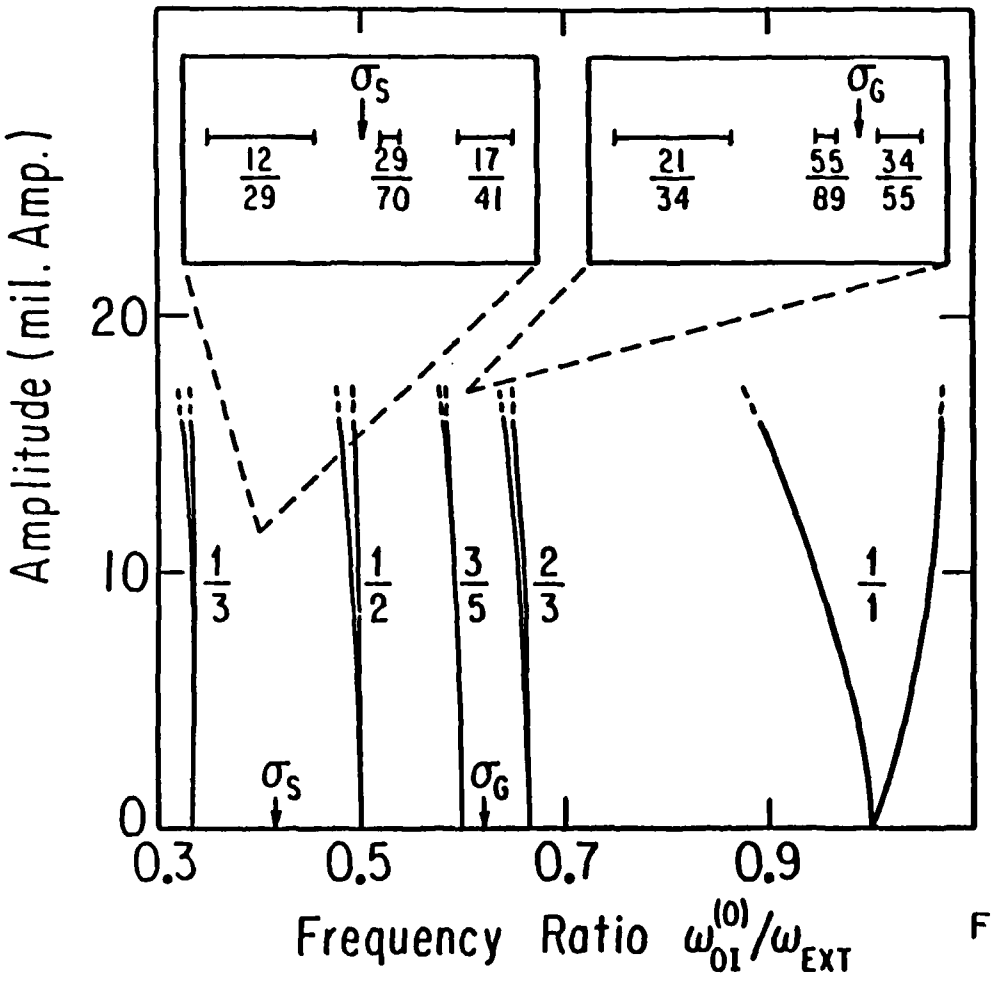
σS
12/29
29/70
17/41
σG
21/34
55/89
34/55
Amplitude (mil. Amp.)
20
10
0
1/3
1/2
3/5
2/3
1/1
σS
σG
0.3
0.5
0.7
0.9
Frequency Ratio ω(0)OI/ωEXT

Fig.1

Directional Solidification of a Dilute Binary Alloy

John Bechhoefer

Physical problems concerning the motion of interfaces have recently attracted wide attention. Together with Albert Libchaber and Francois Heslot, I have studied interface dynamics in the context of the directional solidificaion of an organic molecule called succinonitrile, doped with an impurity.

Our experimental apparatus (figure 1) is adapted from that of Jackson (Jackson and Hunt, 1966).

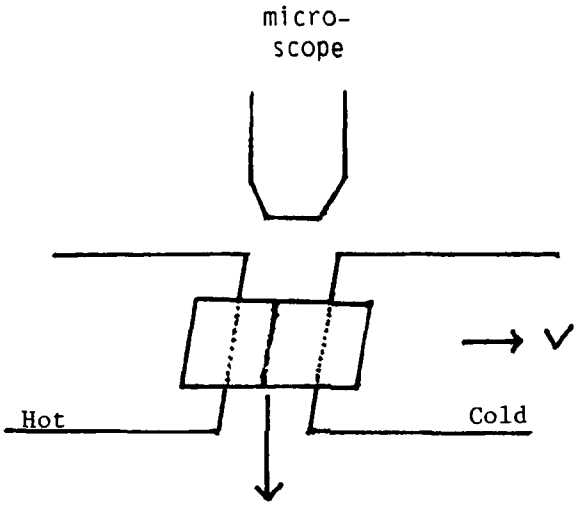

solid-liquid interface

Figure 1

A cell containing a thin (10 μm) layer of succinonitrile ($NC(CH_2)_2$ CN) is placed atop two copper blocks, one of which is at 80°C, the other at 20°C. There is a gap of 2 μm between the blocks. Since the melting temperature of succinonitrile is 60°C, there appears a solid-liquid interface between the blocks. The sample is then pushed at a constant velocity $V \approx 1$ μm/second from the hot to the cold side of the apparatus. The interface acts as a "seed" for new crystallization, and the interface advances. After a transient, which last for several hours, the interface will advance with a velocity -V that just compensates for the pushing of the cell. For slow velocities ($\approx .1$ μm/sec), the interface remains a straight line (figure 2).

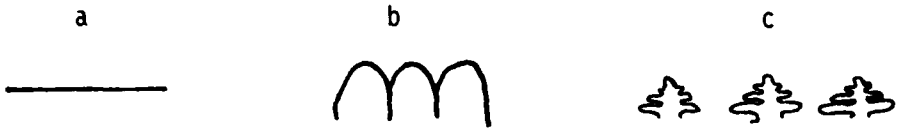

flat cellular dendritic

Figure 2

For higher velocities ($\approx$1 μm/sec) the interface is cellular - it advances with liquid grooves separating solid "fingers" (figure 2b). For still higher velocities ($\approx$ 5 μm/sec) the interface is dendritic - the fingers have developed sidebranches, which themselves can branch, and so on (figure 2c).

The physics of the pattern formation turn out to be governed by the distribution of impurities in the succinonitrile. To visualize this distribution, we have added a dye, rhodamine 6G. The dye is highly soluble in succinonitrile, has a high quantum efficiency (and hence is bright), and is excited by visible light rather than ultraviolet radiation (and hence is easy to work with). Other methods for studying the distribution of impurities exist, but they generally involve freezing the crystal and then performing chemical tests on thin sections of the crystal (Jim and Purdy, 1974). Our method is "noninvasive."

The effect of impurities is illustrated in figure 3.

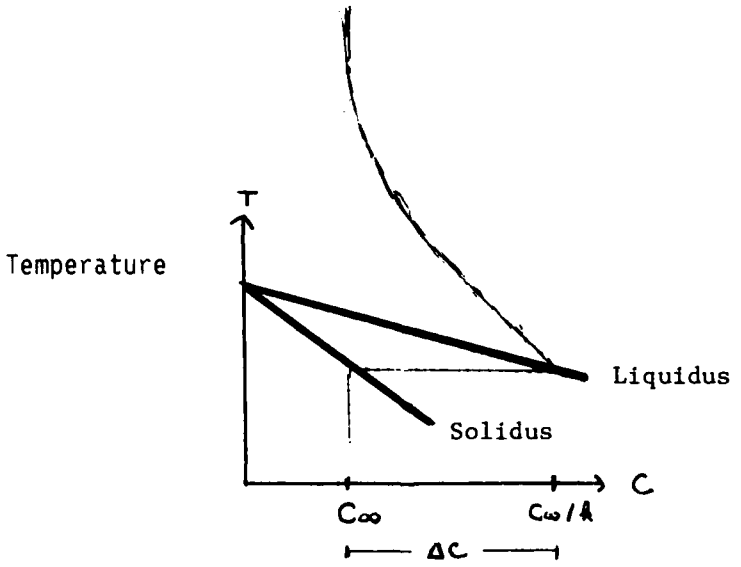

Concentration of Impurities

Figure 3

At a finite average level of impurities c_∞, the melting temperature no longer equals the freezing temperature; rather, liquid and solid coexist over a range of temperature. Also, the concentration of impurities on the solid side of the liquid-solid interface is much less than that on the liquid side. Their ratio, k, is about .1 for succinonitrile and rhodamine. The interface shape is also influenced by the solid-liquid surface tension. A curved interface will be at a temperature that differs from the temperature of a flat interface by $T = T_m d_o \kappa$. Here T_m is the temperature of a flat interface, κ is the local curvature of the interface, and d_o is the capillary length (proportional to the surface tension).

Figure 3 also illustrates the flat interface solution for directional solidification. The concentration is c_∞ on the solid side of the interface, c_∞/k on the liquid side, and decreases exponentially to c at infinity with a decay length of D/V. Here D is the chemical diffusion constant of rhodamine in succinonitrile ($\approx 10^{-5} cm^2/sec.$) and V is the front velocity. As can be deduced from figure 3, when V is increased so that $V\Delta c\ |dT/dc|/GD > 1$, then the decay length will decrease so that the concentration curve passes into the region of coexistence on the phase diagram. Physically, this is the origin of the front instability, as deduced by Mullins and Sekerka (1964).

A key question concerning the shape of the interface is the selection of the length scale of the cells and dendrites. Trivedi and Somboonsk (1984) have investigated the spacing of cells and dendrites. The dependence of these quantities on the velocity and temperature gradient are recorded in figure 4.

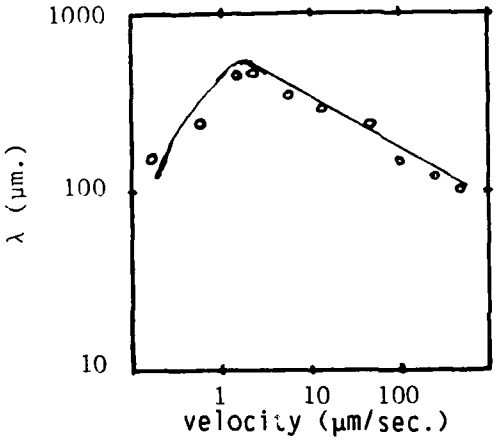

Figure 4

Marginal stability theory accounts for the $V^{-1/2}$ fall off of λ for high velocities but does not account for the growth at smaller velocities.

Another equally basic problem is the shape of the cell. Even in the limit of zero surface tension, no one has found an exact solution for a cell. This is in contrast to other problems of pattern selection, such as the Saffman-Taylor problem, where such a solution exists and is the starting point for further analysis.

We have observed that the patterns selected by the fingers depends upon the orientation of the ⟨100⟩ cubic crystal axis with respect to the thermal gradient (θ) (Heslot and Libchaber, 1985). Roughly, there is a tendency for a finger to grow along the ⟨100⟩ direction which must compete against a tendency to grow along the thermal gradient. For the special case where $\theta = 45°$, there is a second ⟨100⟩ at $\theta = -45°$. Growth is favored along both ⟨100⟩ directions, leading to tip splitting in the cells and a chaotic spatial pattern among the grooves. The nature of the crystalline anisotropy remains in doubt. The anisotropy of the surface tension for succinonitrile has been measured by Glicksman to be less than 5 percent. It is unclear whether such a small anisotropy can account for the variations we see.

We are now carrying out experiments to quantify some of the observations described above. In particular, we are attempting to record the concentration field locally by measuring the intensity of light transmitted through the cell. In addition, we will soon begin observation for velocities just greater than the destabilization velocity of a flat interface. There have been several theoretical studies of the case $V/V_c = 1 + \varepsilon$ that attempt to push the Mullins-Sekerka analysis into the nonlinear regime (Wollkind and Segel, 1970; Ungar and Brown, 1985). Finally, we hope to gain more information about the nature of the crystalline anisotropy by measuring the angle that cells of a fixed orientation grow at for varying velocities.

REFERENCES

Heslot, F. and A. Libchaber, 1985. Physica Scripta T9, 126.

Jackson, R.A., and J.D. Hunt, 1966. Trans. Metal. Soc. of ALME 236, 1129.

Jim, I. and G.R. Purdy, 1974. J. Crystal Growth 23, 37.

Mullins, W.W. and R.F. Sekerka, 1964. J. Appl. Phys. 35, 444.

Trivedi, R. and K. Somboonsk, 1984. Metal. Trans. A15, 967.

Ungar, R. and R. Brown, 1985. Phys Rev. B.

Wollkind, D. and L. Segel, 1970. Phil. Trans. Roy. Soc. Lond. 268, 351.

Fully Developed Phase Turbulence

Stéphane Zaleski

Many systems at the onset of a large scale instability can be described by the Kuramoto-Sivashinsky equation (KSE) (Kuramoto and Tsuzuki, 1976; Sivashinsky, 1977)

$$\varphi_t + \varphi_{xx} + \varphi_{xxxx} + 1/2\ (\varphi_x)^2 = 0,\ 0 < x < L \qquad (1)$$

where the subscripts t and x stand for time and space derivatives. Another interesting form of the KSE is

$$v_t + v_{xx} + v_{xxxx} + vv_x = 0 \qquad (2)$$

where $v = \varphi_x$. For L over 20, the KSE displays a spontaneously chaotic behavior (Pomeau, Pumir and Pelce, 1984). It is thus reminiscent of many models of complex motion, like the Fermi Pasta Ulam chain of oscillators. However, the KSE is a dissipative equation and no soliton solution can be constructed in the proper sense.

Another very interesting analogy can be done with the Navier Stokes equations in 3d (NSE). The same behavior in the infrared region has been predicted for NSE and the KSE (Yakhot, 1981). Renormalization group predictions for long wavelength, long time statistical properties of the NSE and the KSE can thus be tested by a numerical integration of the KSE. Moreover, the detailed statistical analysis required can be performed only in one dimension, due to the restricted computing power of present computers.

We call fully developed phase turbulence the regime where the infrared scaling of the KSE appears, for L over 120 approximately. This should not be confused with fully developed hydrodynamic turbulence, which is the regime in which an inertial range appears at high wavenumber in the NSE. Such an inertial range does not exist for the KSE.

We performed numerical simulations of (i) with periodic boundary conditions (Zaleski and Lallemand, 1985). This allows us to use an efficient spectral code. The time dependency of the Fourier amplitudes was treated at third order in the time step by the approximate solution method. Averages are estimated by starting from 64 randomly chosen initial conditions. We estimated the quantity

$$X(\tau) = \left\langle (\varphi(t+\tau) - \varphi(t))^2 \right\rangle - \left\langle \varphi(t+\tau) - \varphi(t) \right\rangle^2$$

As KSE is invariant in the change $\varphi \to \varphi + c$, φ is a "freely" drifting quantity, and one expects at long times a behavior similar to Brownian motion:

$$X(\tau) = D\tau$$

where D is some constant. The renormalization group predicts instead (Yakhot, private communication)

$$X(\tau) = D\tau^{\mu} \quad \text{with} \quad \mu = 2/3$$

For L large enough, such a scaling law is indeed observed but with $0.48 < \mu < 0.52$. This corresponds to power spectrum for φ of the form

$$\left\langle |\varphi_\omega|^2 \right\rangle \sim \omega^{-1-\mu}$$

and is in some way "less chaotic" than expected (Manneville, 1981).

In conclusion, a deterministic chaotic model like the KSE appears to have a weaker low frequency noise than predicted by the renormalization group analysis.

REFERENCES

Kuramoto, Y. and T. Tsuzuki, 1976. Prog. Theor. Phys. 55, 356.

Manneville, P., 1981. Phys. Lett. 84A, 129. Such a power spectrum was found. In this reference, $\mu = 0.75$, but the simulation was made for L = 64, before the infrared regime is fully developed.

Pomeau, Y., A. Pumir and P. Pelce, 1984. J. Stat. Phys. 37, 39.

Sivashinsky, G.I., 1977. Acta Astron. 4, 1177.

Yakhot, V., 1981. Phys. Rev. A24, 642.

Zaleski, S. and P. Lallemand, September 198.. J. de Physique - Lettres, Paris. (Rigid boundary conditions were nvestigated.)

On the Interaction of Small-Scale Oceanic Internal Waves with Near Inertial Waves

William R. Young

Ray theory is used to investigate the interaction of a short high-frequency progressive internal wave of infinitesimal amplitude with a long progressive near inertial wave of arbitrary amplitude. Weak interaction theory would, if applicable, predict that the largest changes in short wave properties occur when the resonance condition $c = c_g$ is satisfied, where c is the phase velocity of the long wave and c_g is the group velocity of the short wave. The present calculaton confirms this prediction only when the long wave has exceedingly small amplitude (peak velocities of order .1 cm/s).

However, when the background velocity has a realistic amplitude (e.g. oceanic values are of order 20 cm/s) the resonance condition fails to be relevant. For example, waves which initially have $c = c_g$ become trapped in low shear regions and consequently experience very small changes in wavenumber. Other short waves, which initially have $c_g < c$ and hence violate the resonance condition, exhibit large and permanent changes in vertical wavenumber.

Remarkably, it is found that these permanent changes are much more likely to be decreases, rather than increases, in wavenumber. This can be explained as follows. Short waves which enter an inertial wave packet experience both increases and decreases in wavenumber. However, at times when the wavenumber is relatively large, the group velocity is relatively small and the short wave is unlikely to escape from the inertial packet, whereas small wavenumber and large group velocity assist the escape of the short wave group. Consequently the short waves which leave the inertial packet tend to have a smaller average wavenumber than those which enter. Thus the net effect of a near inertial packet on a collection of short waves appears to be an increase in vertical wavelength and frequency.

Probing Turbulence With Large Scale Numerical Simulations

Parviz Moin

Three recent applications of large eddy and direct simulation databases to the study of organized structures in turbulent flows were presented.

An investigation into the existence and frequency of occurrence of hairpin vortices in turbulent channel flow was carried out by Moin and Kim (1985). Using statistical analysis and visualization of the instantaneous vorticity fields in three-dimensional space it was shown that turbulent channel flow consists of a large number of horseshoe (or hairpin) vortices often inclined at 45° to the wall. The hairpins are formed from the roll-up of sheets of spanwise vorticity by random velocity fluctuations and stretching by mean rate of strain. The hairpins do not have legs elongated in the streamwise or spanwise direction as has been proposed by some investigators.

Our observations of the vortical structures in the channel flow led us to conjecture that hairpin vortices are the characteristic structures not only in wall-bounded flows but in all turbulent shear flows. Moin, Rogers and Moser (1985) examined the structure of vorticity field in homogeneous turbulent shear flow using the same techniques as in the channel. Rogallo's (1981) computer program with up to 128x128x128 points was used. The results conclusively showed that homogeneous turbulent shear flow consists of coherent hairpin vortices, verifying the above assertion. The presence of mean shear causes a remarkable organization of the vorticity field in turbulent flows.

Finally, the characteristic eddy decomosition theorem was applied to turbulent channel flow database. This decomposition also known as Lumley's orthogonal decomposition (Lumley 1967) provides a quantitative definition of coherent structures in turbulent flows as well as unambiguous determination of their contribution to turbulence stresses. It is a mathematically elegant procedure for identification of coherent structures and representation of the entire flow field in terms of these eddies. This is an ideal application of the simulation databases because of the large magnitude of the required input data. In this decomposition the instantaneous velocity field is decomposed into a series of deterministic functions (eddies) with random coefficients

$$u_i = \sum_n a_n \phi_i^{(n)}(x) \qquad (1)$$

Given an ensemple of realizations of the velocity field $u_i(x,t)$ the deterministic vector functions or eddies, $\phi_i^{(n)}(x,t)$, are chosen such that they have the highest possible root-mean square correlations with the members of the ensemble. It can be shown the ϕ_i's are the eigenfunctions of a Fredholm eigenvalue problem with the correlation tensor R_{ij} as the kernel (Lumley 1967).

In a recent study a two-dimensional variant of this technique was applied to the channel flow database (Moin 1984). It was shown that the dominant eigenfunction contributed about 30 percent to total turbulent kinetic energy and its contribution to Reynolds shear stress was about 70 percent. When the problem was formulated for the wall region alone, it was pssible to recover virtually all the turbulent kinetic energy and Reynolds shear stress with only five terms in the expansion of equation (1). In the directions of flow homogeneity this expansion is combined with the shot-noise expansion (Rice 1944) to yield the characteristic eddy that is sprinkled in the flow. From second order statistics the characteristic eddy can be obtained to within a phase factor. This phase factor which is essential for determination of the shape of the eddy is recovered from third order statistics. The bi-spectra of the coefficients a_n were calculated from the database, from which the unknown phase angle was determined and the characteristic eddy was constructed. In the wall region the dominant eddy depicts the sweep event (i.e., high speed fluid moving towards the wall); and in the core region it displays the ejection event. These findings are consistent with the measurements of Wallace Eckelmann and Brodkey (1972) using quadrant analysis.

REFERENCES

Lumley, J.L., 1967. The structure of inhomogeneous turbulent flows, Atmospheric Turbulence and Radio Wave Propagation, ed. A.M. Yaglom and V.I. Tatarsky, 166. NAUKA, Moscow.

Moin, P. and J. Kim, 1985. The structure of vorticity field in turbulent channel flow, Part 1, Analysis of the instantaneous fields and statistical correlations, J. Fluid Mech. 155, 441-464.

Moin, P., M. Rogers and R.D. Moser, 1985. Structure of turbulence in the presence of uniform shear, Proc. of the Fifth Symposium on Turbulent Shear Flows, Cornell University, Ithaca, New York, August 7-9, 1985.

Moin, P., 1984. Probing turbulence via large eddy simulation, AIAA paper, 84-0174.

Rice, S.O., 1944. Mathematical analysis of random noise, Bell System Tech. J. 23, 282.

Rogallo, R.S., 1981. Numerical experiments in homogeneous turbulence, NASA TM 81315.

Wallace, J.M., H. Eckelmann and R.S. Brodkey, 1972. The wall region in turbulent shear flow, J. Fluid Mech. 54, 39.

Mixing Layer, Coherence and Two-Dimensional Turbulence

Marcel Lesieur and Chantal Staquet

ABSTRACT: A two-dimensional direct numerical simulation of the temporal mixing layer is performed. It is shown that the successive pairings allow to build up a quasi-stationary longitudinal energy spectrum of slope close to k^{-4}. After two successive pairings the inertial range extends on more than one decade. One shows that the large scales, though coherent, are extremely sensitive to initial conditions, and then unpredictable. This, together with the statistical predictability theory of two-dimensional turbulence, permits to propose a mechanism of exponential growth of spanwise decorrelation which leads in a few turnover times of a given coherent structure to three-dimensionalization. We finally propose a mechanism of recreation of a new coherent structure, based on an eddy-viscosity assumption and the linear instability of the mean inflectional shear.

I. Introduction

The mixing layer between two flows of different velocities U1 and U2 has been extensively investigated experimentally these last 15 years: one can quote for instance the work of Brown and Roshko (1974) showing the persistence far downstream of large structures (usually called "coherent") upon which small scale three-dimensional turbulence superpose, or the observations on the pairing of these structures done by Winand and Browand (1974). An extensive review of the subject has been recently given by Ho and Huerre (1984). Mixing layer type structures can also be found in a lot of atmospheric or oceanic situations, as well as in the atmospheres of Jupiter and Saturn. Such a flow is important to study as a prototype of transitional flow to turbulence. A somewhat controversial issue lies in the concept of coherence applied to the large structures (see e.g. Wood and Bradshaw, 1982). Another important problem is to know to which extent the large quasi-two-dimensional scales have a two-dimesnional dynamics (i.e. obbey two-dimensional Navier-Stokes or Euler equations) and what is their interaction with small scale three-dimensional turbulence.

II. Two-Dimensional Direct Numerical Simulations

In order to decide to which extent the large scales of the mixing layer can be accurately described by two-dimensional processes, we have developed direct numerical large eddy simulations of the two-dimensional Navier-Stokes equations applied to the temporal mixing layer. This type of calculations is of course not new, since the works of Zabusky and Deem (1971), Couet and Leonard (1980), Riley and Metcalfe (1980), Aref and Siggia (1980) or Corcos and Sherman (1984) for instance. Here we have focused on the spectral statistics of the flow, as compared to the homogeneous isotropic two-dimensional turbulence (see e.g. Kraichnan and Montgomery 1980 and Lesieur 1983). We have also looked at the sensitivity of the large scales upon initial random perturbations superposed upon the mean inflectional shear.

In an orthonormal frame Oxyz = Oijk, let us consider a two-dimensional incompressible flow of stream function $\Phi(x,y,t)$ satisfying two-dimensional Navier-Stokes equation

$$[d/dt + J(.,\Phi)]\nabla^2\Phi = \nu\nabla^4\Phi \qquad (2\text{-}1)$$

This corresponds to the advection of the vorticity $\nabla^2\Phi$ by the flow. J(A,B) is the Jacobian operator. Since one is mainly interested by a simulation of the large scales, one will replace the molecular viscous dissipative operator in the r.h.s. of (2-1) by a subgridscale dissipative term $-\nu_1 \nabla^6 \Phi$

$$[d/dt + J(.,\Phi)]\nabla^2\Phi = -\nu_1 \nabla^6 \Phi \qquad (2\text{-}2)$$

This type of biharmonic dissipation is often used by oceanographers (see e.g. Holland 1978). Its relevance is of course questionable, but it seems to allow a good description of the large scales of the flow, with dissipative effects shifted to the cutoff scale. It permits then to artificially increase the Reynolds number. We consider a temporal mixing layer, that is with periodic boundary conditions in the x direction. The boundary conditions in the y direction are no slip boundary conditions with velocities +U and -U respectively. To this temporal mixing layer we will later on associate a spacial problem with two velocities U1 and U2 such that (U1 - U2) = 2U and $x = t\cdot(U_1 + U_2)/2$. This is justified only if one neglects in the spacial layer the streamwise growth on distances of order of the x period of the temporal layer. It is possible that the main results of the following calculations (temporal case) should prove to be valid in the spacial case.

We have carried out a finite differences resolution of (2-2) with the already mentioned boundary conditions. The calculation involves 183^2 grid points. The initial velocity field is $\tanh(2y/\delta i)$, where δi is the initial vorticity thickness, upon which one superposes a white noise random perturbation of small amplitude. It is then well known from linear stability analysis (Drazin and Reid 1981) that a structure corresponding to the most amplified wavenumber is going to appear, since perturbations at all unstable wavenumbers are initially present. The associated most unstable wave length, given by the theory, is equal to $\lambda a = 7\delta i$. In the following calculations, the unit of time will be taken as $\delta i/U$.

We have plotted at the same time the isovorticity lines of the velocity field and the longitudinal spatial energy spectrum obtained by taking the Fourier transform of the velocity and averaging across the layer (in the y direction). Figure 1 shows a calculation involving four eddies, at times 0 (figure 1a), 20 (figure 1b), 37.5 (figure 1c) and 80 (figure 1d). In figure 1a one can see a small peak at the fundamental wavenumber $k^4 = 2\pi/\lambda a$, which corresponds to a small sine perturbation superposed upon the white noise (flat spectrum) in order to accelerate the formation of the four coherent large eddies. At time t = 20 these eddies have been completely formed, and give rise to a peak in the energy spectrum (figure 1b). But nonlinear interactions between modes have already distributed the energy across a broad spectrum. At time t = 37.5 a first pairing has occurred: one clearly sees that the first subharmonic mode $k2 = \pi/\lambda a$ and all the larger wavenumbers collapse on a k^{-4} range (figure 1c). At time t = 80 the second pairing occurs, and the second subharmonic $k1 = \pi/2\lambda a$ collapses on a range of slope close to k^{-4} on 1.5 decade (figure 1d). One will see later on that $\delta(t)$ increases proportionally to t. A schematic scenario of the evolution of the mixing layer could be:

i) an injection of energy and enstrophy at wavenumber $\delta(t)^{-1}$, due to the instability of the inflectional mean shear;

ii) an enstrophy cascade towards smaller scales along a k^{-4} spectrum of constant intensity. The value -4 found for the "enstrophy inertial exponent" differs from the value -3 given by the usual statistical closures of turbulence (Kraichnan 1967) but is in good agreement with direct numerical simulations of two-dimensional homogeneous turbulence (Basdevant and Sadourny 1983). This departure from the k^{-3} enstrophy cascade could be explained by the existence of vorticity shocks (Saffman 1971) or intermittency (Basdevant et al. 1981). Further discussions on this point have been given by Kida and Yamada (1984) and Brachet and Sulem (1984).

One can wonder whether this longitudinal energy spectrum has any relevance to the isotropic energy spectrum of an isotropic ideal two-dimensional turbulence which could for instance be obtained by a random superposition of the mixing layer eddies. Actually, we have checked that the transverse energy spectrum (in the y direction) resembles the x-spectrum, so that finally the turbulence at scales smaller than δ is not far from two-dimensional isotrophy.

This original type of two-dimensional turbulence found in the mixing layer is different from the two classes of homogeneous isotropic turbulent flows which are usually considered: the case with a stationary injection of energy and enstrophy at a fixed wavenumber ki yields a stationary enstrophy spectrum (for $k > ki$) and a quasi-stationary inverse $k^{-5/3}$ inverse energy cascade (for $k < ki$) (Kraichnan 1967, Leith 1968, Pouquet et al. 1975). The freely decaying case leads to a t^{-1} decay of the wavenumber ki(t) characteristic of the energy containing eddies, and an enstrophy cascade

$$E(k,t) = (cte)\ t^{-2}\ k^{-3} \qquad (2\text{-}3)$$

extending for $k > ki(t)$ with an intensity decreasing like t^{-2} (Batchelor 1969). In the case of the mixing layer we have injection of energy and enstrophy from a moving wavenumber $\delta(t)^{-1}$, with a resulting quasi-stationary k^{-4} inertial range extending progressively to smaller and smaller wave numbers.

Figure 2a shows the time evolution of the vorticity thickness $\delta(t)$ in the calculation of figure 1. In this calculation, corresponding to one particular realization of the initial white noise perturbation, there is clearly a growing of $\delta(t)$ associated to the apparition of the first coherent structure and to the first pairing. Figure 2b corresponds to an average done on five independent realizations of the white noise, compared with the linear growth found experimentally by Bernal (1981), and recently confirmed by Lasheras (1984). The agreement of the 2D calculations with the experiments is quite satisfactory up to the time $t = 50$, after which there is essentially one eddy left in the computational domain: this eddy, which is stationary, cannot grow anymore by pairing. After that time ($t = 50$) it is likely that the calculation will differ from the actual mixing layer whose two-dimensional large scales will presumably grow in the same way as given by our calculation before $t = 50$. It seems then that the dynamics of the large structures of a real three-dimensional mixing-layer is correctly described by two-dimensional Navier-Stokes equations with a biharmonic subgridscale dissipation.

III. The Return to Three-Dimensionality

Here one will try to study some aspects of the three-dimensionalization of the mixing layer by looking at spanwise decorrelation developing in a quasi-two-dimensional coherent structure: Indeed, such decorrelations can develop, due for instance to the growth of the translative instability pointed out by Pierrehumbert and Widnall (1981), or non two-dimensional pairings leading to "dislocations". A statistical version of these spanwise decorrelation processes is given by the two-dimensional predictability theory (Alemany et al. 1979, Lesieur 1983, Staquet et al. 1984). Let us consider a quasi-two-dimensional coherent structure, and let u1 and u2 be two cross sections of the flow in the (x,y) plane. If the flow were perfectly two-dimensional, the two random velocity fields u1 and u2 would be perfectly correlated. Then three-dimensionality results in a decorrelation between u1 and u2. One will assume that u1 and u2 evolve according to two-dimensional Navier-Stokes equations. Let $E(k,t)$ be the energy spectrum of u1 and u2 (assumed to be the same) and $E_\Delta(k,t)$ be the "error" spectrum such that

$$(1/4) < (u1 - u2)^2 > \int_0^\infty E_\Delta(k,t)\, dk \qquad (3\text{-}1)$$

One defines then the error rate

$$r(t) = \int_0^\infty E_\Delta(k,t)\, dk \;/\; \int_0^\infty E(k,t)\, dk \qquad (3\text{-}2)$$

The Eddy-Damped Quasi-Normal Markovian theory (EDQNM) (or nearly equivalent Test-Field-Model) was applied to this statistical predictability problem by Leith and Kraichnan (1972) in the case of a stationary enstrophy cascade: they found that for an error initially confined in the large wavenumbers (but not in the dissipation range), the error rate r(t) increases exponentially. The characteristic time of this exponential growth to reach the wavenumber ki is $2\tau(ki)$, where $\tau(ki)$ is the large eddy turnover time at ki. For a decaying 2D turbulence, the same EDQNM theory shows that the characteristic time for the error to contaminate exponentially ki(t) is $4\tau(ki(to))$, where (to) is the time at which the error has been injected (Metais et al. 1983, Metais and Lesieur 1984). Returning to the mixing layer, and considering at time to a quasi-two-dimensional coherent structure of turnover time τo, one can infer from the preceeding results that there will be complete decorrelation between u1 and u2 (i.e. return to three-dimensionality of the structure) in a time of order $2 \sim 4\tau o$. Since we have already seen that the wavelength λa of the large coherent structure is of order $3\delta_o$, one finds:

$$\tau o = \lambda a/U = 3\, \delta o/U \qquad (3\text{-}3)$$

so that the characteristic time of the exponential return to three-dimensionality is of order $6 \simeq 12\ \delta o/U$.

This result of exponential return to three-dimensionality is based on statistical closures of turbulence whose validity has often been doubted. It may then be useful to recover the same kind of result -- i.e. growth of decorrelation between two initially close realizations u1 and u2 of the flow -- even in the strictly two-dimensional case. Figure 3 compares the evolution of the initial inflectional shear with four different realizations of the small initial white noise perturbation, for times t = 20

(figure 3a) and t = 30 (figure 3b). The case 1 corresponds to the calculation shown in figure 1. One sees extremely clearly that a decorrelation develops rapidly between any pair of the flows 1,2,3,4. If one considers these flows as various vertical (x,y) cross sections of the mixing layer, one sees strong spanwise decorrelations develop. If there is no mechanism acting to restaure the two-dimensionality (this of course cannot be proved and will be only a working hypothesis), the mixing layer will explosively return to three-dimensionality in a time of order 6 ~ 12 $\delta o/U$.

In order to assess to EDQNM predictability calculations from the point of view of our present direct numerical mixing layer simulations, we have calculated the time evolution of the spanwise error spectrum corresponding to two different realizations of the mixing layer, the initial random error being superposed to the "developed" layer (i.e. with coherent structures and inertial range formed). Figure 4 presents such a calculation, and shows an inverse cascade of error through the energy spectrum, analogous to the closure prediction of Leith and Kraichnan (1972) or Metais and Lesieur (1985). The error ratio is found to increase exponentially up to t = 80 (corresponding to the second pairing) with a characteristic time of 14 $\delta o/U$.

It must also be noticed that the error spectrum exhibits an intermediate k^{-2} range, which happens then to be proportional to $k^2 E(k,t)$. Then the error spectrum is proportional to the enstrophy spectrum. This had already been noticed in the case of EDQNM two-dimensional turbulence by Metais and Lesieur (1985), who pointed out an analogy with the inertial-convective range of a two-dimensional turbulent passive scalar (Lesieur et al. 1981, Lesieur and Herring 1985). It is remarkable that such an analogy seems to be also valid for the mixing layer.

IV. Transition Coherence/Incoherence

Experiments on the spatial mixing layer behind a splitter plate show generally two different states in the downstream evolution of the layer: close to the plate the coherent structures are well organized and there is no three-dimensional turbulence (transitional region). Then, quite abruptly, three-dimensional turbulence appears and the layer evolves self-similarly (Browand and Ho 1983) (developed region). Similar arguments to those developed in section III have been used in a preceding paper (Lesieur 1983) to propose that the transitional distance Dtr should be proportional to the Logarithm of the Reynolds number based on the initial vorticity thickness θ, namely:

$$[(U1 - U2)/(U1 + U2)]\ (Dtr/\theta) = cte\ ln\ (U\theta]\ t/\nu) + cte \qquad (4\text{-}1)$$

Here we will consider the developed region: several experiments (see e.g. Browand and Troutt 1980) have confirmed that the large coherent structures are still present there, hidden behind the agitation of small scale three-dimensional turbulence. We then consider one of these large structures and assume from the results of the last section that it will return to three-dimensionality: the situation is now a three-dimensional turbulent layer superposed upon a mean inflectional shear of vorticity thickness δ. Let E3D be the three-dimensional turbulent kinetic energy: if E3D were small in front of $(1/2)U^2$ and if the three-dimensional turbulence had a broad band spectrum, Squire theorem would would show that a coherent

structure of wavelength 7δ would appear. Actually, the amplitude of the 3D perturbation is not small, so that that conditions to establish the preceding result are certainly not fulfilled. This result can nevertheless be justified if one assumes that the two-dimensional large scales are renormalized by the three-dimensional turbulence with the aid of an eddy viscosity ν_t. The value of ν_t can be evaluated either by measuring experimentally the Reynolds stresses (Wignanski and Fiedler 1970) or by recourse to the concept of eddy-viscosity in spectral space introduced by Kraichnan (1976). This yields

$$\nu_t = 30 \sim 40 \quad U\delta \tag{4-2}$$

Then a perturbation superposed on the mean shear and initially small, will satisfy an Orr-Sommerfeld equation and the most amplified coherent structure $\lambda a = 7\delta$ will appear in a characteristic time $10\delta/U$. This time is of the same order as the spanwise decorrelation time (characteristic time of return to three-dimensionality.)

Then the evolution of the mixing layer in the coherent region could be characterized by a cyclic exchange of energy between two and three-dimensional turbulence:" starting from a two-dimensional structure ("coherent structure"), spanwise decorrelation would develop exponentially to such a point that the coherence would be lost and it would break into three-dimensional turbulence. Then the ambient mean inflectional shear would act -- by linear stability mechanism -- to build a new coherent structure.

V. Conclusion

This paper has studied the large coherent structures of the temporal mixing layer from a two-dimensional point of view: direct numerical simulations have shown that these structures were turbulent in the sense that they are extremely sensitive to initial conditions ("unpredictable") and that they develop an enstrophy cascading like energy spectrum of slope close to k^{-4}. This inertial range is close to be stationary. The spectrum peaks at the inverse of the vorticity thickness $\delta(t)$ which increases like t and evolves in good agreement with the spacial mixing layer experiments. It could be expected that this evolution would keep on for ever for a mixing layer developing in an infinite domain.

The ideas of exponential loss of predictability in a two-dimensional turbulent flow, based both on EDQNM closure and direct numerical simulations, have also been used to propose in the mixing layer an exponential spanwise decorrelation which will eventually result into a three-dimensionalization of the structure. A new coherent structure will then be reformed due to the action of the mean inflectional shear. Since the times for the destruction (and possibly the reformation) of the coherent structure depend logarithmically upon the amplitude of initial perturbations, the exchange between "coherence" (two-dimensional turbulence) and "chaos" (three-dimensional turbulence) will be intermittent as soon as the perturbations are randomly distributed in space.

REFERENCES

Alemany, A., R. Moreau, P.L. Sulem and U. Frisch, 1979. Influence of an external magnetic field on homogeneous MHD turbulence, J. de Mecanique 18, 277-314.

Aref, H. and E.D. Siggia, 1980. Vortex dynamics of the two-dimensional turbulent shear layer, J. Fluid Mech. 100, 705-737.

Basdevant, C., B. Legras, R. Sadourny and M. Beland, 1981. A study of barotropic model flows: Intermittency, waves and predictability, J. Atmos. Sci. 38, 2305-2326.

Basdevant, C. and R. Sadourny, 1983. Modelling of virtual scales in numerical simulation of two-dimensional turbulent flows, J.M.T.A. special issue "Two-dimensional turbulence," R. Moreau Ed., 243-269.

Batchelor, G.K., 1969. Computation of the energy spectrum in homogeneous two-dimensinal turbulence, Phys. Fluids Suppl. 12, II.233.

Bernal, L.P., 1981. The coherent structure of turbulent mixing layers, Ph.D. Thesis, Calif. Inst. Technol., Pasadena.

Brachet, M.E. and P.L. Sulem, 1984. Direct numerical simulation of two-dimensional turbulence, Fourth Beer Sheva Seminar on MHD Flows and Turbulence. Proceedings in A.I.A.A. Progress in Aeronautics and Astronautics.

Browand, F.K. and T.R. Troutt, 1980. A note on spanwise structure in the two-dimensional mixing layer, J. Fluid Mech. 93, 325-336.

Browand, F.K. and C.M. Ho, 1983. The mixing-layer: An example of quasi-two-dimensional turbulence, J.M.T.A., special issue "Two-dimensional turbulence," R. Moreau, Ed., 99-120.

Brown, G.L. and A. Roshko, 1974. On density effects and large structure in turbulent mixing layers, J. Fluid Mech. 64, 775-816.

Corcos, G.M. and F.S. Sherman, 1984. The mixing layer: Deterministic models of a turbulent flow, Part 1: Introduction and the two-dimensional flow, J. Fluid Mech. 139, 29-65.

Couet, B. and A. Leonard, 1980. Mixng layer simulation by an improved three-dimensional vortex-in-cell algorithm, In Proc. 7th Intl. Conf. on Numerical Methods in Fluid Dynamics, Stanford-Ames.

Drazin, P.G. and W.H. Reid, 1981. Hydrodynamic stability, Cambridge University Press.

Ho, C.M. and P. Huerre, 1984. Perturbed free shear layers, Ann. Rev. Fluid Mech., 365-424.

Holland, W.R., 1978. The role of mesoscale eddies in the general circulation of the ocean, J. Phys. Ocean 8, 363-392.

Kida, S. and M. Yamada, 1984. Turbulence and chaotic phenomena in fluids, edited by T. Tatsumi, North-Holland, 339-350.

Kraichnan, R.H., 1967. Inertial ranges in two-dimensional turbulence, Phys. Fluids 10, 1417-1423.

Kraichnan, R.H., 1976. Eddy viscosity in two and three dimensions, J. Atmos. Sci. 33, 1521-1536.

Kraichnan, R.H. and D. Montgomery, 1980. Two-dimensional turbulence, Reports Progr. Phys. 43, 549-619.

Lasheras, J.C., J.S. cho and Y. Maxworthy, 1984. On the origin and scale of streamwise vortical structures in a plane, free shear-layer, submitted to J. Fluid Mech.

Leith, C.E., 1968. Diffusion approximation for two-dimensional turbulence, Phys. Fluids 11, 671-673.

Leith, C.E. and R.H. Kraichnan, 1972. Predictability of turbulent flows, J. Atmos. Sci. 29 29, 1041.

Lesieur, M., J. Sommeria and G. Holloway, 1981. Zones inertielles du spectre d'un contaminant passif en turbulence bidimensionnelle, C.R. Acad. Sc., 5.292, serie II, 271-274.

Lesieur, M., 1983a. Turbulence and chaotic phenomena in fluids, edited by T. Tatsumi, North-Holland, 339-350.

Lesieur, M., 1983b. Introduction to two-dimensional turbulence, J.M.T.A. special issue "Two-dimensional turbulence," R. Moreau Ed., 5-20.

Lesieur, M. and J. Herring, 1985. Diffusion of a passive scalar in two-dimensional turbulence, J. Fluid Mech., to appear.

Metais, O., J.P. Chollet and M. Lesieur, 1983. Predictability of the large scales of freely-evolving three- and two-dimensional turbulence, Proc. A.I.P. Conf. n^{o} 106, Predictability of fluid motions, Ed. G. Holloway and B.J. West, 303-319.

Metais, O. and M. Lesieur, 1985. Statistical predictability of decaying turbulence, J. Atmos. Sci., to appear.

Pierrehumbert, R.T. and S.E. Widnall, 1981. The structure of organized vortices in a free shear layer, J. Fluid Mech. 102, 301-313.

Pouquet, A., M. Lesieur, J.C. Andre and C. Basdevant, 1975. Evolution of high Reynolds number two-dimensional turbulence, J. Fluid Mech. 4, 72, 305-319.

Riley, J.J. and R.W. Metcalfe, 1980. Direct numerical simulation of a perturbed turbulent mixing layer, A.I.A.A. 18th Aerospace Sci. Meeting, Pasadena, 80-0274.

Saffman, P.G., 1971. On the spectrum and decay of random two-dimensional vorticity distributions of large Reynolds number, Stud. Appl. Math. 50, 377-383.

Staquet, C., O. Metais and M. Lesieur, 1984. Study of the mixing layer from the point of view of two-dimensional turbulence, C.R. Acad. Sci. t. 300, serie II, 833-838.

Winand, C.D. and F.K. Browand, 1974. Vortex pairing, the mechanism of turbulent mixing layer growth at moderate Reynolds number, J. Fluid Mech. 63, 237-255.

Wood, D.H. and P. Bradshaw, 1982. A turbulent mixing layer constrained by a solid wall, J. Fluid Mech. 122, 57-90.

Zabusky, N.J. and G.S. Deem, 1971. Dynamical evolution of two-dimensional unstable shear flows, J. Fluid Mech. 47, 353-379.

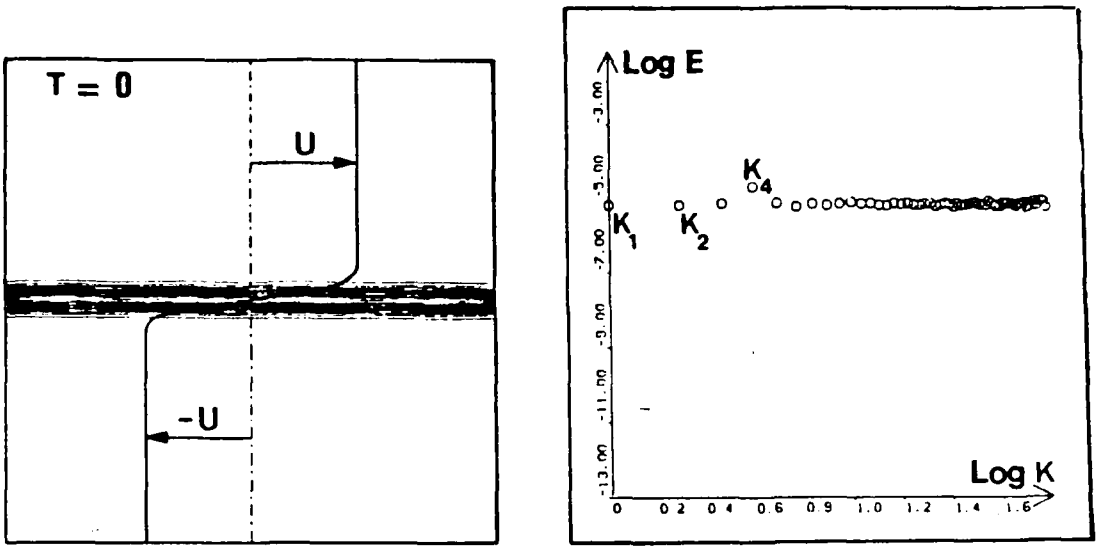

Figure 1a

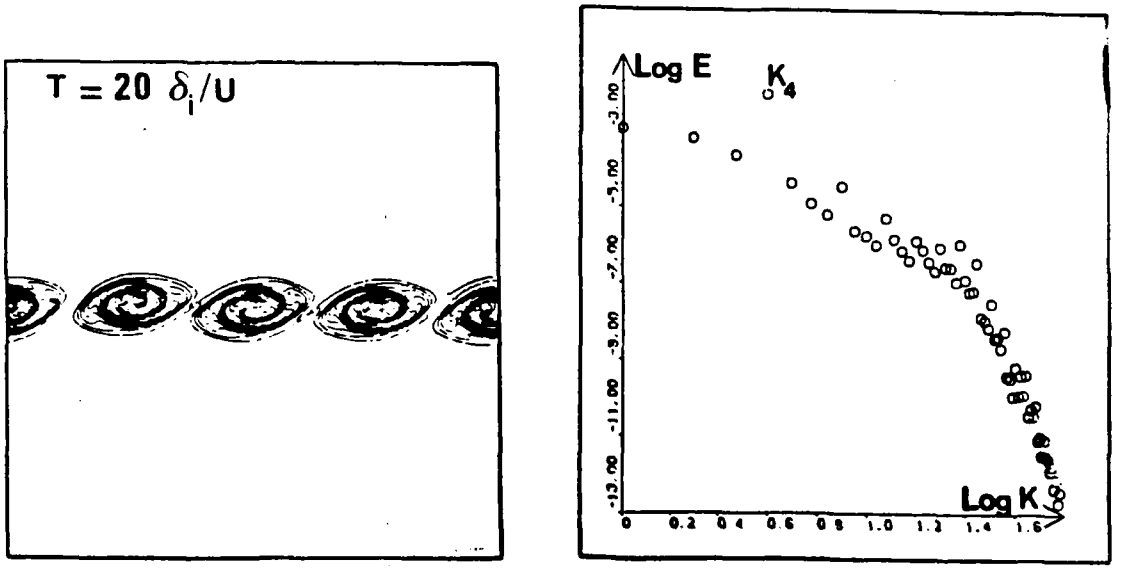

Figure 1b

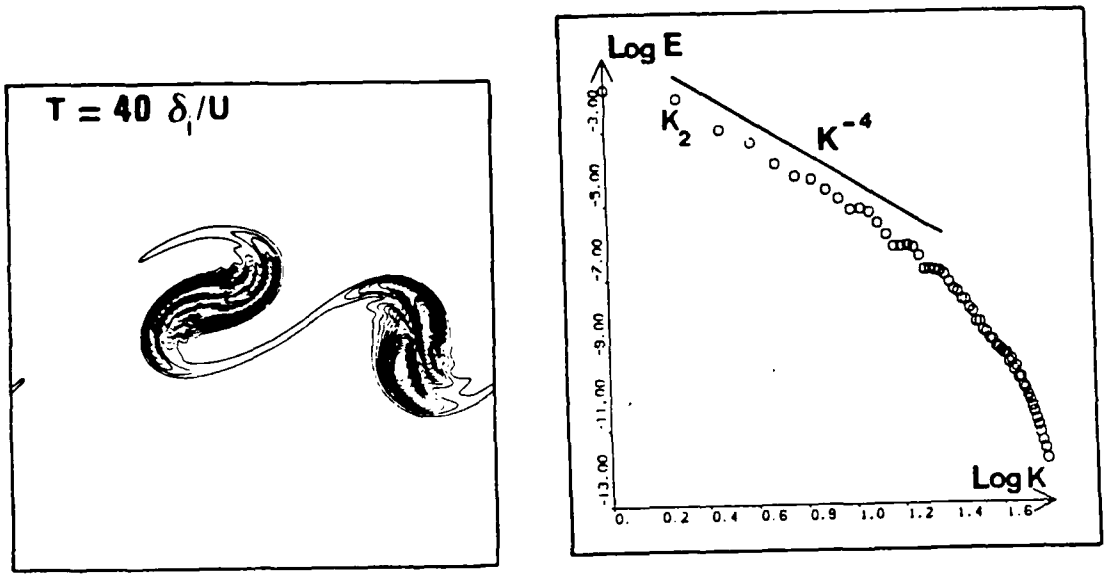

Figure 1c

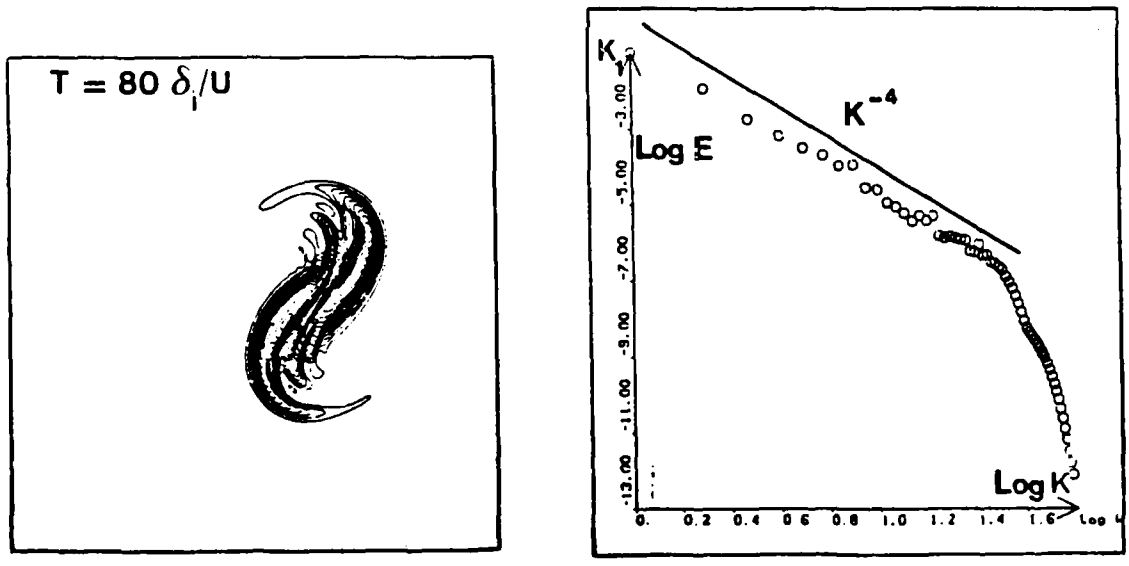

Figure 1d

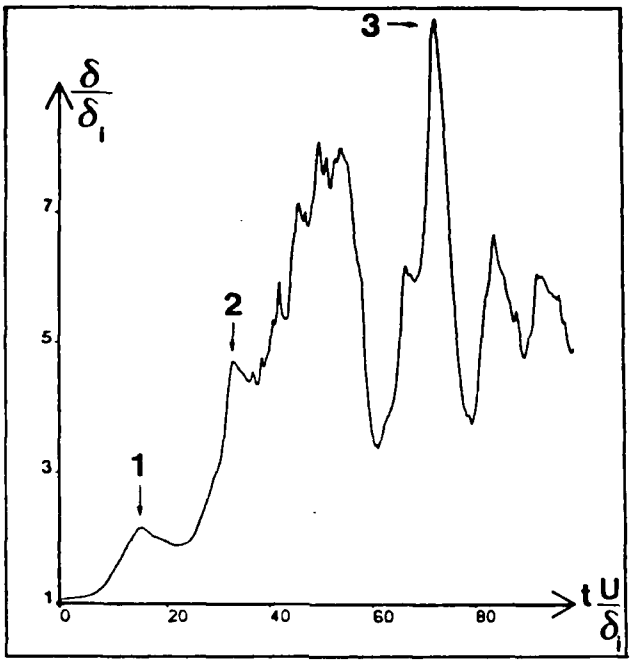

Figure 2a: Vorticity Thickness

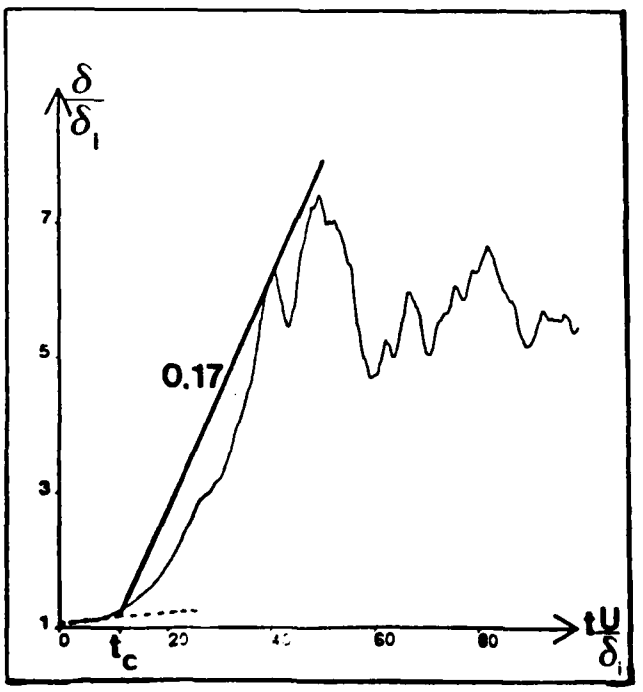

Figure 2b

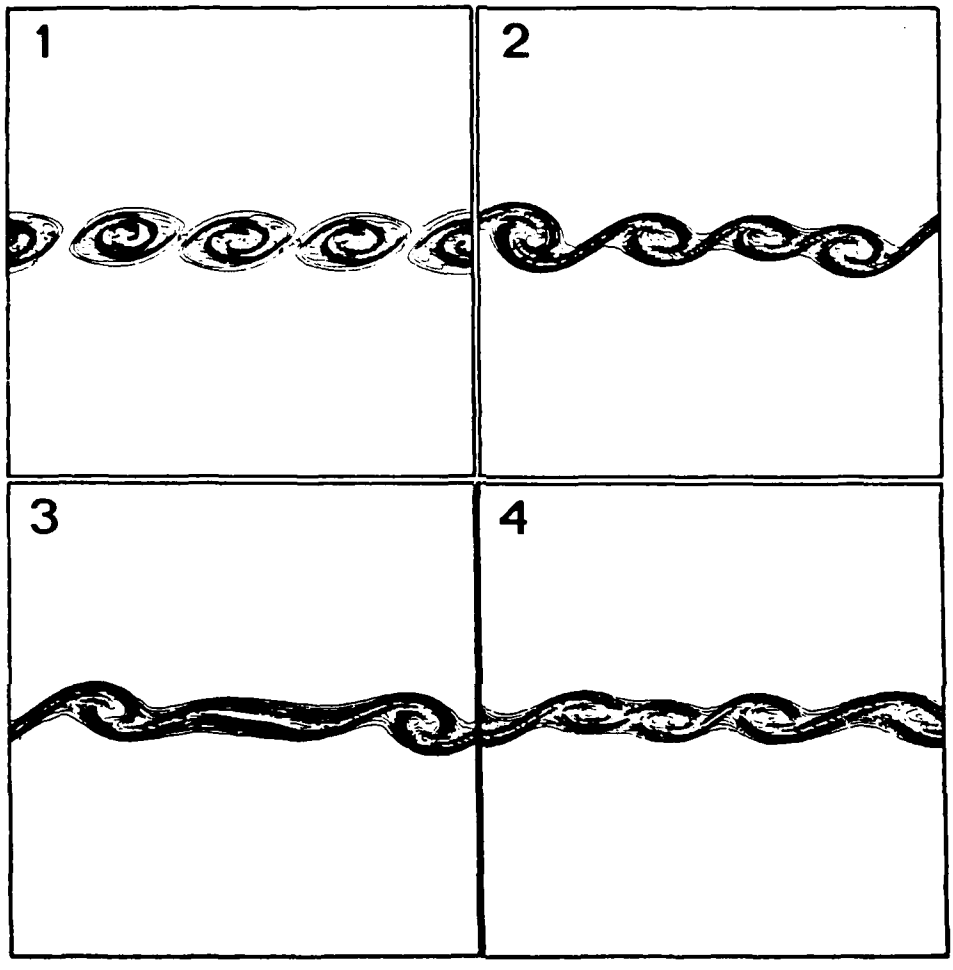

$t = 20 \times \delta i/U$

Figure 3a: Sensitivity to Initial Conditions of the Coherent Structures.

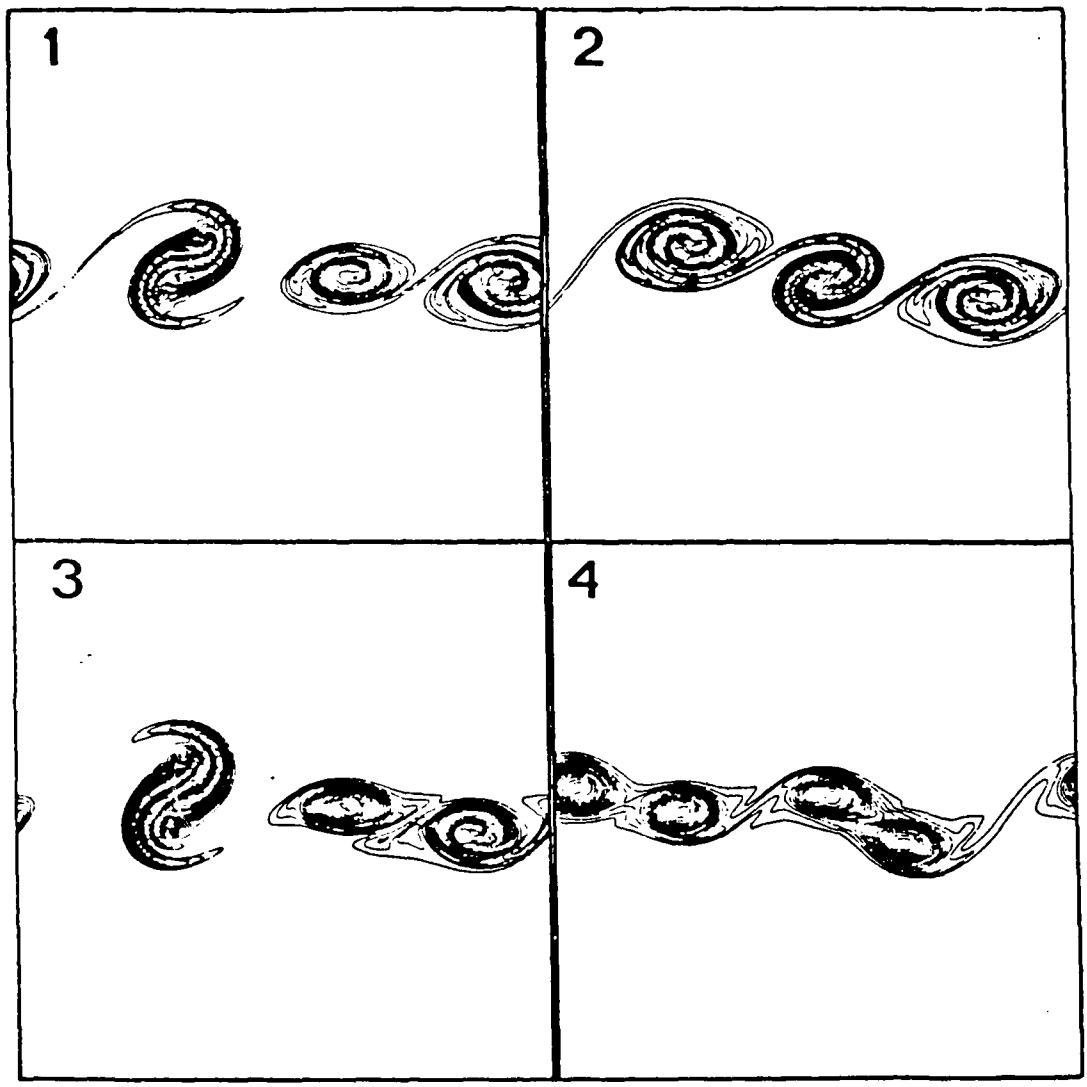

$t = 30 \frac{\delta i}{U}$

Figure 3b

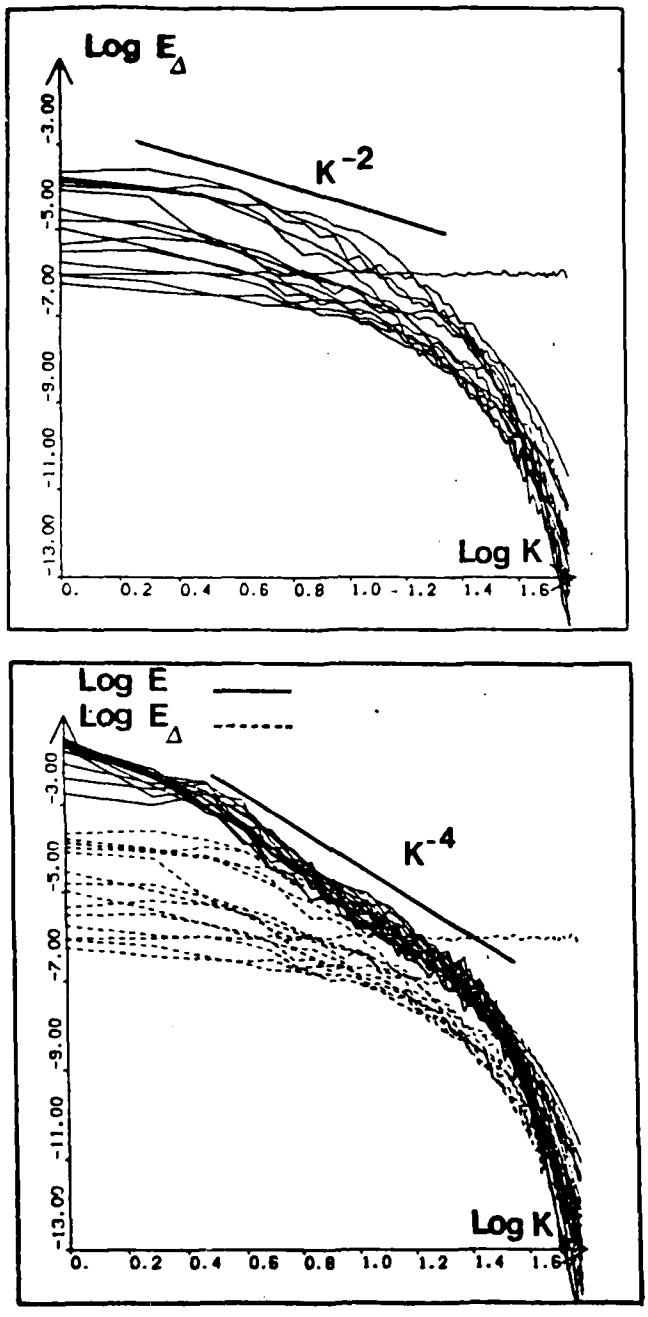

Figure 4

Error Spectrum $\langle (u^{(1)} - u^{(2)})^2 \rangle$ from $t = 20 \frac{\delta i}{U}$ to $t = 80 \frac{\delta i}{U}$.

Experiments and Theory in Double-diffusive Convection

L. N. Howard

I. Experiments of R. Krishnamurti and the author on double diffusive convection, stabilized by a solute and thermally destabilized, were described. The first series utilized salt or boric acid, and made use of saturated solutions to fix the solute concentration at the lower boundary, a permeable membrane separating the working layer from a stirred reservoir. The concentration at the similar upper boundary was maintained at a slightly lower value by constant flushing of the upper reservoir (also stirred), and the temperature of this reservoir was controlled by a cooling coil connected to a constant temperature circulator. Measurement of input and output concentrations in the upper reservoir, together with the flushing rate, gave the net solute flux. Heat was added to the lower reservoir by an electric heater, and forced to leave only through the membrane by surrounding this reservoir by a guard bath maintained at the same temperature. Thus the controlled external variables were concentration difference (or solute Rayleigh number R_S) and heat flux, while the measured variables were solute flux and temperature difference. A preliminary description of these measurements was given at WHOI last summer by Krishnamurti. More recent experiments have been made using sugar as the solute, and maintaining both concentrations by flushing so that saturated solutions are not required. The flushing of the two reservoirs is done alternately so that at all times at least one reservoir is completely closed -- this avoids the danger of accidental flow across the membranes (such flow due to pressure fluctuations associated with the convection or stirrers was found to be negligible, but it is difficult to avoid if both reservoirs are simultaneously flushed). In addition to providing a different value of the diffusivity ration $\tau = \kappa S/\kappa T$ (about 3×10^{-3} for sugar and 10^{-2} for salt or boric acid), the non-ionic sugar permits use of the thymol blue dye technique to obtain some flow visualization.

The small values of τ used in these experiments indicate that the lowest linear instability is oscillatory, and for the fairly large values of $R_S(10^5 - 10^7)$ used, the bifurcation is probably subcritical. Indeed if the solute gradient is established first, with no heating, and then the heating rate is slowly increased, the Nusselt numbers are found to remain at unity until the thermal Rayleigh number R_T reaches a value near, though somewhat below, that of the lowest linear instability. Convection then starts abruptly and the temperature difference (heat flux being fixed) drops quickly so that the thermal Nusselt number rises to about 3 or 4. Further increase of the power input gives a slow increase in Nusselt numbers. Once convection has started, however, the power input can be decreased greatly without the convection ceasing. As the heat flux is slowly reduced, the thermal Nusselt number decreases, but not very much so until the heat flux is reduced by a factor of the order of ten, when it rather quickly falls back to unity. The solute Nusselt number appears to be rather larger than the thermal one when convection first begins, and to decrease more rapidly as the power is reduced. We are attempting to determine how these minimal conditions for the maintenance of convection depend on the other parameters. Only one of the earlier experiments dealt with this; it suggested that convection could be maintained until the density ratio $\beta\Delta S/\alpha\Delta T = R_S/R_T$ reached a value of about 18. The

sugar experiments give somewhat lower values and indicate a definite dependence on the solute Rayleigh number qualitatively similar to that suggested by the theory of Proctor (1981). However, Proctor's theory assumes that $\tau^{1/2}R_S$ (or $\tau^{2/3}R_S$ for rigid boundary conditions) is small, which is not true of these experiments; it is also for steady two-dimensional flow. Some instances of apparently steady subcritical convection were observed, as well as some apparently periodic ones, but near the lowest values of heating rate at which subcritical convection could be sustained we generally found irregular oscillations, and the motion seemed to be three dimensional.

II. The numerical calculations of Huppert and Moore (1976) also do not directly apply to these experiments, because they are for two-dimensional convection with free boundary conditions, and do not cover the range of Prandtl number, τ and R_S needed. In a qualitative way there is some resemblance, but the experiments are not yet complete enough to permit, say, the delineation of parameter ranges for steady, periodic or irregular motion. With regard to the least value of R_T at which convection can be sustained we might look to absolute stability bounds obtained by the energy method. Unfortunately the best result obtained by Shir and Joseph (1968) in this regard, for the case of thermal destabilization and solute stabilization, is that convection is only excluded for $R_T < R_c$ ($\approx$1708) -- no effect of R_S is found at all by these methods. In the lecture an extension of the energy method, which also utilizes another integral relation obtained from the temperature and solute equations jointly (and not used by Shir and Joseph), was described. Some simple but rather weak estimates applied to this show that convection cannot occur if $R_T < \tau R_S + R_c$, so this method does enlarge the excluded region obtained by Shir and Joseph. Stronger results that this can be obtained by this approach, but the details are not yet complete; the above estimate at any rate suggests that R_S has <u>some</u> effect.

REFERENCES

Huppert, H.E. and D.R. Moore, 1976. Nonlinear double-diffusive convection, <u>J. Fluid Mech.</u> <u>78</u>, 821-854.

Proctor, M.R.E., 1981. Steady subcritical thermohaline convection, <u>J. Fluid Mech.</u> <u>105</u>, 507-521.

Shir, C.C. and D.D. Joseph, 1968. Convective Instability in a Temperature and Concentration Field, <u>Arch. Rational Mech. Anal.</u> <u>30</u>, 38-80.

LECTURES OF FELLOWS

Model Equations for Pattern Selection in Finite Systems

James W. Swift

In spite of many years of experimental and theoretical study, the problem of pattern selection in convection remains unsolved. There is not even concensus as to which patterns are observed experimentally in a container with given dimensions. One reason for the confusion is the large number of dimensionless parameters needed to characterize a real experiment. In addition to the Rayleigh and Prandtl numbers, two aspect ratios of a rectangular box (or one for a cylinder, etc.) and the relative conductivity of the fluid and plates, all have an effect on pattern formation. The boundary conditions vary from experiment to experiment and between experiment and theory. Some experimentalists fix heat flux, others fix the temperature difference; some raise the temperature difference slowly through threshold, others drop down to slightly subcritical values from a turbulent state; some force an initial pattern, others allow spontaneous pattern selection.

Furthermore, all experiments have imperfections -- the plates are neither parallel nor flat, there may be horizontal heat flux at the lateral boundaries, and non-Boussinesq effects are always present to some degree.

The Boussinesq equations for convection are complicated; they are difficult to study analytically and difficult to simulate numerically. For this reason many researchers study model equations for convection in which the vertical dependence of the fields is suppressed. It is hoped that these models contain the essential features of pattern selection which are independent of the details of a given experiment. Since the vertical eigenfunctions are "quantized," the vertical structure of the fields is dominated by the first mode to go unstable. These model equations are simplifications of the normal form equations one finds when the vertical structure is removed using the "physicist's center manifold" technique (see Spiegel's lecture #5, this volume).

The Swift*-Hohenberg (1977) equation is the first and simplest of the model equations. A single real field ψ -- often thought of as the vertical velocity -- is a function of the horizontal domain D and time,

$$\dot{\psi}(\underset{\sim}{x},t) = [\varepsilon - (1 + \nabla^2)^2]\psi - \psi^3, \qquad (1a)$$

with boundary conditions that ψ and its normal derivative vanish

$$\psi/_{\partial D} = \partial_n\psi/_{\partial D} = 0. \qquad (1b)$$

The linear terms in equation (1) model an instability with a preferred wavelength normalized to $k^2 = 1$. The equations have the symmetry of rotations and translations in the plane (although this symmetry is broken by the boundaries). The neutral stability curves for plane waves (in an infinite domain) for the model and Boussinesq equations are compared in figure 1.

* no relation to author

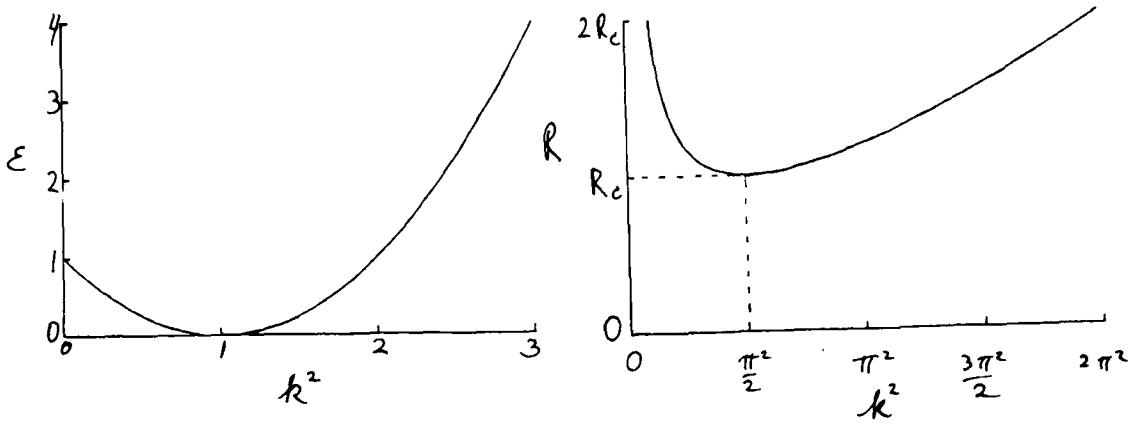

Figure 1

The neutral stability curves for (a) $L_\varepsilon \equiv \varepsilon - (1 + \nabla^2)^2$ and (b) Bénard convection. Near threshold the correspondence is $\varepsilon\alpha(R - R_c)/R_c$. The critical wavenumber is normalized to 1 by scaling x, and the curvature of the parabola at the minimum is set to 1 by scaling ε.

When lateral boundaries are included the eigenvalue problem

$$(1 + \nabla^2)^2\psi = \varepsilon\psi \qquad (2)$$

for the critical Rayleigh number (ε) is no longer trivial. The corresponding linear problem for convection with realistic boundary conditions is only solvable numerically. This is why model equations are often used to study the onset of convection in finite geometries.

In this paper, we solve the eigenvalue equation (2) in one dimension and, less completely, in a circular disk. It appears that closed form solutions are impossible in rectangular geometry since the biharmonic operator $(\nabla^2)^2$ is nonseparable in rectangular coordinates. There is a large qualitative difference between linear stability theory for rigid (no-slip) and free (stress-free) boundary conditions at the sidewalls.

For certain interval lengths L in the one-dimensional problem there are two patterns (corresponding m and (m-1) rolls), which go unstable simultaneously. We study the nonlinear competition between these two solutions. There is a quantitative (but not qualitative) difference between rigid and free boundaries which does not go away in the limit $L \to \infty$.

The implications of these results for convection in finite containers, and for wavenumber selection in equation (1) are discussed.

Physical Interpretation of the Model Equations

When presented with the model equations, an obvious question is "What is ψ physically?". One answer is that ψ is the "order parameter," some characterization of the state of the system. This is not much help.

In the one-dimensional model equations, corresponding to two-dimensional convection, ψ is best interpreted as the horizontal velocity, evaluated on some horizontal plane: $\psi(x) = u(x, z=z_o)$. Clearly, we want $\psi = 0$ at the boundaries. The continuity equation $\nabla \underset{\sim}{u} = \partial_x u + \partial_z w = 0$ implies that $\partial_x \psi = 0$ at the boundaries ($w=0$). If we assume that the vertical dependence of the fields separates out (not true for rigid top and bottom plates), then we can identify $\partial_x \psi$ with the vertical velocity.

$$\underset{\sim}{u} = \psi(x) \cos \pi z, \quad w = -1/\pi \ \partial_x \psi \sin \pi z.$$

For stress-free boundaries at the sidewalls, the correct boundaries conditions are $\psi = (\partial_n)^2 \psi = 0$.

In the two-dimensional models for three dimensional convection, there are two possible interpretations of ψ; (1) the vertical velocity, and (2) the velocity potential.

For the following discussion, let $\underset{\sim}{u} = (\underset{\sim}{v}, w)$, where $\underset{\sim}{v}$ is the horizontal velocity and w is the vertical velocity.

In interpretation (1),

$$\psi(x, y) = w(x, y, z=z_o).$$

When ε is very small we have the approximate identity

$$\underset{\sim}{v} \approx -\nabla \psi,$$

which leads naturally to the "rigid" boundary conditions

$$\underset{\sim}{u} = 0 \Rightarrow \psi = \partial_n \psi = 0.$$

This interpretation is not very satisfactory in small boxes. The deviation from $\underset{\sim}{v} = -\nabla \psi$ can be quite large, and the eigenfunctions can have the undesirable property that the average of ψ over the layer is nonzero.

The second interpretation (2) is

$$-\nabla \psi(x, y) = \underset{\sim}{v}(x, y, z=z_o).$$

This has the consequence that $w \approx \nabla^2 \psi$. The rigid boundary condition $\underset{\sim}{v} = 0$ implies that $\nabla \psi = 0$. In a simply connected domain, ψ must be constant on the boundary. This constant can be chosen to be zero, giving the boundary conditions (1b).

In real convection there is a third boundary condition -- involving the temperature -- which has no analogue here. The model equation are biharmonic ($(\nabla^2)^2$), thus two boundary conditions are needed, whereas the full convection equations are triharmonic ($(\nabla^2)^3$) and need three boundary conditions. Drazin (1975) has studied a more realistic linear model for two-dimensional convection; he assumes idealized boundary conditions at the top and bottom plates so that the equations separate. A sixth-order ODE in the horizontal direction results, and all the boundary conditions can be satisfied, but the results are quite complicated.

Nonlinear Terms

In one spatial dimension, where ψ represents the horizontal velocity, an alternative to the model equation (1) includes the advection nonlinearity, $\dot{\psi} = L_\varepsilon\psi + \psi\,\partial_x\psi$ where $L_\varepsilon = (\varepsilon - (1 + \nabla^2)^2)$ (see Pomeau and Zaleski, 1980, 1981).

In two dimensions, an advection term like $\psi\nabla\psi$ is not rotationally invariant. Greenside and Cross (1985) discuss many possible nonlinear terms

$$\begin{aligned}\dot{\psi} = L_\varepsilon\psi &- a\psi^3 \\ &- b\psi|\nabla\psi|^2 \\ &- c\psi\nabla^2\psi \\ &- d(\nabla^2\psi)|\nabla\psi|^2 \\ &- e(\partial_i\psi)(\partial_j\psi)(\partial_i\partial_j\psi).\end{aligned} \tag{3}$$

One of the important distinctions between various models is whether or not they are derivable from a potential. For equation (1) there is a potential

$$V[\psi] = \int_D d^2\underset{\sim}{x}\{-1/2\ \varepsilon\psi^2 + 1/2\ [(1 + \nabla^2)\psi]^2 + 1/4\ \psi^4\}$$

such that

$$\dot{\psi} = \frac{-\delta V[\psi]}{\delta\psi}$$

This potential is a Lyapunov functional; it is bounded from below and its time derivative is negative unless $\dot{\psi} = 0$

$$\dot{V}[\psi] = \int_D d^2\underset{\sim}{x}\ \delta V/\delta\psi \cdot \dot{\psi} = -\int_D d^2x\ (\dot{\psi})^2 \leq 0.$$

Such models are called variational, or relaxational, and the system always evolves towards a local minimum of the potential. Limit cycles or chaotic behavior are impossible in these models.

Time dependence which appears to continue indefinitely is experimentally observed very near threshold (Ahlers et al., 1985). Nonvariational models are needed to describe this time dependence, although the lowest order amplitude equations (Segel, 1969; Newell and Whitehead, 1969) are nonvariational.

For a general functional

$$V[\psi] = \int_D d^2\underset{\sim}{x}\ (\psi, \nabla\psi, \nabla^2\psi, \ldots),$$

the functional derivative is

$$\delta V/\delta\psi\ [\psi] = \partial\mathcal{V}/\partial\nabla - \nabla[\partial\mathcal{V}/\partial(\nabla\psi)] + \nabla^2[\partial\mathcal{V}/\delta(\nabla^2\psi)] - \ldots$$

(assuming that there are no contributions from the boundary terms in the integrations by parts). Note that there are two rotationally symmetric terms for $\mathcal{N}$ which have two powers of ∇ and four powers of ψ:

$$\mathcal{N} \sim |\nabla\psi|^2\psi^2, \quad \mathcal{N} \sim (\nabla^2\psi)\psi^3.$$

Both of these terms give (up to a constant) the same variational dynamics:

$$\dot{\psi} \propto (\psi|\nabla\psi|^2 + \psi^2\nabla^2\psi)$$

Thus the model (3) can be variational only if b=c. Similarly, if e = 2d in (3), then the last two terms are derivable from a potential with $\mathcal{N} = (|\nabla\psi|^2)^2$.

A realistic treatment of the cross-roll instability requires the presence of the term proportional to e in equation (3). The analysis of three-dimensional instabilities (including the cross-roll instability) involves the interaction of two rolls oriented at some relative angle φ. For the first four nonlinear terms in (3), this interaction is independent of φ. In real convection, the "lattice function" which measures this interaction of two rolls, is a complicated function of $\cos^2\varphi$. A local model equation, with a finite number of derivatives, cannot have the same lattice function as real convection. The equation (3) with a nonzero $\mathcal{L}$ term can, however, model the relative stability of rolls and squares.

Linear Theory in One Dimension

As the Rayleigh number (ε) is increased, a stationary mode bifurcates from the origin when $L_\varepsilon\psi = 0$. In order to find the critical ε, we must solve the eigenvalue problem

$$(1 + \nabla^2)^2\,\psi(x) = \varepsilon\psi(x), \quad x \in \mathbb{R}.$$

We will solve this equation in one dimension subject to two sets of boundary conditions:

$$\text{FREE:} \quad \psi(\pm L/2) = \psi''(\pm L/2) = 0$$

$$\text{RIGID:} \quad \psi(\pm L/2) = \psi'(\pm L/2) = 0.$$

For free boundaries, the eigenvalue problem is trivial since a pure sine wave satisfies both of the boundary conditions. The eigenfunction with p bumps is

$$\psi_p(x) = \sin\left[\frac{p\pi(x + L/2)}{L}\right].$$

The eigenvalue for this eigenfunction is

$$\varepsilon_p = [1 - (p\pi/L)^2]^2$$

The eigenvalues as a function of L, the length of the box, are drawn in figure 2.

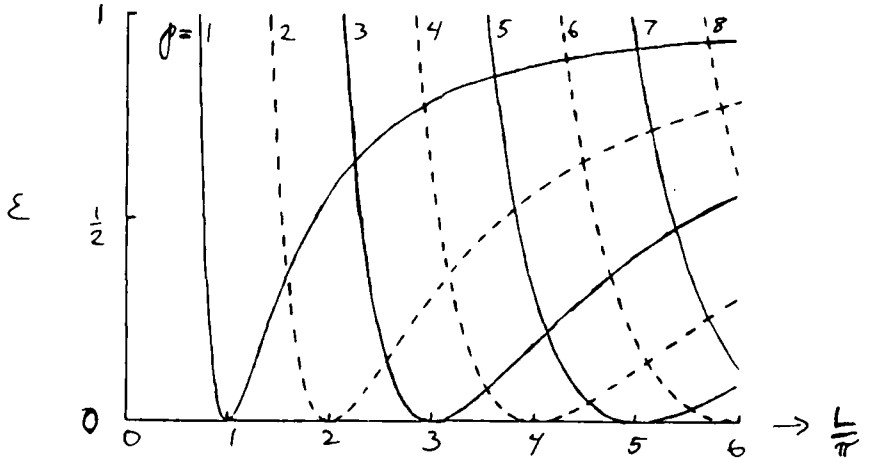

Figure 2: The eigenvalues ε of $(1 + \nabla^2)^2$ for free boundaries, as a function of the box length L. Only eigenvalues smaller than 1 are shown. The integer p indicates the number of half wavelengths, each corresponding to a roll which fits in the box. The solid lines are even solutions, and the dotted lines are odd solutions.

The eigenvalue problem with rigid boundaries is more difficult, although it is straightforward. It is a one-dimensional ODE with constant coefficients, so the eigenfunctions are sums of exponentials,

$$\psi = \sum_{\alpha} A_\alpha e^{ik_\alpha x},$$

where k_α are the roots of the quardic in k, $(1 - k^2)^2 = \varepsilon$. The two positive roots (for $0 < \varepsilon < 1$) are

$$k_+ = \sqrt{1 + \sqrt{\varepsilon}} \quad , \quad k_- = \sqrt{1 - \sqrt{\varepsilon}} \; .$$

Due to the reflectional symmetry about $x = 0$, the eigenfunctions are either even or odd,

$$\psi^{(e)}(x) = a \cos(k_+ x) + b \cos(k_- x)$$

$$\psi^{(o)}(x) = c \sin(k_+ x) + d \sin(k_- x),$$

where the constants are determined by the boundary conditions. (Only the boundary conditions at $x = L/2$ need be satisfied, the others follow from the symmetry.)

The rigid boundary conditions for even solutions can be written as

$$\begin{pmatrix} \cos(k_+L/2) & \cos(k_-L/2) \\ k_+\sin(k_+L/2) & k_-\sin(k_-L/2) \end{pmatrix} \begin{pmatrix} a \\ b \end{pmatrix} = 0$$

(A similar expression holds for the odd solutions.) The determinant of the matrix must vanish when there are nontrivial solutions. This yields the eigenvalue relations for the even (and odd) solutions:

$$\sin(\alpha_-L) = \begin{matrix} - \\ + \end{matrix} (\alpha_-/\alpha_+)\sin(\alpha_+L), \qquad \begin{matrix} \text{EVEN } (-) \\ \text{ODD } (+) \end{matrix} \qquad (4)$$

where

$$\alpha_- = (k_+-k_-)/2, \quad \alpha_+ = (k_++k_-)/2.$$

These two eigenvalue relations are transcendental equations relating ε and L. We can solve them graphically by letting L vary with ε (and therefore $\alpha_\pm$) fixed.

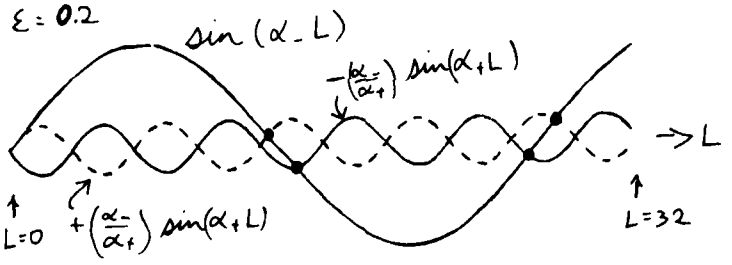

Figure 3: The eigenvalue relations (4) solved graphically. Intersections at $L \neq 0$ correspond to even (solid curve) or odd (dotted curve) solutions. For small ε there are two solutions near $\alpha_-L = n\pi$. For any ε between 0 and 1 there is one even solution and one odd solution in the interval $(n - 1/2)\pi < \alpha_-L < (n + 1/2)\pi$, $n \geq 1$.

It is easy to find the approximate solutions for small ε.

$$0 < \varepsilon << 1 \Rightarrow \alpha_+ = 1 + O(\varepsilon), \quad \alpha_- = 1/2\sqrt{\varepsilon} + O(\varepsilon^{3/2})$$

The intersection of the two sine waves occurs for

$$\alpha_-L \approx n\pi \Rightarrow \varepsilon \approx (2\pi n/L)^2$$

This result corresponds to modulation theory, where the carrier waves with $k = 1$ are modulated by $\sin[n\pi(x+L/2)/L]$. Modulation theory is insensitive to the phase of the carrier wave, so the even and odd solutions are degenerate. The even and odd eigenfunctions have slightly different eigenvalues:

$$\varepsilon = (2\pi n/L)^2 \left[1 \mp (-1)^n (2/L) \sin(L) + O(1/L^2)\right] \quad \begin{matrix} \text{EVEN } (-) \\ \text{ODD } (+) \end{matrix} \qquad (5)$$

This expression holds for small ε, which implies that L is large.

When $L \cong n\pi$ the even and odd solutions are degenerate. These degeneracies can be found exactly by inspection of the eigenvalue relations. Even and odd solutions occur at the same (ε, L) when

$$\alpha_- = (n\pi/L), \quad \alpha_+ = (m\pi/L), \qquad 1 \leq n < m \qquad (6)$$

The wavenumbers $k_\pm$ are

$$k_- = p\pi/L \quad , \quad k_+ = q\pi/L \quad , \qquad (7)$$

where

$$p = m - n, \; q = m + n.$$

Note that p and q are either both even or both odd. The two degenerate "special eigenfunctions" are

$$\psi^{(c)}_{p,q}(x) = \cos\left[\frac{p\pi(x + L/2)}{L}\right] - \cos\left[\frac{q\pi(x + L/2)}{L}\right] \qquad (8)$$

$$\psi^{(s)}_{p,q}(x) = \sqrt{\frac{2}{p^2+q^2}} \left\{ q \sin\left[\frac{p\pi(x + L/2)}{L}\right] - p \sin\left[\frac{q\pi(x + L/2)}{L}\right] \right\} \qquad (9)$$

These eigenfunctions are normalized so that their square has an average of 1. The cosine-type eigenfunction $\psi^{(c)}$ are even if p and q are even, and odd if and q are odd. Some of the eigenfunctions are plotted in figure 4. The eigenvalues of these special eigenfunctions satisfy

$$\varepsilon = [1 - (p\pi/L)^2]^2 = [1 - (q\pi/L)^2]^2.$$

These equations can be solved simultaneously to give

$$\varepsilon = \left(\frac{q^2 - p^2}{q^2 + p^2}\right)^2 = 4\left(\frac{nm}{n^2 + m^2}\right)^2 \qquad (10)$$

where the eigenfunctions fit in a box of length

$$L = \pi\sqrt{n^2 + m^2} = (\pi/\sqrt{2})\sqrt{p^2 + q^2}. \qquad (11)$$

The eigenvalue relations (4) implicitly determine a set of curves in the ε-L plane, corresponding to critical Rayleigh numbers as a function of L. The following observations aid the drawing of these curves.

The special solutions to the eigenvalue relations give discrete points in the ε-L plane where curves of even and odd eigenfunctions intersect.

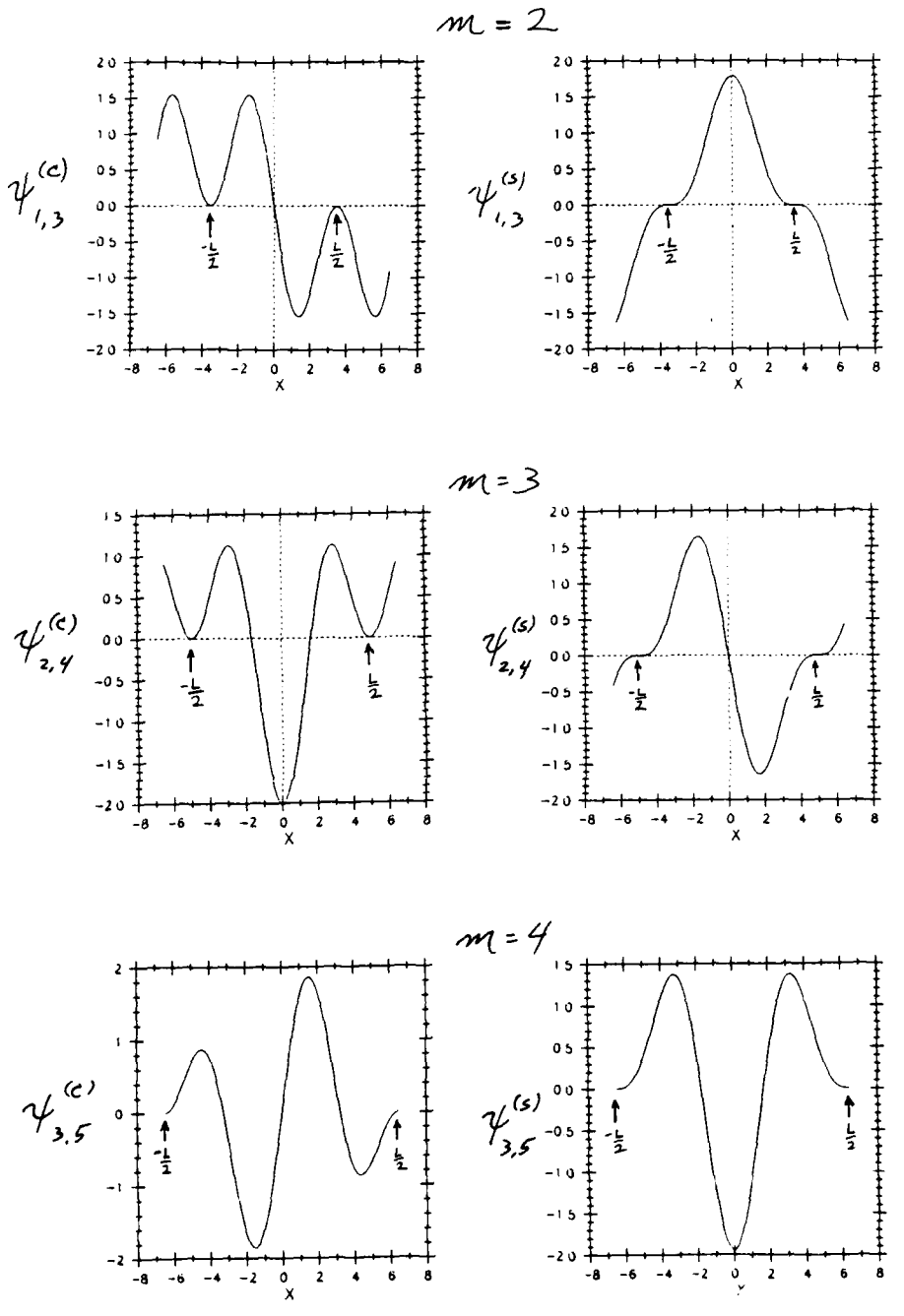

Figure 4: The special eigenfunctions $\psi^{(c)}_{p,q}$ (left column) and $\psi^{(s)}_{p,q}$ (right column). (See equations (8) and (9).) These are the two degenerate eigenfunctions at special values of the box length L. All eigenfunctions shown have $n = (p-q)/2 = 1$, thus they are the first modes to go unstable as ε is increased. For n=1, $\psi^{(c)}_{p,q}$ has m rolls and $\psi^{(s)}_{p,q}$ has (m-1) rolls, where $m = (p+q)/2$. The roll boundaries are at $\psi=0$, since ψ represents the horizontal velocity.

It can be seen from (7) that these points in the rigid case correspond to points in figure 2 (for stress-free boundaries) where two even solutions (p and q odd) or two odd solutions (p and q even) intersect.

REMARK: At these points where two solution curves meet, one of the curves has zero slope. Furthermore, these are inflection points rather than minima; each branch of solution curves is monotonically decreasing.

PROOF: The flat places on the solution curves are found by differentiating (4) with respect to L:

$$\cos(\alpha_- L) = \begin{matrix}\text{EVEN } (-) \\ \mp \\ \text{ODD } (+)\end{matrix} \cos(\alpha_+ L).$$

This must be solved simultaneously with (4). The only solutions are the special solutions (10) and (11), where

$$(-1)^n = \begin{matrix}\text{EVEN } (-) \\ \mp \\ \text{ODD } (+)\end{matrix} (-1)^m \Rightarrow (-1)^{n-m} = (-1)^p = \begin{matrix}-\\ \mp \\ +\end{matrix} 1$$

Thus the even or odd solution curve (depending on p) has zero slope whenever the curves intersect. By differentiating (4) again, we find that the curvature is zero when the slope is zero. (End of proof)

As the eigenvalue ε approaches 1, the eigenvalue relations (4) reduce to

$$\sin(L/\sqrt{2}) = 0 \qquad \text{EVEN}$$

$$\tan(L/\sqrt{2}) = L/(2\sqrt{2}) \qquad \text{ODD.}$$

Thus the even solution curves reach $\varepsilon = 1$ at $L = n\pi\sqrt{2}$, and for large L the odd solution curves approach $\varepsilon = 1$ at $L = \sqrt{2}\,(n + 1/2)\pi$.

The solution curves are drawn in figure 5.

Note the differences in figures 2 and 5. With stress-free boundaries the eigenfunctions with p rolls fall on continuous curves. With rigid boundaries, the number of rolls on a solution branch changes when two new rolls are pushed in from the boundaries. The number of rolls for the lowest lying (n=1) set of solutions curves is indicated in figure 6. The new rolls are formed at the boundaries when $\psi''(\pm L/2) = 0$. This occurs for $\psi^{(s)}_{p,q}$ (see figure 4 or equation (9)).

Davis (1967) found the eigenfunctions for convection in a three-dimensional rigid boundary box. He numerically solved for ε versus L assuming a fixed number of rolls, therefore he did not find results like figure 6 where the number of rolls changes along a solution branch.

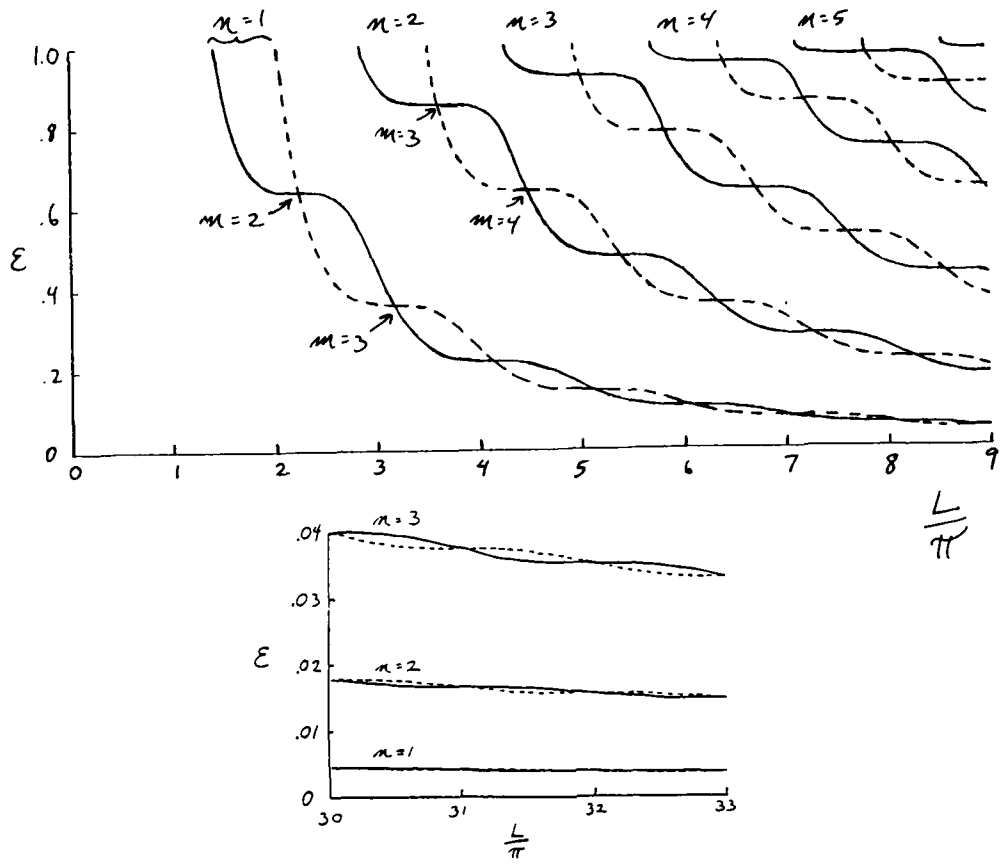

Figure 5: As for figure 2, except with rigid boundaries. The integers n and m are defined in equation (6). The bottom figure shows the solution curves in the large L limit, given by equation (5).

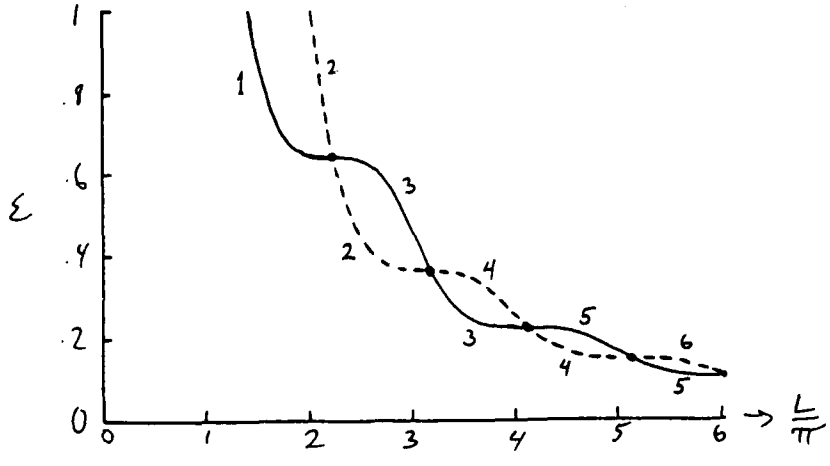

Figure 6: The two n = 1 solution curves are shown, and the number of rolls is indicated. The number of rolls jumps by 2 at the dots; one roll is created at each boundary.

The Competition Between m and m-1 Rolls

In this section, we analyze the effects of rigid versus free sidewalls on the competition between m and m - 1 rolls in the one-dimensional model equation (1a). When the length L of the box is set at special values, two eigenfunctions bifurcate at the same Rayleigh number ε. As ε and L are varied in the neighborhood of the intersection there is a codimension-two bifurcation. We are concerned primarily with the n = 1 intersections shown in figure 6, where m and m - 1 rolls bifurcate simultaneously at

$$L_m = \pi(1 + m^2)^{1/2}, \quad \varepsilon_m = 4m^2/(1 + m^2)^2$$

Near the codimension-two bifurcation, the two critical eigenfunctions have the largest amplitude, and the field can be written as (see equations (8) and (9) and figure 4)

$$\psi(x,t) = \sqrt{4/3}\ (A_m(t)\psi^{(c)}_{p,q}(x) + A_{m-1}(t)\psi^{(s)}_{p,q}(x)) + \ldots$$

where

$$p = m - 1, \quad q = m + 1$$

The linear theory of the last section gives the linear ODE

$$\dot{A}_m = \mu A_m$$

$$\dot{A}_{m-1} = \nu A_{m-1},$$

where

$$\begin{aligned} \mu &= \varepsilon - \varepsilon_m + c_m(L - L_m) + O(L - L_m)^3 \\ \nu &= \varepsilon - \varepsilon_o, \qquad\qquad + O(L - L_m)^3, \end{aligned} \tag{12}$$

and the constants c_m are the slopes of the m-roll branch. For large m equation (5) implies $c_m \approx 16/(\pi m^3)$.

The true field ψ is a superposition of eigenfunctions of $(1 + \nabla^2)^2$ at the fixed L. These eigenfunctions are orthogonal, so we can project out the amplitude dependence by taking the inner products

$$\langle \psi^{(c)}_{p,q} \cdot \dot{\psi} \rangle = \langle \psi^{(c)}_{p,q} \cdot (L_\varepsilon \psi - \psi^3) \rangle \tag{13}$$

and

$$\langle \psi^{(c)}_{p,q} \cdot \dot{\psi} \rangle = \langle \psi^{(s)}_{p,q} \cdot (L_\varepsilon \psi - \psi^3) \rangle, \tag{14}$$

where the brackets are an average over the layer:

$$\langle f(x) \rangle = 1/L \int_{-L/2}^{L/2} f(x)dx$$

Using the even and odd symmetry properties of the eigenfunctions, and the fact that

$$\langle (\psi^{(c)}_{p,q})^2 \rangle = \langle (\psi^{(s)}_{p,q})^2 \rangle = 1$$

we see that equations (13) and (14) reduce to

$$\dot{A}_m = \mu A_m - 4/3\, A_m[\langle(\psi^{(c)})^4\rangle\ A_m^2 + \langle(\psi^{(c)})^2(\psi^{(s)})^2\rangle\, A_{m-1}^2] + \ldots$$

$$\dot{A}_{m-1} = \nu A_{m-1} - 4/3\, A_{m-1}[\langle(\psi^{(s)})^4\rangle\ A_{m-1}^2 + \langle(\psi^{(c)})^2(\psi^{(s)})^2\rangle\, A_m] + \ldots$$

A calculation of the nonlinear terms gives for ($q \neq 3p$)

$$\dot{A}_m = \mu A_m - A_m(3A_m^2 + A_{m-1}^2) + O(A^5)$$

$$\dot{A}_{m-1} = \nu A_{m-1} - A_{m-1}\left[\frac{2(q^4 + 4q^2p^2 + p^4)}{(q^2 + p^2)^2}\ A_{m-1}^2 + A_m^2\right] + \ldots$$

This ODE is actually calculated for any nonresonant ($q \neq 3p$) p and q. In the present case, the complicated coefficient can be simplified:

$$\frac{2(q^4 + rq^2 + p^4)}{(q^2 + p^2)^2} = 2 + \left(\frac{m^2-1}{m^2+1}\right)^2 \lesssim 3.$$

The competition between 1 and 2 rolls ($p = 1$, $q = 3$) must be treated separately. The ODE is

$$\dot{A}_2 = \mu A_2 - A_2\left(\frac{7}{4}\, A_2^2 + \frac{21}{20}\, A_1^2\right) + \ldots$$

$$\dot{A}_1 = \nu A_1 - A_1\left(3 \cdot \frac{99}{100}\, A_1^2 + \frac{21}{20}\, A_3^2\right) + \ldots.$$

With stress-free boundaries, the calculations are much simpler. The field is

$$\psi(x) = \sqrt{2}\ \{A_m \sin\left[\frac{m\pi(x + L/2)}{L}\right] + A_{m-1}\sin\left[\frac{(m-1)\pi(x + L/2)}{L}\right]\} + \ldots$$

The ODE near the codimension-two bifurcation is

$$\dot{A}_m = \mu A_m - A_m(3/2\, A_m^2 + A_{m-1}^2) + O(A^5)$$

$$\dot{A}_{m-1} = \nu A_{m-1} - A_{m-1}(3/2\, A_{m-1}^2 + A_m^2) + O(A^5)$$

where μ and ν are obtained from linear theory.

Note that the normal form for rigid boundaries does not approach the normal form for free boundaries as $m \to \infty$.

The analysis of this normal form can be found in Guckenheimer and Holmes (1983) so we will give a brief treatment here. In all cases the normal form can be written

$$\begin{aligned} \dot{A}_m &= \mu A_m - A_m(\alpha A_m^2 + A_{m-1}^2) \\ \dot{A}_{m-1} &= \nu A_{m-1} - A_{m-1}(\beta A_{m-1}^2 + A_m^2) \end{aligned} \qquad (15)$$

where

$$\left.\begin{aligned}\alpha &= 3\\ \beta &= 2 + [(m^2-1)/(m^2+1)]^2\end{aligned}\right\} \quad \text{RIGID } (m \neq 2)$$

$$\alpha = \beta = 3/2 \qquad \text{FREE}$$

Note that the ODE has the symmetry of a rectangle in the plane:

$$\begin{aligned}(A_m, A_{m-1}) &\longrightarrow (-A_m, A_{m-1})\\ &\longrightarrow (A_m, -A_{m-1})\\ &\longrightarrow (-A_m, -A_{m-1})\end{aligned} \qquad (16)$$

There are four solution types:

TRIVIAL	$A_m = A_{m-1} = 0$
m ROLLS	$A_m^2 = \mu/\alpha$, $A_{m-1} = 0$
m-1 ROLLS	$A_m = 0$, $A_{m-1}^2 = \nu/\beta$
ASYMMETRIC	$A_m^2 = (\beta\mu-\nu)/(\alpha\beta-1)$, $A_{m-1}^2 = (\alpha\nu-\mu)/(\alpha\beta-1)$

Of course, these solutions only exist when $A_m^2 \geq 0$ and $A_{m-1}^2 \geq 0$. Figure 7 shows the phase plane behavior as a function of the parameters μ and ν.

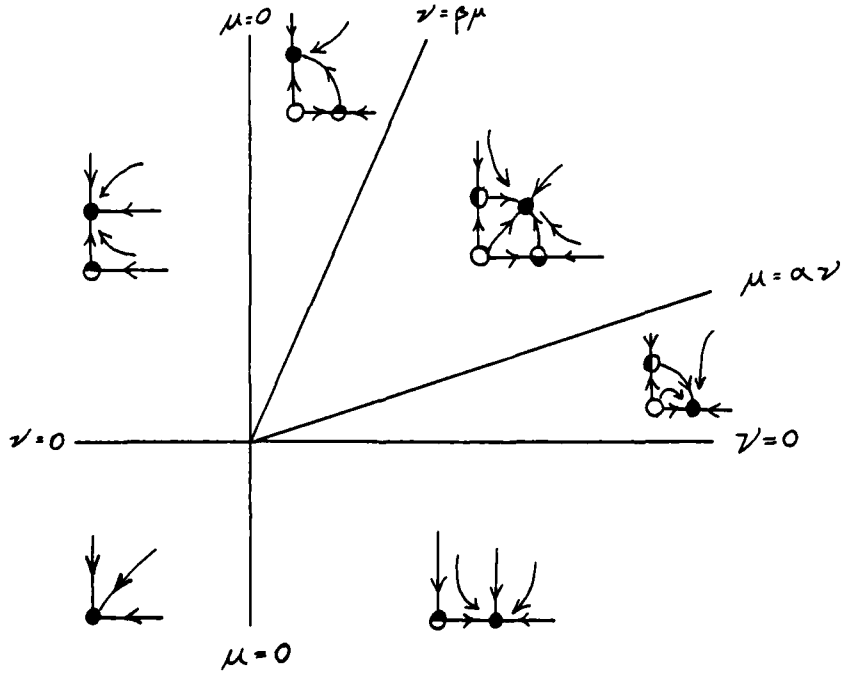

Figure 7: Equation (15) with $\alpha > 1$ and $\beta > 1$. The parameter space is divided into six regions by the lines $\mu = 0$, $\nu = 0$, $\nu = \beta\mu > 0$, and

$\mu = \alpha\nu > 0$. One quarter of the $A_m - A_{m-1}$ phase plane is drawn for six choices of μ and ν fixed. The rest of the phase planes are obtained by the symmetries (16). The asymmetric solutions are stable in the wedge at the upper right corner in μ-ν space.

As ε is increased in the original problem, the system traverses the μ-ν plane toward the upper right at 45° (see equation (12)). Since $\alpha > 1$ and $\beta > 1$, we always end up in the region with stable asymmetric solutions.

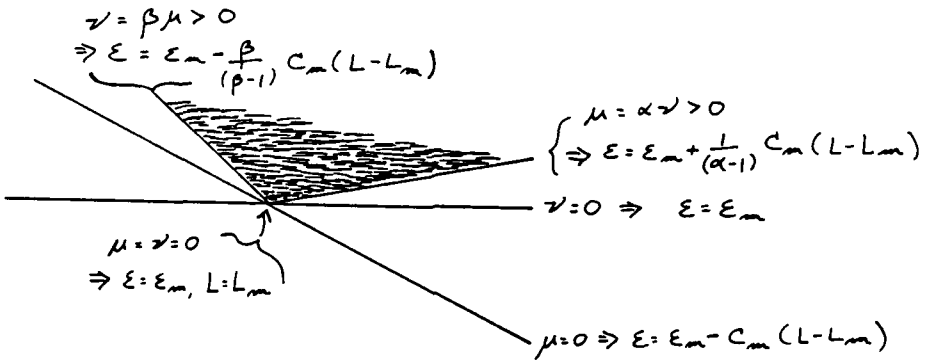

Figure 8: The codimension-two bifurcation in the original parameter space (the ε-L plane). The asymmetric solutions are stable in the shaded region. For large m the shaded region occupies almost the whole region where nontrivial solutions exist.

The bifurcation diagrams, which plot $\langle\psi^2\rangle$ versus ε, can now be drawn for the original system at fixed L.

Discussion

The codimension-two analysis presented here is only valid for small amplitudes, certainly only for ε small enough that the $n = 2$ branches of solutions are not reached (see figure 5). The results strongly suggest, however, that the stable solutions at larger ε will be neither even nor odd. If so, this contradicts the results of Pomeau and Zaleski (1981).

Knobloch and Guckenheimer (1983) analyzed the competition between m and (m-1) rolls in two-dimensional convection with stress-free boundaries. As they appreciated, the results might change significantly if rigid boundary conditions are used. Such a calculation -- even the linear theory -- could only be done numerically for the convection equations. Therefore, we have studied the simple model equation (1).

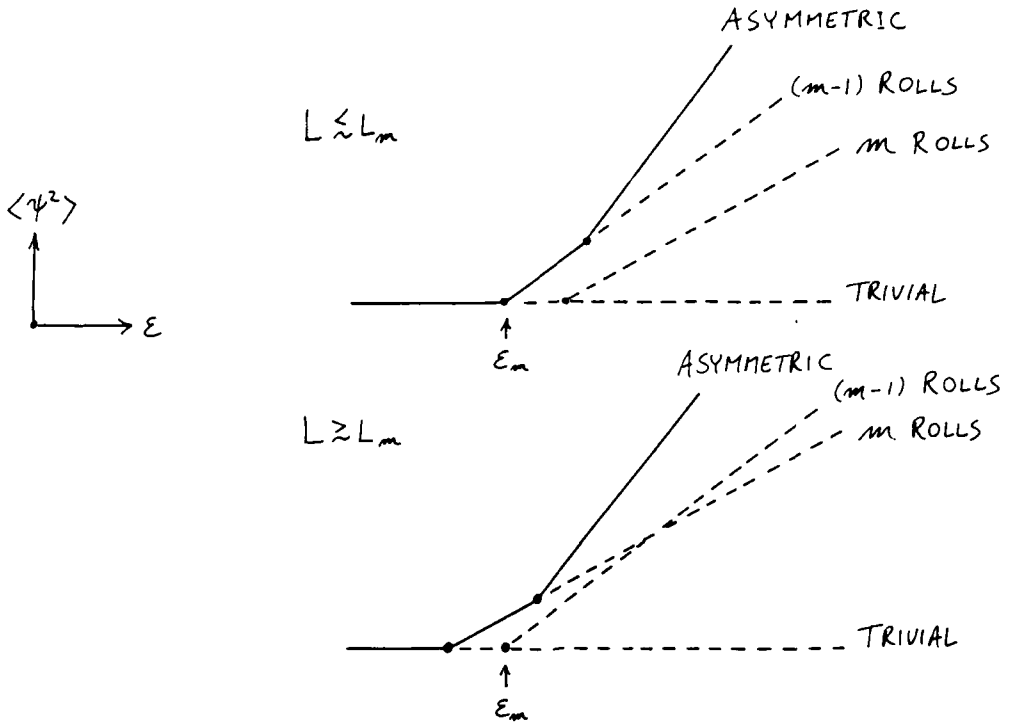

Figure 9: Bifurcation diagrams for the competition between m and (m-1) rolls in the Swift-Hohenberg equation (1). Solid lines indicate stable solutions, dotted lines indicate unstable solutions. The asymmetric solution is a superposition of m and (m-1) rolls.

The linear theory reveals a striking difference in the "strong resonsances" possible with rigid versus free boundaries. If the Boussinesq symmetry does not hold, there is the possiblity of quadratic terms in the amplitude equations when the ratio of wavelengths is 2:1. These quadratic terms would cause subcritical instabilities.

The strong resonances for a "non-Boussinesq" model

$$\dot{\psi} = L_\varepsilon \psi + \delta\psi^2 - \psi^3$$

would occur for the competition between one and two rolls in the stress-free case, as expected. Suprisingly, with rigid boundaries the 2:1 resonance in k-space occurs when two and three rolls coexist. This can be seen from linear theory alone: two and three rolls coexist when $p = 2$ and $q = 4$ (see equation (7) and figure 4).

Admittedly, this result is due to the detailed form of the assumed linear operator, but the effect will be present in more realistic calculations whenever the eigenfunctions are not pure exponentials. The results may have relevance to Libchaber and Maurer's (1981) experiments on the competition between two and three rolls.

Appendix: The Linear Problem in a Circular Disk

The eigenvalue problem (2) does not separate in rectangular coordinates, and solutions must be found numerically (Normand, 1983). In polar coordinates, the general solution to (2) can be written as

$$\psi(r,\theta) = \sum_n [A_+(n)J_n(k_+r) + A_-(n)J_n(k_-r)]e^{in\theta}.$$

The boundary conditions for a circle of diameter D are

$$\psi(D/2, \theta) = \partial/\partial r\, \psi(D/2, \theta) = 0.$$

The eigenfunctions are pure n modes in the general solution, where the constants satisfy

$$0 = A_+(n)\, J_n(k_+D/2) + A_-(n)\, J_n(k_-D/2)$$

$$0 = A_+(n)k_+J_n'(k_+D/2) + A_-(n)k_-J_n'(k_-D/2).$$

There is a nontrivial solution provided the eigenvalue relation holds:

$$k_-\, J_n'(k_-D/2)\cdot J_n(k_+\, D/2) - k_+\, J_n'(k_+D/2)\cdot J_n(k_-D/2) = 0$$

This relation has "special solutions," analogous to the one-dimensional case

$$k_-D/2 = j_{n,p} \quad , \qquad k_+D/2 = j_{n,q}'$$

or

$$k_-D/2 = j_{n,p}' \quad , \qquad k_+D/2 = j_{n,q}$$

where j_{np} is the p^{th} zero of $J_n(x)$, and j_{np}' is the p^{th} zero of $J_n'(x)$.

In the limit of $k_-D \gg 1$ (for n fixed) we can use an asymptotic expression for the Bessel function

$$J_n(x) \sim \sqrt{2/\pi x}\, \cos(x - \tfrac{1}{2} n\pi - \pi/4) + O(n^2/x).$$

If this first term is substituted into the eigenvalue relation, it yields the asymptotic eigenvalue relation

$$\sin(\alpha_-D) = -(-1)^n(\alpha_-/\alpha_+)\, \cos(\alpha_+D)$$

Note that in this approximation the eigenvalues are the same for all even and all odd n. The next term in the asymptotic expansion should split this degeneracy, but it leads to a mess.

At the onset of convection in a cylinder, many modes come in at almost the same Rayleigh number; the nonlinear terms are responsible for pattern selection. In a large cylinder, we expect that many modes will combine to give an approximate roll solution (recall the expansion of a plane wave in terms of Bessel functions). There is a cut-off when

$\pi D \sim n$, because then the wavelength of the "rim mode" is approximately 1. In this rim mode there is a single amplitude maxima, concentrated at the rim, and the nodes are radial.

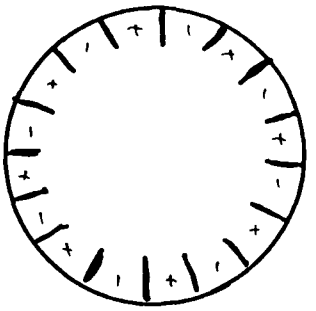

n = 8
"Rim node"

Acknowledgements: I would like to thank Yves Pomeau, George Veronis, Willem Malkus and Ed Spiegel for helpful and stimulating discussions. I enjoyed the exceptional atmosphere at Walsh Cottage this summer; thanks go to all of the participants.

REFERENCES

Ahlers, G., D.S. Cannell and V. Steinberg, 1985. Time dependence of flow patterns near the convective threshold in a cylindrical container, Phys. Rev. Lett. 54, no. 13, 1373-1376.

Cross, M.C., P.G. Daniels, P.C. Hohenberg and E.D. Siggia, 1983. Phase-winding solutions in a finite container above the convective threshold, J. Fluid Mech. 127, 155-183.

Cross, M.C. and A.C. Newell, 1984. Convective patterns in large aspect ratio systems, Physica 10D, 299-328.

Davis, S.H., 1967. Convection in a box: linear theory, J. Fluid Mech. 30, part 3, 465-478.

Drazin, P.G., 1975. On the effects of sidewalls on Benard convection, ZAMP 26, 239-243.

Greenside, H.S. and M.C. Cross, 1985. Stability analysis of two-dimensional models of three-dimensional convection, Phys. Rev. A 31, no. 4, 2492-2501.

Guckenheimer, J. and P. Holmes, 1983. Nonlinear oscillations, dynamical systems and bifurcations of vector fields, Springer Series in Applied Mathematical Sciences 42.

Heutmaker, M.S., P.N. Fraenkel and J.P. Gollub, 1985. Convection patterns: Time evolution of the wave-vector field, Phys. Rev. Lett. 54, no. 13, 1369-1372.

Knobloch, E. and J. Guckenheimer, 1983. Convective transitions induced by a varying aspect ratio, Phys. Rev. A 27, no. 1, 408-417.

LeGal, P., A. Pocheau and V., Croquette, 1985. Square versus roll pattern at convective threshold, Phys. Rev. Lett. 54, no. 23, 2501-2504.

Manneville, P., 1983. A two-dimensional model for three-dimensional convective patterns in wide containers, J. Physique 44, 759-765.

Newell, A.C. and J.A. Whitehead, 1969. Finite bandwidth, finite amplitude convection, J. Fluid Mech. 38, part 2, 279-303.

Normand, C., 1981. Convective flow patterns in rectangular boxes of finite extent, ZAMP 32, 81-96.

Pomeau, Y. and S. Zaleski, 1980. Selection du nombre d'onde dans les structures cellulaires convectives, C.R. Acad. Sci. 290B, Paris, 505-507.

Pomeau, Y. and S. Zaleski, 1981. Wavelength selection in one-dimensional cellular structures, J. Physique 42, 515-528.

Segel, L.A., 1969. Distant side-walls cause slow amplitude modulation of cellular convection, J. Fluid Mech. 38, part 1, 203-224.

Swift, J. and P.C. Hohenberg, 1977. Hydrodynamic fluctuations at the convective instability, Phys. Rev. A. 15, no.1, 319-328.

Zippelius, A. and E.D. Siggia, 1983. Stability of finite-amplitude convection, Phys. Fluids 26 (10), 2905-2915.

Dynamics of Vortices in Background Rotating Flows

William Collins

Abstract

A method for computing the motion of a concentrated vortex embedded in a rotating fluid is developed. The radius of curvature of the filament is taken to be much larger than its diameter. A variational technique is used to show that the vortex is marginally stable to infinitesimal displacements off its rotation axis. A nonlinear treatment which reduces the Euler equations to two ordinary differential equations for the position of the vortex axis follows from approximating the flow field as nearly two-dimensional.

I. Introduction

Solitary nonaxisymmetric waves have been observed on concentrated vortex cores in several recent experiments (Hopfinger et al., 1982; Maxworthy et al., 1985). The most frequent wave geometries observed are in the form of kinks and twists (figure 1). These waves propagate stably over the length of the experimental apparatus. Similar waves have been photographed on tornadoes and waterspouts (figure 2). The solitons observed under laboratory conditions are often formed by pumping fluid out of a tank filled with rotating fluid. The resulting isolated vortex cores have rotational frequencies $\omega \approx 250\ s^{-1}$, an order of magnitude larger than that of the surrounding fluid, but the circulation in the cores is much less than the circulation of the fluid in the tank. Rossby numbers for these vortices are typically order ten or greater. It is claimed that the background rotation has a negligible effect on the form and propagation of these solitary waves.

In the absence of ambient rotation, the velocity of a point on a concentrated vortex is (Hama, 1962):

$$\vec{v} = \frac{\Gamma\kappa}{4\pi}\vec{b}\ln\left(\frac{L}{\sigma}\right) \tag{1}$$

where Γ is the vortex circulation, κ is the curvature, $\vec{b}$ is the binormal to the filament, and σ is the core radius (figure 3).

This expression is obtained from the Biot-Savart law for the velocity in the limit $\kappa^{-1} \gg \sigma$ assuming that the internal structure of the vortex is unaffected by its motion. In the limit $\sigma \to 0$, the logarithmic factor forces the self-induced velocity to diverge as expected for a line vortex. The maximum distance for interaction between two points on the vortex is set to a constant $L/2$ of the order of κ. Using the Frenet-Seret formulae to describe the filament, Betchov has derived time-evolution equations for the curvature and torsion τ of the filament from equation (1). Hasimoto has combined Betchov's equations into a single nonlinear Schrödinger equa-

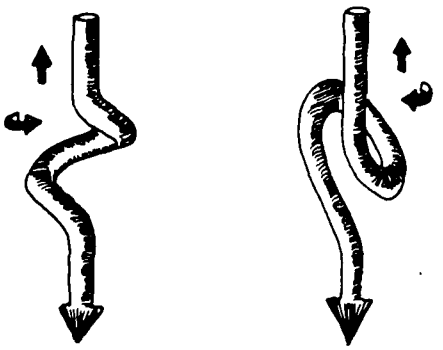

Figure 1: Twist(left) and kink(right) solitary waves. The filament vorticity is in the $-\vec{z}$ direction and the wave velocity is in the $+\vec{z}$ direction (Hopfinger et al., 1982).

tion

$$-i\frac{\partial\psi}{\partial t} = \frac{\partial^2\psi}{\partial s^2} + \frac{1}{2}\left(|\psi|^2\right)\psi$$

for the quantity

$$\psi = \kappa \exp\left(i\int_0^s \tau ds\right)$$

where s is the arclength along the filament. All possible steady waveforms have been classified using Hama's local-induction approximation formula (1). The family of solitary waves calculated by Hasimoto and Kida is qualitatively similar to the ''twist'' waves observed by Hopfinger et al.

However, there is no a priori reason to neglect the effects of the background circulation on the filament. Aref and Flinchem (1984) have performed numerical studies of vortices embedded in a transverse shear flow. In their experiments the velocity of the filament is modified by an additional shear velocity; the back reaction of the filament is neglected on the basis of a scaling argument. They find that a vortex initially supporting a twist wave rapidly develops large transverse waves which continue to grow in amplitude (figure 4). The authors attribute this stretching to the advection of the waves by the shear flow. Locally a finite amplitude perturbation of a vortex filament from the rotation axis is also in a large-scale shear flow and therefore advection should disrupt the soliton. Aref and Flinchem mention that the shear velocity must be much larger than the self-induced velocity in order for the waves to develop before the soliton has travelled many times its own length. In this note two calculations pertaining to the stability and motion of concentrated vortices in rotating flows are described. In section II the frequency of oscillation of the filament is calculated using

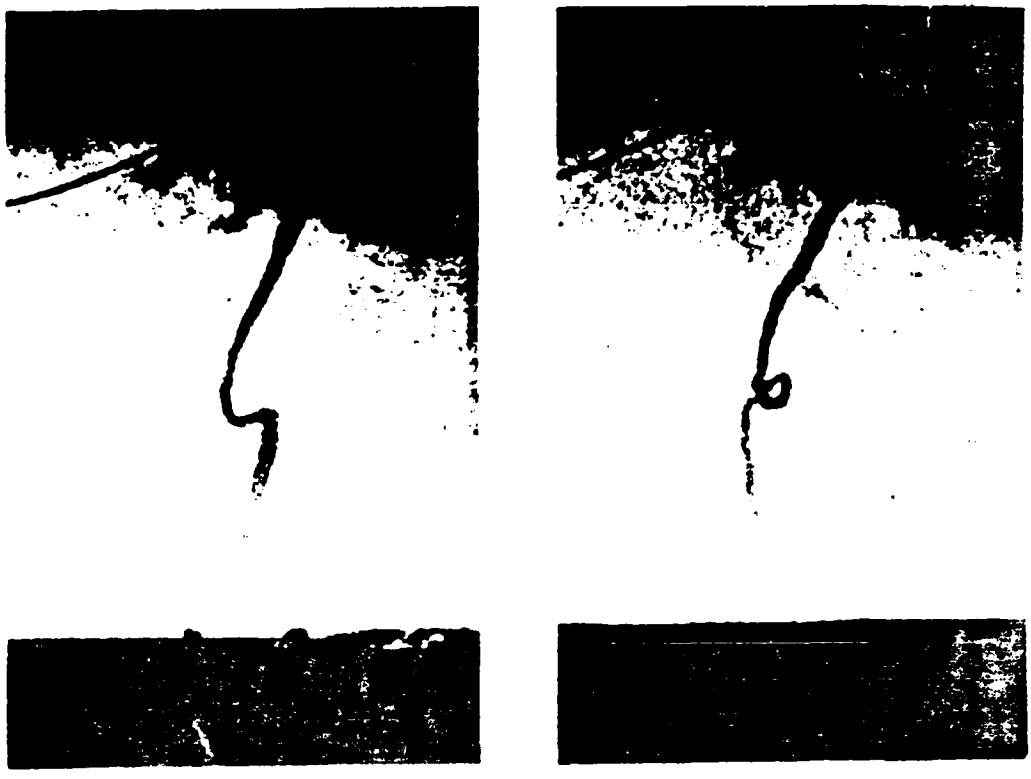

Figure 2: Two photographs of a tornado near Brameur, Oklahoma(1978) showing a finite-amplitude twist (Aref and Flinchem, 1984).

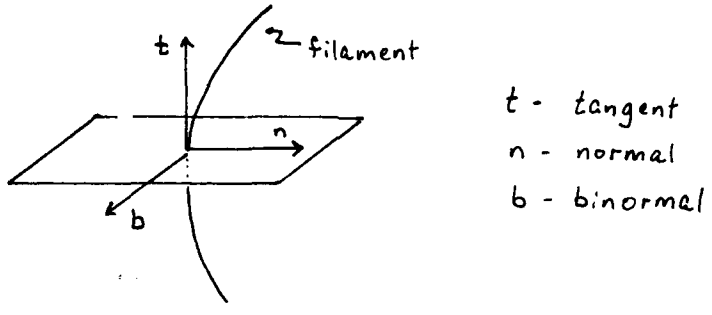

Figure 3: Vectors defined the intrinsic geometry of the filament.

a linear variational method and compared with measurements reported by Hopfinger et al (1982). The vortex is shown to be marginally stable to infinitesimal displ<acements from the rotation axis. In section III the velocity of a vortex supporting long wavelength finite amplitude perturbations is determined to $O(k^2)$ using an expansion of the full Euler equations for a quasi-2D field.

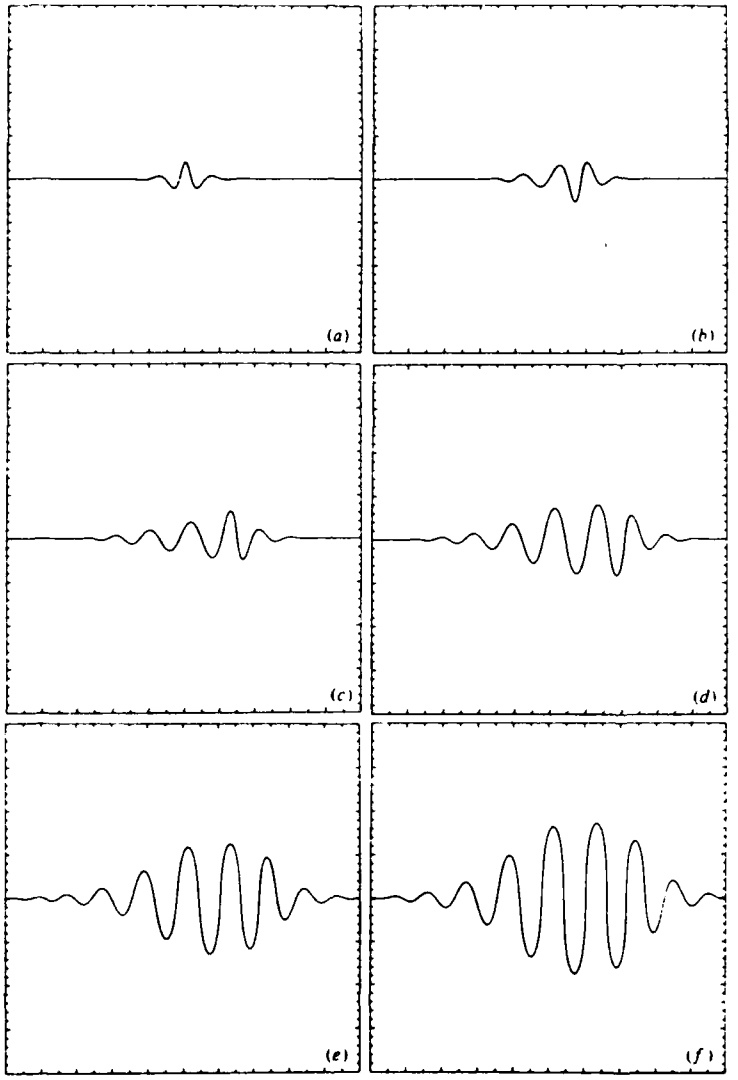

Figure 4: Dispersion of a twist-type soliton by a background shear flow. These frames are projections onto the z-x plane with time increasing from (a) → (f). The shear velocity is $u = U_0 \tanh(z/L)\vec{y}$. (Aref and Flinchem 1984).

II. Marginal linear stability of vortices in rotating flows

In the limit of displacements from the rotation axis small compared to the core radius r_1, the local induction approximation reduces to the linear stability problem for a nearly straight vortex. The relevant eigen-

mode has an $m = 1$ azimuthal angular dependence. For longitudinal wavenumber $k = 0$ this mode is a rigid lateral displacement of the vortex from the rotation axis, and for $k \neq 0$ this mode is a helical wave. Higher $m$modes add foliations to the vortex, and the $m = 0$ mode is a varicose wave. The induction equation requires neglecting all perturbations to the structure of the core which oscillate on timescales comparable to the vortex rotation time. When the surrounding fluid is irrotational, the following eigenvalue calculation should recover the dispersion relation implied by the induction approximation.

The longitudinal wavelength is taken to be large compared to r_1 so the growth rate σ may be expanded as a series in k:

$$\sigma = \sigma_0 + \sigma_2 k^2 + \ldots .$$

A variational calculation is used to determine the lowest order correction. Terms odd in k vanish because the system is invariant under $z \rightarrow -z$. The fluid is in a cylindrical tank with rigid-wall slip boundary conditions on the sides. The steady< piecewise-continuous velocity profile is

$$v_\theta(r) = \begin{cases} \omega_1 r & r < r_1 , \\ \omega_2 r + (\omega_1 - \omega_2) r_1^2 r^{-1} & r_1 \leq r_2 \ . \end{cases} \tag{2}$$

For axisymmetric disturbances the Rayleigh criterion for the circulation

$$\mathrm{D}(\Gamma^2) = 0 \tag{3}$$

where $\mathrm{D} = d/dr$ is a necessary and sufficient condition for stability. When the disturbance is two-dimensional a necessary condition for instability is the existence of a point of inflection in the vorticity where $\mathrm{D}\omega(r)$ changes sign. Leibovich and Stewartson (1983) show that sufficient condition for instability to fully three-dimensional perturbations is

$$v_\theta(\mathrm{D}\Omega)^2 \mathrm{D}\Gamma < 0$$

where Ω is the angular velocity v_θ/r. However, this inequality follows from an asymptotic analysis for large m modes and does not apply to $m = 1$. A sufficient condition for stability obtained by Howard and Gupta (1962) is

$$\frac{k^2}{\Gamma^3}\mathrm{D}\Gamma^2 - \frac{1}{4}(m\mathrm{D}\omega)^2 \geq 0 \ .$$

For $m = 0$ this is the axisymmetric condition (3). If $m \neq 0$, this condition is always violated for sufficiently small k. The stability of the $m = 1$ mode is not predicted by the general theory.

If the perturbing velocity and pressure depend on t, z, and θ only through $exp[i(\omega t + kz + m\theta)]$, the continuity equation and the Euler equations may be combined into an equation for the radial velocity alone (Howard and Gupta):

$$\gamma^2 \mathrm{D}S\mathrm{D}_* v_r - [\gamma^2 + \gamma a(r) + b(r)] v_r = 0 \tag{4}$$

AD-A164 601 SUMMER STUDY PROGRAM IN GEOPHYSICAL FLUID DYNAMICS 3/3
WOODS HOLE OCEANOGRAPH..(U) WOODS HOLE OCEANOGRAPHIC
INSTITUTION MA G VERONIS ET AL. NOV 85 WHOI-85-36
UNCLASSIFIED N00014-82-G-0079 F/G 20/4 NL

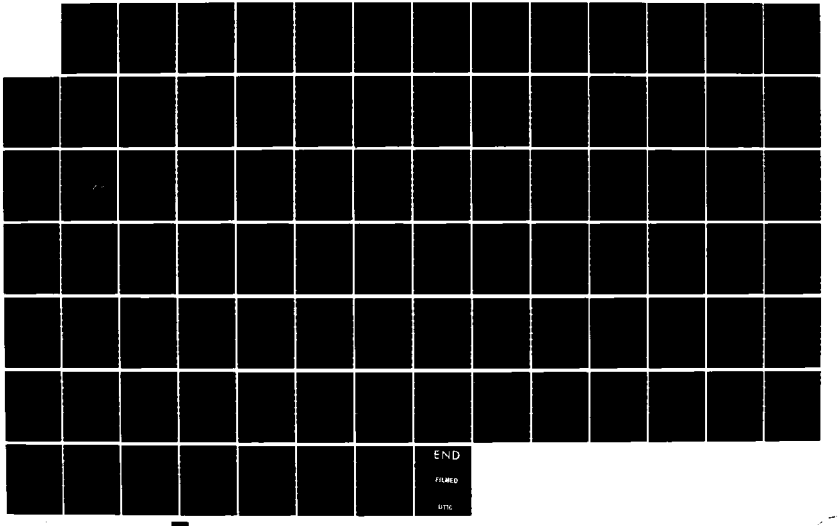

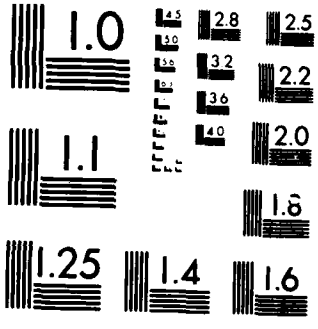

with

$$D_* = D + r^{-1},$$
$$\gamma = \sigma + \frac{v_\theta}{r},$$
$$a = rD\left[S\left(D_*\left(\frac{v_\theta}{r}\right) + 2\frac{v_\theta}{r^3}\right)\right],$$
$$b = -2\frac{k^2}{r^2}v_\theta S(D_* v_\theta),$$
$$S = \frac{r^2}{(1+k^2r^2)} .$$

The boundary conditions on the solution are

$$Dv_r = 0 \qquad r = 0,$$
$$v_r = 0 \qquad r = r_2 \qquad \text{(rigid-walls)} ,$$
$$v_r|_-^+ = 0 \qquad r = r_1 \qquad \text{(continuity at vortex boundary)} .$$

For computing σ_2 only terms through $O(k^2)$ in equation (4) need to be retained. It is convenient to define $\psi = -irv_r$. Expanding S in series form and grouping k-dependent terms gives

$$r^{-1}D[rD\psi] - r^{-2}\psi - \frac{D(D_* v_\theta)}{\gamma_0 r}\psi = k^2\left[r^{-1}D(r^3 D\psi) - \frac{D(r^2 D_* v_\theta)}{\gamma_0 r}\psi + \frac{2v_\theta D_* v_\theta}{\gamma_0^2 r}\psi\right] + O(k^4) \quad (5)$$

where $\gamma_0 = \sigma_0 + v_\theta/r$.

Consider the $k = 0$ problem first. Because of the jump discontinuity in the vorticity at $r = r_1$, the equation for ψ_0 must be solved separately inside and outside the vortex. The solutions are joined at r_1 by requiring ψ_0 to be continuous and imposing a jump condition on $D\psi_0$:

$$D\psi_0|_-^+ - \frac{2(\omega_2 - \omega_1)}{\gamma_0 r}\psi_0 = 0 \qquad r = r_1.$$

The solution to

$$r^{-1}D(rD\psi_0) - r^{-2}\psi_0 = 0 \qquad r \neq r_1$$

consistent with the boundary conditions is

$$\psi = \begin{cases} r & r < r_1 \\ -\frac{\mu}{(1-\mu)}r + \frac{r_1^2}{(1-\mu)}r^{-1} & r \geq r_1 \end{cases}$$

where $\mu = (r_1/r_2)^2$. The jump condition requires

$$\frac{\sigma_0}{\omega_1} = (1-\mu)(1-\omega) - 1$$

with $\omega = \omega_1/\omega_2$. When $\omega_1 = \omega_2$, the filament should oscillate with frequency ω_1, and when $r_1/r_2 \to 0$, so the filament occupies a negligible volume

fraction of the cylinder, the frequency should be ω_2. The expression for σ_0 has these limiting values for $\omega \to 1$ and $\mu \to 0$.

The second-order correction follows from varying an integral of the equation for v_r with respect to k^2. Multiplying equation (5) by $r\psi$ and integrating by parts from 0 to r_2 yields

$$-\int_0^{r_2} \left[r(\mathrm{D}\psi)^2 + r^{-1}\psi^2 + \gamma^{-1}\mathrm{D}(\mathrm{D}_* v_\theta)\psi^2\right] dr$$
$$= -k^2 \int_0^{r_2} \left[r^3(\mathrm{D}\psi)^2 + \gamma^{-1}\mathrm{D}(r^2\mathrm{D}_* v_\theta)\psi^2 - 2\gamma^{-2} v_\theta \mathrm{D}_* v_\theta \psi^2\right] dr + O(k^4) \tag{6}$$

Substituting the second-order solution $\psi = \psi_0 + k^2\psi_2$ with the corresponding eigenvalue $\sigma = \sigma_0 + k^2\sigma_2$ into this equation leaves the right-hand side unchanged through $O(k^2)$. The left-hand side has two additional term proportional to ψ_2 and σ_2. However, the ψ_2 term

$$\delta I = -2\int_0^{r_2} \left[r(\mathrm{D}\psi_0)(\mathrm{D}\psi_2) + r^{-1}\psi_0\psi_2 + 2\gamma_0^{-1}\mathrm{D}(\mathrm{D}_* v_\theta)\psi_2\psi_0\right] dr$$

after integration by parts becomes

$$\delta I = \int_0^{r_2} 2\psi_0 r \left[r^{-1}\mathrm{D}(r\mathrm{D}\psi_2) - r^{-2}\psi_2 - \frac{\mathrm{D}(\mathrm{D}_* v_\theta)}{r\gamma_0}\psi_2\right] dr.$$

Since ψ_2 satisfies the equation of motion, $\delta I = 0$. The resulting equation for σ_2 is

$$\sigma_2 = \left[\int_0^{r_2} \gamma_0^{-2}\mathrm{D}(\mathrm{D}_* v_\theta)\psi_0^2 dr\right]^{-1} \left\{\int_0^{r_2} \left[-\gamma_0^{-1}\mathrm{D}(r^2\mathrm{D}_* v_\theta) + 2\gamma_0^{-2} v_\theta \mathrm{D}_* v_\theta\right]\psi_0^2 dr \right.$$
$$\left. - \int_0^{r_2} r^3(\mathrm{D}\psi_0)^2 dr\right\}$$
$$= \frac{f_1}{2\nu_1} r_2{}^2 \frac{\mu}{(1-\mu)^2} \left\{ -\left\langle \tilde{\nu}_1(1-\mu)^2 + 2\nu_1(1-\mu)^2 + \tilde{\nu}_2(1-\mu^2) + 2\nu_2\tilde{\nu}_2\mu(1-\mu) \right.\right.$$
$$\left. - 4\tilde{\nu}_2(1+\nu_2\mu)(1-\mu) + 2\tilde{\nu}_2(1+\nu_2\mu)^2 \ln\left[\frac{1+\nu_2\mu}{\mu(1+\nu_2)}\right]\right\rangle$$
$$+ \left\langle \tilde{\nu}_1^2(1-\mu)^2 + \tilde{\nu}_2^2(1-\mu^2) + 2\nu_2\tilde{\nu}_2\mu(1-\mu) - 4\tilde{\nu}_2^2(1+\nu_2\mu)(1-\mu) \right.$$
$$+ 2\nu_2\tilde{\nu}_2\mu(1-\mu)(1-\tilde{\nu}_2) + 2\nu_2\tilde{\nu}_2(1-\tilde{\nu}_2)(1+\nu_2\mu)\frac{(1-\mu)}{(1+\nu_2)}$$
$$\left. \left[2\tilde{\nu}_2^2(1+\nu_2\mu)^2 - 4\nu_2\tilde{\nu}_2\mu(1-\tilde{\nu}_2)(1+\nu_2\mu)\right] \ln\left[\frac{1+\nu_2\mu}{\mu(1+\nu_2)}\right]\right\rangle$$
$$\left. - \left\langle \frac{3}{2}(1-\mu) - \frac{1}{2}\ln\mu \right\rangle \right\} . \tag{7}$$

where

$$f_1 = \sigma_0 + \omega_1 \ , \qquad f_2 = \sigma_0 + \omega_2 \ ,$$
$$\tilde{\nu}_2 = \frac{\omega_1}{f_1} \ , \qquad \tilde{\nu}_2 = \frac{\omega_2}{f_2} \ ,$$
$$\nu_2 = \frac{(\omega_1 - \omega_2)}{f_1} \ , \text{and} \qquad \nu_2 = \frac{(\omega_1 - \omega_2)}{f_2} \ .$$

Through second order the filament is marginally stable to the $m = 1$ perturbation regardless of the relative magnitude and sign of ω_1 and ω_2. This follows from the correspondence of this perturbation to an infinite-wavelength Kelvin-Helmholtz mode. The boundary of the vortex is embedded in a shear flow layer of width dr (figure 5).

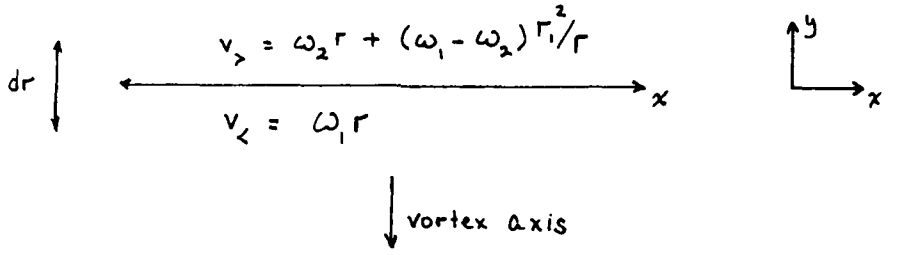

Figure 5: The shear flow at the vortex periphery ($dr \ll r_1$)

The curvature of the filament manifests itself at $|x| \to \infty$. This layer is unstable to long wavelength perturbations and is marginally stable to infinite wavelength disturbances. The $m = 1$ mode also shifts the entire layer out to $|x| \to \infty$ along the y axis and therefore no shear instabilities are excited.

In the limit $\omega_2 = 0$ the dispersion given by $\sigma_2 k^2$ should equal the dispersion for the local-induction approximation. A helical perturbation with wavenumber k and amplitude $a \ll k^{-1}$ has curvature

$$\kappa = \frac{k}{(1 + a^2 k^2)} \approx k$$

and a phase velocity given by equation (1). The dispersion relation is

$$\sigma = k c_p = \frac{\gamma k^2}{4\pi} \ln\left(\frac{L}{r_1}\right). \tag{8}$$

When $\omega_2 = 0$ the eigenvalue σ_2 simplifies considerably since $\tilde{\nu}_2 = 0$. Also, in the experiment of Hopfinger et al., the core radius is typically 1.5

mm. in a tank 40 cm. wide so $\mu \approx 5 \times 10^{-5}$. The leading term in $\sigma_2 k^2$ when $\mu \ll 1$ is

$$\sigma_2 k^2 = \left(\frac{f_1 \gamma_2^2 \mu}{4\nu_1} \ln \mu \right) k^2$$

$$\approx \frac{\gamma k^2}{4\pi} \ln \mu \ .$$

If $\omega_2 \neq 0$, the leading term becomes

$$\sigma_2 k^2 = \frac{\gamma_v k^2}{4\pi} \left(\frac{\gamma_t}{\gamma_v} \right)^2$$

where γ_v is the vortex circulation and γ_t the circulation in the entire tank. The oscillation frequency depends on the volume of fluid surrounding the vortex and increases as that volume is increased with fixed ω_2. Waves with this frequency were not observed. Hopfinger et al. fit equation (8) to their results and found

$$\ln \left(\frac{L}{r_1} \right) \approx 1.4$$

gave good agreement. However, the circulation ratio is

$$\left(\frac{\gamma_t}{\gamma_v} \right)^2 \approx 2.5 \times 10^5.$$

There are several possible explanations for this discrepancy. The small expansion parameter is $kr_2 \ll 1$ so the perturbation couples to the radius of the tank. Also, these measurements are not for isolated vortices. The experimental values quoted are for one vortex selected from twenty-five. Each vortex is screened from the walls of the cylinder by its neighbors. The effective tank circulation in one of these cells is only 4% of the total circulation so

$$\left(\frac{\gamma_{eff}}{\gamma_v} \right) \approx 400.$$

Since the $\approx$ 5 cm. wavelength of the solitons is comparable to the width of the cell, $kr_{cell} \sim O(1)$. A determination of ω_2 for $kr_2 \geq 1$ might help eliminate the discrepancy.

III. Vortex Motion in a Quasi-2D flow field.

In the limit $\omega_2 \approx 0$, $kr_1 \ll 1$, and $\mu \ll 1$, a vortex oscillates very slowly compared to circulation timescales. Its motion may be calculated using the full Euler equations if the flow is nearly two-dimensional.

The velocity and pressure in the flow depend on the coordinates and time through

$$\vec{u} = \vec{q}(x, y, \varsigma, \tau) + w(x, y, \varsigma, \tau)\hat{z}$$
$$\vec{q} = u\hat{x} + v\hat{y}$$
$$p = p(x, y, \varsigma, \tau)$$

where $\varsigma = \epsilon z$ and $\tau = \epsilon t$. The slow-time scaling follows from the characteristic time-scale implied by the local-induction approximation. A vortex moves through its radius of curvature in a time

$$t^{-1} = |v|\kappa = \frac{\Gamma\kappa^2}{4\pi} \ln\left(\frac{L}{r_1}\right).$$

Therefore the ratio between t^{-1} and the circulation frequency is of order $(\kappa r_1)^2 \ln(L/r_1) \ll 1$. It is possible to tune the dimensions r_1 and r_2 and vorticities ω_1 and ω_2 so that the $m = 1$ frequency $k^2\sigma_2$ is also much less than ω_1. The linear analysis presented in section II provides the ''slow'' time-scale needed for a non-linear calculation of the vortex motion. Both $\vec{u}$ and p are expanded as series in ϵ:

$$\vec{q} = \vec{q}_0 + \epsilon\vec{q}_1 + O(\epsilon^2)$$
$$w = w_0 + \epsilon w_1 + O(\epsilon^2)$$
$$p = p_0 + \epsilon p_1 + O(\epsilon^2) \ .$$

In the quasi-two-dimensional approximation, the zeroth order flow is that of an axisymmetric columnar vortex in a surrounding incompressible inviscid flow with streamlines uniformly displaced for each ς by $\vec{d} = \xi(\varsigma, \tau)\hat{x} + \eta(\varsigma, \tau)\hat{y}$ (figure 6). The displacement may be of finite amplitude. The flow in each plane is

$$\vec{q}_0 = Q(r)\hat{\theta} \tag{10}$$

where r and θ are coordinates relative to the center of the streamlines and therefore depend on ξ and η. In the experiments of Maxworthy et al., the axial velocity is much less than the circulation velocity. If there is no uniform axial flow, the zeroth-order velocity field is

$$\vec{q}_0 = \nabla \times (\psi\hat{z})$$
$$\psi(x, y) = \Psi_0\left(|(x - \xi)^2 + (y - \eta)^2|^{1/2}\right) \tag{11}$$
$$w_0 = 0 \ .$$

The solution for the motion of the vortex consists of evolution equations for ξ and η obtained from solvability conditions. These conditions follow from requiring that the higher-order corrections to the velocity

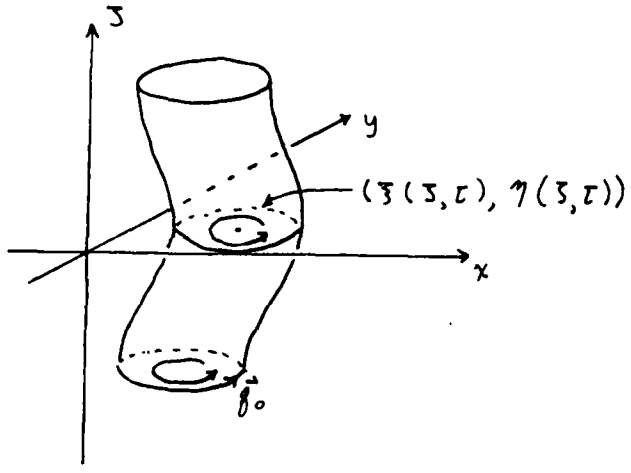

Figure 6: The zeroth-order velocity field in the quasi-2D approximation, equation (11).

and pressure be single-valued under $\theta \to \theta + 2\pi$. For example, the vertical momentum equation is

$$\frac{\partial w}{\partial \tau} + (\vec{q}\cdot\nabla)w + w\frac{\partial w}{\partial \zeta} + \frac{\partial p}{\partial \zeta} = 0 \ .$$

After expansion in ϵ it has the form

$$(\vec{q}_0\cdot\nabla)w_n = f(\vec{q}_0,\ldots,\vec{q}_{n-1};w_0,\ldots,w_{n-1};p_{n-1}) \ .$$

Using equation (10), this may be integrated along the zeroth-order streamlines to give w_n so long as

$$\int_0^{2\pi} f\,d\theta = 0 \ .$$

There are similar conditions that arise in solving for $\vec{q}_n$ and p_n. The pressure corrections are obtained by integrating the horizontal momentum equations

$$\frac{\partial \vec{q}}{\partial \tau} + (\vec{q}\cdot\nabla)\vec{q} + w\frac{\partial \vec{q}}{\partial \zeta} + \nabla_2 p = 0$$

where $\nabla_2 = \partial_x\hat{x} + \partial_y\hat{y}$. The $\vec{q}_n$ terms follow from the equations for continuity and vertical vorticity:

$$\nabla_2\cdot\vec{q} + \frac{\partial w}{\partial \zeta} = 0$$

$$\frac{\partial \omega_z}{\partial \tau} + \cdots\frac{\partial \omega_z}{\partial \zeta} + (\vec{q}\cdot\nabla)\omega_z - \omega_z\frac{\partial w}{\partial \zeta} - \left(\omega_x\frac{\partial}{\partial x} + \omega_y\frac{\partial}{\partial y}\right)w = 0.$$

For this preliminary calculation the fluid domain is infinite. The consistency of the solutions with rigid-wall boundary conditions at the outer cylindrical surface is ignored. The ensatz for the zeroth-order velocity field (equation 11) implies a radial outflow at infinity unless $\xi = \eta = 0$. Also, the assumption that the perturbation of the surrounding rotational flow by the vortex has constant amplitude over distances r large compared to r_1 is justifiable only if $r \ll r_2$. The calculation of the motion of the vortex and the surrounding fluid is considered as an ''inner'' problem to be matched with an ''outer'' flow field.

At lowest order the Euler and continuity equations are

$$(\vec{q}_0 \cdot \nabla_2)\vec{q}_0 + \nabla_2 p_0 = 0$$
$$\vec{q}_0 \cdot \nabla_2 w_0 = 0$$
$$\nabla_2 \cdot \vec{q}_0 = 0 \ .$$

The second two equations are identically satisfied. The solution for p_0 balances the centrifugal term:

$$p_0 = \int_0^r \frac{Q^2(r')}{r'} dr'.$$

At first order the vertical velocity follows from

$$(\vec{q}_0 \cdot \nabla) w_1 + \frac{\partial p_0}{\partial \zeta}|_{x,y} = 0 \ .$$

The pressure gradient is nonzero because at each ζ the streamline intersecting the line (x, y) = constant and the pressure p_0 are determined by the displacement $\vec{d}$. The variation of r and θ with ζ is

$$\frac{\partial r}{\partial \zeta} = -(\xi' \cos\theta + \eta' \sin\theta)$$
$$\frac{\partial \theta}{\partial \zeta} = (\xi' \sin\theta - \eta' \cos\theta)$$

where $' = d/d\zeta$. Equations (21) and (22) imply

$$w_1 = \int Q(r)(\xi' \cos\theta + \eta' \sin\theta) d\theta$$
$$= rQ(r)\frac{\partial \theta}{\partial \zeta} + W_1(r; \zeta, \tau)$$

This represents a flow from regions of higher to lower pressure (figure 7).

The equations for $\vec{q}_1$ are

$$\nabla_2 \cdot \vec{q}_1 = 0$$

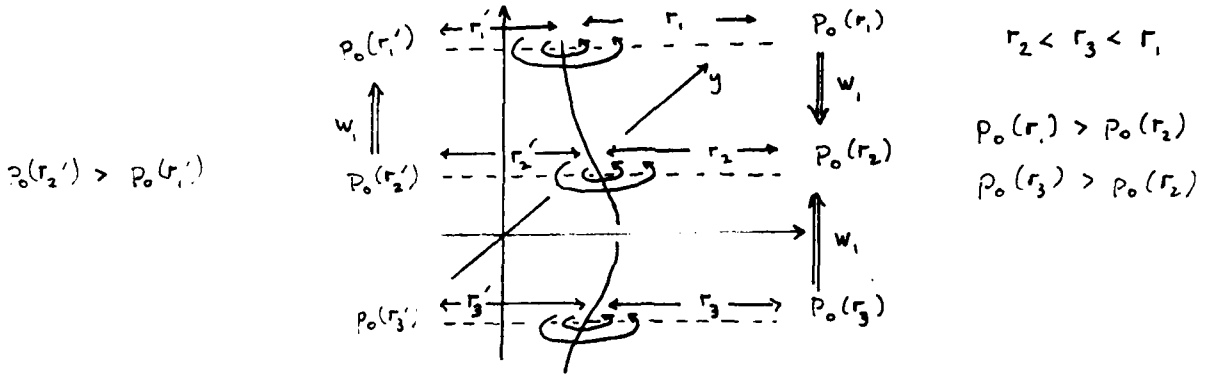

Figure 7: Vertical pressure gradients induce axial flow.

$$\frac{\partial \omega_0}{\partial \tau} + (\vec{q}_0 \cdot \nabla_2)\omega_1 + (\vec{q}_1 \cdot \nabla_2)\omega_0 = 0.$$

The simplest solution is

$$\vec{q}_1 = \xi'\hat{x} + \eta'\hat{y}.$$

The fluid in each plane moves uniformly with the streamline center. The equations for q_n are difficult to solve by inspection for $n \geq 2$ but they can be separated into equations for q_{nr} and $q_{n\theta}$. For any n the continuity and vertical vorticity equations have the form

$$\nabla_2 \cdot \vec{q}_n + \frac{\partial w_{n-1}}{\partial \zeta} = 0$$
$$(\vec{q}_0 \cdot \nabla)\omega_n + (\vec{q}_n \cdot \nabla)\omega_0 = F_n$$

where F_n depends on the velocity and pressure fields at lower order. Continuity implies

$$\frac{\partial \vec{q}_{n\theta}}{\partial \theta} = -r\frac{\partial w_{n-1}}{\partial \zeta} - \frac{\partial (r\vec{q}_{nr})}{\partial r}. \tag{12}$$

Substituting this into the vorticity equation gives

$$L(q_{nr}) = -Q^{-1}F_n - r^{-2}\frac{\partial (r^2 w_{n-1})}{\partial r} \tag{13}$$

with

$$L = \frac{\partial^2}{\partial r^2} + \frac{3}{r}\frac{\partial}{\partial r} + \frac{1}{r^2}\left(1 - \frac{\partial^2}{\partial \theta^2} - \frac{r^2 D\omega_0}{Q}\right).$$

This is separable in r and θ.

At this order the vortex may be stretched. Since circulation is conserved, the angular velocity increases as the vortex radius decreases.

Let λ be a lagrangian coordinate along the vortex. Then the arclength between $\vec{r}(\lambda)$ and $\vec{r}(\lambda + d\lambda)$ is

$$ds^2 = \left|\frac{\partial \vec{r}}{\partial \lambda}(\lambda, t)d\lambda\right|^2$$

At a time δt later, the arclength separation has changed to

$$\begin{aligned} ds'^2 &= \left|\frac{\partial \vec{r}}{\partial \lambda}(\lambda, t+\delta t)d\lambda\right|^2 \\ &= ds^2 + 2\frac{\partial \vec{r}}{\partial \lambda}\cdot\frac{\partial}{\partial \lambda}\left(\frac{\partial \vec{r}}{\partial t}\right)\delta t d\lambda^2 + O(\delta t^2) \end{aligned}$$

In the local-induction approximation, the filament is not stretched. At some time t let λ equal the arclength s so the stretching term is proportional to $\vec{t}\cdot(\vec{t}\cdot\nabla)\vec{v}$ where $\vec{v}$ is given by equation (1). Using the Frenet-Seret formulae one can show this is identically zero. For the quasi-2D approximation choose $\lambda = \zeta$. At first order,

$$\frac{\partial \vec{v}}{\partial \lambda}|_{r=0} = \frac{\partial \vec{v}}{\partial \zeta}|_{r=0} = W_1'(0;\zeta,\tau) + (\dot{\xi}'\hat{x} + \dot{\eta}'\hat{y})$$

and therefore

$$ds'^2 - ds^2 = \left[\frac{d}{dt}(\xi'^2 + \eta'^2) + \dot{W}_1\right] d\lambda^2 \delta t + O(\delta t^2).$$

The first term in brackets is just the change in the arclength of the centerline of the vortex. If the vortex is being concentrated, radial inflow at the periphery of the vortex will have to appear at second order.

The vertical velocity w_2 satisfies

$$(\vec{q}_0\cdot\nabla)w_2 = -\frac{\partial w_1}{\partial \tau} - (\vec{q}_1\cdot\nabla_2)w_1 - \frac{\partial p_1}{\partial \zeta}.$$

In terms of the coordinates ξ and η,

$$\begin{aligned} (\vec{q}_1\cdot\nabla_2)w_1 = &-DQ\left[-\frac{1}{2}\dot{\xi}\xi'\sin 2\theta + \frac{1}{2}\dot{\xi}\eta'(1+\cos 2\theta) - \frac{1}{2}\dot{\eta}\xi'(1-\cos 2\theta) + \frac{1}{2}\dot{\eta}\eta'\sin 2\theta\right] \\ &- \frac{Q}{r}\left[\frac{1}{2}\dot{\xi}\xi'\sin 2\theta + \frac{1}{2}\dot{\xi}\eta'(1-\cos 2\theta) - \frac{1}{2}\dot{\eta}\xi'(1+\cos 2\theta) - \frac{1}{2}\dot{\eta}\eta'\sin 2\theta\right] \end{aligned}$$

and

$$\frac{\partial w_1}{\partial \tau} = -(\vec{q}_1\cdot\nabla_2)w_1 + Q[\dot{\xi}'\sin\theta - \dot{\eta}'\cos\theta] + \dot{W}_1.$$

Imposing a solvability condition $\dot{W}_1 + p_1' = 0$ and integrating around the streamlines yields

$$w_2 = -rQ[\dot{\eta}' \cos\theta + \dot{\xi}' \sin\theta].$$

In principle one could now calculate the velocity $\vec{q}_2$ using equations (12) and (13). The most important feature of the solution, however, is not $\vec{q}_2$ but the solvability conditions required to obtain it. These conditions are presumably equations of motion for ξ and η. One such equation can be found without first solving for q_{2r} and $q_{2\theta}$ if $\partial_r \omega_0 \neq 0$ in the vortex domain. In regions of constant vorticity a similar conditions applies. Equation (28) may be rewritten in the form

$$\frac{Q}{r}\frac{\partial \omega_n}{\partial \theta} + q_{nr} \mathrm{D}\omega_0 = F_n.$$

Dividing by $\mathrm{D}\omega_0$, applying L to both sides, and using equation (13) gives

$$L\left[\frac{Q}{r\mathrm{D}\omega_0}\frac{\partial \omega_n}{\partial \theta}\right] - \left[\frac{F_n}{Q} + \frac{1}{r^2}\frac{\partial}{\partial r}\left(r^2 \frac{\partial w_{n-1}}{\partial r}\right)\right] = L\left(\frac{F_n}{\mathrm{D}\omega_0}\right).$$

Since ∂_θ commutes with L, the first term on the left-hand side averages to 0 after integration around a streamline:

$$-\int_0^{2\pi}\left[\frac{F_n}{Q} + \frac{1}{r^2}\frac{\partial}{\partial r}\left(r^2 \frac{\partial w_{n-1}}{\partial r}\right)\right] d\theta = \int_0^{2\pi} L\left(\frac{F_n}{\mathrm{D}\omega_0}\right) d\theta.$$

This must hold for all r. The resulting solvability condition is expressed in terms of the flow fields only through order n-1. At second order the terms involving ξ and ζ all have angular dependence and therefore integrate to 0 so the condition is trivially satisfied.

Presumably a nontrivial condition is required at third order and will depend on the matching of this ''inner'' calculation to the ''outer'' fluid domain. It can only depend on the first and second time derivatives of $\vec{d}$. If the first derivatives appear, the condition is an expression for the velocity of the filament and should reproduce the Biot-Savart result when the surrounding fluid is irrotational. This may require a renormalization of time by a factor corresponding to $\ln(L/r_1)$. Since stretching of the vortex can occur, the equation should indicate that solitary waves may be disrupted in finite time by large-amplitude transverse waves.

Acknowledgements

I would like to thank Steve Childress and Ed Spiegel for their suggestion of this problem and for many helpful discussions, especially in the latter part of August. I would also like to thank the other students and staff of the GFD program for a very enjoyable summer.

References

Aref, H., and Flinchem, E., 1984. Dynamics of a vortex filament in shear flow, J. Fluid Mech., 148, 477-497.

Betchov, R., 1965. On the curvature and torsion of an isolated vortex filament, J. Fluid Mech., 22, 471-479.

Childress, S., 1985. Nearly two-dimensional Euler flows, preprint.

---------, 1985. Vortex stability and inertial-range cascades, preprint.

Hama, F. R., 1962. Progressive deformation of a curved vortex filament by its own induction, Phys. Fluids, 5, 1156-1162.

Hasimoto, H., 1972. A soliton on a vortex filament, J. Fluid Mech., 51, 477-485.

Hopfinger, E., Browand, F., and Gagne, Y., 1982. Turbulence and waves in a rotating tank, J. Fluid Mech., 125, 503-534.

Kida, S., 1981. A vortex filament moving without change of form, J. Fluid Mech., 112, 397-409.

Leibovich, S., and Stewartson, K., 1983. A sufficient condition for the instability of columnar vortices, J. Fluid Mech., 126, 335-356.

Maxworthy, T., Hopfinger, E., and Redekopp, L., 1985, Wave motions on vortex cores, J. Fluid Mech., 151, 141-165.

Thompson, Sir W., 1880. Vibrations of a columnar vortex, Phil. Mag., 5, 155-168.

A Hamiltonian Form of the Anelastic Equations

Leslie Smith

Abstract: A new set of equations capable of describing convection and internal gravity waves in the atmosphere is derived using Hamilton's principle. These equations filter acoustic waves, as they must to avoid the use of very small time steps in numerical integration. Further, they are less restrictive than those previously obtained because they do not require prescription of a horizontally averaged basic state. An additional advantage is that they conserve exact mass, energy, momentum and potential vorticity.

I. Introduction

When modelling convection one must remove acoustic waves to avoid the use of very small time steps in numerical integration. The goal is to eliminate acoustic waves without altering the other essential physics. The Boussinesq equations are successful in shallow layer systems but the anelastic equations derived for deep stratified layers are much less adequate.

The Boussinesq equations were first written down by Boussinesq based on physical assumptions and later derived formally using scaling techniques and an asymptotic expansion (Malkus, 1964). The formal derivation requires both that the depth of the layer be small compared to the depth of the associated adiabat and that temperature fluctuations be small compared to the mean. In addition the ratio of depth and length scales must be of order unity. If these conditions hold, the density can be considered a constant everywhere except in the buoyancy term of the momentum equation. The continuity equation is therefore

$$\nabla \cdot (\rho_0 \underset{\sim}{u}) = 0$$

where ρ_0 is the constant density. One sees immediately that sound waves have been eliminated.

Similar formal scalings and asymptotic derivations of the anelastic equations, valid in the atmosphere, have been given by Ogura and Phillips (1962) and Gough (1969). Now the shallow layer assumption is relaxed while the small temperature fluctuation condition remains. Both result in the following continuity equation:

$$\nabla \cdot (\bar{\rho}(z)\underset{\sim}{u}) = 0$$

where $\bar{\rho}(z)$ is a prescribed mean density field from which one perturbs. Sound waves are thus eliminated but at the expense of fixing the mean field for all variables.

The requirement of a prescribed mean field seems much too artificial and one asks if it might be avoided with a completely different approach to the derivation of the equations. Here is presented a Hamiltonian formulation of anelastic equations where no such restriction is needed. A constraint is attached to the exact Lagrangian for a perfect fluid that

removes the cause of sound waves: small scale pressure fluctuations on the density. The constraint is a condition on the thermodynamic equation only.

The difference between the new approach and the old is in how one chooses to eliminate high frequency waves from the equation relating density and pressure for a perfect fluid:

$$\partial^2\rho/\partial t^2 = \nabla^2 P + g\,\partial\rho/\partial z + \nabla\cdot(\rho\underset{\sim}{u}\cdot\nabla\underset{\sim}{u}) - \nabla\cdot(\underset{\sim}{u}\,\partial\rho/\partial t)$$

where ρ is the density, P the pressure, $\underset{\sim}{u}$ the velocity and g the gravitational constant. The traditional method is to drop the $\partial^2\rho/\partial t^2$ term while here is proposed removing part of the $\nabla^2 P$ term. Mass then becomes an important invariant. As will be shown, not only do the new equations conserve exact mass, they also conserve exact momentum, energy and potential vorticity. The new equations are simple and eliminate sound waves. In addition they obey all of the relevant conservation laws. Thus they are superior to the old.

A review of Hamilton's principle and a derivation of the exact equations for a perfect fluid are given in section II. Section III contains examples of constraints on the equation of state that all remove sound waves, including a critique of their usefulness. A proposal for the best constraint and the equations that result from using it are presented in section IV. Sections V and VI discuss, respectively, conservation laws and the linear perturbation analysis. Finally, in section VII, the constraint is assessed further.

II. Hamiltonian Formulation of the Exact Equations

Hamilton's principle states that variations of the action must vanish. That is,

$$\delta\int_{-\infty}^{\infty} L\,d\tau = 0,$$

where

$$L = \iiint_{-\infty}^{\infty} da\,db\,dc\,[1/2\,(\partial\underset{\sim}{x}/\partial\tau)^2 - V(\underset{\sim}{x})]$$

is the Lagrangian. The position of fluid particles $x = x(a,b,c,\tau)$ is a function of curvilinear labelling coordinates $\underset{\sim}{a} = (a,b,c)$ and time τ. The labelling coordinates remain constant following particles and are chosen so that mass is conserved following particles: $da\,db\,dc = d(\text{mass}) = \rho\,dx\,dy\,dz$. Notice that $\partial/\partial\tau$ means fixed (a,b,c) and thus $\partial/\partial\tau = D/Dt$. $V(\underset{\sim}{x})$ is the potential energy.

The exact Lagrangian for an infinite perfect fluid is

$$L = \iiint_{-\infty}^{\infty} d\underset{\sim}{a}\,[1/2\,(\partial\underset{\sim}{x}/\partial\tau)^2\,gz - E(\alpha,S)]$$

where α is the specific volume and

$$\alpha = 1/\rho = \partial(x,y,z)/\partial(a,b,c).$$

Finally,

$$D\rho/Dt + \rho\nabla \cdot \underset{\sim}{u} = 0. \tag{2.2}$$

Conservation of potential temperature follows also from definition:

$$D\theta/Dt = 0. \tag{2.3}$$

Together with the thermodynamic equation

$$DP/Dt = c^2 D\rho/Dt \tag{2.4}$$

where $c^2 = \partial P/\partial\rho$, equations (2.1) - (2.3) form a closed set.

III. Examples of Thermodynamic Constraints That Eliminate Sound Waves

There are many constraints on the thermodynamic equation of state that will remove the cause of sound waves: small scale pressure fluctuations on the density. One would like to find the least restrictive such constraint. The constraint may be written as acting on the function that gives pressure in terms of density and potential temperature, $P = -\partial E/\partial\alpha = F(\rho, \theta)$, or equivalently as acting on the function that gives density in terms of pressure and potential temperature, $\rho = G(P, \theta)$.

The most obvious choice is to require that the pressure be constant:

$$\rho = G(P_0, \theta)$$

where P_0 is a reference temperature. It follows that density is a function of the labelling coordinates only:

$$\rho = \rho(a,b,c). \tag{3.1}$$

A worse choice is to require that the pressure and the potential temperature be constant

$$\rho = G(P_0, \theta_0)$$

where P_0 and θ_0 are reference values. Then

$$\rho = \rho_0 = \text{constant}. \tag{3.2}$$

It is here proposed that the best choice is to constrain the pressure to be its hydrostatic value in the equation of state

$$F(\rho, \theta) = P_0 - \int_0^z \bar{\rho} g dz' \tag{3.3}$$

where P_0 is a constant by conservation of mass.[1]

---

[1]The usual definition of hydrostatic pressure $P = \int_z^\infty \rho g dz'$ becomes upon using the horizontally averaged density ρ:

$$P = \int_z^\infty \bar{\rho} g dz' = \int_0^\infty [\iint_{-\infty}^\infty \rho dx'dy' / \iint_{-\infty}^\infty dx'dy'] g dz' - \int_0^z \bar{\rho} g dz' = P_0 - \int_0^z \bar{\rho} g dz'$$

where the last equality follows by conservation of mass.

The entropy S is a function only of the labelling coordinates. The internal energy $E(\alpha,S)$ is a given function, determined by choice of fluid. The thermodynamic equation of state is

$$dE = \partial E/\partial\alpha \; d\alpha + \partial E/\partial S \; dS = -Pd\alpha + TdS.$$

Henceforth potential temperature $\theta = \Theta(a,b,c)$ will be used instead of entropy: the two are equivalent.

Independent variations δx of the action $\int_{-\infty}^{\infty} L_{exact}\, d\tau$ give the exact momentum equations for a perfect fluid

$$D\underset{\sim}{u}/Dt = -gk - 1/\rho \; \nabla P. \qquad (2.1)$$

For example, δz:

$$0 = \int_{-\infty}^{\infty}\!\!\int\!\!\int\!\!\int d\underset{\sim}{a}\, d\tau \left[\frac{\partial z}{\partial \tau} \frac{\partial(\delta z)}{\partial \tau} - g\delta z - \frac{\partial E(\alpha,\Theta)}{\partial \alpha} \frac{\partial(x,y,\delta z)}{\partial(a,b,c)} \right].$$

After integration by parts one finds

$$0 = \int_{-\infty}^{\infty}\!\!\int\!\!\int\!\!\int d\underset{\sim}{a}\, d\tau \left[\frac{-\partial^2 z}{\partial \tau^2} - g - \frac{\partial(x,y,\partial E/\partial\alpha)}{\partial(a,b,c)} \right] \delta z.$$

with $\delta x \to 0$ as $|\underset{\sim}{a}|, |\tau| \to \infty$. One can rewrite this as

$$0 = \int_{-\infty}^{\infty}\!\!\int\!\!\int\!\!\int d\underset{\sim}{a}\, d\tau \left[\frac{-\partial^2 z}{\partial \tau^2} - g - \alpha \frac{\partial(x,y,\partial E/\partial\alpha)}{\partial(x,y,z)} \right] \delta z.$$

For arbitrary δz this yields the $\hat{k}$ component of the momentum equation

$$Dw/Dt = -g - 1/\rho \; \partial P/\partial z$$

where $\underset{\sim}{u} = u\hat{i} + v\hat{j} + w\hat{k}$.

One obtains conservation of mass by definition:

$$\partial/\partial\tau \left[1/\rho = \partial(x,y,z)/\partial(a,b,c)\right]$$

$$-1/\rho^2 \; \partial\rho/\partial\tau = \partial(u,y,z)/\partial(a,b,c) + \partial(x,v,z)/\partial(a,b,c) + \partial(x,y,w)/\partial(a,b,c)$$

$$-1/\rho^2 \; \partial\rho/\partial\tau = \partial(x,y,z)/\partial(a,b,c) \left[\partial u/\partial x + \partial v/\partial y + \partial w/\partial z\right]$$

$$-1/\rho^2 \; \partial\rho/\partial\tau = 1/\rho \; \nabla \cdot \underset{\sim}{u}.$$

The approximate Lagrangian using the constraint (3.1) is

$$L = \iiint d\underset{\sim}{a}[1/2(\partial \underset{\sim}{x}/\partial \tau)^2 - gz - E(\alpha,\theta) + \pi(a,b,c,\tau)(\partial(a,b,c)/\partial(x,y,z) - \rho(a,b,c)]$$

where $\pi = \pi(a,b,c,\tau)$ is a Lagrange multiplier. Independent variations δx of the corresponding action yield the following momentum equation:

$$D\underset{\sim}{u}/Dt = -1/\rho \ \nabla F - g\hat{k} + 1/\rho \ \nabla(\pi\rho^2).$$

Noticing, however, that $F = P_0$ is a constant, reduces the above to

$$D\underset{\sim}{u}/Dt = 1/\rho \nabla(\pi\rho^2) - g\hat{k}. \tag{3.4}$$

Independent variations $\delta\pi$ give the constraint equation. One time derivative following particles of the constraint equation then gives

$$\nabla \cdot u = 0. \tag{3.5}$$

By definition

$$D\rho/Dt = 0 \tag{3.6}$$

$$D\theta/Dt = 0. \tag{3.7}$$

If one now redefines the pressure as $P = \pi\rho^2$, equations (3.4) - (3.7) are similar to the inviscid Boussinesq equations. The difference is that density is a function of temperature everywhere.

The approximate Lagrangian using the constraint (3.2) is

$$L = \iiint d\underset{\sim}{a}[1/2(\partial \underset{\sim}{x}/\partial \tau)^2 - gz - E(\alpha,\theta) + \pi(\partial(a,b,c)/\partial(x,y,z) - \rho_0)].$$

Independent variations $\delta\underset{\sim}{x}$ and $\delta\pi$ of the action yield, respectively,

$$D\underset{\sim}{u}/Dt = -g\hat{k} - 1/\rho_0 \nabla P \tag{3.8}$$

$$\nabla \cdot \underset{\sim}{u} = 0. \tag{3.9}$$

Again, by definition

$$D\rho/Dt = 0 \tag{3.10}$$

$$D\theta/Dt = 0. \tag{3.11}$$

This, of course, is the Euler set.

IV. New Equations for Convection in the Atmosphere

New anelastic equations result from constraining the exact Lagrangian with the constraint (3.3):

$$F(\rho,\theta) = P_0 - \int_0^z \bar{\rho} g dz'$$

where P_0 is a constant and $\bar{\rho} = \iint dx'dy'\rho / \iint dx'dy'$. Again, the pressure is required to be its hydrostatic value only in the thermodynamic equation of state. The approximate Lagrangian is then

$$L = \iiint d\underset{\sim}{a}[1/2(\partial \underset{\sim}{x}/\partial\tau)^2 - gz - E(\alpha,\theta) + \rho\, \partial\pi/\partial z\, (F(\rho,\theta) - P_0 + \int_0^z \bar{\rho} g dz')]$$

where the Lagrange multiplier is chosen to be $\rho\partial\pi/\partial z$ for convenience. Independent variations δx of the action give the momentum equation

$$D\underset{\sim}{u}/Dt = -g\hat{k} - 1/\rho\ \nabla F - g\ \partial\bar{\Psi}/\partial z\ \hat{k} + \nabla(\partial\Psi/\partial\ \partial F/\partial\rho) - 1/\rho\ \partial\Psi/\partial z\ \partial F/\partial\theta\ \nabla\theta \qquad (4.1)$$

where $\Psi = \pi(x,y,z,t) - \pi(x,y,\infty,t)$ with $\Psi > 0$ as $z \to \infty$.

Noticing that $\nabla F = -g\bar{\rho}\hat{k}$ and defining $P = \rho c^2 \Psi_z$ one can rewrite the momentum equation as

$$\rho\, D\underset{\sim}{u}/Dt = -\nabla P - (\rho - \bar{\rho})g\hat{k} + g/c^2\,(\bar{\rho}P/\rho^2 - \rho\bar{P}/\rho^2)\hat{k}. \qquad (4.2)$$

The conservation of mass and potential vorticity equations follow from definition:

$$D\rho/Dt + \rho\ \nabla\cdot\underset{\sim}{u} = 0 \qquad (4.3)$$

$$D\theta/Dt = 0 \qquad (4.4)$$

The equation of state $DF/Dt = c^2\, D\rho/Dt$ becomes

$$g(\omega\bar{\rho} - \overline{\omega\rho}) = c^2\, D\rho/Dt \qquad (4.5)$$

Equations (4.2) - (4.5) form a closed set that differs from the exact set only in the $\hat{k}$ component of the momentum equation and the equation of state. The new equations are hardly more complicated than the exact and they filter acoustic waves. Furthermore, they conserve exact mass and, as will be discussed in section V, exact energy, momentum and potential vorticity.

To assess the accuracy of the new anelastic equations allow the definition $P_H = F$ where the H means hydrostatic. If the vertical scale of motion is much smaller than the depth of the atmosphere, c^2/g, then the momentum equation (4.2) reduces to

$$\rho D\underset{\sim}{u}/Dt = -\rho g\hat{k} - \nabla(P - P_H)$$

where the term proportional to g/c^2 has been dropped because it is much

smaller than the remaining. If, then, the height of the convective cells is small compared to the depth of the atmosphere, the new equations are accurate: they are within a small error of the exact equations. The pressure is now given in terms of its departure from the hydrostatic pressure.

One can argue that the new equations are not very restrictive as the convective cells may be quite deep and still be small compared to the depth of the atmosphere. Also notice that in the horizontally averaged equations the extra terms vanish identically.

A final important quality of the new equations is that they are easily solved numerically and therefore practical for computation. In order to time step the physical variables one must determine P at each time. The equation for P is found by taking a partial time derivation of the thermodynamic equation (4.5). Substituting for $D\rho/Dt$ from (4.3) and for $\partial \underset{\sim}{u}/\partial t$ from (4.2) one finds

$$c^2\rho\ \nabla \cdot \underset{\sim}{A} - g\bar{\rho}\underset{\sim}{A} \cdot \hat{k} - g\rho\bar{\underset{\sim}{A}} \cdot \hat{k} = c^2\rho\nabla \cdot \underset{\sim}{B} + g\bar{\rho}\underset{\sim}{B} \cdot \hat{k} + g\rho\bar{\underset{\sim}{B}} \cdot \hat{k}$$
$$+ g(\omega\ \nabla \cdot \overline{\rho\underset{\sim}{u}} + \overline{\omega\nabla \cdot \rho\underset{\sim}{u}}) - (\rho F_{\rho\rho} + c^2)\ \nabla \cdot \rho\underset{\sim}{u}\ \nabla \cdot \underset{\sim}{u} \qquad (4.6)$$

where $\underset{\sim}{A} = -1/\rho\ \nabla P + g/c^2\ (\bar{\rho}P/\rho^2 - \rho\bar{P}/\bar{\rho}^2)\hat{k}$

and $\underset{\sim}{B} = -\underset{\sim}{u} \cdot \nabla\underset{\sim}{u} - g/\rho\ (\rho - \bar{\rho})\hat{k}.$

Equation (4.6) is a linear, second-order, elliptic equation for P. The relevant boundary conditions are

$$P \to 0 \quad \text{as } z \to \infty \qquad (4.7)$$

and

$$(\rho - \bar{\rho})g + g/c^2\ (\bar{\rho}P/\rho^2 - \rho\bar{P}/\bar{\rho}^2) + \partial P/\partial z = 0 \text{ at } z = 0 \qquad (4.8)$$

Equation (4.8) follows from the $\hat{k}$ component of momentum and the fact that $\underset{\sim}{u} \cdot \hat{n} = 0$ at $z = 0$. This is a well-posed, numerically tractable problem.

V. Conservation Laws

The conservation laws for the exact equations (2.1) - (2.4) result from the symmetry properties of the exact Lagrangian. Translational invariance in time implies conservation of momentum:

$$\partial/\partial t \int_{-\infty}^{\infty}\int\int d\underset{\sim}{x}\ \ \rho\underset{\sim}{u} = 0. \qquad (5.1)$$

Translational invariance in space gives conservation of energy:

$$\partial/\partial t \int_{-\infty}^{\infty}\int\int dx\ [1/2\rho\underset{\sim}{u}^2 + \rho gz + \rho E(\alpha,\theta)] = 0. \qquad (5.2)$$

Conservation of potential vorticity follows from the fact that the labelling coordinates (a,b,c) enter the Lagrangian only through the Jacobian:

$$\frac{D}{Dt}\left[\frac{(\nabla \times \underset{\sim}{u}) \cdot \nabla \theta}{\rho}\right] = 0. \tag{5.3}$$

The new anelastic equations (4.1) - (4.5) must also conserve exact momentum, energy and potential vorticity because the approximate Lagrangian obeys the same symmetry properties stated above. This is straightforward to prove.

For example, consider the energy. To show that the new equations conserve exact energy one adds the inner product of $\underset{\sim}{u}$ and the momentum equation (4.1) to the continuity equation (4.3) multiplied by $1/2\ \underset{\sim}{u}^2$. Then one integrates over the entire domain. Since one knows that this process gives (5.2) for the exact equations, one must show that all the extra terms introduced by the approximate equations are zero. That is, one must show that

$$\iiint d\underset{\sim}{x}\ \rho \underset{\sim}{u} \cdot [\ \nabla(g\overline{\Psi} - \Psi_z F_\rho) + 1/\rho\ \Psi_z F_\theta \nabla \theta] = 0. \tag{5.6}$$

First one integrates the first term by parts to find

$$\iiint dx\ [-(g\overline{\Psi} - \Psi_z F_\rho)\ \nabla \cdot \rho \underset{\sim}{u} + \Psi_z F_\theta\ \underset{\sim}{u} \cdot \nabla \theta]$$

where the boundary terms vanish because $\rho \to 0$ as $z \to \infty$ and $u \cdot \hat{n} = 0$ at $z = 0$. Substitution from (4.3) and (4.4) gives

$$\iiint d\underset{\sim}{x}\ [g\overline{\Psi}\ \partial\rho/\partial t - \partial/\partial z\ (\Psi\ \partial F/\partial t) + \Psi\ \partial^2 F/\partial z \partial t]. \tag{5.7}$$

But notice that

$$\begin{aligned}
\iiint d\underset{\sim}{x}\ \Psi\ \partial^2 F/\partial z \partial t &= \iiint d\underset{\sim}{x}\ \Psi \partial^2 F/\partial t \partial z \\
&= -\iiint d\underset{\sim}{x}\ \Psi\ \partial/\partial t \iint dx'dy' \rho g \\
&= -\iiint dx'dy'dz\ \ \partial\rho/\partial t\ g \iint dxdy\ \Psi \\
&= -\iiint d\underset{\sim}{x}\ g\overline{\Psi}\ \partial\rho/\partial t.
\end{aligned}$$

Then (5.7) becomes

$$\iiint d\underset{\sim}{x}\ \ -\partial/\partial z(\Psi\ \partial F/\partial t) = -\iint dxdy\ \Psi\ \partial F/\partial t \Big|_{z=0}^{\infty} = 0$$

because $\Psi \to 0$ as $z \to \infty$ and $\partial F/\partial t = 0$ at $z = 0$. Conservation of exact energy is thus established. Conservation of momentum and potential vorticity can similarly be verified.

VI. The Linear Perturbation Equations

The check that the linearized form of the new equations does indeed filter sound waves one perturbs from a basic state as follows. Let

$$\underset{\sim}{u} = 0 + \underset{\sim}{u}'(x, y, z, t)$$

$$\rho = \bar{\rho}(z) + \rho'(x, y, z, t)$$

$$F = \bar{F}(z) + F'(x, y, z, t)$$

$$\theta = \bar{\theta}(z) + \theta'(x, y, z, t)$$

$$P = 0 + P'(x, y, z, t)$$

Now one assumes each perturbation to be a plane wave in the horizontal: $\Psi' = \hat{\Psi}(z)e^{i(kx - \omega t)}$ where Ψ' is any perturbation quantity. The y dependence has been dropped because it is exactly symmetrical to the x dependence.

The constraint equation (3.3) becomes

$$\hat{F} = -\int_0^z g\,\overline{\hat{\rho}(z)e^{i(kx - \omega t)}}\,dz' = 0 \qquad (6.1)$$

because the horizontal average of a plane wave is zero. Also, by definition,

$$\hat{F} = \partial F(\bar{\rho},\bar{\theta})/\partial\rho\ \hat{\rho} + \partial F(\bar{\rho},\bar{\theta})/\partial\theta\ \hat{\theta}. \qquad (6.2)$$

Together equations (6.1) and (6.2) require that

$$\hat{\rho} = F_\theta/c^2\ \hat{\theta}. \qquad (6.3)$$

One sees immediately that sound waves have been eliminated since the density perturbation amplitude depends only on temperature perturbations and not on pressure perturbations.

VII. Discussion

One can also filter sound waves with the following constraint:

$$F(\rho,\theta) = P_0 - \int_0^z \rho g\,dz'$$

where P_0 is a constant.[2] That is, the pressure is again its hydrostatic value in the equation of state but now calculated using the exact density.

---

[2]In this case P_0 is not a constant by conservation of mass. The restriction P_0 = constant is now necessary to eliminate Lamb waves.

There are advantages to calculating the hydrostatic pressure with an average density and advantages to using the exact density. It makes sense to use an average because it is an average density that balances the pressure gradient in the z direction while a perturbation density balances the convective velocity in the z direction. This follows from the $\hat{k}$ component of the momentum equation

$$\rho \, D\omega/Dt = -\rho g - \partial P/\partial z .$$

On the other hand, consider the atmosphere stretching over a continent and an ocean. If the weather differs dramatically over land and water, which it often does, then the average density will be a poor representative of either. The best choice of density is probably a running average where one averages over a distance large compared to the width of a convective cell but small compared to the length of the domain.

Finally, it is important to recognize that this method of deriving anelastic equations is completely different from those used previously. It is therefore dangerous to attempt to apply scaling techniques to the Lagrangian. A scaling of terms in the Lagrangian does not imply the same scaling of corresponding terms in the variational equations. For example, in the exact Lagrangian the internal energy $E(\alpha,S)$ is larger than the kinetic and potential energies by many orders of magnitude. In the momentum equation derived using the exact Lagrangian, however, the term corresponding to internal energy, $-1/\rho \, \nabla P$, is of the same order of magnitude as those corresponding to kinetic and gravitational potential engeries, $D\underset{\sim}{u}/Dt$ and $g\hat{k}$, respectively. It follows that evaluation of error in equations derived using Hamilton's principle is necessarily carried out $\grave{a}$ posteriori.

Acknowledgements: I would like to thank Rick Salmon for his invaluable guidance throughout our collaboration. I also thank Nigel Weiss for suggesting this problem and Ed Spiegel for his advice and encouragement for the future.

REFERENCES

Gough, D.O., 1969. The anelastic approximation for thermal convection, J. Atmos. Sci. 26, 448-456.

Malkus, W.V.R., 1964. Boussinesq equations and convection energetics, unpublished.

Ogura, Y. and N.S. Phillips, 1962. Scale analysis of deep and shallow convection in the atmosphere, J. Atmos. Sci. 19, 173-179.

Crossing Chaotic Boundaries in the Disc Dynamo

Kirk Brattkus

Abstract: We study the third order system which describes the motion of the disc dynamo and find new chaotic solutions to these modified Lorenz equations. Also, motivated by the record of geomagnetic reversals, we introduce a slow modulation of the Rayleigh number across the boundaries of chaos and observe a form of intermittent chaos.

Introduction

The disc dynamo has long been studied as a simple low order system which possibly models much more complex behaviors arising in fluid dynamos consisting of electrically conducting fluid spheres. It is a very simple machine composed of a rotating disc connected by a ring of brushes to a coaxial current loop which, after winding around the axle, ends there with a set of brushes. If a torque is applied to the wheel in the presence of an external magnetic field, there is an induced E.M.F. across the disc and a current is established in the coil. This current produces a magnetic field that reinforces the pre-existing field as long as the loop is wrapped counter-clockwise as viewed from above (up is taken in the direction of the initial magnetic field). In fact, the initial field was only required to start up the dynamo and after the current begins to flow it is no longer necessary. After start up, this machine has become a self exciting dynamo; a so-called homopolar dynamo (figure 1).

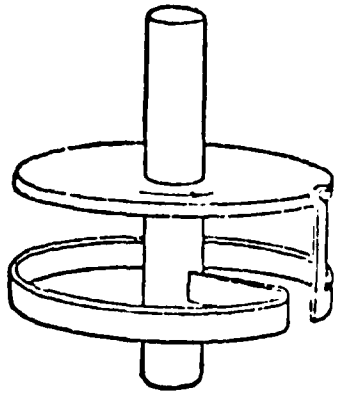

Figure 1: The Disc Dynamo

Disc dynamos similar to the one described behave in ways not only analogous to fluid dynamos but these systems have also been shown to exhibit reversals in an apparently stochastic sequence. The first of these discovered was the Rikitake dynamo where two homopolar dynamos are coupled by wrapping the current loop of one around the axle of the other and vice versa. The random reversals caused considerable interest among investigators looking for analogues in fluid dynamos to the pattern of reversals in the geomagnetic record. The record shows that the earth's dipole magnetic field reverses direction on time scales of 10^4 years and that these reversals are highly erratic (figure 2).

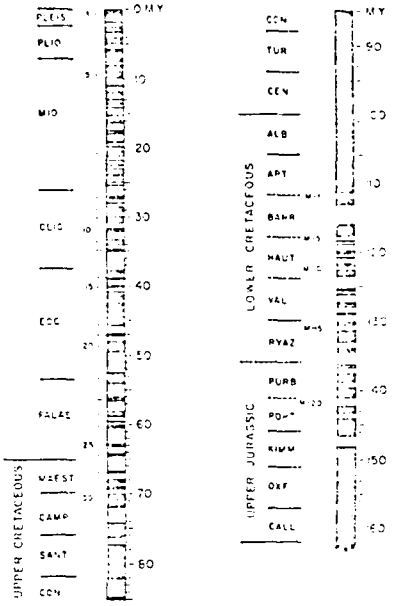

Figure 2: Reversals of the earth's magnetic field over the last 160 m.y.

The Rikitake dynamo exhibits similar properties of the geodynamo but it lacks the simplicity of the homopolar dynamo. Malkus (1972) noted that if the induction and resistance of the brushes were incorporated into the homopolar dynamo, the currents in the disc and the coil could dephase, thus causing reversals.

The Dynamo Equations

The Malkus dynamo is an extension of the homopolar dynamo where a resistive shunt is placed across the current loop and the impedance between the coils and the brushes are included (figure 3). Robbins (1976) has shown that this system also describes the fields associated with the averaged fluid dynamo equations.

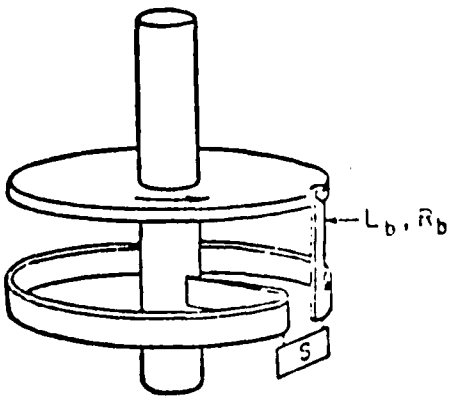

Figure 3: Dynamo with brush impedence

There are three dynamic variables in the model: J, the current in the disc; I, the current in the coil; and ω, the angular velocity, which are governed by the following set of ODE's:

$$C\dot{\omega} = G - MIJ - \nu\omega$$

$$(L_b + L_s)\dot{I} + (R_b + R_s)I = M\omega J - (R_c + R_s)J \qquad (1)$$

$$(L_c + L_s)\dot{J} + (R_c + R_s)J = L_s\dot{I} + R_s I$$

where ν is the viscous damping term, C is the moment of inertia of the disc, and the L's and R's are the inductance and resistance of the coil, brushes, and shunt. The introduction of an inductance for the brushes allows the currents in the coil and the disc to get out of phase with one another and eventually cause reversals through the Lorenz torque on the disc.

Linear Stability Analysis

The nondimensional form of the dynamo equations are:

$$\dot{a} = bc - a$$

$$\dot{b} = r - b - ac \qquad (2)$$

$$\dot{c} = \sigma(a - c) + \sigma\sigma^{-1} a$$

which have two stationary solutions a=c=0, b=r or a=c=r-1, b=1. Here a, b, c are the nondimesional current in the coil, the angular velocity, and the current in the disc respectively. Linear stability analysis about the first of these gives a characteristic polynomial for the eigenvalues of the linearized problem as:

$$(\lambda + 1)(\lambda^2 + (\sigma - \sigma r/\sigma_1 + 1)\lambda + \sigma(1-r)) = 0$$

The zero solution is stable when $r < 1$ and $\sigma - \sigma r/\sigma_1 + 1 > 0$. There are pure imaginary roots when $r_1 = \sigma_1(1 + 1/\sigma) < 1$ which corresponds to a Hopf bifurcation with an initial frequency, $\omega^2 = \sigma(1-4)$. If we linearize about the second stationary solution, we find

$$\lambda^3 + (\sigma - \sigma/\sigma_1 + 2)\lambda^2 + (r(1 + \sigma/\sigma_1) + \sigma - 2\sigma/\sigma_1)\lambda + 2\sigma(r - 1) = 0.$$

At $r = 1$, $\lambda = 0$ is an eigenvalue and the steady state is locally stable if $1 + \sigma/\sigma_1 + \sigma > 0$, i.e. if there is no Hopf bifurcation in $r < 1$.

There is a Hopf bifurcation off of the cellular solution in the Lorenz equations so we look for one in the dynamo equations by setting $\lambda = i\omega$, $\omega \in R$:

$$\omega^2 = \frac{2\sigma(r_2 - 1)}{(\sigma - \sigma/\sigma_1 + 2)} = (r_2(1 + \sigma/\sigma_1) + \sigma - 2\sigma/\sigma_1) \qquad (3)$$

where $r_2 > 1$ is the position of the bifurcation. This gives real ω only if

$$\sigma - \sigma/\sigma_1 + 2 > 0 \tag{4.a}$$

$$r_2(1 + \sigma/\sigma_1) + \sigma - 2\sigma/\sigma_1 > 0 \tag{4.b}$$

and if these hold then (3) gives

$$r_2 = \frac{2\sigma + (\sigma - 2\sigma/\sigma_1)(\sigma - \sigma/\sigma_1 + 2)}{2\sigma - (1 + \sigma/\sigma_1)(\sigma - \sigma/\sigma_1 + 2)} \tag{5}$$

If we wish to consider regions in parameter space where both r_1 and r_2 correspond to Hopf bifurcations, then we are required to satisfy $\sigma - \sigma/\sigma_1 + 2 > 0$ and $\sigma - \sigma/\sigma_1 + 1 < 0$. Consistency between these and both (5) and (4.b) implies that

$$2\sigma - (1 + \sigma/\sigma_1)(\sigma - \sigma/\sigma_1 + 2) < 0 \tag{6}$$

This gives a very limited region in (σ, σ_1) space where one Hopf branch connects the two steady solutions (figure 4).

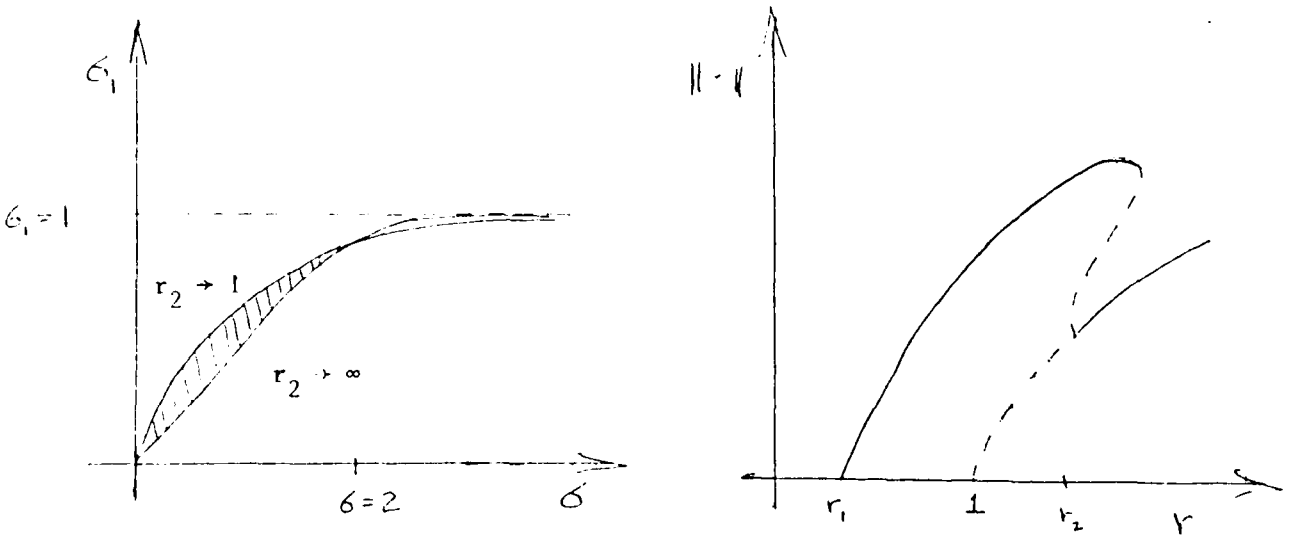

Figure 4: Bifurcation structure for a region of (σ, σ_1) space.

As the graph indicates, the oscillatory branch hits the second stationary branch at r_2 which tends to infinity as (σ, σ_1) approaches the curve $2\sigma - (1 + \sigma/\sigma_1)(\sigma - \sigma/\sigma_1 + 2) = 0$ but which tends toward $r_2 = 1$ as (σ, σ_1) approaches $1 - \sigma/\sigma_1 + \sigma = 0$. However $1 - \sigma/\sigma_1 + \sigma = 0$ also implies that $r_1 = 1$ and along this curve we have a codimension two bifurcation.

Elsewhere in parameter space: If $\sigma + 1 - \sigma/\sigma_1 < 0$ outside of the slice shown in figure 4, the Hopf bifurcation remains above the second branch which never gains stability. If we remove the restriction that there exists a Hopf bifurcation in front of the second branch, there is another section of parameter space described by (4) and (5) which corresponds to a Hopf bifurcation off of the second branch analogous to that seen in the Lorenz system (figure 5).

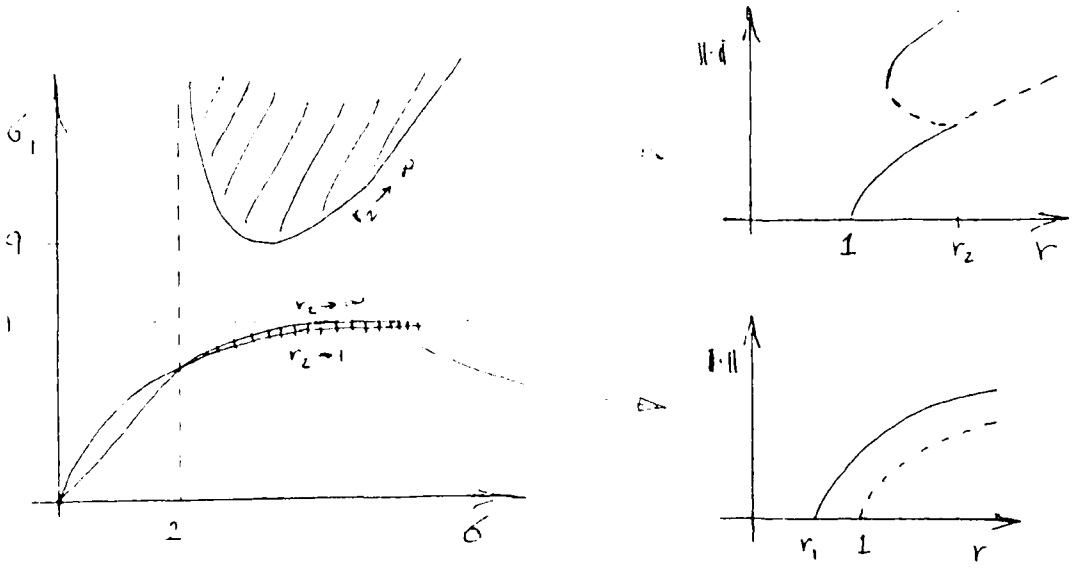

Figure 5: Other Regions

Chaos in the Disc Dynamo

When $\sigma_1^{-1} = 0$ the dynamo equations reduce to the Lorenz system (Lorenz, 1963) where the chaos has been extremely well studied (Sparrow, 1982). Following Robbins (1977), (r, σ) space can be separated into regions where a subcritical Hopf bifurcation either does or does not exist (figure 6).

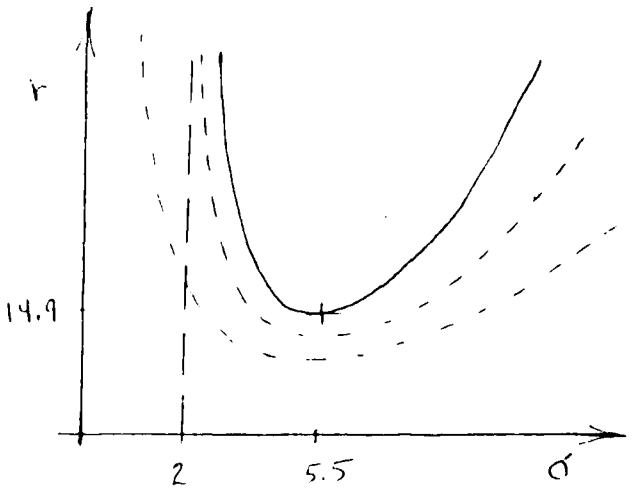

Figure 6 (Robbins, 1977)

Associated with this curve are two dashed curves. The first curve corresponds to the onset of a homoclinic orbit that Sparrow labels as a homoclinic explosion which generates an unstable strange invariant set (Sparrow, 1982). The second curve determines when the strange invariant set becomes stable and appears as a strange attractor. These curves are modified when $\sigma_1^{-1} \neq 0$ by introducing cutoff values for σ other than $\sigma_\ell = 2$, $\sigma_u = \infty$ as in the Lorenz case (figure 7).

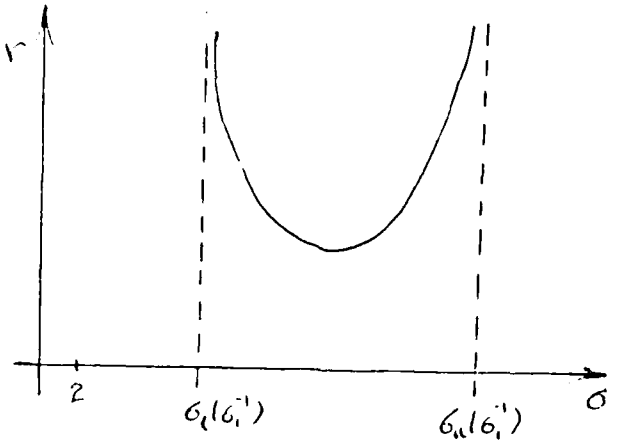

Figure 7: Cutoff values for the appearance of a Hopf bifurcation.

We can assume that there are similar dashed curves associated with the new boundary when $\sigma_1^{-1} \neq 0$ although these must be determined numerically. Note that as $\sigma_1 \to 9^+$, $\sigma_u(\sigma_1) - \sigma_\ell(\sigma_1) \to 0$ and there is no longer a Lorenz type Hopf bifurcation.

This region in parameter space exhibits merely an order ϵ change in the behavior of chaotic solutions from the Lorenz system, so we look to other regions with Hopf bifurctions for chaos; but, before going further, a necessary condition for chaos is that there be some global bound on the orbits in the form of a Lyapunov functional. If we define

$$E = a^2/2 + (r-b)^2/2 + (\sigma^{-1}c + \sigma_1^{-1}a)^2$$

then

$$\dot{E} = -(1 + \sigma_1^{-1}) - \sigma^{-1}c^2 - (r-b)^2 + (r + (\sigma^{-1} + \sigma_1^{-1}))ac$$

and $\dot{E} < 0$ outside of some ellipse which implies that the orbits are contracting outside this region.

Chaos also exists in other parts of parameter space. The unfolding of the codimension two bifurcation that occurs near $1 + \sigma - \sigma/\sigma_1 = 0$ has been examined by Knobloch (1981) and the supercriticality of the steady bifurcation necessitates the existence of a homoclinic orbit. Chaotic solutions are observed when the unstable limit cycles shed from the homoclinic explosion begin to interfere with the oscillatory solutions in the manner of S'ilnikov. Figure 8 shows the oscillatory one cycle bifurcate into a two cycle at $\sigma = 1.0$, $\sigma_1 = .4176450$, $r = 2.0625$. As r is increased further the two cycle loses symmetry and proceeds to go chaotic. There is a similar route to chaos for much of the region depicted in figure 4.

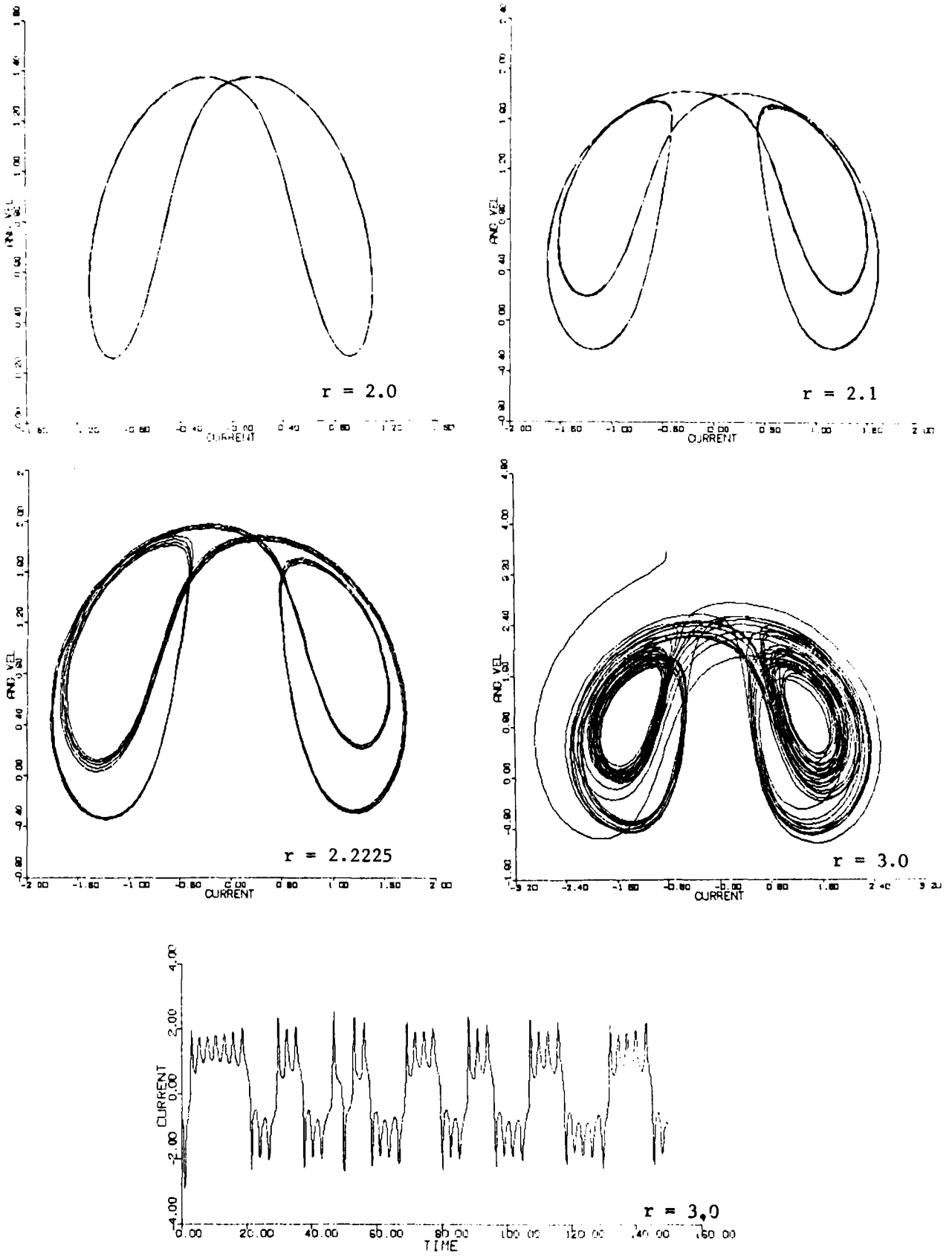

Figure 8: Evolution to Chaos with increasing r.

Statistical Averages of the Dynamo Equations

The limit of zero inductance on the brushes, $\sigma_1^{-1} = 0$, leads to the well studied Lorenz equations (Lorenz, 1963):

$$\begin{aligned} \dot{a} &= bc - a \\ \dot{b} &= r - b - ac \\ \dot{c} &= \sigma(a - c) \end{aligned} \tag{7}$$

Due to the statistical nature of the solutions to these equations when r is sufficiently large, it seems natural to introduce the moments of each component and determine the dynamics of the averages in much the same way that most theories of turbulence do. Numerical studies along these lines were first done by Lucke (1976) and substantiated theoretically by Knobloch (1978) who developed various stochastic differential equations governing the second order moments of the solutions.

If we introduce the average value as $\overline{(\quad)} = \lim_{t\to\infty} \frac{1}{t}\int_0^t (\quad)dt'$ then it immediately follows from (7) that $\overline{bc} = \overline{a}$, $r = \overline{b} + \overline{ac}$, $\overline{a} = \overline{c}$. An infinite number of such relations can be formed by noting that

$$\overline{\frac{d}{dt} A(a,b,c)} = \overline{\frac{\partial A}{\partial a}\dot{a}} + \overline{\frac{\partial A}{\partial b}\dot{b}} + \overline{\frac{\partial A}{\partial c}\dot{c}} = 0$$

Malkus (1972), who derived the Lorenz equations from a closure to the equations describing convection of a heated fluid in a ring, discovered a useful relation giving the average heat flux in terms of its value while in steady rolls plus other negative definite terms.

The result is:

$$\overline{ac} = r - 1 - \frac{\overline{\dot{c}^2}}{\sigma^2\,\overline{c^2}} - \frac{\overline{(b - \overline{b})^2}}{\overline{c^2}}$$

In the full dynamo equations an equivalent relation is given by:

$$\overline{ac} = r - \frac{(1 + \sigma\sigma_1^{-1})\,\overline{c^2}}{(1 + 2\sigma\sigma_1^{-1})(c^2 + \sigma\sigma_1^{-1}a^2)} - \frac{2\sigma\sigma_1^{-1}(1 + \sigma\sigma_1^{-1})\,\overline{a^2}}{(1 + 2\sigma\sigma_1^{-1})\,c^2 + \sigma\sigma_1^{-1}a^2)} \tag{9}$$

$$- \frac{\overline{(b - \overline{b})^2}}{\overline{c^2} + \sigma\sigma_1^{-1}\overline{a^2}} - \frac{\sigma_1^{-2}(1 + \sigma\sigma_1^{-1})\,\overline{\dot{a}^2}}{\sigma^2(1 + 2\sigma\sigma_1^{-1})(\overline{c^2} + \sigma\sigma_1^{-1}\overline{a^2})} - \frac{(1 + \sigma\sigma_1^{-1})\,\overline{\dot{c}^2}}{\sigma^2(1 + 2\sigma\sigma_1^{-1})(\overline{c^2} + \sigma\sigma_1^{-1}\overline{a^2})}$$

which reduces to (8) in the limit $\sigma_1^{-1} \to 0$ and also gives $\overline{ac} = r - 1$ on the steady branch where $\overline{\dot{a}^2} = \overline{\dot{c}^2} = \overline{(b - b)^2}$ and $\overline{a^2} = \overline{c^2}$.

These averages correspond to physical observables such as the average heat flux for the convecting fluid or the average back reactance of the magnetic field on the disc dynamo. Just as in many physical systems, we expect these averages to undergo a discontinuous change as the system passes through a subcritical bifurcation where the stable flow field on the lower branch has radically different properties than its corresponding stable state on the upper branch. Such discontinuities of physical observables are commonplace in flows with subcritical bifurcations, for example, the torque required to drive the cylinders in Taylor-Couette flow drops dramatically as Taylor convection sets in.

The subcritical bifurcation in the Lorenz equations is associated with the onset of its strange attractor and the depth of subcriticality of the Hopf bifurcation is usually considered to be the value of r where the strange invariant set first becomes stable. Since $\overline{c^2}$ and $(\overline{b} - b)^2$ are nonzero for the chaotic orbits, $\overline{ac}$ must decrease from its value in steady rolls, $\overline{ac} = r - 1$. Figure (9) exhibits numerically calculated

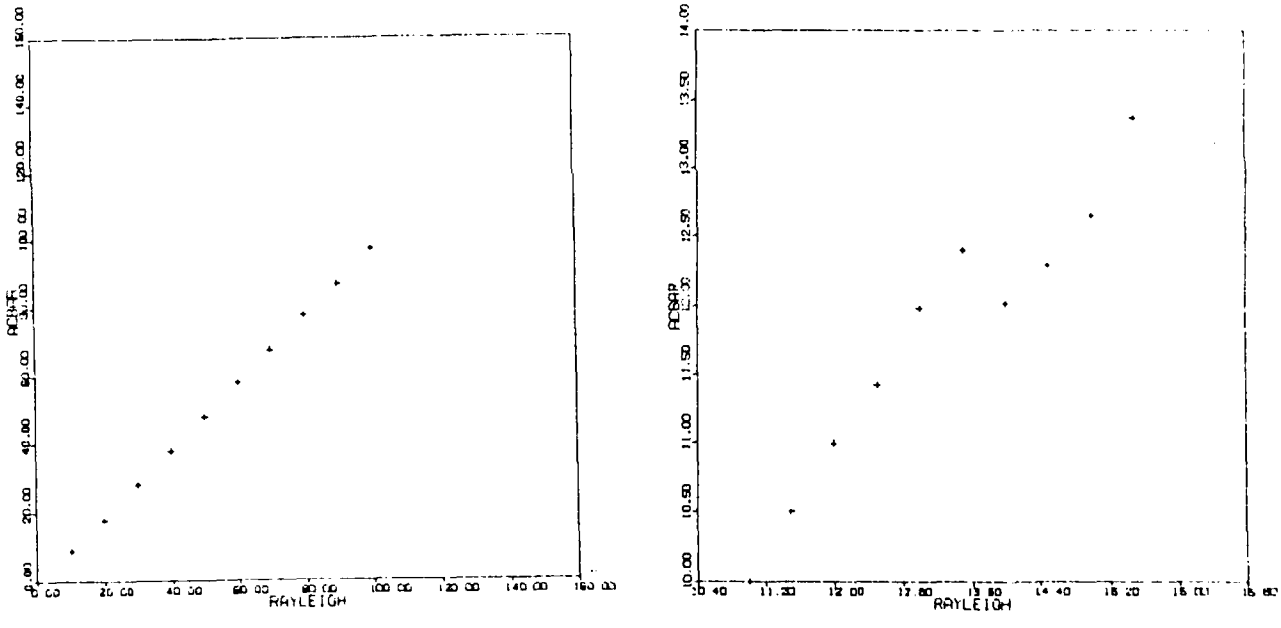

Figure 9: Heat flux vs. Rayleigh number: Subcritical jump.

averages of ac as functions of the Rayleigh number for the Lorenz system with $\sigma = 5.0$. The gap at $r = 14.0$ indicates the stabilization of chaos and the graph is somewhat incomplete since $\overline{ac} = r - 1$ is linearly stable until the Hopf bifurcation at $r = 15.0$, i.e., there is a hysteresis effect as is standard with subcritical bifurcations. The size of the gap can be easily estimated by noting that $(\overline{b} - b)^2 / \overline{c^2} = O(1/r)$ and since the frequency of the Hopf bifurcation is of order $\sqrt{r}$, $\dot{c} \doteq \sqrt{rc}$ on the attractor so that $(1/\sigma^2)\ \overline{\dot{c}^2} / \overline{c^2} = O(r/\sigma^2)$ which gives that $[\overline{ac}]_{r = 14.0} \sim r/\sigma^2 \sim .5$.

A similar study can be carried out with the full dynamo equations, where both r and σ remain fixed and the induction, σ_1, is varied. As σ_1 is decreased from its value near the onset of the Hopf bifurcation, the position where the Hopf branch hits the steady solution moves toward infinity and eventually passes the chosen value of r. With r = 5.0 and σ = 1.0 the cells lose absolute stability to a subcritical Hopf bifurcation which then proceeds to develop into various stages of chaos to emerge in states of noisy periodicity (figure 10).

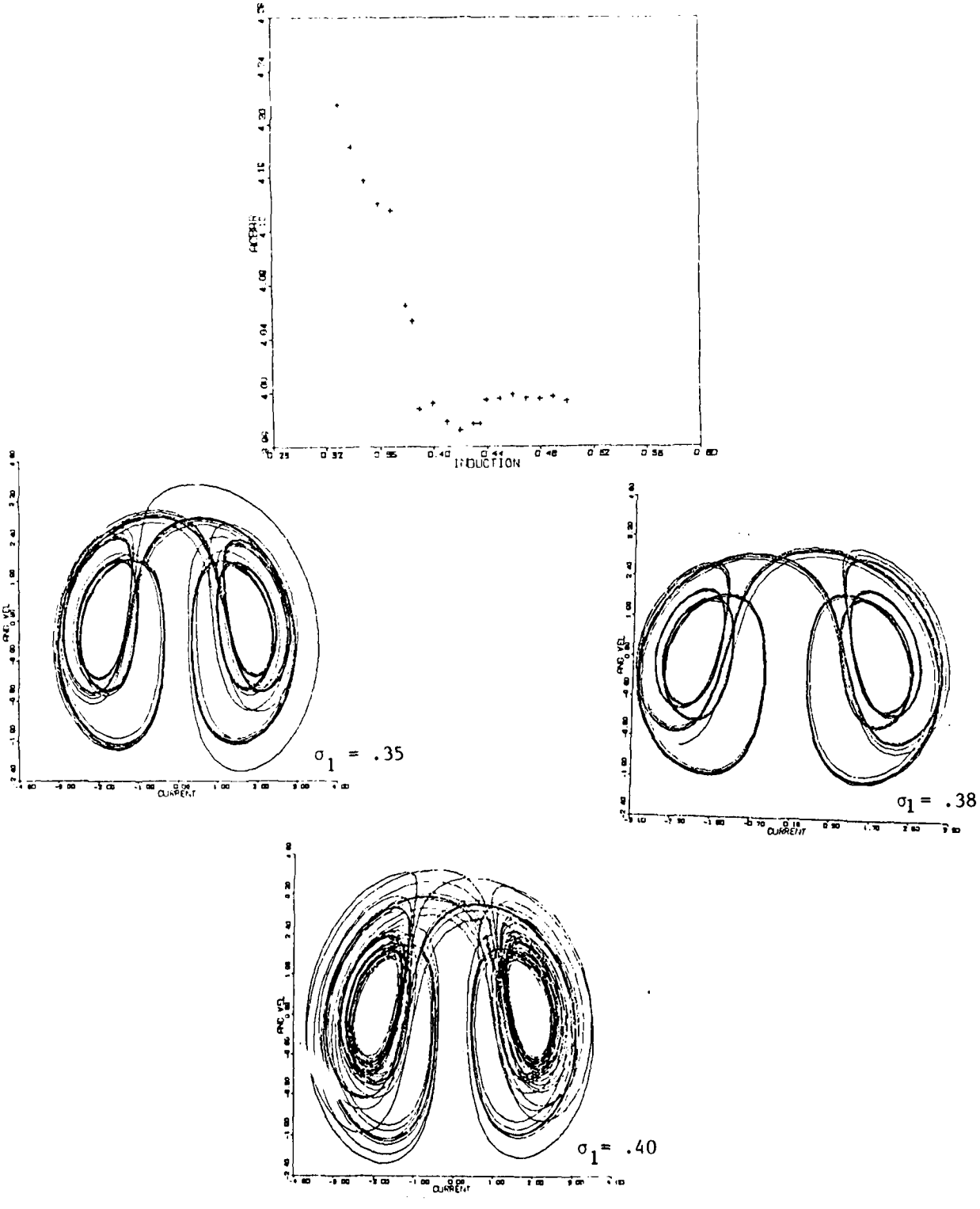

Figure 10

Modulation of Rayleigh Number

The statistics of the geomagnetic record underwent a dramatic change about 40 million years ago when the frequency of reversals became significantly smaller. There is a period between 88 and 110 million years ago in which no reversals occurred (figure 2). Connections have been made to regions of the Lorenz attractor where the system spends longer than average times orbiting one fixed point before reversing (Bullard, 1978) but these would hardly seem to account for the extended periods of nonreversal in the earth's record.

It is quite possible that there is a slow time modulation of the internal parameters in the geodynamo; there are precessional effects and coremantle interactions not to mention a multitude of other possibilities. If these slow modulations were to occur near the boundaries of the chaotic behavior in the dynamo, we would expect to see rolls stabilized on a much longer time scale. These rolls would then lose stability as the parameters slowly moved into regions allowing chaotic reversals.

This is basically just a time dependent bifurcation problem where the Rayleigh number now evolves on a slow time scale near the discontinuity in the heat flux. It seems natural that the processes controlling the modulation of r are linked to the physical state of the system which might be characterized by the average heat flux. If this is the case, lacking knowledge of any physics behind the modulation, we seek to model the slow time evolution of r so that it is increasing below the onset of chaos and decreasing above it. In light of the discontinuity of $\overline{ac}$, where it drops by about 4 , we can introduce a model equation for the modulation as:

$$\dot{r} = \epsilon[ac - \gamma(r - 1)] \tag{10}$$

where $\epsilon << 1$ and $.96 < \gamma < 1$. If ϵ is small enough, we should expect to be able to replace the average of ac by its local value assuming that ac has equilibrated on a time scale of $1/\epsilon$. This allows us to replace the integro differential equation by a much simpler differential equation:

$$\dot{r} = \epsilon[ac - \gamma(r - 1)]$$
$$\epsilon << 1, \; .96 < \gamma < 1 \tag{11}$$

It is easy to see that equation (10) exhibits the proper behavior with $\dot{r} < 0$ below chaos and $\dot{r} > 0$ above. If ϵ is not too large, equation (11) should behave similarly.

The addition of this equation modifies the system and the solutions now show bursts of intermittent chaos separated by periods of relaminarization which lasts on the time scale of $\tau_k \sim 1/[\epsilon(1-\gamma)]$(figure 11). The length of the bursts are proportional to $\tau_B \sim 1/(\gamma-.96)$ which leads to $\tau_B/\tau_R = [\epsilon(1-\gamma)]/(\gamma-.96)$.

Conclusion

We have found that there are regions in parameter space where the disc dynamo can undergo chaotic reversals in a manner quite unlike that associated with the approximation of zero brush inductance. Chaos develops as a result of the development of a homoclinic orbit which arises on the Hopf branch that merges into the supercritical steady bifurcation.

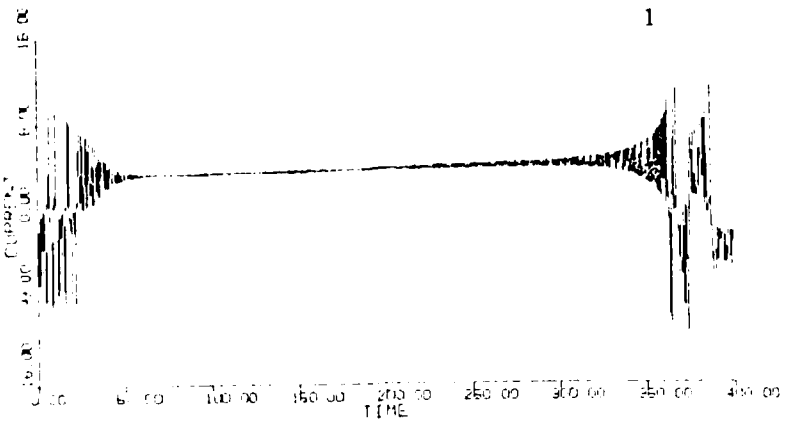

ϵ =.1, γ=.09, τ_R=500, τ_B=50

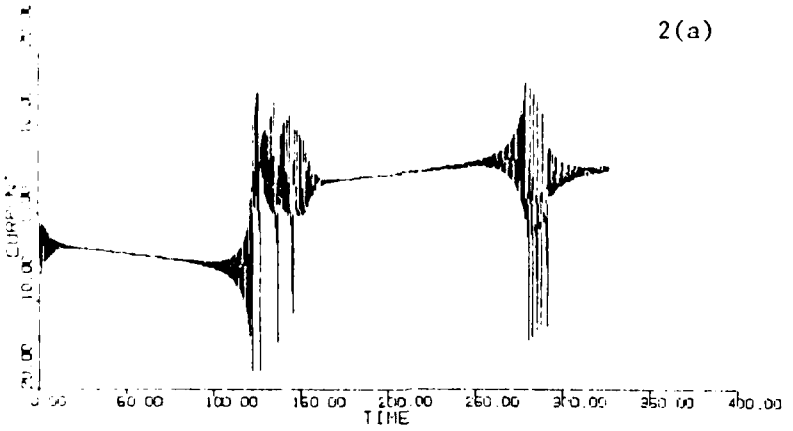

ϵ=.5, γ= .98, τ_R=100, τ_B=50

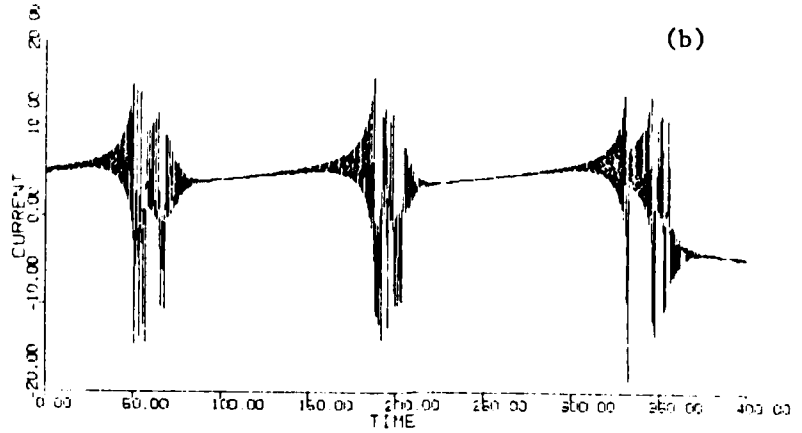

Figure 11: Periodic bursting in the modulated Lorenz Equations. 2(b) is a continuation of the integration begun in (2a).

The second part of this paper has been a motivational treatment of parameter modulation in the disc dynamo model of geodynamo. This is based on the observation that many self equilibrating flows fluctuate near metastable boundaries. The model for modulation was strictly contrived and produced bursting which was much too regular to have any direct correlation to the geodynamo, however, it gives a possible mechanism for the long periods of nonreversal observed.

This system is now a fourth order set of ODE's where we have significant control over the length and periods of the chaotic bursts through the parameters ε and δ. Intermittency is a fairly common phenomena in higher order systems, but its appearance and disappearance are difficult to determine and even more difficult to "tune". In this modulated Lorenz system, as δ increases toward $\delta = 1$, the length of nonreversing roll solutions increases to infinity. Likewise, as δ decreases to approximately $\delta = .96$, the length of chaotic reversals increases to infinity. Any combination of these two extremes can be obtained and the added parameter ε determines the relative time scales on which the solution is either chaotic or laminar.

Acknowledgements: I would like to sincerely thank Willem Malkus for his interesting discussion, outdoor barbeques and extra C.L.O.C. tickets. I also thank George Veronis for making the summer such a pleasure.

REFERENCES

Bullard, E., 1978. Topics in Nonlinear Dynamics, AIP Conference Proceedings no. 46. New York American Institute of Physics.

Knobloch, E., 1978. WHOI Report no. 78-67, 91-109.

Knobloch, E., 1981. WHOI Report no. 81-102.

Lorenz, E.N., 1963. Atmos. Sci. 20, 130.

Lucke, M., 1976. J. Stat. Phys. 15, 455.

Malkus, W.V.R., 1972. Trans. Amer. Geophys. Un. 53, 617.

Malkus, W.V.R., 1972. Memoires Soc. Roy. des Sciences de Liege 4, 6th series, 125-128.

Robbins, K.A., 1977. Math. Proc. Camb. Phil Soc. 82, 309.

Robbins, K.A., 1976. Proc. Natl. Acad. Sci. U.S.A. 73, no. 12, 4297.

Sparrow, C., 1982. The Lorenz Equations: Bifurcations, Chaos, and Strange Attractors, Applied Math. Sciences, Vol. 41, Springer-Verlag.

Convection with Mixed Up Boundary Conditions

William Morrell

Abstract: We explore the dynamics of thermohaline convection subject to nonstandard boundary conditions as a problem archetypal of the excitation of large scale modes by small scale motions. In particular we choose fixed salt flux and fixed temperature boundary conditions. A finite amplitude perturbation expansion is done for the special case of no vertical salinity forcing. We find that horizontal gradients generate fronts in the salt concentration which directly reflect the phase of the slow modulation of the forced thermal convection. The zero flux calculation can be posed as a problem in estuary dynamics, and we also argue for its application to certain astrophysical problems.

I. Introduction

The excitation of large scale structures by small scale motions is a common problem in geophysical and astrophysical fluid dynamics. The dynamo problem relies on such mechanisms as do many meteorological problems. This type of process can often be characterized by a renormalized diffusion of the property in question - momentum, vorticity, etc. In the case of vertical vorticity in Rayleigh-Benard convection, a phase instability occurs resulting in the concentration and oscillation of vertical vorticity (Busse, 1978). Such so-called "phase instabilities" are common in secondary bifurcations of dynamical systems which involve the interaction of two instabilities. The problem of vertical vorticity in a convecting layer near onset has been extensively studied (Siggia and Zippelius, 1981), but the three dimensional nature of the vertical vorticity field renders the analysis quite difficult, masking the dynamics of the generic instability. Such generic problems have been analyzed using normal form theory and symmetry arguments (Coullet and Fauve, 1984), but no simple physical model is known for many cases. Below we address the problem of realizing a phase instability at the onset of thermal convection in a simple two-dimensional model.

The analysis will be organized in the following way. In section II we introduce a simple physical problem which has the characteristics necessary to generate phase instabilities at the onset of convection. Equations for the amplitude of the coupled modes of the system are derived by standard perturbative methods and discussed. We examine solutions of these equations and derive conditions for their stability. Section III is a general discussion of the problem and possibilities for future analysis. Most of the calcultions will be presented in the appendix, although those necessary to follow the development will be sketched where appropriate.

II. The Model

Figure 1 depicts the physical set up we have in mind. A layer of fluid large in horizontal extent is heated from below. At a critical value of the Rayleigh number, buoyancy forces overcome viscous damping and motion occurs. However, the boundary conditions on the appropriate scalar field are crucial in determining the scale at which the motion

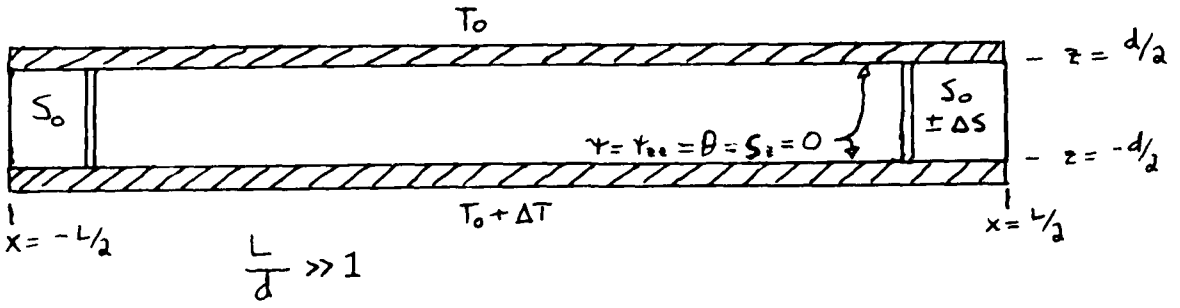

Figure 1

will occur. In particular, for fixed temperature boundary conditions, large scale motions cannot be supported and small scale motions are damped so the system first goes unstable to a mode with a finite wavenumber, K_c. On the other hand, for fixed flux boundary conditions, the system first becomes unstable at zero wavenumber (Spiegel, 1981), i.e., infinite wavelength. This important difference motivates our choice of boundary conditions on the fluid. The temperature at the boundaries is fixed; the flux of salt through the boundaries is taken to be zero. This choice results in a thermal instability at a finite wavenumber exciting a haline instability at zero wavenumber.

The choice of kinematic boundary conditions is based on mathematical simplicity. That is, we choose stress-free boundaries above and below in order to simplify the eigenfunctions of the linear problem. The dynamics of the instability we have in mind will not critically depend on this choice.

The motion is taken to be two dimensional and our results may depend on this assumption, but we will leave that question to the discussion. The fluid is taken to satisfy the Boussinesq approimation and we leave the choice of boundary conditions at the edges of the layer to later in the development. Under these assumptions the nondimensional equations of motion are

$$(\sigma^{-1}\partial_t - \Delta)\Delta\psi = -R\theta_x + \partial_x\Sigma + \sigma^{-1}J(\psi,\Delta\psi) \tag{2.1}$$

$$(\partial_t - \Delta)\theta = -\partial_x\psi + J(\psi,\theta) \tag{2.2}$$

$$(\partial_t - \tau\Delta)\Sigma = J(\psi,\Sigma) \tag{2.3}$$

where

$$\underset{\sim}{V} = (\partial_z\psi, -\partial_x\psi) \qquad J(A,B) = \partial_x A\partial_z B - \partial_x B\partial_z A$$

$$\theta = (T - T_c)/\Delta T \qquad \Delta = \partial_x^2 + \partial_z^2$$

$$\Sigma = S/\Delta S \qquad \tau = \kappa S/\kappa T$$

$$R = g\alpha\Delta T d^3/\kappa_T\nu \qquad \sigma = \nu/\kappa T$$

where ΔS is a characteristic horizontal variation of the background salinity, which varies on long length scales only, and T_c is the motionless conductive state.

Note that the equation for salinity couples only nonlinearly to the velocity field due to the assumption of no imposed vertical gradient in salinity, and the assumption that the horizontal gradient in salinity is of $O(\varepsilon)$ relative to the temperature and velocity variation. Accordingly, the perturbed or inhomogeneous salinity field should be independent of the vertical at lowest order.

Linear Theory

The equations of motion may be rewritten for convenience in the following form:

$$V = \begin{pmatrix} \psi \\ \theta \\ \Sigma \end{pmatrix} \quad ; \quad MV = \partial_t LV + N(V,V) \tag{2.4}$$

where M and L are linear operators and N is strictly nonlinear. The linear problem is then given by

$$MV = \partial_t LV.$$

This equation admits two normal modes. One is a mode which consists only of velocity and temperature and it is identical to the mode of linear theory for simple thermal convection. The other is a salt mode which is estimated for long wavelengths (see appendix). They are

$$V_T = e^{S_1 t}\begin{pmatrix} \cos\pi z \sin Kx \\ \cos\pi z \cos Kx \\ 0 \end{pmatrix} \quad \text{and} \quad V_S = e^{S_2 t}\begin{pmatrix} KF_1(z)\sin Kx + O(K^3) \\ K^2F_2(z)\cos Kx + O(K^4) \\ \cos Kx \end{pmatrix}$$

where $s_1 = (R - R_c)/R_c - \xi_0(K - K_c)^2 + O(K - K_c)^3$ and $s_2 = -\tau K^2$ and ξ_0 is a constant.

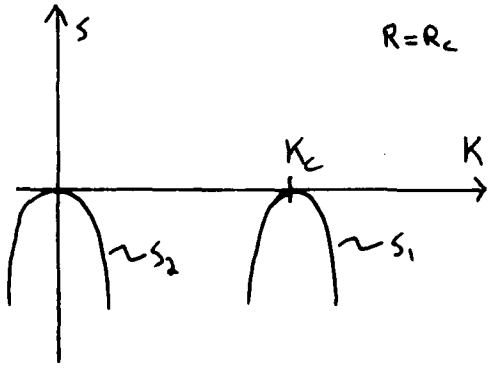

Figure 2

Figure 2 depicts the growth rates at the value of $R = R_c$ given by linear theory for the onset of convection at a finite wavelength.

For R slightly above R_c, a finite band of modes in K-space is unstable but the salt modes are still marginal. To admit the finite band of modes one allows a slow modulation of the linear eigenfunctions in the usual way. We let

$$R = R_c(1 + \varepsilon^2)$$

$$X = \varepsilon x$$

$$T = \varepsilon^2 t$$

where the scaling of the growth rates and long length scales are determined by the structure of the growth rate curve, i.e., parabolic. Then the operators become

$$\partial_x \rightarrow \partial_x + \varepsilon \partial_X$$

$$\partial_t \rightarrow \varepsilon^2 \partial_T$$

and we expand all the operators and state vectors in equation (2.4) in powers of ε.

The situation we choose to exmaine is that of an order one salinity field varying only in the slow variables at the onset of thermal convection. This is expressed in the ansatz

$$V = \begin{pmatrix} 0 \\ 0 \\ \Sigma_0(XT) \end{pmatrix} + \varepsilon A(XT) \begin{pmatrix} \psi_1 \\ \theta 1 \\ \Sigma_1 \end{pmatrix} + \ldots$$

where the salinity mode has no temperature of velocity field in the limit as $K \rightarrow 0$.

We equate powers of ε and at each order we must remove secularities by applying a solvability condition. The system then becomes a set of linear inhomogeneous equations the details of which are presented in appendix B.

If B is the amplitude of the vertically averaged salinity field then the amplitude equations, written in terms of the fast variables, are:

$$B_t = [(\tau + \xi(|A|^2 + \gamma B_x^2))B_x]_x \qquad (2.5)$$

$$\lambda A_t = [r - (\eta B_x^2 + (\pi^2/4)|A|^2)]A + 4A_{xx} \qquad (2.6)$$

where

$$\lambda = (\sigma + 1)/\sigma \qquad \xi = 2/3\,\tau$$

$$r = 3\pi^2/2\ (R-R_c/R_c) \qquad \gamma \cong 1/2000$$

and $\eta \cong 1/(670\,\tau^2)$ for τ small, σ large.

There is a number of important features to note about these equations. First, the salt equation is a diffusion equation with a renormalized diffusion coefficient. Similarly, A evolves according to diffusion and a renormalized Rayleigh number. The presence of B_x^2 in the A equation is a result of the shear flow generated by the salinity gradient, which is known to stabilize the fluid, i.e., it decreases the effective Rayleigh number. The $|A|^2$ and B_x^2 terms in the B equation are the result of increased transport of salt due to the presence of the convective rolls and shear flow, respectively. Indeed, the presence of the reciprocal of the diffusion in the coefficients of $|A|^2$ and B_x^2 is reminiscent of Taylor shear dispersion.

If we multiply B times (2.5) and integrate over the domain we get the following power integral:

$$\partial_t \int_{-L/2}^{L/2} 1/2\ B^2 = -\int_{-L/2}^{L/2} (\tau + \xi(|A|^2 + \gamma B_x^2))B_x^2 + [(\tau + \xi(|A|^2 + \gamma B_x^2)BB_x]_{-L/2}^{L/2}$$

That is, if we do not impose a horizontal density contrast across the layer then the variance of the salinity must decrease monotonically (the integral can be taken to be a Lyapunov function). With this in mind we see that there is a steady solution to the equations given by

$$B_0 = pX \qquad A_0 = Qe^{iqx}$$

where $r - \eta p^2 - \pi^2/4\ Q^2 - 4q^2 = 0$ and p and Q are real constants. This solution corresponds to changing the wavenumber of the roll pattern from K_c to $K_c + q$, but keeping the amplitude constant in space and time and imposing a horizontal density contrast through the sidewall boundary conditions.

The next issue, of course, is the stability of this simple solution. We linearize the equations and perturb this solution as indicated below

$$A = (Q + a)e^{iqx}$$

$$B = B_0 + b$$

where a is complex and b is real. If we write $a = \rho + i\varphi$, ρ and φ both real, and let ρ, φ and b all vary as e^{iKx+st}, then we have a third order eigenvalue problem governing the linear stability of the above steady solution to perturbations of wavenumber K. The perturbations must satisfy

$$\begin{pmatrix} (\lambda S + \pi^2/2\, Q^2 + 4K^2) & 8iqK & 2i\eta pQK \\ -8iqK & (\lambda S + 4K^2) & 0 \\ -2p\xi Qi K & 0 & S + \zeta K^2 \end{pmatrix} \begin{pmatrix} \rho \\ \varphi \\ b \end{pmatrix} = 0$$

where

$$\zeta = \tau + \xi (Q^2 + 3\gamma_\rho^2).$$

The equation for the growth rate S is then given by the condition that the determinant of the coefficients vanishes:

$$\lambda^2 S^3 + \lambda S^2[\lambda \zeta K^2 + \pi^2/2\, Q^2 + 8K^2]$$

$$+ S[4K^2 E + \lambda\zeta K^2(\pi^2/2\, Q^2 + 8K^2) - \lambda\chi Q^2 K^2]$$

$$-4K^4(\zeta E - \chi Q^2) = 0$$

where $\chi = 4p^2\eta\xi$ and $E = \pi^2/2\, Q^2 + 4K^2 - 16q^2$, the 'Eckhaus discriminant'. In the case where $p = 0$, then, direct instability occurs for $E < 0$. That is, the system is unstable to a perturbation of wavenumber K if

$$K^2 < r - 3\pi^2 Q^2/8.$$

The condition for instability of the uniform gradient solution is given by

$$\zeta E - \chi Q^2 > 0$$

$$4E - \lambda\chi Q^2 + \zeta(\pi^2/2\, Q^2 + 8K^2) < 0$$

Rewriting these inequalities to clarify the restrictions on K we find:

$$\left((\lambda\zeta - 4)\frac{\chi}{8\zeta^2} - \frac{\pi^2}{16}\right) Q^2 > K^2 > r - \frac{3\pi^2}{8} Q^2 + \left(\frac{\xi Q^2}{\zeta} - 1\right)\eta p^2.$$

If Q and p are of the same order of magnitude and $\tau \simeq 0.01$, as for water, then $\zeta \simeq \xi Q^2$, and we estimate

$$\frac{\lambda\eta p^2}{2} - \frac{2\eta p^2}{Q^2} - \frac{\pi^2}{16} Q^2 > K^2 > r - \frac{3\pi^2}{8} Q^2$$

For $\tau \simeq 0.01$, $\xi \simeq 200/3$ and $\eta \simeq 15$, so to first order this amounts to

$$\frac{15\lambda}{2} p^2 - \frac{\pi^2}{16} Q^2 > K^2 > r - \frac{3\pi^2}{8} Q^2$$

Thus direct instability occurs in a band of K space which borders the region which is Eckhaus unstable.

There is another range in parameter space where direct instability always occurs, namely as $K \to 0$. If we return to the cubic equation for the growth rates and neglect terms of order K^3 and higher we get

$$\lambda^2 S^3 + \lambda\frac{\pi^2}{2} Q^2 S^2 - K^2(64q^2 + \chi)S = 0$$

In particular, $S = 0$ is always a solution, and there is also always a positive root for S found by solving the quadratic equation which results from removing the $S = 0$ root:

$$S = \frac{-\pi^2 Q^2}{4\lambda} + \frac{1}{4\lambda}\left(\pi^4 Q^4 + 16K^2(64q^2 + \chi)\right)$$

$$\simeq 2(64q^2 + \chi)\frac{K^2}{\lambda}$$

At marginality the perturbation solutions are given by

$$\begin{pmatrix} \rho \\ \varphi \\ b \end{pmatrix} = \begin{pmatrix} \frac{-i}{2} & \frac{K}{q} \\ 1 & \\ \frac{p\xi Q}{\zeta q} & \end{pmatrix} e^{iKx} .$$

From this we can see that as $K > 0$, we do indeed have a phase instability, for ρ vanishes like K. Even for K finite we see that the velocity perturbation is out of phase with the steady solution, i.e., a phase rather than amplitude instability:

$$\rho + i\varphi = i(1 - K/2q)\varphi_0 e^{iKx}.$$

This instability is a bit surprising as the shear generated by the density gradient would normally be expected to stabilize the system, but here the fluid system is capable of altering the forcing, and this is apparently what is happening. A full solution of the linear perturbation problem has not yet been done but preliminary results indicated that there may be a Hopf bifurcation accessible to the system.

To see what this instability corresponds to, we examine the steady equations. For a steady solution the following equations hold

$$(\tau + \xi(|A|^2 + \gamma B_x^2))B_x = \text{constant} \qquad (2.7)$$

$$(r - (\eta B_x^2 + \pi^2/4\ |A|^2))A + 4A_{xx} = 0 \qquad (2.8)$$

If we imagine that a perturbation does not initially change the wavenumber of A, then we may perturb B_x^2 and ask for the following balances:

$$B_x^2 \rightarrow B_x^2 + \delta$$

then

$$|A|^2 \rightarrow |A|^2 - 4\eta/\pi^2\delta \quad \text{from (2.8).}$$

Then to maintain the balance in (2.7) we find that

$$\gamma B_x^2 + |A|^2 \rightarrow B_x^2 + |A|^2 + \delta(\gamma - 4\eta/\pi^2) \cong B_x^2 + |A|^2 + \delta(1/2000 - 1/300\tau^2)$$

Now the last term in parentheses is negative for τ small, so to maintain the balance in equation (2.7) we must further increase $|B_x|$. That means that the perturbation will grow, whether positive or negative. Note also that the effect is independent of the sign of B_x.

Since the mean gradient must be preserved to first order, this suggests that the uniform gradient will be unstable to a perturbation similar to that shown in figure 3. Where the perturbation in the salt gradient squared was positive, the gradient will be steep and the amplitude of the rolls will be small; the opposite will hold where δ was negative.

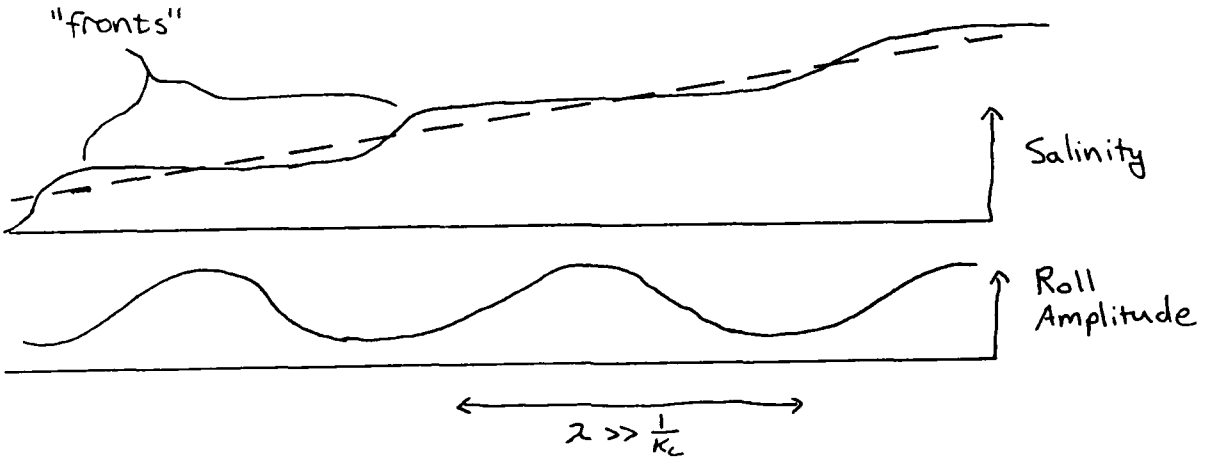

Figure 3

The form of this perturbation may also be understood to be an adjustment of the system to the shear flow suppressing the rolls. When such an instability is developed, the regions where the shear is strong are localized in regions where the amplitude is small and vice versa. The development of these salt fronts allows the rolls to exist in the presence of the shear generated by the salt gradient.

The full structure of the perturbation problem remains to be seen, but, as usual, the limited time available in one summer has restricted the completeness of this aspect of the research. We consequently turn to the general discussion of the problem.

III. Discussion

One may regard this problem as an exploration of estuary dynamics in the presence of thermal convection. Young (1983) has considered this problem in the case of no convection. The result here, then, is the calculation of a renormalized diffusion of a dynamically important solute in the presence of eddies preferentially oriented in the vertical. The instability of the simple uniform gradient solution indicates that the system can develop inhomogeneities on long length scales. Physically this is counter-intuitive, particularly in the case of a solute, where

one would expect convection to homogenize the fluid. A simple, although nonrigorous argument suggests that fronts in salinity may form in such a convection zone.

This fact suggests another interesting problem for future study. If a convection layer lies above a quiescent region, so-called penetrative convection, and there is a perturbation to the horizontal salinity field, the gradient might develop fronts which would locally be gravitationally unstable. Physically this would be exciting as it would provide a mechanism for mixing and transport of a solute in an initially homogeneous fluid. Such mixing has been invoked in astrophysical problems without a definite mechanism to support the theory, so the discovery of a transport process which is self-sustaining would be a breakthrough. We hope to begin exploration of this problem in the near future.

Another point worth remarking on is the relationship of the two-dimensional problem to the full three-dimensional problem. Usually the presence of shear flow in a single direction merely forces the rolls to align parallel to the shear, but here, where the shear is not externally forced, but internally generated, a mechanism has been suggested for the reorganization of the shear forcing which may allow rolls aligned perpendicular to the imposed salt gradient to exist in comparable amplitude with those aligned with the shear. This becomes a pattern selection problem, and is hence fully three dimensional, but one may attempt to suppress the full problem by considering model equations which control planform without the difficulties of a three-dimensional representation (Swift, 1985). This too is a hope for future study.

The full problem of a vertically forced salinity field remains to be studied. Also, alternate scalings may simplify the analysis, avoiding dreaded reconstitution, or mixing of orders (see appendix). It seems we have posed more questions than we have answered, but perhaps this is typical of problems of this nature. While the lack of closure is regrettable, it is also exciting in the prospects it brings to scrutiny.

Appendix

A. Computation of Near Infinite Wavelength Salt Mode

If we take an x-derivative of equation (2.1) to eliminate odd derivatives and let fields vary like exp(st + iKx) for K small then we have:

$$(-\sigma^{-1}s\Delta + \Delta^2)w = R_T K^2 \theta - K^2 \Sigma$$

$$(s - \Delta)\theta = w$$

$$(s - \tau\Delta)\Sigma = 0$$

The equation for Σ is satisfied if Σ is a constant in the vertical and $s = -\tau K^2$, and this is in fact the most general solution. Then we expand in powers of K^2 and we have at O(1)

$$D^2\theta_0 = -w_0$$

$$D^4 w_0 = 0$$

for which the most general solution satisfying boundary conditions is

$$\theta_0 = w_0 = 0.$$

At $O(K^2)$ we get

$$D^2\theta_1 = -w_1$$

$$D^4 w_1 = -\Sigma$$

The solution to these equations are polynomials of fourth- and sixth-order for w and θ, respectively, the F_1 and F_2 of the mode in the linear analysis. Since ψ is an x integral of w, we lose one power of K and the mode is

$$\begin{pmatrix} \psi \\ \theta \\ \Sigma \end{pmatrix} = \begin{pmatrix} K\,P_1(z)\sin Kx \\ K^2 P_2(z)\cos Kx \\ \cos Kx \end{pmatrix} e^{-\tau K^2 t} + \text{h.o.t.}$$

where P_1 is fourth-order, P_2 is sixth order and h.o.t. indicates terms depending on higher powers of K. Note, however, that the Σ solution is exact.

B. The Linear Inhomogeneous System

We start with the dimensional equations

$$(\partial_t - V\Delta)\Delta\psi = -g\alpha\theta_x + g\beta s_x + J(\psi, \Delta\psi) \qquad \text{(B.1)}$$

$\underset{\sim}{V} = (\psi_z, -\psi_x)$

$$(\partial_t - K_T\Delta)\theta = -\overline{T}_z w + J(\psi, \theta) \qquad \text{(B.2)}$$

$$(\partial_t - K_S\Delta)s = J(\psi, s) \qquad \text{(B.3)}$$

We nondimensionalize as follows

$$w = \frac{\kappa_T}{d} w' \qquad t = \frac{d^2}{\kappa_T} t' \qquad \psi = \kappa_T \psi' \qquad \nabla = \frac{\nabla'}{d} \qquad \theta = -\overline{T}_z d\theta'$$

dropping primes we have:

$$s = \frac{G}{\beta} \quad \text{where} \quad R = \frac{-g\alpha T_z d^4}{\kappa_T \nu}, \quad G = \frac{gd^3}{\nu\kappa_T}$$

$$(1/\sigma\,\partial_t - \Delta)\Delta = -R_T\theta_x + \Sigma_x + 1/\sigma\, J(\psi, \Delta\psi)$$

$$(\partial_t - \Delta)\theta = -\psi_x + J(\psi, \theta)$$

$$(\partial_t - \tau\Delta)\,\Sigma = J(\psi, \Sigma)$$

Rewriting this as $MV = \partial_t LV + N(U,U)$ where

$$V = \begin{pmatrix} \psi \\ \theta \\ \Sigma \end{pmatrix} \qquad M = \begin{pmatrix} \Delta^2 & -R_T\partial_X & \partial_X \\ -\partial_X & \Delta & 0 \\ 0 & 0 & \tau\Delta \end{pmatrix} \qquad L = \begin{pmatrix} \Delta/\sigma & 0 & 0 \\ 0 & 1 & 0 \\ 0 & 0 & 1 \end{pmatrix}$$

$$N(V,V) = \begin{pmatrix} -\sigma^{-1}J(\psi, \Delta\psi) \\ -J(\psi, \theta) \\ -J(\psi, \Sigma) \end{pmatrix}$$

We scale slow space, slow time and the amplitude of the motion on ε, where $\varepsilon^2 = R - R_c$.

$$X = \varepsilon x, \quad T = \varepsilon^2 t$$

$$\partial_x = \partial_x + \varepsilon\partial_X, \quad \partial_t = \varepsilon^2\partial_T$$

$$R_T = \ldots = R_c(1 + \varepsilon^2)$$

Expanding the operators themselves in powers of ε facilitates the expansion procedure, and this is done as follows:

$$\Delta' = \partial_x^2 + \partial_z^2 \qquad \Delta = \Delta' + \varepsilon 2\partial_x\partial_X + \varepsilon\partial_X^2$$

$$\Delta^2 = \Delta'^2 + 4\varepsilon\Delta'\partial_x d_X + \varepsilon^2\partial_X^2(4\partial_x^2 + 2\Delta') + \varepsilon(4\partial_X\partial_x^3) + \ldots$$

Then

$$M = M_0 + \varepsilon M_1 + \ldots$$
$$L = L_0 + \varepsilon L_1 + \ldots$$
$$N = N_0 + \varepsilon N_1 + \ldots$$

$$M_0 = \begin{pmatrix} \Delta'^2 & -R_T\partial_X & \partial_X \\ -\partial_X & \Delta' & 0 \\ 0 & 0 & \tau\Delta' \end{pmatrix} \qquad M_1 = \begin{pmatrix} 4\Delta'\partial_x\partial_X & -R_T\partial_X & \partial_X \\ -\partial_X & 2\partial_x\partial_X & 0 \\ 0 & 0 & 2\tau\partial_x\partial_X \end{pmatrix}$$

$$M_2 = \begin{pmatrix} \partial^2_X(4\partial_x^2+2\Delta') & -R_T\partial_X & 0 \\ 0 & \partial^2_X & 0 \\ 0 & 0 & \tau\partial^2_X \end{pmatrix} \qquad M_3 = \begin{pmatrix} 4\Delta'\partial_x\partial_X & -R_T\partial_X & 0 \\ 0 & 0 & 0 \\ 0 & 0 & 0 \end{pmatrix}$$

$$L_0 = \begin{pmatrix} \alpha^{-1}\Delta' & 0 & 0 \\ 0 & 1 & 0 \\ 0 & 0 & 1 \end{pmatrix} \qquad L_1 = \begin{pmatrix} \alpha^{-1}2\partial_x\partial_X & 0 & 0 \\ 0 & 0 & 0 \\ 0 & 0 & 0 \end{pmatrix} \qquad L_2 = \begin{pmatrix} \alpha^{-1}\partial^2_X & 0 & 0 \\ 0 & 0 & 0 \\ 0 & 0 & 0 \end{pmatrix}$$

$$N(A,B) = (L\partial_x A)(E^+\partial_z B) - (L\partial_z A)(E^+\partial_x B) \qquad E^+ = (1,0,0)$$

$$N_0 = (L_0\partial_x A)(E^+\partial_z B) - (L_0\partial_z A)(E^+\partial_x B)$$

$$N_1 = (L_1\partial_x A + L_0\partial_X A)(E^+\partial_z B) - (L_1\partial_z A)(E^+\partial_x B) - (L_0\partial_z A)(E^+\partial_X B)$$

$$N_2 = (L_1\partial_X A + L_2\partial_x A)(E^+\partial_z B) - (L_2\partial_z A)(E^+\partial_x B) - (L_1\partial_z A)(E^+\partial_X B)$$

$$N_3 = (L_2\partial_X A)(E^+\partial_z B) - (L_2\partial_z A)(E^+\partial_X B)$$

We imagine bringing the thermal Rayleigh number past its critical value, as determined by linear theory, in the presence of an O(1) salt concentration which varies only on the slow scale X. Accordingly we set

$$U = U_0 + \varepsilon U_1 \ldots = \varepsilon_A V + B \begin{pmatrix} 0 \\ 0 \\ 1 \end{pmatrix} + \ldots$$

where V contains only ψ and θ. Then the scaled order one equations read:

$$M_0 U_0 = N_0(V_0, V_0) = 0$$

and our slowly varying B_0 is a solution. At $O(\varepsilon)$:

$$M_0 U_1 = -M_1 U_0 + N_0(U_0, V_1) + N_0(U_1, V_0) + N_1(V_0, V_0)$$

All the *nonlinear* terms vanish for our slowly varying salt concentration B_0, so this reduces to

$$\begin{pmatrix} \Delta^2 & -R_T\partial_x & \partial_x \\ -\partial_x & \Delta' & 0 \\ 0 & 0 & \tau\Delta' \end{pmatrix} \begin{pmatrix} \psi_1 \\ \theta_1 \\ \Sigma_1 \end{pmatrix} = \begin{pmatrix} -B_{0X} \\ 0 \\ 0 \end{pmatrix}.$$

Since the most general solution for the salt equation with fixed flux boundaries is $\Sigma_1 = B_1(XT)$, this equation yields the typical trignometric solutions modulated on the slow scales X, T as in the linear problem with an additional shear flow term generated by the variation of density in the horizontal. That is,

$$V_1 = \begin{pmatrix} (Ae^{iKx} + \overline{A}e^{-iKx})\cos\pi z - B_{0X}P_1(z) \\ (Ae^{iKx} - \overline{A}e^{-iKx})(-iK/q^2)\cos\pi z \\ B_1 \end{pmatrix} \begin{matrix} A = A(XT) \\ B_1 = B_1(XT) \end{matrix}$$

where subscripts denote derivatives. P is given by the conditions $0^4 P_1 = 1$

$$P_{1zzzz} = 1$$

$$P_{1zz} = P_1 = 0 \text{ at } z = \pm 1/2$$

$$\text{and} \qquad P_1 = z^4/4! - 3/2\ z^2/4! + 5/16 \cdot 4!.$$

The variation of the density on the slow scales has generated a flow which does not depend on the fast x-scale, a O-K mode. This mode in turn generates a response at next order as will be seen below. At $O(\epsilon^2)$:

$$M_0U_2 = -M_1U_1 - M_2U_0 + \partial_T L_0U_0 + N_0(U_2,V_0), + N_0(V_0,V_2) + N_0(V_1,V_1)$$
$$+ N_1(V_0, V_1) + N_1(V_1,V_0) + N_2(U_0,V_0)$$

Solvability requires that $B_{0T} = B_{0XX}\tau$ and all other terms are nonresonant. The $O(\epsilon^2)$ solution is:

$$\begin{pmatrix} \psi_2 \\ \theta_2 \\ \Sigma_2 \end{pmatrix} = \begin{matrix} -B_{1X}P_1(z) - B_{0X}iK(Ae^{iKx} - \bar{A}e^{-iKx})\,\hat{\psi}_2 \\ 1/6\pi|A|^2\sin 2\pi z - B_{0XX}P_2(z) - (2/9\pi^2)(A_Xe^{iKx} + \bar{A}_Xe^{-iKx})\cos\pi z \\ B_{0X}\,\pi/(\tau q^2)\,(Ae^{iKx} + \bar{A}e^{-iKx}) - B^2{}_{0X}\,P_3(z)/\tau + B_2 \end{matrix}$$

where P_2 and P_3 satisfy

$$P_2 = P_{2_{zz}} = P_{3_z} = 0 \qquad z = \pm 1/2$$

$$P_{2_{zz}} = P_1 \qquad\qquad P_{3_{zz}} = P_{1_z}$$

and $\hat{\psi}_2$ and $\hat{\theta}_2$ are products of polynomials, sines and cosines which are omitted here.

At $O(\epsilon^3)$ the solvability condition yields equation (2.6). On the basis of symmetry and the no net horizontal flow imposed by the Ψ boundary conditions we need only calculate Σ_3 to get at $O(\epsilon^4)$

$$B_{2T} = \tau B_{2XX} + (2/3\tau)(B_{0X}|A|^2)_X + \beta/\tau\,(B_0X)^3X$$

where $\beta \cong 1/6000$ from the solvability condition. We then define

$$B = B_0 + \epsilon^2 B^2$$

where we may scale away B_1. Then rewriting the B equation in terms of the fast variables x and t yields equation (2.5).

This mixing of orders or reconstitution is a delicate matter, however it is frequently necessary in codimension two problems. It may also be possible to avoid it by using different scalings for space and time.

Acknowledgements: I would like to thank Ed Spiegel for enthusiasm and support as my advisor in this work, and George Veronis for his sage comments and direction. Conversations with other staff and visitors, seemingly too numerous to list, were of immeasurable help. Stephan Fauve, Bill Young, Stephane Zaleski and Albert Libchaber were particularly helpful and informative in their comments. This work received support from NSF grant number OCE-8410154.

REFERENCES

Busse, F.H., 1978. Rep. Prog. Phys. 41, 1929.

Coullet, P.H. and S. Fauve, 1984. Combustion and Turbulence, Conf. Proceedings, preprint.

Siggia, E.D. and A. Zippelius, 1981. Phys. Rev. A24, 1036-1049.

Spiegel, E.A., 1981. GFD Proceedings, Report no. WHOI-81-102.

Swift, J.W., 1985. GFD Proceedings, this volume.

Young, W., 1983. GFD Proceedings, Report no. WHOI-83-41.

A Simple Model for Interface Evolution and Tip-splitting

Michael Landman

Abstract: Geometrical models for the motion of an interface are discussed, in which a local equation for the dynamics is intended to capture some of the phenomena of moving boundary problems. In particular we characterize the essential features of tip-splitting and thereby conjecture the existence of a nonlinear cascade to small length scales and a fractal geometry in finite time.

I. Introduction

In the light of current developments in nonlinear dynamics and fractal geometries, there has been considerable interest in the dynamics of an interface between two regions of different phase. Such moving boundary problems can arise in solidificaion and dendritic growth (Langer, 1980), viscous fingering problems (Robinson, 1985), contour dynamical models of vorticity (Stern, this volume), viscous gravity currents (Huppert, 1984) and biological growth models (Kiermayer, 1981). In most of these physical problems the dynamical equations are extremely complex and not even tractable numerically at the present time.

This has motivated workers in the field (Brower et al., 1983; Ben-Jacob et al., 1983) to formulate simpler phenomenological models of moving curves in two dimensions which attempt to capture some of the essential features of the physical problem. In particular their interests have been to model the dendritic growth of a crystal which is solidifying out of the supercooled liquid phase. Their studies have helped to clarify which features of the model control the growth of a curve, in the hope that there may be some type of universality principle underlying problems in interfacial dynamics, as has been found true for other large classes of dynamical systems (Cvitanovic, 1984). For example, it is suggested numerically from these models that anisotropy is a necessary ingredient for dendritic growth of a needle crystal with side branching, and that lack of this factor leads to tip-splitting behavior (Kessler et al., 1984).

Our interest in these types of models is different, however, and is twofold in nature. First, we are interested in developing a model exhibiting tip-splitting at an interface in analogy to current experiments in Hele-Shaw fingering (Robinson, 1985) and unidirectional crystal growth (Heslot and Libchaber, 1985). Second, and perhaps more importantly, we seek to find a model displaying a nonlinear cascade to smaller length scales in analogy to an inertial-range cascade hypothesized for turbulent flows. In this way we seek a self-similar or near self-similar cascade of tip-splitting events on the moving curve as a simple one-dimensional dynamical model for the transition to a fractal geometry as time develops. If such a cascade occurs one would then like to reduce the self-similar development to a low dimensional map which can be applied to the dynamics over a large range of length scales independent of initial conditions (Childress, 1985).

In section II we consider the purely geometric aspects of tip-splitting of an interface, in order to give a feel for the dynamical behavior for which we should be looking. We then concentrate on the model introduced by Brower and his co-workers (1983, 1984) which assumes a local equation of motion for the interfacial curve in two dimensions. We consider a different dynamical law than theirs, however, in order to preserve the scale invariance which is a desirable property if we want to have access to self-similar dynamics. The derivation of the model is outlined in section III; in section IV we describe some of its properties. The next section deals with a local analysis of the dynamical model and we are able to find tip-splitting behavior as suggested in section II. In section VI we show some results from a full numerical simulation of the equations of motion which provide some evidence that tip-splitting can occur but is generally inconclusive. The last section summarizes and discusses the results and suggests some possible further investigations.

II. A Geometrical Model

As a first step to understanding the necessary geometrical condition for an interface to undergo tip-splitting, we consider an elementary description of a curve in the plane which has such a transition.

Consider the interface given by $y = y(x,t)$ where x and y are cartesian coordinates and t is a parameter which should be thought of as time. As $|x| << 1$ we suppose that locally

$$y = a(t)x^m + b(t)x^n + o(x^n) \quad \text{as } x \to 0 \tag{2.1}$$

where to retain symmetry m and n are even integers with $n > m$. We assume that at $t = 0$ the tip of this curve at $x = 0$ undergoes a splitting; that is, $a(t)$ goes from positive to negative as t increases through zero, and $b(t)$ remains order 1 as $|t| \to 0$.

Let κ be the curvature, s the arclength and θ the angle the curve makes with the x-axis. Then by definition

$$\begin{aligned} \tan\theta &= y' \\ \kappa &= d\theta/ds = y''/(1 + y'^2)^{3/2} \end{aligned} \tag{2.2}$$

By assumptions on (2.1), at $t = 0$ as $x \to 0$, $\theta \to 0$ and we may set $s \to 0$. In this limit we have the asymptotic behavior

$$\begin{aligned} &y \sim x^n, \ \theta \sim x^{n-1} \\ &\kappa \sim x^{n-2} \sim s^{n-2} \sim \theta^{(n-2/n-1)} \end{aligned} \qquad \text{as } x, \theta, s \to 0 \text{ and } t = 0.$$

Note then that in $\kappa - \theta$ space, a singularity will occur for integers $n > 2$ as $t \to 0$. This is an important point that we will return to later.

In the "generic" case for symmetric tip-splitting we set $m = 2$, $n = 4$ and $a(t) = t$ for simplicity of parameterization, and thus consider the model equation

$$y = x^2(x^2 - t) \tag{2.3}$$

This curve is shown for successive values of t in figure (2.1). The curvature for the curve (2.3) can be given only implicitly as a function of angle θ ; i.e. from the formulae (2.2)

$$\kappa = 2(6x^2 - t)\cos^3\theta \tag{2.4}$$

where $x(\theta)$ is given by

$$4x^3 - 2tx - \tan\theta = 0 \tag{2.5}$$

When $t < 0$, (2.5) is single valued for $x(\theta)$. When $t > 0$ (2.5) has three solutions for θ sufficiently small and thus κ becomes triple valued. In fact as $\theta \to 0$ we can write

$$\theta^2 \sim 1/108\ (\kappa + 2t)\ (\kappa - 4t)^3$$

which has the characteristic cusp singularly of $\kappa \sim \theta^{2/3}$. A picture of κ versus θ is shown in figure 2.2 for a series of times, and is exemplary of a cusp catastrophy. The tip-splitting is far less dramatic, however, if viewed in arclength coordinates, as shown in figure (2.3). κ is analytic in s and in the generic case has local quadratic form where the minimum of $\kappa(s)$ passes through zero at $t = 0$ i.e.

$$\kappa \sim -2t + 12s^2 \quad \text{as} \quad |t| < s^2 \to 0 \tag{2.6}$$

These features of our description of tip-splitting will appear later when we develop a dynamical model for the curve.

One aspect of our simple discussion so far that may trouble the reader is the use of the word "generic" in the choice of exponents in equation (2.1). In the symmetric cases when m and n are even much the same scenario as for $n = 4$, $m = 2$ occurs except that the exponents in the expansions for κ may alter. Symmetry breaking is of course not particularly atypical in physical systems. We argue that the inclusion of a cubic term, say, in the example (2.3) means only the addition of an imperfection from the symmetric case, i.e., if

$$y = -tx^2 + \varepsilon x^3 + x^4$$

then when $|x| << |t/\varepsilon|$ the parabolic tip behavior is dominant and when $|x| >> |\varepsilon|$ the far-field quartic behavior is dominant. See figure (2.4) to (2.6) as a comparison to figures (2.1) to (2.3). In this way most of this study will concentrate on seeking symmetric tip-splitting from our dynamical models wherever this symmetry is supported, though we will keep in mind that asymmetric perturbations may and probably will occur.

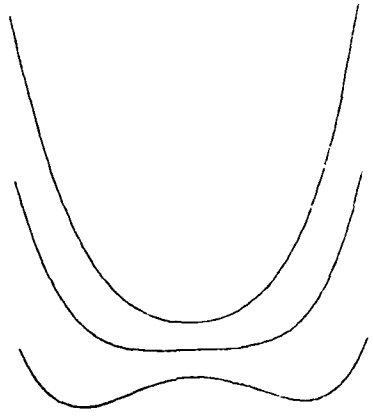

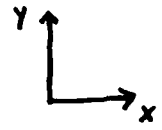

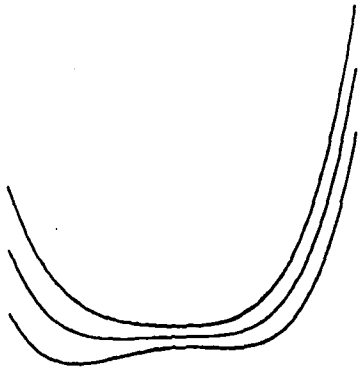

2.1

2.4

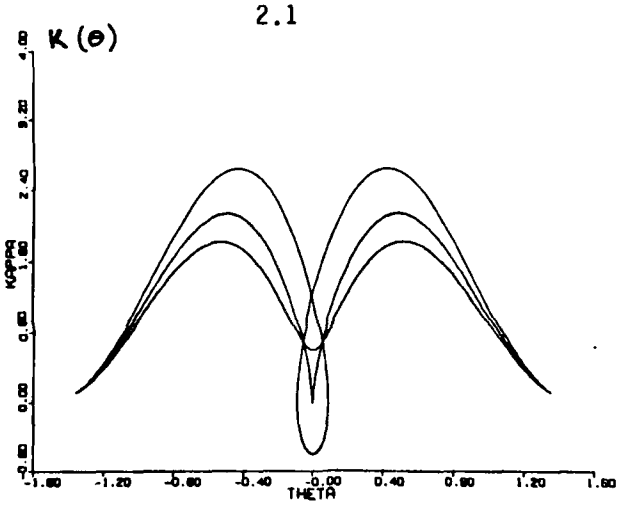

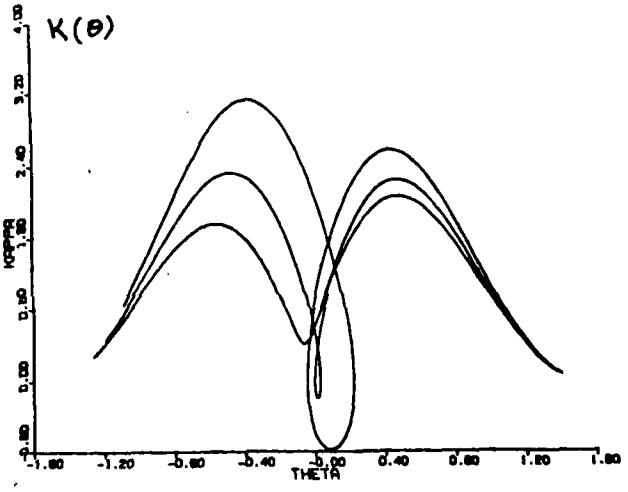

2.2

2.5

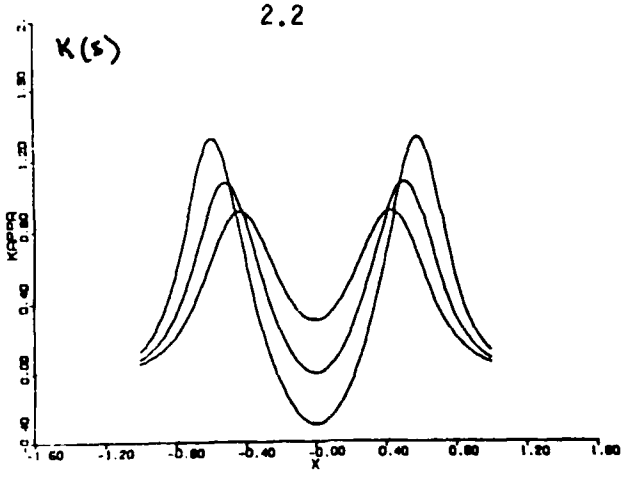

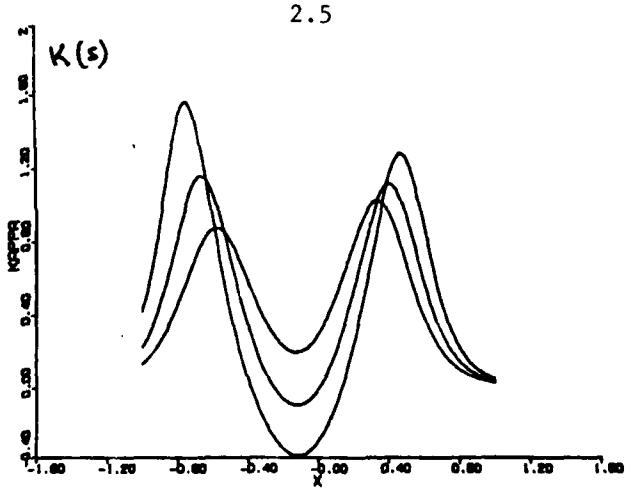

2.3

2.6

Symmetric

Asymmetric

Figures 2.1 - 2.6: Geometrical Model of Tip-Splitting.

III. A Dynamical Model

We now describe the model on which our study will concentrate - that is, a phenomenological model for interface evolution based upon the motion of a curve in the plane which is given a simple dynamical law. This model has been discussed primarily by Brower, Kessler et al. in a series of papers (see references), and we shall use their kinematic model though we will choose a different dynamical law as will be explained below.

We suppose that a moving curve C develops according to the rule that at any point on the curve its velocity V is normal to C and is a functional of local curvature κ. Hence, if $\vec{r} = (x,y)$ is the position vector of C, we have that

$$(\partial\vec{r}/\partial t)_{s_0} = -V[\kappa]\,\vec{n} \tag{3.1}$$

where $\vec{n}$ is the unit inward normal. We think of s_0 as a Lagrangian coordinate along C which may be set equal to arclength at $t = 0$ and uniquely specifies each point on C. In general the actual length of C, $L(t)$, is a function of time due to induced curve stretching, so that the "Eulerian" arclength s is constrained such that $0 \leq s < L(t)$. To obtain an equation describing the evolution of $\kappa(s,t)$, we use the Frenet formulae for the unit normal and tangent vectors $\vec{n}$ and $\vec{\tau}$ respectively

$$\partial\vec{n}/\partial s = -\kappa\vec{\tau}\ ,\ \partial\vec{\tau}/\partial s = \kappa\vec{n}. \tag{3.2}$$

See figure 3.1.

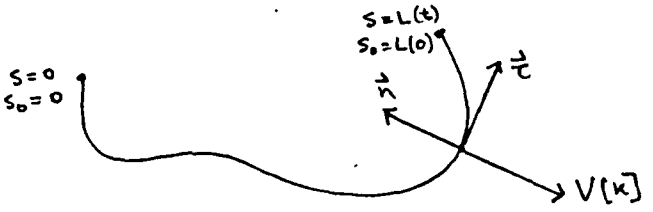

Figure 3.1: Moving Curve Model

As differentiation with respect to space and time commute in the Lagrangian coordinates but not Eulerian, we derive first the Lagrangian kinematics using the Jacobian for $s = s(s_o, t)$

$$J \equiv \partial s/\partial s_0. \tag{3.3}$$

Differentiating (3.1) with respect to s_0 and using $\partial\vec{r}/\partial s = \vec{\tau}$ gives

$$\left(\frac{\partial J}{\partial t}\right)_{s_0}\vec{\tau} + J\left(\frac{\partial\vec{\tau}}{\partial t}\right)_{s_0} = -J\frac{\partial V}{\partial s}\vec{n} - JV\frac{\partial\vec{n}}{\partial s_0}\ . \tag{3.4}$$

Substituting the first of (3.2) into the above and resolving normal and tangential components gives the two equations

$$\left(\frac{\partial J}{\partial t}\right)_{s_0} = \kappa V J\ ,\quad \left(\frac{\partial\vec{\tau}}{\partial t}\right)_{s_0} = -\frac{\partial V}{\partial s}\vec{n}\ . \tag{3.5}$$

Differentiating the second of (3.2) with respect to s_0 yields

$$\frac{\partial}{\partial t}\left(J\kappa\vec{n}\right) = -J\frac{\partial^2 V}{\partial s^2}\vec{n} + \kappa J\frac{\partial V}{\partial s}\vec{t} \qquad (3.6)$$

whose normal component gives the equation

$$\kappa\left(\frac{\partial J}{\partial t}\right)_{s_0} + J\left(\frac{\partial \kappa}{\partial t}\right)_{s_0} = -J\frac{\partial^2 V}{\partial s^2} . \qquad (3.7)$$

On eliminating the Jacobian using the first of (3.5) we get the equation of motion

$$\left(\frac{\partial \kappa}{\partial t}\right)_{s_0} + \kappa^2 V + \frac{\partial^2 V}{\partial s^2} = 0 . \qquad (3.8)$$

We now need to rewrite this equation in the Eulerian frame making s and t independent variables using the relation

$$\left(\frac{\partial}{\partial t}\right)_{s_0} = \left(\frac{\partial}{\partial t}\right)_s + \left(\frac{\partial s}{\partial t}\right)_{s_0}\left(\frac{\partial}{\partial s}\right)_t .$$

The "stretching" term is derived using the first of (3.5); we find that on integration and setting an arbitrary origin for s that

$$\left(\frac{\partial s}{\partial t}\right)_{s_0} = \int_0^s \kappa V\, ds' . \qquad (3.9)$$

In this way the equation of motion becomes

$$\frac{\partial \kappa}{\partial t} + \frac{\partial}{\partial s}\left[\kappa\int_0^s \kappa V\, ds'\right] + \frac{\partial^2 V}{\partial s^2} = 0 \qquad (3.10)$$

$$0 \le s < L(t)$$

where s and t are now independent variables. We now perform another change of variables in order to make the total arclength independent of time. Let

$$\sigma = s/L(t).$$

From (3.9)

$$\frac{dL}{dt} = \int_0^L \kappa V\, ds'$$

so that

$$\left(\frac{\partial \kappa}{\partial t}\right)_s = \left(\frac{\partial \kappa}{\partial t}\right)_\sigma - \frac{s}{L^2}\int_0^L \kappa V\, ds' \cdot \frac{\partial \kappa}{\partial \sigma}$$

It is also advantageous to define stretched curvature and velocity

$$u = \kappa(s,t)\, L(t) \quad , \quad \mathbf{v} = V[\kappa]\, L^3(t)$$

and a stretched time scale τ :

$$d\tau = L^{-4}(t)dt.$$

Finally then the kinematic equation becomes

$$\frac{\partial u}{\partial \tau} + \frac{\partial}{\partial \sigma}\left[u\left(\int_0^\sigma uv\,d\sigma' - \sigma\int_0^1 uv\,d\sigma'\right)\right] + \frac{\partial^2 v}{\partial \sigma^2} = 0 \qquad (3.11)$$

$$0 \le \sigma < 1 .$$

Note that although σ and u are dimensionless arclength and curvature, v and τ are dimensional but will be made dimensionless once we have chosen the velocity functional v, which we do below. We should point out that all the formulae up to equation (3.10) hold for a curve of infinite length, and it is only the introduction of σ coordinates that requires L(t) to be finite.

In previous work on this model (Kessler et al., 1984) V was chosen to be the form

$$V = (\kappa + A\kappa^2 - B\kappa^3 + \gamma\,\partial^2\kappa/\partial s^2)\,(1 + \varepsilon\cos m\theta) . \qquad (3.12)$$

This is an example of the general velocity law

$$V = F(\kappa) + \gamma\,\partial^2\kappa/\partial s^2 \qquad (3.13)$$

with an added isotropy factor which gives a preferred growth direction. The rationale behind (3.13) is that in general pattern formation at an interface is due to competition between stabilizing and destabilizing forces. We think of $F(\kappa)$ as a local forcing of the velocity of the interface and the derivative term as the smoothing term which acts similar to surface tension in a real interface problem (this analogy is revealed in the Mullins-Sekerka type instability analyzed in section IV). The Kessler law (3.12) is motivated by the physics of the solidification of a dendrite and the reader is referred to the literature for their rationalization; ε is the anisotropy factor and θ the tangent angle defined earlier. In their numerical studies, Kessler et al. have concluded that in order to achieve a stable growth of dendrite like structures, a critical value of γ must be exceeded or the dendritic tip splits (Kessler et al., 1984, 1985; see figure 3.2). Most of their recent work has focused on the anisotropic problem and the resulting velocity selection criterion of the dendritic tip, which is still open to speculation for real dendritic growth (Langer, 1980).

It is our interest however, to search for some scale invariant cascade within the dynamics of the tip-splitting mechanism. Thus it is desirable for there to be a scale invariant transformation of the equation taking (s, t, κ, V) into $(cs, c_1 t, c_2\kappa, c_3 V)$. From (3.12) we see that $c_2 = c^{-1}$ and from the general form (3.13) we therefore select a cubic for $F(\kappa)$. We thus choose

$$V = a\kappa^3 + \gamma\,\partial^2\kappa/\partial s^2 . \qquad (3.14)$$

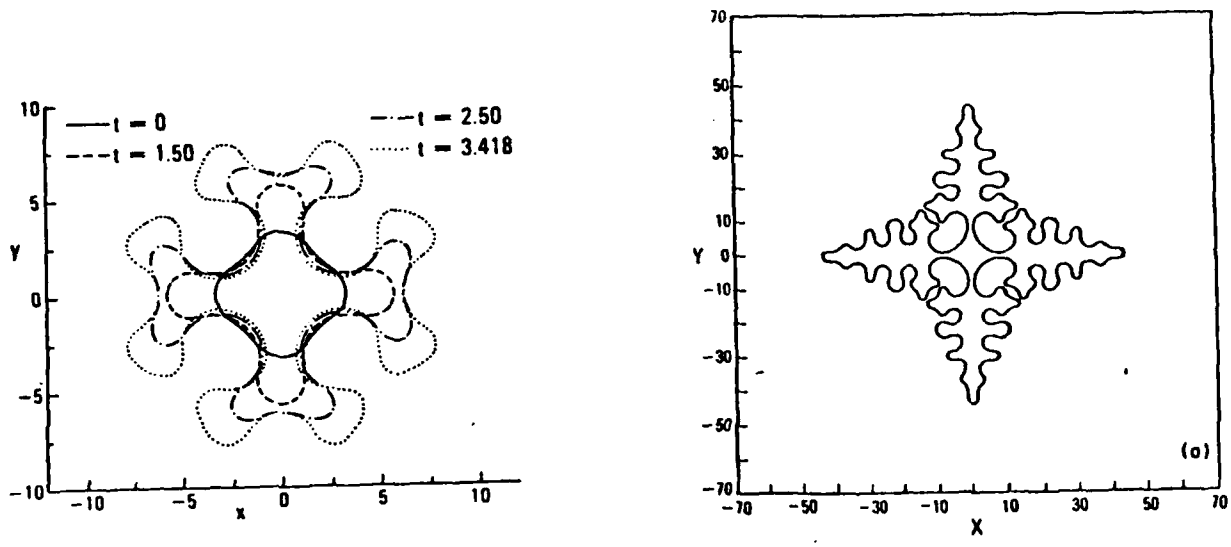

ε=0 A=1 B=1/4 γ=1/4 ε=3/20 A=4 B=2 M=4 γ=1

Figure 3.2: Numerical Results from Kessler et al. (1984) for velocity law (3.12).

Note that with this choice, $V(-\kappa) = -V(\kappa)$ so that the evolution of κ is independent of its sign. The invariance of equation (3.10) is therefore

$$(s,t,\kappa,V) \rightarrow (cs, c^4t, c^{-1}\kappa, c^{-3}V) \qquad (3.15)$$

We may set $a = 1$ without loss of generality. In stretched coordinates the transformation

$$v \rightarrow av \quad , \quad \tau \rightarrow a^{-1}\tau$$

renders these variables dimensionless and the velocity law is

$$v = u^3 + \gamma\, \partial^2 u/\partial\sigma^2 \qquad (3.16)$$

where γ is dimensionless.

The kinematic equation (3.10) and its equivalent stretched form (3.11), although far simpler than the real interfacial dynamic problem, are nonetheless not easily solved numerically, let alone analytically. There is a change of variables, however, that converts the integro-partial differential equation into a local equation. Recall the angle variable θ defined

$$\theta(s,t) = \int_0^s \kappa(s,t)ds'$$

We desire to find κ as a function of θ and t alone. Now

$$\left(\frac{\partial}{\partial t}\right)_s = \left(\frac{\partial}{\partial t}\right)_\theta - \left[\kappa \int_0^s \kappa V \, ds' + \frac{\partial V}{\partial s}\right] \frac{\partial}{\partial \theta}$$

and on transforming equation (3.10) we get simply

$$\frac{\partial \kappa}{\partial t} + \kappa^2 \left(1 + \frac{\partial^2}{\partial \theta^2}\right) V = 0 \,. \tag{3.17}$$

Using the dynamics proposed for V, we have that

$$V = \kappa \left(1 + \frac{\gamma}{2} \frac{\partial^2}{\partial \theta^2}\right) \kappa^2 \tag{3.18}$$

which gives the equation at motion of C in θ - t coordinates as

$$\frac{\partial \kappa}{\partial t} + \kappa^2 \left(1 + \frac{\partial^2}{\partial \theta^2}\right) \kappa \left(1 + \frac{\gamma}{2} \frac{\partial^2}{\partial \theta^2}\right) \kappa^2 = 0 \,. \tag{3.19}$$

Though we seem to have reduced the complexity of the equation for the curvature by reparameterizing in θ, we are faced with the added complication of the possiblity of κ being nonanalytic and multivalued in θ at a fixed time. Recall this was the case found for the geometric model of tip-splitting discussed in section II.

IV. Some Properties of the Model

We will describe in this section some simple analytic solutions that can be found for the evolution of the moving curve. We will consider steady profile solutions, though note that steady in one of the coordinates s, σ or θ does not necessarily imply steady in another.

There are a number of time independent solutions carrying zero normal velocity. Using (3.18) we have

$$\kappa = 0 \text{ or } \kappa^2 = A \cos \sqrt{2/\gamma} \; (\theta - \theta_0). \tag{4.1}$$

The first is the plane interface solution which, with (3.14), is stable to infinitessimal disturbances due to the dominant influence of the linear "surface tension" term. The second of (4.1) gives a periodic curved interface provided $\gamma < 8$, and for those with a taste for 19th century mathematics we can transform the solution to arclength coordinates and write the steady profile as a Jacobi elliptic function

$$\kappa = A \, \mathrm{cn}(sA/\sqrt{\gamma}) \,.$$

Observe that these solutions can cause self intersection of the curve depending on the parameters γ and A. It is worth noting here that the two conditions necessary for the solution to satisfy if it is a closed curve are shown easily to be

$$\int_0^{L(t)} \kappa(t,s')ds' = 2\pi \quad \text{and} \quad \int_0^{L(t)} e^{i\theta}(t,s') \, ds' = 0 \,. \tag{4.2}$$

Also more generally the equations of motion for the curvature are in conservation form so

$$\int_0^{L(t)} \kappa(s,t)ds = \int_0^1 u(\sigma,\tau)d\sigma = \text{constant.} \qquad (4.3)$$

A more general set of steady solutions for $\kappa(\theta,t)$ can be found from equations (3.19) by setting

$$\partial_t \mathcal{L} U = \mathcal{M} U \qquad (4.4)$$

If we seek moving finger solutions in the x-direction where $\kappa \to 0$ as $\theta \to 0$ and π, then we can show by modifying the arguments of Brower et al. (1984) that these solutions will only exist for a few values of γ. Writing (4.4) as a first order system of equations

$$d\theta/ds = \kappa$$

$$d\kappa/ds = \beta$$

$$\partial\beta/\partial s = 1/\gamma\ (A\sin\theta - \kappa^3)$$

then we seek solutions emanating from the critical point $(\theta, \kappa, \beta) = (0,0,0)$ and approaching $(\pi,0,0)$ as s goes from $-\infty$ to ∞ (i.e. a heteroclinic orbit in phase space). Stability arguments by linearizing about these points show that at $\theta = 0$ the unstable manifold is one dimensional and at $\theta = \pi$ the stable manifold is one dimensional. Thus one can argue that only at exceptional values of γ do these manifolds connect and yield a moving finger solution. For $\gamma = 1/2$ such a solution can be found, where

$$\kappa = c \sin\theta = c\ \text{sech}\ (cs)$$

$$V = (c^3/2)\ \text{sech}\ (cs)$$

and c is an arbitrary constant. The equations for the curve in the plane may be found by integration and are

$$x(s,t) = (-1/c)\ \ln(\cosh cs) + (1/2)\ c^3 t + x_0 \qquad (4.5)$$

$$y(s,t) = (2/c)\ \tan^{-1}(\sinh cs) + y_0$$

which gives a finger of steady shape moving in the y direction with a parabolic tip of curvature c/4.

One solution of considerable interest is that for which $\kappa = 2\pi/L(t)$ which satisfies constraints (4.2) and corresponds to an expanding circular interface. We find

$$\kappa(s,t) = [4(t + t_0)]^{-1/4}$$

$$L(t) = 2\pi\,[4(t + t_0)]^{1/4}$$

It is easiest to consider the problem in stretched σ coordinates for which $u(\sigma,\tau) = 2\pi$ is the solution for all time. Performing a linear

stability analysis of the interface, we perturb it by writing

$$u = 2\pi + \varepsilon u' \quad \text{where} \quad \int_0^1 u' d\sigma = 0$$

which follows from equation (4.3). Substituting this expression into (3.11) and linearizing in u' yields the equation

$$L_\gamma u' = (\partial/\partial\tau + 4(2\pi)^4 + (3+\gamma)(2\pi)^2 \partial^2/\partial\sigma^2 + \gamma \partial^4/\partial\sigma^4)u' = 0 \quad (4.6)$$

which we can solve by expanding u' in the normal modes

$$u'_m = e^{P\tau} e^{2\pi i m\sigma} \qquad 0 < \sigma < 1.$$

The dispersion relation that results is

$$P = -(2\pi)^4 [\gamma m^4 - (\gamma + 3)m^2 + 4]$$

which indicates there is a band of unstable wavenumbers for sufficiently small γ (see figure 4.1). The m = 1 mode is always stable and corresponds

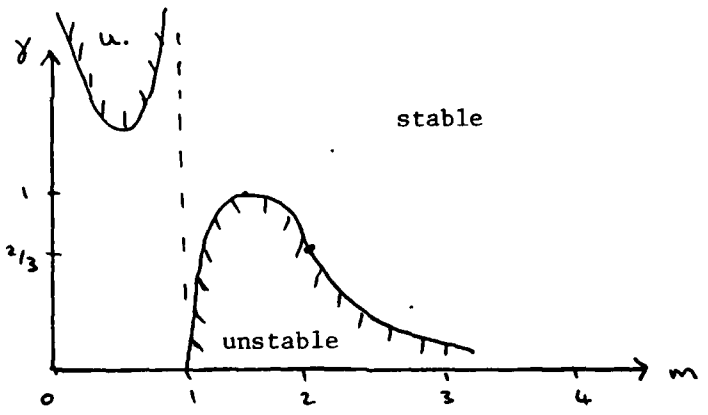

Figure 4.1: Linear stability diagram for circular solutions.

to a uniform translation. The elliptic m = 2 mode is the first mode to go unstable as γ is reduced past $\gamma_c = 2/3$. The maximum growth rate occurs at the wavenumber

$$m = \sqrt{\frac{\gamma+3}{2\gamma}}$$

which means that the shortest wavenumbers become most unstable as $\gamma \to 0$. It is these properties of the circular solution which bear a notable resemblance to the Mullins-Sekera instability experienced in the full solidificiation equations. This instability describes the evolution of perturbations on a flat or spherical interface and occurs because an

outward bump of frozen material will grow faster than its surroundings due to the more efficient conduction of latent heat away from the bump. The stabilizing force is the surface tension, and as with γ in our model this acts to control the growth and leads to a band of unstable wavenumbers.

In an attempt to determine if there is any nonlinear stabilization of the unstable modes, a multiple scales analysis of the growth of the elliptic mode was carried out for γ near $\gamma_c = 2/3$. As a regular perturbation expansion for u breaks down at third order, the relevant scales are

$$\gamma - \gamma_c = \varepsilon^2 \qquad \tilde{\tau} = \varepsilon^2 \tau$$

$$u = 2\pi + \varepsilon u_1(\tau, \tilde{\tau}, \sigma) + \varepsilon^2 u_2(\tau, \tilde{\tau}, \sigma) + \ldots$$

Using equation (3.11), one obtains a series of equations

$$L_{2/3} u_i = f_i$$

where $L_{2/3}$ is given by (4.6). Writing

$$u_1 = A(\tilde{\tau}) \cos(4\pi s + \Phi(\tilde{\tau}))$$

at $O(\varepsilon^2)$ one finds no secularity in f_2 provided we set $\Phi \equiv 0$. This however does not constrain u_1 due to the rotational invariance in the problem. The solution for u_2 contains a second harmonic of u_2 - hence at $O(\varepsilon^3)$ we are forced to apply a solvability condition to remove resonant terms. Suppressing the usual algebraic complexities, we derive the amplitude equation

$$\partial A/\partial \tilde{\tau} = 192\pi^4 A + 210/29\ \pi^2 A^3$$

which suggests that there are no supercritical steady solutions near $\gamma = 2/3$.

V. Local Dynamics of Tip-Splitting

We wish to demonstrate in this section that locally, at least, our model supports tip-splitting behavior. One approach we took to this problem was to look for similarity solutions for curvature as a function of θ, recalling that in section II tip-splitting corresponded to a cusp singularity in these coordinates. It turns out that this nonlinear analysis was too complicated compared to our ultimate simple conclusions - yet it is felt that a brief discussion of this approach has some value and may be applicable to other systems where singularities occur.

We seek a similarity solution for equation (3.19) which as $t^* = t - t_0 \to 0$ has singular derivatives in θ. Taking as our ansatz

$$\kappa^2 \sim |t^*|^2 F(\eta), \eta = \theta |t^*|^{-\beta} \quad \text{as } t^* \to 0 \tag{5.1}$$

the dominant balance of terms in the equation becomes

$$\partial\kappa/\partial t + \gamma/2\ \kappa^2 \{\partial^2/\partial\theta^2\ \kappa\ (\partial^2/\partial\theta^2\ \kappa^2)\} = 0 \tag{5.2}$$

Substitution of (5.1) into (5.2) yields

$$\mathrm{sgn}(\tau) \cdot 2/\gamma \, [\alpha F - \beta \eta /2 \, F'] + F^{3/2}[F^{1/2}F'']'' = 0 \qquad (5.3)$$

$$\alpha - \beta = -1/4 \qquad (5.4)$$

and we are left with a degree of freedom to choose α. Our aim is to find solutions to (5.3) on either side of the singularity in θ at $t^* = 0$ and to match them as $t^* \to 0$ by matched asymptotics as $\eta \to \infty$.

To see how a cusp singularity as discussed in section II could occur for solutions of equation (5.3), we assume that

$$F \sim \eta^{\mu} \quad \eta \to \infty \quad \text{and} \quad F \sim \eta^{\lambda} \quad \eta \to 0. \qquad (5.5)$$

Also we hypothesize that the asymptotic shape of the interace at the tip is given by

$$y \sim a x^n - b t^{*p} x^m \quad \text{as} \quad x \to 0, \; m < n \quad . \qquad (5.6)$$

Matching the asymptotics of equations (5.5) and (5.6) leaves us with four equations in seven unknowns α, β, m, n, p, λ and μ. Coupled with equation (5.4), we obtain one relation between m, n, and p, so

$$p = 1/4 \; (n - m) \qquad \mu = 2(n-2)/n-1$$
$$\alpha = 1/4 \; (n - 2)$$
$$\beta = 1/4 \; (n - 1) \qquad \lambda = 2 \; (m-2/m-1)$$

If we assume a generic tip-splitting in the sense of section II, we set $m = 2$, $n = 4$, $p = 1/2$ and we get

$$\kappa \sim \pm \, | t^* |^{1/2} \, F^{1/2} \, (\theta \, | t^* |^{-3/4}). \qquad (5.8)$$

We observe however that the time dependence of the curve is not analytic at $t^* = 0$ which causes a problem with the validity of this solution in a neighborhood of that point. This is unfortunate as figures 5.1 and 5.2 show a numerical solution of equation (5.3) for similarity form (5.8), which bear a remarkable resemblance to figure 2.2. In fact the solutions on either side of the singularity can be shown to have identical asymptotic form as $\eta \to \infty$ to all algebraic orders for the unique choice of $\alpha = 1/2$, $\beta = -3/4$, due to the fact that $F = \eta^{4/3}$ is an exact solution of (5.3). Why then have we found a solution for $\kappa(\theta, t)$ that for fixed time gives the local form of a tip for which we are looking that can be shown to be analytic in s but is not analytic in time?

The answer to why we get this behavior from a highly nonlinear equation lies in our choice of coordinate θ. It is rather amusing to take the approximate equation (5.2) and transform back to arclength coordinates. Making the approximation that near tip-splitting $\kappa << 1$ so $V \simeq \gamma \, \partial^2\kappa/\partial s^2$ obtain the <u>linear</u> equation

$$\partial\kappa/\partial t + \gamma \, \partial^4\kappa/\partial s^4 = 0 \quad . \qquad (5.11)$$

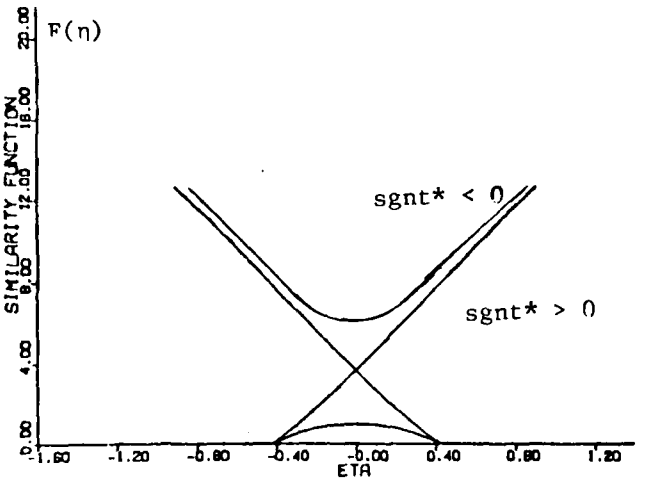

Figure 5.1: Numerically determined similarity solution.
(The singularities at F = 0 were handled using local analysis.)

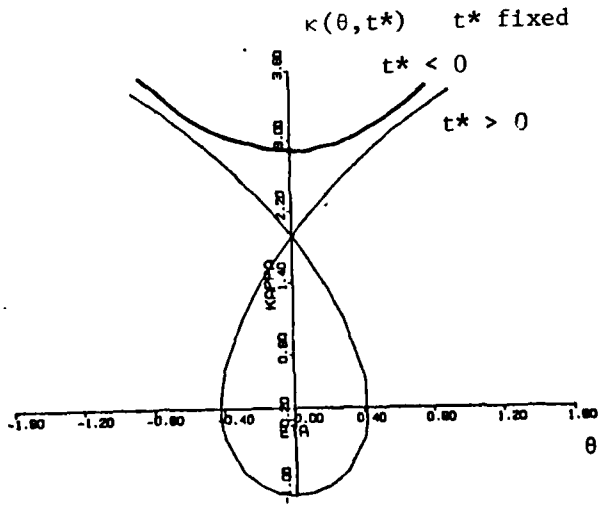

Figure 5.2: Corresponding curvature (see figure 2.2).

In retrospect then it is fairly obvious that we were just linearizing the full equation for κ (s,t) and looking for similarity solutions with

$$\kappa = |t^*|^{\nu} G(\xi) \quad , \quad \xi = s^*/|t^*|^{1/4} \quad , \quad s^* = s - s_0 \, . \qquad (5.12)$$

It is clear then that although θ - variables were attractive due to the dramatic nature in which tip-splitting takes place, this transformation obscured the approximations being made about the critical time $t^* = 0$.

We thus concentrate on the linear equation (5.11) as a local model equation for tip-splitting. It is worth noting that we have approximated the normal velocity functional V independent of the choice of $F(\kappa)$ in (3.13). We have discussed that the general solution to (5.12) is not analytic as $t^* \to 0$. But by the unique choice of $G = a\xi^2$, $\nu = 1/2$ which corresponds to $F(\eta) = a^2 \eta^{4/3}$ we get the exact solution of (5.11)

$$\kappa = as^{*2} \tag{5.13}$$

which gives the flattened interface at splitting. Now if we consider a linear combination of similarity solutions

$$\kappa = \sum_{\nu_i} |t^*|^{\nu_i} G_i(\xi)$$

which gives κ analytic in t^* and s^*, then in effect we are writing κ in a double power series in t^* and s^* which could then be substituted into the full equation for $\kappa(s,t)$. In particular we observe that an exact solution to (5.11) is

$$\kappa = At^* + Bs^{*2} - (A/24\gamma)s^{*4} \tag{5.14}$$

which is a local expansion for κ to be compared with equation (2.6) for the geometric model. Note we can add asymmetric terms in s^* and s^{*3} to (5.14) which also satisfy the linear equation exactly.

The above suggests that locally the symmetric tip-splitting event can be characterized by the two constants A and B. It is this hypothesis plus the fact that our equation of motion has no natural length scale and is invariant under the transformation (3.15) that leads us to the following conjecture concerning an infinite cascade to small length scales, which is summarized schematically in figure 5.2. Given that the dynamics of a tip is primarily local due to small structures having time scales far smaller than larger structures, then a cascade can occur where $\kappa(s,t)$ develops increasingly many zeros. This will lead to a cascade of tip-splittings characterized by the sequence

$$\{A_1, B_1, A_2, B_2, \ldots A_n, B_n, \ldots\} \tag{5.15}$$

where (A_n, B_n) are the values of A, B in the local expansion (5.14) at the time when $\kappa = s^* = t^* = 0$, A being found from the fourth derivative of κ with respect to s^*.

The n^{th} stage of the cascade can be locally described by

$$\kappa = A_n t^* + B_n s^{*2} - (A_n/24\gamma)\, s^{*4} \qquad \begin{aligned} t^* &= t - t_n \to 0 \\ s^* &= s - s_n \ll 1 \end{aligned}$$

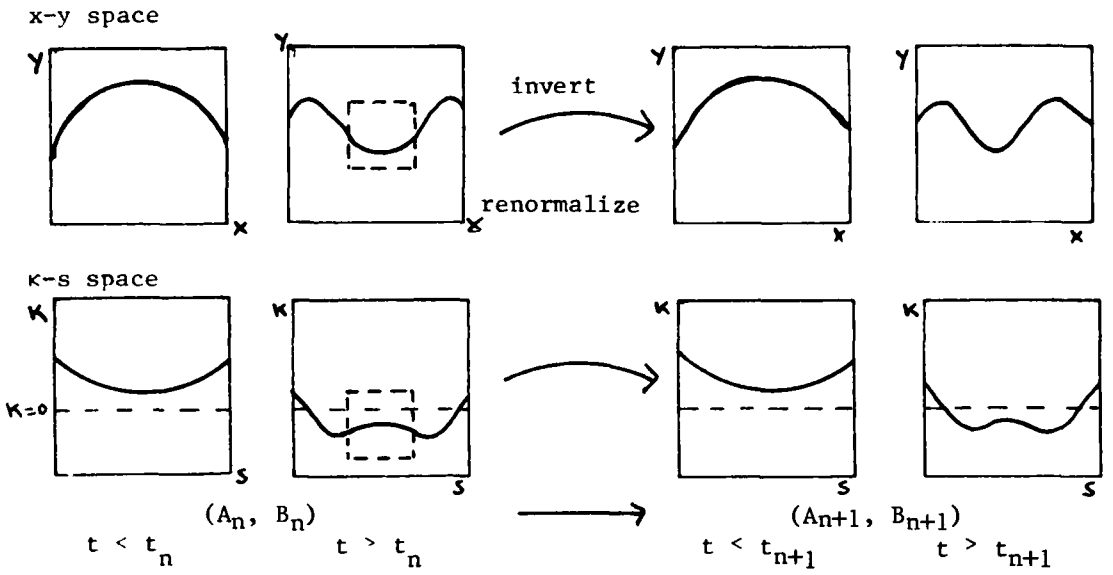

Figure 5.2: Two steps of a tip-splitting cascade. The dashed box is inverted and renormalized at each stage.

If we rescale so $s \to cs$ then

$$\kappa = \bar{A}_n t^* + \bar{B}_n s^{*2} - (\bar{A}_n/24) s^{*4}$$

where $\bar{A}_n = c^5 A_n$, $\bar{B}_n = c^3 B_n$. We thus observe that the shape factor

$$f_n = A_n^{1/5}/B_n^{1/3} \tag{5.16}$$

is a characteristic parameter describing the local geometry of the tip at splitting which is invariant to a change in length scale. Hence each step of the cascade can be reduced to a one dimensional map

$$f_{n+1} = F(f_n) \tag{5.17}$$

where we assume that each stage of tip-splitting is dependent only on the previous one. In the case of a strict self-similar cascade to a fractal curve, (5.17) will have a fixed point $f_{n+1} = f_n$ for all n. Granted then that this highly idealized scenario can occur, we cannot expect strict similarity due to the influence of initial conditions and asymmetries. If a term in s^* is included in (5.14) then a second parameter measuring this asymmetry will be involved in the local description in addition to f_n. By scaling arguments similar to those above, if near splitting we have

$$\kappa = A_n t^* + \varepsilon_n s^* + B_n s^{*2} - (A_n/24) s^{*4}$$

then we can define this asymmetry parameter as

$$g_n = \varepsilon_n^2/B_n.$$

A two dimensional map will then arise for f_n and g_n which has equation (5.17) as an invariant subspace.

In any case, this type of renormalization technique and reduction to a low-dimensinoal map is an attractive scenario for any model of a nonlinear cascading process. As simple self-similar examples of this in turbulence theory, the reader is referred to the β-model for the inertial range cascade of vortices (Frisch et al., 1978) and the γ-model for the cascade of helical vortices (Childress, 1985).

VI. Numerical Simulation

In order to verify whether the above local analysis is applicable in the global problem, a numerical code was written in order to perform a full simulation of the dynamics of equation (3.11) for $u(\sigma, \tau)$. A pseudo-spectral method in space (where derivatives are taken in Fourier space by fast Fourier transforms) was chosen giving periodic boundary conditions on [0,1] and readily allows computations for closed curves in the plane. An implicit method was chosen in time. This reduces the large restriction put on the time step if the usual explicit time stepping methods such as leap frog are used due to the differential equation being fourth order in space. Noting that the equation can be written

$$\partial u/\partial \tau + \partial^4 u/\partial \sigma^4 + \{\partial^2 u^3/\partial \sigma^2 + \partial/\partial \sigma\ (u \int_0^\sigma u v d\sigma' - \sigma u \int_\sigma^1 u v\, d\sigma')\}$$

$$v = u^3 + \gamma^2 u/\partial \sigma^2 \qquad (6.1)$$

we treat the first two linear terms by Crank-Nicholson and the bracketed nonlinear terms by an Adams-Bashforth 2-step scheme giving a second order implicit time stepping method.

Due to a lack of known solutions to (6.1) for closed curves, it proved difficult to test the code. We do have the results from the linear stability of the circle $u = 2\pi$ discussed in section IV, and our computations confirmed the predicted instabilities of modes for various values of γ. In all numerical experiments at least 64 grid points were used and the time step was less than 10^{-5}, being reduced as u became large.

Initial conditions were taken as $u = 2\pi$ with a perturbation of white noise in the Fourier spectrum. As an example of the limited computations performed, figures 6.1 and 6.2 show the instability of the circular solution at $\gamma = 0.2$ when the 3-mode is most unstable. The curves in the plane are reconstructed from $u(\sigma, \tau)$ by integrating

$$\partial x/\partial \sigma = \cos(\int_0^\sigma u d\sigma'), \quad \partial y/\partial \sigma = \sin(\int_0^\sigma u d\sigma')$$

so that the time dependence due to the length L(t) and normal velocity $v(\sigma, \tau)$ has been supressed. The real curve would be stretched and translated according to those quantities, but qualitatively the shape of the curves are as in figure 6.2.

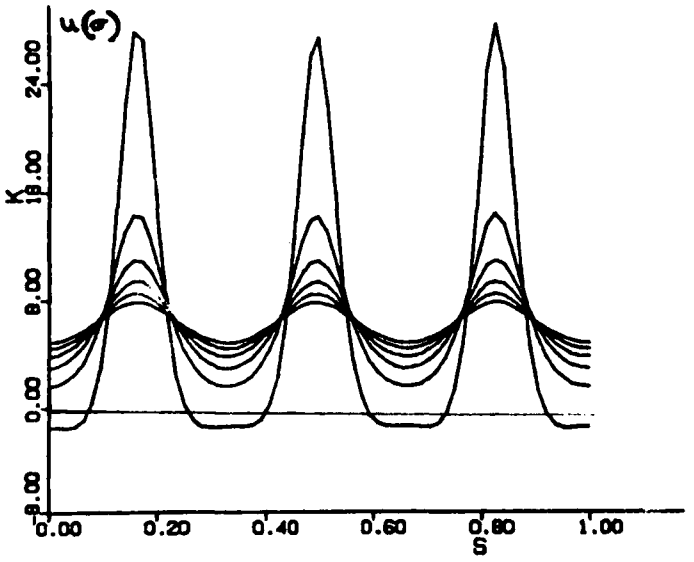

Curvature - arclength

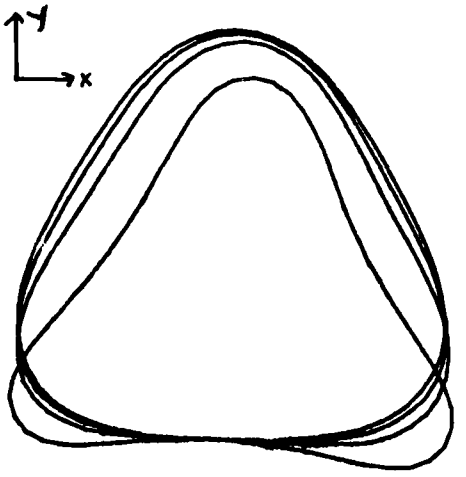

The curve

Figures 6.1 and 6.2: Instability of a circle for γ = 0.2 at successive times close to where curvature changes sign.

We have thus been able to compute a change in sign in curvature corresponding to three tip-splittings which nearly retain the three-symmetry of the most unstable mode.

Note that the calculation was at the limits of numerical resolution by the last stage shown due to the highly localized peaking of curvature. This caused the highest modes in the Fourier decomposition to be excited (and thus numerical breakdown) and was the factor found to rapidly limit our computations for values of γ of interest (i.e. sufficiently small to allow destabilization). The reason that the Kessler model of equation (3.12) allows computation more readily (see figure 3.2) is that velocity law contains a polynomial term to control the growth of curvature. We argue that the length scale on which the diffusive term controls the growth of the cubic term in our dynamical law (3.16) is very sensitive to the value of γ and for small values of this parameter the length scales at which V is renormalized are inhibitively small to be resolved by our limited computations.

We intend to perform numerical computations for more marginal values of γ (eg. γ near 2/3) where we expect this problem to be less severe.

VII. Conclusion

We have shown that a moving curve model with scale invariant dynamics can support tip-splitting behavior by local arguments. We present a conjecture concerning the existence of a sequence of tip-splittings that would lead to a cascade to a fractal curve, which can be described by a low dimensional map.

Limited numerical computation suggests a single tip-splitting can occur, but we are unable to reliably continue the calculation due to numerical error. We hope in the future to demonstrate that at least two successive tip-splittings can occur by more suitable choice of the stabilizing parameter δ in our computations, which would help substantiate the above conjecture. Another possible method to compute the motion of the curve would be to work with the actual curve and describe it by a set of points in the plane. High order spline interpolation could be used, and then explicit time stepping of the curve would be carried out using the given velocity law.

Acknowledgements: It is with great appreciation that I acknowledge the kind supervision of Dr. Stephen Childress, whose work and thought forms much of the basis for the above project. I would also like to thank the staff, my fellow fellows and in particular George Veronis for making this summer a most valuable and enjoyable one.

REFERENCES

Ben-Jacob, E., N. Goldenfeld, J.S. Langer, Gerd Schon, 1983. Dynamics of Interfacial Pattern Formation, Phys. Rev. Letts. 51, no. 21, 1930-32.

Brower, R.C., D.A. Kessler, J. Koplik, H. Levine, 1983. Geometrical Approach to Moving Interface Dynamics, Phys. Rev. Letts. 51, no. 13, 1111-14.

Brower, R.C., D.A. Kessler, J. Koplik, H. Levine, 1984. Geometrical Models of Interface Evolution, Phys. Rev. A 29 no. 3, 1335-42.

Cvitanović, P., 1984. Universality in Chaos, Adam Hilger Ltd.

Childress, S., 1985. Vortex Stability and Inertial Range Cascades Lecture Notes in Physics 230, Springer Verlag, 81-99.

Frisch, U., P.-L. Sulem, M. Nelkin, 1978. J. Fluid Mech. 87, 719-736.

Heslot, F. and A. Libchaber, 1985. Unidirectional Crystal Growth and Crystal Anisotropy, Physica Scripta T9, 126-129.

Huppert, H., 1985. Viscous Gravity Currents, WHOI Tech. Rept., WHOI-84-44 49-65.

Kessler, D.A., J. Koeplik, H. Levine, 1984. Geometrical Models of Interface Evolution II, Numerical Simulation, Phys. Rev. A30 no. 6, 3161-74.

Kessler, D.A., J. Koeplik, H. Levine, 1984. Geometrical Models of Interface Evolution III, Theory of Dendritic Growth, Phys. Rev. A31, no. 3, 1712-17.

Kirmayer, O., 1981. Cell Biology Monographs, Vol. 8, Springer, 147.

Langer, J.S., 1980. Instabilities and Pattern Formation in Crystal Growth, Rev. of Mod. Phys. 52, no. 1, 1-28.

Robinson, A.L., 1985. Fractal Fingers in Viscous Fluids, Science 228, 1077-80.

Fronts and Subcriticality

Janet M. Becker

ABSTRACT

The growth or decay of isolated finite amplitude disturbances is examined for a specific subcritical instability, thermal convection subject to a spatially periodic forcing. The amplitude equation describing this instability is derived by symmetry considerations and the bifurcation structure is presented. As this equation can be written in the form $A_t = -\delta V/\delta A$, variational arguments are given in order to infer the growth or decay of this finite amplitude perturbation as a function of the control parameter in the problem. Equivalently, these results are obtained by considering the propagation velocity c of a front, defined to be the interface between a finite amplitude perturbation and the underlying flow. Fronts separating this perturbation from the basic flow with c positive represent growing perturbations while those with c negative represent decaying perturbations. The concept of a front has the advantage of being independent of the existence of a variational structure to the dynamics.

Properties of this front velocity c as a function of the control parameter are determined numerically and by topological considerations. The above analysis is contrasted with that for a temporal oscillatory instability that does not possess a variational structure. Finally, the coefficient of the term in the amplitude equation due to the spatial forcing is examined for a porous medium with inconclusive results.

Introduction

The propagation and growth or decay of finite amplitude, isolated disturbances is a phenomenon widely studied by hydrodynamicists (Cantwell 1981). Specifically, for flow in a pipe, Wygnanski and Champagne (1973) observed the propagation of turbulent puffs (generated by large disturbances at the pipe inlet) and turbulent slugs (caused by the instability of the boundary layer to small disturbances at the pipe inlet). Their measurements of the velocity of the leading and trailing edge of these fronts for three different pipes is presented in figure 1a. These measurements are independent of downstream distance, but depend upon the nature of the inlet disturbance. Slugs have a well defined leading and trailing interface, the velocity of these front interfaces being constant across the pipe (figure 1b). Thus, the growth of the slugs can be assessed from these measurements. For this Poiseuille flow, the instability observed is subcritical (Maslowe 1981); for a given range of control parameter, there exists more than one linearly stable state. For a system considered to be of infinite extent, the asymptotic behavior in time of the flow in this parameter range is dependent upon initial conditions. This is contrasted with a supercritical instability, where linear stability arguments determine the long time behavior of a given flow configuration (Malkus abstract, this volume; Joseph 1976).

When the dynamics of a flow is described by a variational principle

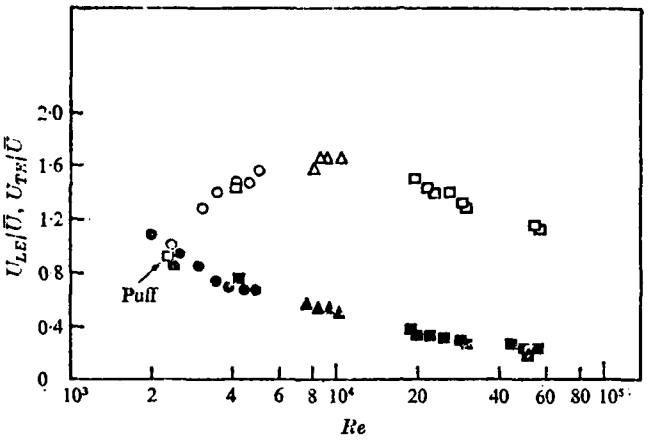

The propagation speed of puffs and slugs at various Reynolds numbers. ○, Lindgren (1957); △, Wygnanski (1971); □, present results; - - -, Lindgren (1969) theoretical result for the propagation of the rear boundary at $Re \to \infty$.

Figure 1(a)

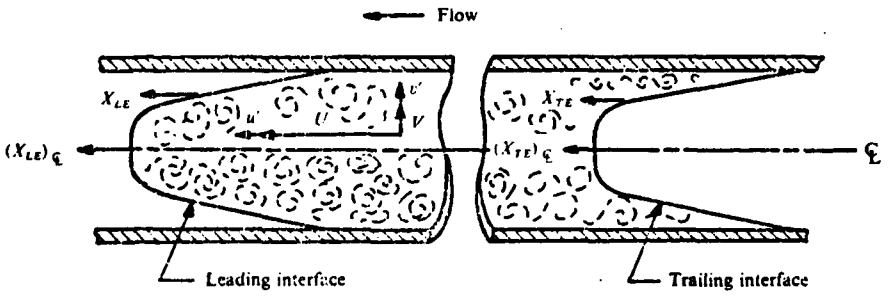

Figure 1(b)

(i.e. one may write the governing dynamical equation as $A_t = -\delta V/\delta \bar{A}$) the evolution of a given isolated finite amplitude perturbation is determined by energy arguments. If the "potential energy' of the perturbation is lower than that of the surrounding flow, it will grow; conversely if its "potential energy" is higher than that of its surroundings, it will decay. The dynamics of many fluid flows of interest however, are not described by a variational principle; thus a criterion that determines the asymptotic behavior in time of the perturbation with respect to the basic flow that is independent of this variational structure is needed. The experiment of Wygnanski and Champagne (1973) suggests that the velocity difference between the leading and trailing edge of a front separating the basic flow from an isolated, finite amplitude perturbation will determine the stability of the flow with respect to this perturbation; a growing perturbation ($U_{LE} - U_{TE} > 0$) indicates the instability of the basic flow while a decaying ($U_{LE} - U_{TE} < 0$) implies that the underlying flow is stable. (Wygnanski and Champagne reported only growing perturbations for slugs. For puffs, they found cases where $U_{LE} = U_{TE}$ and the disturbance propagated without expanding or contracting. In this report, the idea of inferring the long time behavior of a finite amplitude perturbation from a propagating front is applied to a problem from thermal convection possessing a subcritical instability as a starting point for this analysis.

Amplitude Equation From Symmetry Considerations

Recently Lowe and Gollub (1983, 1985) have measured the effects of applying a spatially periodic steady electric field to a layer of a nematic liquid crystal at the onset of an electrohydrodynamic instability (Lowe et al. 1983; Lowe et al. 1985; Gollub abstract, this volume). They find one dimensional stable states where the convective rolls are phase locked to the external forcing (commensurate states). In order to describe these commensurate states near the onset of the convective instability, one uses an amplitude equation that governs the evolution of the slowly varying (in space and tims) amplitude of the marginally stable convective rolls. This equation may be derived by standard asymptotic methods (Newell and Whitehead 1969, Segel 1969), however the form of the equation may be determined more efficiently by symmetry considerations (Coullet abstract). Here the system is assumed one dimensional and unbounded in the horizontal direction, a good approximation for the large aspect ratio conveection observed in Lowe and Gollub's experiments. The governing physics of the unforced problem is described by

$$\partial_t \underset{\sim}{U} + L\underset{\sim}{U} = N(\underset{\sim}{U})$$

$$\underset{\sim}{U} = A\underset{\sim}{\phi} e^{ik_o x} + cc + D$$

where L is a linear operator and N represents nonlinear effects accounted for in the slowly varying amplitude A. Here k_o is the finite wave number of the marginally stable mode corresponding to the minimum control parameter of the marginal stability curve snd D represents linear and nonlinear corrections from the damped modes. This system is invariant under

i) space translations $x \to x + d \Rightarrow A \to Ae^{ik_o d}$
ii) space reflections $x \to -x \Rightarrow A \to \bar{A}$
iii) time translations $t \to t + \phi$.

The equation describing the evolution of the roll envelope can be written in general as

$$A_t = \mu A + \beta(\partial_x)^2 A + N^l(U) \qquad (1)$$

Here μ is the linear growth rate of the marginal mode near onset and N^l is a nonlinear operator. β is assumed to be $O(1)$. The smallest ℓ consistent with constraint (ii) and the fact that we are expanding about k_o, the wave number corresponding to the minimum control parameter of the assumed quadratic marginal stability curve is $\ell = 2$. The lowest order nonlinear term consistent with invariance under space translaters is $|A|^2A$ thus (1) becomes

$$A_t = \mu A + \beta A_{xx} - \gamma|A|^2 A + \text{h.o.t.} \qquad (2)$$

For the scalings $A \sim \mu^{1/2}$, $\partial_x \sim \mu^{1/2}$, $\partial_t \sim \mu$, $\gamma \equiv O(1)$, the terms neglected are $O(\mu^2)$. Moreover as (2) is invariant under space reflections. μ•β and γ are real. Equation (2) is the asymptotic equation obtained by Newell and Whitehead (1969) and Segel (1969).

The imposed periodic spatial forcing breaks the invariance in (2) to arbitrary space translations. For $k_F = 3k_o$ (k_F = wavenumber of forcing) (2) must be invariant to $A \to Ae^{2(\pi/3)}$. Thus, the lowest order nonlinear term that must be added to (2) is $\alpha\bar{A}^2$ and the amplitude equation that includes the effects of the forcing is

$$A_t = \mu A + \beta A_{xx} - \gamma|A|^2 A + \alpha\bar{A}^2 + \text{h.o.t.} \qquad (3)$$

Here, a consistent scaling for α is $\alpha \sim \mu^{1/2}$. While symmetry considerations yield the form of the amplitude equation, they do not give information about the coefficients of the nonlinear terms (except that they are real). For $\alpha = 0$, the sign of β determines whether the bifurcation is super- or subcritical. In (3) the sign of α is irrelevant since the underlying dynamics ($\alpha = 0$) is invariant to space translations. Here, this symmetry breaking forcing renders the bifurcation subcritical. (More precisely, this bifurcation is transcritical Benjamin (1978).)

Bifurcation Structure of Amplitude Equation

As the equation describing the physics of a nematic liquid crystal is quite complicated, the following analysis will consider forced Rayleigh Benard convection in a fluid. Physically, the imposed horizontal temperature gradient induces rolls trapped near the top plate (but, see discussion following for forced rolls that penetrate the bulk of the fluid), the wave length of the rolls being that of the perturbative forcing (see figure 2a). Distinct physical states consist of

a) trapped forced rolls alone

b) trapped forced rolls plus rolls generated by the convective instability rotating in phase

c) trapped forced rolls plus rolls generated by the convective instability rotating out of phase

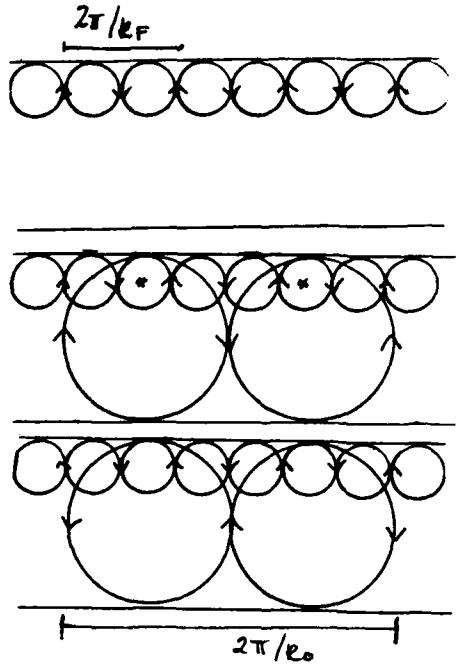

Figure 2

Notice that all of the rolls of wavenumber k_o are unstable (in phase) in figure 2c. Convective rolls with insufficien amplitude to overcome the recirculation of the interior roll * in figure 2b are unstable in amplitude while those of larger amplitude are stable, establishing the subcritical nature of the bifurcation.

In order to quantify the physical description of the forced convection problem

Scale:

$$A \sim \alpha/\gamma$$

$$t \sim \gamma/\alpha^2$$

$$x \sim \sqrt{\beta\gamma}/\alpha$$

Define:

$$\mu \equiv \mu\gamma/\alpha^2$$

in (3) to obtain

$$A_t = \mu A + \bar{A}^2 - |A|^2 A + A_{xx} \qquad (4)$$

With the substitution $A = Re^{i\theta}$ equation (4) becomes

$$R_{xx} - \theta_x^2 R + \mu R - R^3 + R^2\cos 3\theta = R_t \qquad (5a)$$

$$R\theta_{xx} + 2R_x\theta_x - R^2\sin 3\theta = \theta_t R \qquad (5b)$$

The stationary, homogeneous solutions of (5b) are

$$\theta = 0,\ \pi/3,\ 2\pi/3\ \ldots$$

where the odd multiples of $\pi/3$ are linearly unstable (corresponding to the convective rolls out of phase with the forcing, figure 2c). By choosing $\theta = 0$ (equivalently $\theta = 2\pi/3,\ 4\pi/3,\ \ldots$) in 5a one may examine the bifurcation structure of the state where the convective rolls are phase locked to the forcing (figure 2b). Then

$$R_{xx} + \mu R - R^3 + R^7 = R_t \qquad (6)$$

The homogeneous stationary solutions of (6) are

$$R = 0$$

$$R_\pm^* = 1/2 \pm \sqrt{1/4+\mu}$$

For $R = 0$ to be stable; $\mu < 0$. For R_+^* to exist $\mu > -1/4$. Then R_+^* is linearly stable and R_-^* is unstable. The corresponding bifurcation diagram is presented in figure 3a.

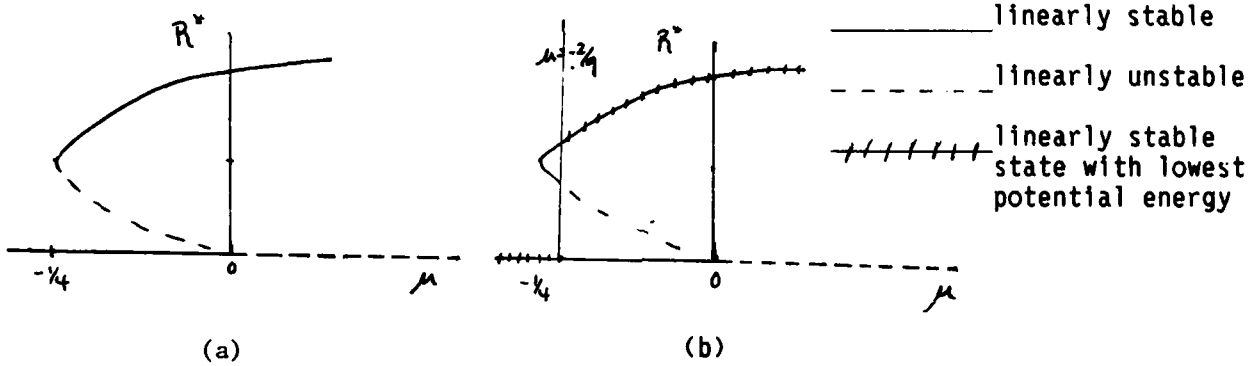

Figure 3

The Evolution of Isolated Finite Amplitude Perturbations

For $-1/4 < \mu < 0$, there exist two linearly stable states. Imagine that in this parameter range, the flow is in state 2a (forced rolls). Now introduce a finite amplitude perturbation to this flow that is made up of state 2b (convective and forced rolls). It is of interest to predict whether this perturbation will grow or decay. To the order considered, equation (6) may be written as a variational principle.

$$R_t = -\partial U/\partial R \qquad (7a)$$

$$U = \int dx\{-\mu R^2/2 - R^3/3 + R^4/4 + (R_x^2/2)\} \qquad (7b)$$

Then $U_t = -(\partial U/\partial R)^2$ and if the introduced perturbation has a potential U higher than that of the initial flow configuration, it will eventually decay, while if its potential is lower than its surroundings, it will amplify. (Note that the integrand of (7b) is a constant for $R = 0, R_+^*$ so integrate over a periodic domain rather than an ∞ interval.) For

$\partial = -2/9$	$U(R_+^*) = U(0)$ and 2a and 2b coexist simultaneously
$-2/9 > \mu > -1/4$	$U(0) < U(R_+^*)$ and the perturbation decays
$0 > \mu > -2/9$	$U(0) > U(R_+^*)$ and the perturbation grows

Figure 3b indicates the bounds determined from these energy considerations. This idea of a system minimizing its Lyapunov functional has been tested experimentally for a convective system (Lowe et al. 1983; Gollub abstract, this volume) with good qualitative agreement for convection a finite μ past onset.

Alternatively, one may examine uniformly propagating solutions to (6) that asymptote to the steady, linearly stable solutions 0 and R_+^* at $x = \pm\infty$. Here we replace $\partial_t = -c\partial_x$ where c is identified with the velocity of the front. Rewriting (6) as

$$R_{xx} + cR_x + \partial V/\partial R = 0 \quad V = 1/2\mu R^2 - R^4/4 + R^3/3 \qquad (8)$$

we see that (8) describes the motion of a particle in a force field $-\partial V/\partial R$ with c being the dissipation (notice that $V = -U$ in (7); thus stable stationary solutions in space (x) correspond to unstable stationary solutions in time (t)).

Again examine the model problem of a figure 2b perturbation on a figure 2a flow for $-1/4 > \mu > -2/9$. The "potential energy" as a function of R is presented in figure 4.

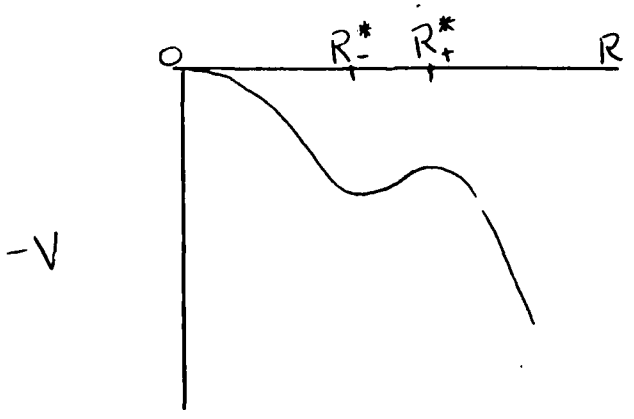

Figure 4

Solving (8) subject to the conditions $R(-\infty) = 0$, $R(\infty) = R_+^*$ yields a front that models the trailing edge of the perturbation. This front corresponds

to the trajectory of a particle starting from rest at R = 0, rolling down hill and stopping at R_+^*; thus c > 0 and R = 0 invades $R = R_+^*$. (The convective rolls are unstable with respect to the forced rolls existing alone.) It is important to note that since the potential energy V is a function of the control parameter μ, the front velocity c is a function of this control parameter also. Similarly the leading edge of the front is represented by solving (8) subject to $R(-\infty) = R_+^*$, $R(\infty) = 0$.

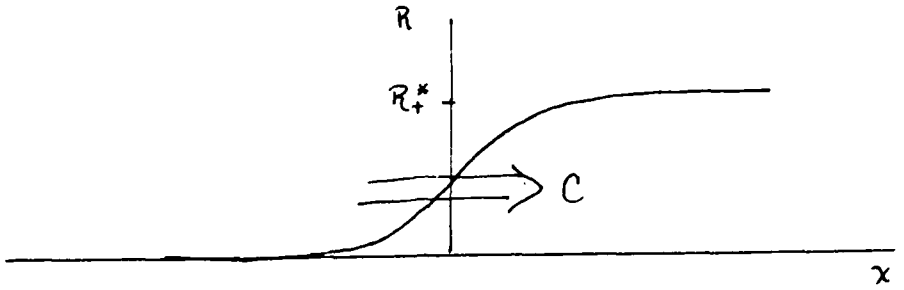

Front modeling trailing edge of perturbation

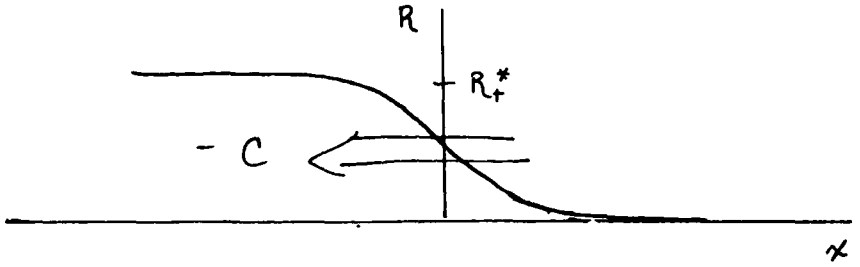

Front modeling leading edge of perturbation

Again R = 0 is the stable flow since c < 0 for this case (one needs to add energy to get the particle up the potential hill). For $-2/9 < \mu < 0$ the perturbation grows while for $\mu = -2/9$, c = 0, and the two states of figures 2a and 2b coexist simultaneously. For this stationary front, an analytic expression can be obtained readily:

$$R_{xx} + \partial V/\partial R = 0$$

A first integral of the motion is

$$1/2R_x^2 + V = 0 \qquad V = -R^2/9(1-R/R_+^*)^2$$

Thus

$$R(x) = 2/3 \; \frac{e^{\sqrt{2}x/3}}{1+e^{\sqrt{2}x/3}} \qquad (9)$$

This solution is presented in figure 5. Front solutions for other values of were obtained numerically using a shooting method. These front profiles are qualitatively similar to the stationary front case. differences being largely due to the boundary contition $R(\mu) = R_+^*$ changing with μ. Qualitatively, for $-1/4 < \mu < -2/9$ the front interface becomes broader as $R_+^*(\mu) < R_+^*(\mu = -2/9)$. For $-2/9) < \mu < 0$, the front interface steepens as $R_+^*(\mu) > R_+^*(\mu = 2/9)$. (See figure 5.)

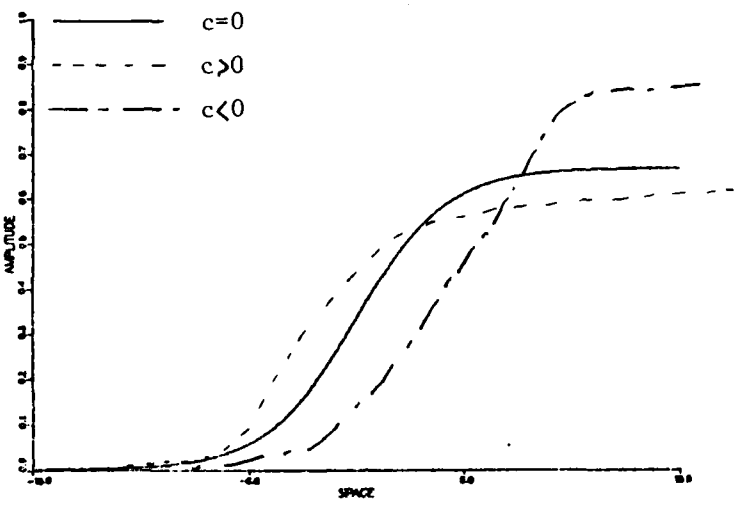

Figure 5

It can be shown that a stationary front solution to equation (2) with $A = \tanh x/\sqrt{2}$ (this front separates convective rolls rotating in opposite senses) is unstable to purely imaginary (phase) perturbations. Here the forcing (represented by $\alpha\bar{A}^2$ in (3)) adds a restoring force to the phase and the front solution to (8) for arbitrary c in linearly stable (see appendix).

The Front Velocity c as a Function of the Control Parameter

The velocity of the front c, determined numerically for various values of is presented in figure 6. Referring to equation (5) with the boundary conditions $R(-\infty) = 0$, $R(\infty) = R_+^*$, one may obtain an implicit expression for c.

$$c = V(R_+^*)/\int_{-\infty}^{\infty} R^2 dx \qquad (10)$$

For c close to zero ($\mu = -2/9 + \delta\mu$), $c(\mu)$ is linear in $\delta\mu$ and an analytic expression for the slope may be obtained from (10) by replacing $R_+^* = 2/3 + 3\delta\mu$ and R_x by the derivative of equation (9), the stationary front. Thus

$$c \approx 6.4\delta\mu \equiv M\delta\mu \quad \text{as} \quad \delta\mu \to 0$$

Numerically for $\delta\mu = .008$, $6.7 < M < 7.1$ and for $\delta\mu = -.01$, $5.6 < M < 6.0$.

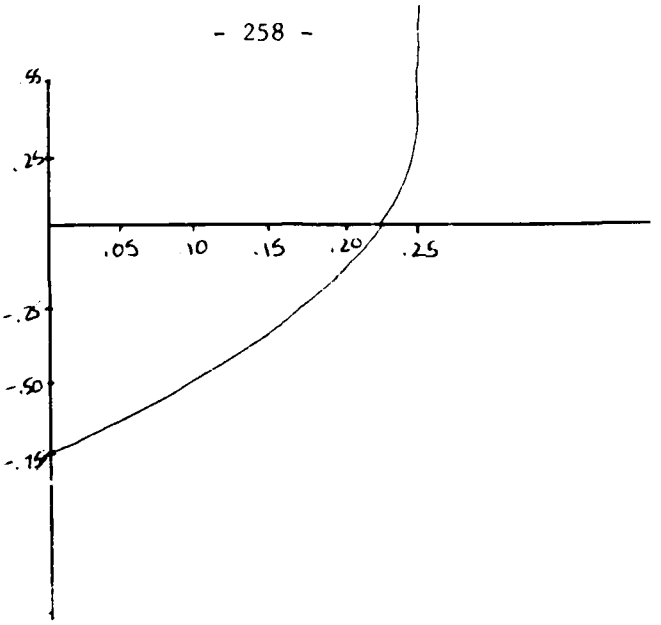

Figure 6

Other properties of this curve are deduced from topological considerations. That the front solution to (5) that satisfies $R(-\infty) = 0$, $R(\infty) = R_+^*$ has a unique velocity c associated with it is established by the following.

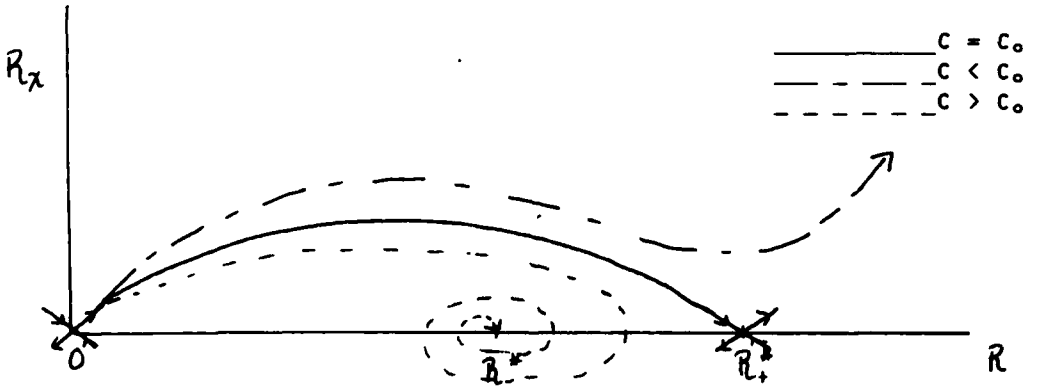

Figure 7a. Phase space trajectories (R_x vs R) of equation (5) for various values of the front velocity c.

Only the flow trajectory leaving R = 0 with $c = c_o$ makes it to R_+^*. Similarly that c varies monotonically with μ can be seen by examing the variation of $R_+^* = 1/2 + \sqrt{1/4+\mu}$ with μ. Since

$$R_+^*(\mu - |\delta\mu|) < R_+^*(\mu) < R_+^*(\mu + |\delta\mu|),$$

one sees that

$$c(\mu + |\delta\mu|) < c_o(\mu) < c(\mu - |\delta\mu|).$$

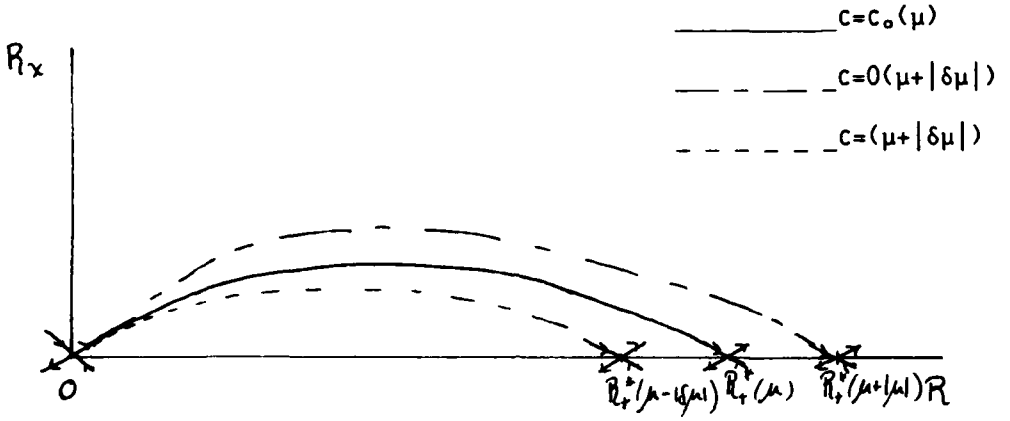

Figure 7b. Phase space trajectories (R_x vs R) of equation (5) subject to $R(-\infty) = 0$, $R(\infty) = R_+^*(\mu)$ for various values of μ. When $\mu = 0$ or $\mu = -1/4$, the "potential energy" V(R) exhibits an inflection point. Here a continium at front velocities c satisfies equation (6) and the boundary conditions. Figure 7c presents this behavior for $\mu = -1/4$. The inflection point (R_I corresponds to R_+^* and R_-^* coalescing; and trajectory with $c \geq c_{11m}$ (where c_{11m} labels the trajectory that enters R_I along the stable manifold) will end up at R_I by entering along the center manifold.

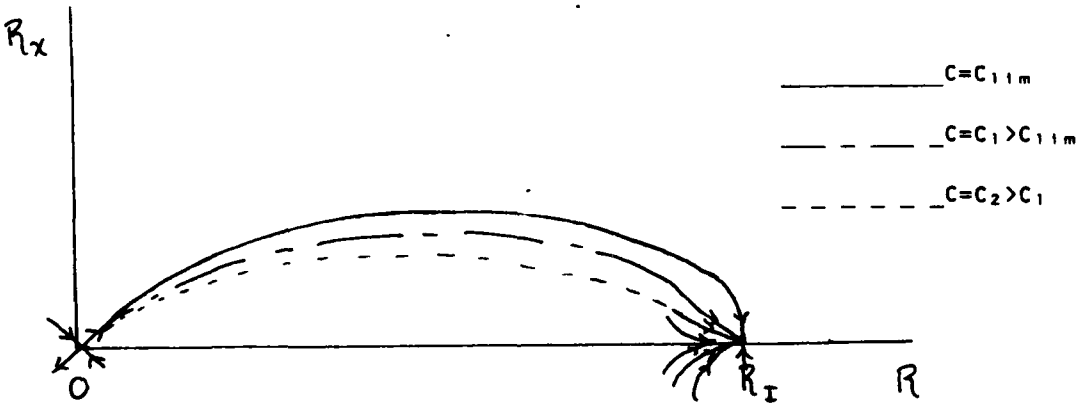

Figure 7c. Phase space trajectories (R_x vs R) of equation (5) and boundary conditions for $\mu = -1/4$. Here a continium of $c > c_{11m}$ satisfies (5) and the boundary conditions.

The limiting behavior of $c(\mu)$ as $\mu \to 0$ and $\mu \to -1/4$ is deduced by expanding the potential about the inflection point. In the limit $\mu \to -1/4$ set $R = 1/2 + z$, $\mu = -1/4 + \epsilon$, ($\epsilon > 0$) in (5) to obtain

$$z_{xx} + cz_x = 1/2(z^2 - \epsilon) \qquad (11)$$

For $\epsilon = 0$, equation (11) describes the local behavior of the flow field at the inflection point. For $\epsilon \neq 0$, the phase space trajectory that satisfies the boundary conditions $R(-\infty) = 0$ and $R(\infty) = R_+^*(\mu)$ is modified due to two effects.

(i) For $z \leq \epsilon^{1/2}$, the topology of the fixed point at $x = \infty$ changes from that of an inflection point (figure 7c) to that of a saddle point (figure 7a).

(ii) $\Delta c = c(\mu = -1/4) - c(\mu = -1/4 + \epsilon) = 0$. The front velocity associated with the flow trajectory that satisfies the boundary conditions changes since μ changes.

Effect (ii) modifies the trajectory globally; $c(-1/4+\ )$ labels a different trajectory leaving $R(-\infty) = 0$ then $c(\mu = -1/4)$. Effect (i) modifies the trajectory locally for $z \leq \epsilon^{1/2}$ and therefore will only be considered to modify the trajectory through the modified boundary condition $R(\infty) = R_+^*(-1/4) + O(\epsilon^{1/2})$.

For $\epsilon = 0$ and $cz_x >> z^2/2$, phase space trajectories enter the parabolic region defined by $z_x = z^2/2c$ surrounding the inflection point parallel.

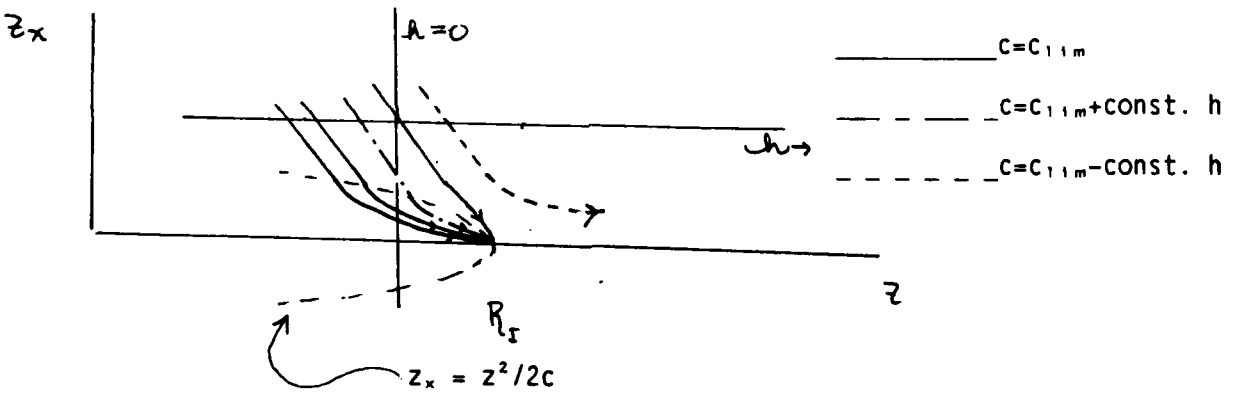

Figure 7d. Local behavior of phase space trajectories (z_x vs z) for $\mu = -1/4$. h is the horizontal projection of the distance between neighboring trajectories. c_{1im} labels trajectory entering along stable manifold.

Thus the distance between neighboring trajectories h is linearly proportional to Δc. Then the modified boundary condition at $R(\infty)$ is satisfied for $h \sim \epsilon^{1/2} \sim \Delta c$ and $c = c_{1im} - \epsilon^{1/2} = c_{1im} - \sqrt{\mu+1/4}$ as $\mu \downarrow -1/4$. Similarly around $\mu = 0$ replace $R = z$; $\mu = -\epsilon (\epsilon > 0)$ in (5) to obtain

$$z_{xx}\, cz_x = \epsilon z - z^2$$

An analgous argument to that given above yields

$$c = c^o_{1im} + \epsilon = c^o_{1im} - \mu \quad \text{as } \mu \uparrow 0$$

This limiting behavior of $c(\mu)$ is explified in figure 6.

The front velocity is a quantity that can be measured in the laboratory. A possible experiment with which to check these results would involve mechanically varying μ by changing the spacing between the plates confining the fluid until one obtains a critical value of $\mu = \mu_c$ that sustains the stationary front. Then one has a controlled state to begin from and by changing μ and μ_c (by changing the temperature gradient for example), the measured velocity of the front may be compared with the velocity predicted from this theory (figure 6).

A Nonvariational Case; An Oscillatory Instability

For many dynamical systems of nonequilibrium phenomenon, the amplitude equation does not possess a variational structure (Pomeau et al., 1983). As the concept of a moving front is independent of the existence of a variation principle it is applicable to a wide class of problems. For example, at the onset of an oscillatory instability, the coefficients in the amplitude equation are no longer real as there is no reflectional property in time as there is in space (Coullet and Fauve, 1984). Thus, the amplitude equation that describes this Hopf bifurcation with external temporal periodic forcing at $\omega_f = 3\omega_o$ ($\omega_o \equiv$ natural (resonant) frequency of system) is

$$A_t = \mu(1+i\mu')A + \bar{A}^2 - (1-i\gamma)A^2A + (1+i\beta)A_{xx} \qquad (12)$$

For $\gamma = \mu' = \gamma \equiv \gamma << 1$, one may treat this problem perturbatively. Letting $A = Re^{i\theta}$ and $\partial_t \equiv c\partial_x$ in (12) yields

$$-cR_x = \mu R + R^2\cos 3\theta - R^3 + R_{xx} - 2\gamma R_x\theta_x - \theta_x^2 R + \gamma\theta_{xx}R \qquad (13)$$

$$-c\theta_x R = \mu\gamma R - R^2\sin 3\theta + \gamma R^3 + \gamma R_{xx} + 2R_x\theta_x - \gamma\theta_x^2 R + \theta_{xx}R$$

In order to obtain the solution to (13) expand

$$R = R_o + \gamma R_1 + \ldots$$

$$\theta = \gamma\theta_1 + \gamma^2\theta_2 + \ldots$$

$$c = c_o + \gamma c_1$$

At lowest order, one has the front of figure 5.

$$R_{oxx} + c_o R_{ox} + \mu R_o - R_o^3 + R_o^2 = 0 , \qquad (14a)$$

$$\theta_o = 0, \qquad (14b)$$

$$R_o(-\infty) = 0,\ R(\infty) = R_+^* \qquad (14c)$$

At $O(\gamma)$

$$LR_1 = -c_1 R_{ox} \qquad (15a)$$

$$J\theta_1 = -R_o - R_{oxx}/R_o - \mu \qquad (15b)$$

$$\theta_1 = 1/3(R_+^* + \mu/R_+^*) \quad \text{at} \quad x = \infty \qquad (15c)$$

$$L = \partial_{xx} + c_o\partial_x + (\mu+2R_o-3R_c^2)$$

$$J = \partial_{xx} + (2R_{ox}/R_o - c_o)\partial_x - 3R_o$$

Differentiate (1a) with respect to x to verify that L has a nontrivial kernel (R_{ox}). Thus, the solvability condition for (15a) demands that $c_1 = 0$ and R_1 is set to zero. Then equation (15b) for θ_1 may be solved numerically, taking care of the boundary condition on θ_1 at $x = -\infty$. Here $R_o = 0$ and θ_1 is not fixed. Letting $R_o = e^{\sigma x}$ as $x \to -\infty$ one may determine $\theta_1(-\infty)$ in terms of two free parameters.

At $O(\gamma^2)$

$$LR_2 = -c_2R_{ox} + 2R_{ox}\theta_{1x} + \theta_{1x}R_o + \theta_{1xx}R_o + 9/2R_o\theta_1 \qquad (16a)$$

$$J\theta_2 = 0 \qquad (16b)$$

And we see that c_2 is determined by solvability at this order. Define ϕ to be the kernal of the adjoint operator of L

$$L^+\phi = 0$$

Then by defining a suitable scalar product, one obtains

$$\langle\phi, LR_2\rangle = 0$$

and c_2 is determined by

$$C_2 = \langle\phi,\ 2R_{ox}\theta_{1x} + \theta_{1x}R_o + \theta_{1xx}R_o + 9R^2\theta^2/2\rangle \ /\ \langle\phi, R_{ox}\rangle$$

Thus the front velocity is modified at $O(\gamma^2)$ from that of figure 6.

The Effects of Spatial Periodic Forcing on a Porous Medium

An attempt was made to calculate the coefficient of the symmetry breaking term in the amplitude equation from the fluid equations for convection in a porous medium. In a porous medium, the flow of interest occurs on a scale h. The layer depth, while the viscous term $\nu\Delta V$ is dominantly due to friction in small pores of length scale $l << h$ (see figure 8). The dimensional Boussinesq equations for the perturbation temperature T and velocity V about a mean state $V = 0$, $T = T_o - \delta T(Z/h) + \theta$ (Palm, 1975) are

$$\theta_t + V\ \nabla\theta = K\Delta\theta + W\delta T \qquad (17)$$

$$V_t + V\ \nabla V = -\nabla P/\rho_o + \alpha g\theta z + \nu\Delta V \qquad (18)$$

Here

ν = kinematic viscosity
K = thermal diffusivity
α = coefficient of expansion
g = gravity

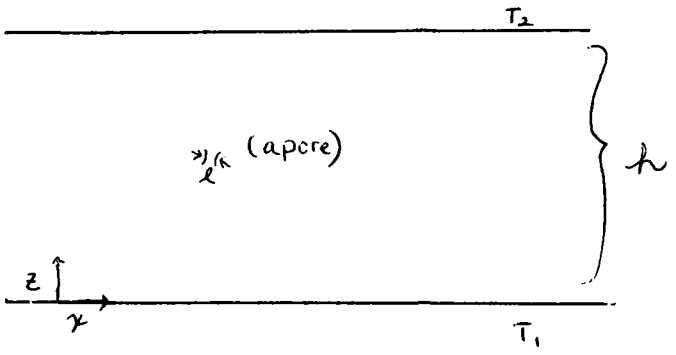

Figure 8

For $l \ll h$, the Darcy approximation is valid

$$\nu \Delta V = -V/\tau \qquad (\tau \text{ constant} \sim \ell^2/\nu) \tag{19}$$

Then the effective Reynolds number of the flow is $Re = U\tau/h \ll 1$ and the inertial terms in (13) are neglected.

Using the scalings

$$V \sim K/h \qquad (x,z) \sim h$$

$$t \sim h^2/K \qquad P \sim K\rho_o/\tau$$

$$\theta \sim K/\alpha\tau gh$$

and defining

$$R = \alpha g \delta T h \tau / K$$

the nondimensional porous medium (Darcy-Boussinesq) equations are

$$X = -\nabla P + \theta \hat{z} \tag{20}$$

$$\theta_t + V \cdot \nabla \theta = \Delta\theta + RW \tag{21}$$

$$U_x + W_z = 0 \tag{22}$$

The boundary conditions are

$$w = 0 \quad \text{at} \quad z = 0,1 \tag{23a}$$

$$\theta = 0 \quad \text{at} \quad z = 0 \tag{23b}$$

$$\theta = ge^{3ik_c x} + cc \quad \text{at} \quad z = 1 \tag{23c}$$

One may combine (20), (21), and (22) to obtain ($\Delta_h \equiv \partial_{xx}$)

$$-\Delta\psi_t + R\Delta_h\psi + \Delta^2\psi = \Delta_h\psi\Delta_z - \psi_{xz}\Delta\psi_x \tag{24}$$

with $\psi = \int^z P dz$. (23) becomes

$$\text{(a)} \quad \psi = 0 \quad \text{at} \quad z = 0,1$$

$$\text{(b)} \quad \psi_{zz} = 0 \quad \text{at} \quad z = 0 \tag{25}$$

$$\text{(c)} \quad \psi_{zz} = ge^{3^{1/2}k_c x} + cc \quad \text{at} \quad z = 1$$

In order to determine k_c, the wave number of the marginal mode, set $\psi = \sin\pi z e^{i k_c x} e^{\sigma t}$ in the linear part of (24) to obtain the marginal stability curve ($\sigma = 0$) given by (26) and diagrammed in figure 9.

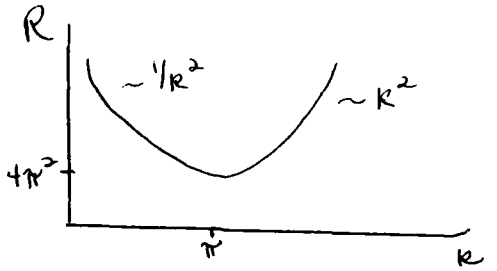

Figure 9

$$R = (\pi^2 + k^2)^2/k^2 \tag{26}$$

Rewrite (24) as

$$L\dot{} = S(\psi, \psi)$$

$$L \equiv -\Delta\partial_t + (4\pi^2 + \epsilon)\Delta_h + \Delta^2$$

$$S(\psi, \psi) = \Delta_h\psi\Delta\psi_z - \psi_{xz}\Delta\psi_x$$

and proceed to determine α by standard perturbative methods

$$\psi = \sqrt{\epsilon}\psi_o + \epsilon\psi_1 + \epsilon^{3/2}\psi_2$$

$$R = 4\pi^2 + \epsilon$$

$$L\psi_o = 0$$

$$\psi_o = \psi_f + \psi_h$$

where $\psi = (Xe^{iKx} + cc)\sin\pi z$ satisfies homogeneous boundary conditions and $\psi_f = ge^{hi3^{1/2}\pi x} + cc)\phi(z)$; $\phi(z) = -a \sinh \sqrt{3}\,\pi z + c \sinh \sqrt{15}\,\pi z$ where a and c are positive constants. Notice that the z dependence of ψ_f causes the forced rolls to be trapped near the top plate. At $O(\epsilon)$, the relevant terms that determine α are $S(\psi_f,\psi_h)$. ($S(\psi_h,\psi_h)$ gives the incorrect x dependence).

The solution of $L\psi_1 = S(\psi_f,\psi_h)$ at this order is

$$\psi_1 = e^{2i\pi x}\mathcal{G}(z)$$

$\mathcal{G}(z) = gX^*[A\sinh 2\sqrt{2}\pi - K'/32\pi^4\ (1-i\sqrt{3})\sinh(\sqrt{3}+1)\pi + cc]$ A,K' constants.

Next at $O(\epsilon^{3/2})$, α is determined by solvability and this analysis yields $\alpha = 0$. This does not imply that the forcing has no effect at this order; it modifies the linear growth rate (although this effect has not been explicitly calculated at this time). The calculation leading to $\alpha = 0$ at third order was completed during the last week of the program so this calculation was not taken to higher order to calculate the symmetry breaking term. At fifth order this term could consist of a combination of $g|g|^2\bar{A}^2$ and $g|A|^2\bar{A}^2$. Swift (1984) indicates that a similar result has been found where if one only breaks the Boussinesq symmetry through the boundary conditions (i.e. rigid bottom, free top) and the linear problem is self adjoint (as it is here) the first symmetry breaking term in the amplitude equation occurs at fifth order. The result $\alpha = 0$ may be related to this. As this expansion to fifth order will involve a lot of algebra, before proceeding to this order this calculation will be reformulated by representing the spatially periodic forcing as a source term in the temperature equation, thus affecting the bulk fluid, rather than acting as a skin effect. That this forcing does render the bifucation transcritical has been shown for Rayleigh Benard convection (Kelley and Pal, 1979; Benjamin, 1978). The result that $\alpha = 0$ for this calculation as likely to be related to violation of property (5) of Benjamin 1978, page 6.

In summary, for a simple model, a uniformly propagating front has been used to infer the long time behavior of finite amplitude perturbations imposed on a basic flow. This theory is independent of the existence of a variational structure of the dynamics and yields a physical quantity c (that is a function of the parameters of the problem, that can, and has been measured. The connection of this model with the porous medium equations needs to be completed in order to see how the symmetry breaking term arises from these dynamics.

Future work involves applying these ideas to hexagons as they possess a subcritical instability intrinsically (not dependent upon the forcing as in the present problem).

Also, this theory will be extended in order to attempt to explain the measureaents of figure 1a. Returning to figure 1a, an asymmetry about the center line between the leading and trailing edge velocities develops for $Re > 10^4$. This cannot be accounted for in this theory as it stands as the amplitude equation possesses reflectional symmetry in space. This and other effects will be taken into account as these ideas are extended to more complicated physical systems.

Acknowledgements: I would like to thank the staff of the GFD program who are responsible for this unique opportunity to do research in hydrodynamics. Conversations with S. Fauve, J. Gollub, A.Libchaber. A. Pumir and S. Zaleski were greatly appreciated. I would especially like to thank Pierre Coullet and Yves Pomeau for suggesting this problem and for their continued advice and direction. This material is based upon work supported under a National Science Foundation Graduate Fellowship.

REFERENCES

Benjamin, T.B., 1978. Bifurcation Phenomena in Steady Flows of a Viscous Fluid. Proc. R. Soc. Lond. A359. 1-26.

Cantwell, B.J., 1981. Organized Motion in Turbulent Flow, Ann. Rev. Fluid Mech. 13, 457-515.

Coullet, P. and S. Fauve, 1984. Collective Modes of Periodic Structures Conference Proceedings, Combustion and Turbulence, Les Houches.

Joseph, D.D., 1976. Stability of Fluid Motions, I, II. Springer Tracts in Natural Philosophy 28, Springer-Verlag Berlin.

Kelley, R.E. and D. Pal, 1979. Three Dimensional Thermal Convection Produced by Two Dimensional Thermal Forcing, Heat Transfer Division of ASME 18th National Heat Transfer Conference.

Lowe, M., J.P. Gollub and T.C. Lubensky, 1983. Commensurate and Incommensurate Structures in a Nonequilibrium System, Phys. Rev. Letts. 51(9), 786-789.

Lowe, M. and J.P. Gollub, 1985. Solitons and the Commensurate-Incommensurate Transition in a Convecting Nematic Fluid, Phys. Rev. A31, 3893.

Maslowe, S.A., 1981. Shear Flow Instabilities and Transition, Hydrodynamic Instabilities and the Transition to Turbulence, H.L. Swinney and J.P. Gollub, editors, Springer-Verlag Berlin Heidelbert, NY.

Newell, A.C., J.A. Whitehead, 1969. Finite Bandwidth. Finite Amplitude Convection, J. Fluid Mech. 38(2), 279-303.

Palm, E., 1975. Nonlinear Thermal Convection, Ann. Rev. Fluid Mech., 39-61.

Pomeau, Y., S. Zaleski, P. Manneville, 1983. Dislocation Motion in Cellular Structures, Phys. Rev. A. 27(5), 2710-2726.

Segel, L.A., 1969. Distant Side-Walls Cause Slow Amplitude Modulation of Cellular Convection, J. Fluid Mech. 38, 203-224.

Swift, J.W., 1984. Bifurcation and Symmetry in Convection, Ph.D. dissertation, University of California, Berkeley.

Wygnanski, I.J. and F.H. Champagne, 1973. On Transition in a Pipe Part I. The Origin of Puffs and Slugs and the Flow in a Turbulent Slug, J. Fluid Mech. 59(2), 281-335.

Appendix

The linear stability of the front R_o (real) that is the solution of

$$A_{xx} + (\partial V/\partial \bar{A}) = A_t \quad V = \mu|A|^2 + [(\bar{A}^3+A^3)/3] - (|A|^4/2) \qquad (A1)$$

$$A(-\infty) = 0 \quad A(\infty) = R_+^*(\mu) \quad R_{o_t} \equiv -cR_{o_x}$$

is determined by substituting

$$A = R_o + \delta A_1 e^{\sigma t} \quad \delta A_1 = \delta R + i\delta r$$

into (A1), linearizing and examining the eigenvalues σ. This yields

$$\delta R_{xx} + c\delta R_x + (\mu+2R_o-3R_o^2)\delta R = \sigma\delta R \equiv L_1\delta R \qquad \text{(A2a)}$$

$$\delta r_{xx} + c\delta r_x + (\mu-2R_o-R_o^2)\delta r = \sigma\delta r \equiv L_2\delta r \qquad \text{(A2b)}$$

Changing variables in order to make the linear operators on the l.h.s. of (A2) self adjoint yields

$$\delta\tilde{R}_{xx} + (-c^2/4 + \mu + 2R_o - 3R_o^2)\delta\tilde{R} = \sigma\delta\tilde{R} \qquad \text{(A3a)}$$

$$\delta\tilde{r}_{xx} + (-c^2/4 + \mu - 2R_o - R_o^2)\delta\tilde{r} = \sigma\delta\tilde{r} \qquad \text{(A3b)}$$

$$\delta\tilde{R} \equiv e^{(c/2)x}\delta R \quad \delta\tilde{r} \equiv e^{(c/2)x}\delta r$$

First examine the stability of R_o to purely imaginary perturbations (A3b). As the front has localized structure in space, one is interested in examining localized perturbations thus $\delta\tilde{r}(\infty) = \delta r(-\infty) = 0$. Multiplying (A3b) by $\delta\tilde{r}$, integrating over x $(-\infty, \infty)$ one obtains

$$-\int_{-\infty}^{\infty} dx[(\delta\tilde{r}_x)^2 + |\mu-2R_o-R_o^2|(\delta\tilde{r})^2] = \sigma\int_{-\infty}^{\infty}(\delta\tilde{r})^2 dx$$

and $\sigma \leq 0$; R_o is stable to phase perturbations since the l.h.s. is nonpostive definite. In order to determine the stability of R_o to real perturbations (A3a), one recognizes that R_{o_x} is an eigenfunction of (A2a) with eigenvalue zero. Moreover, R_{o_x} has no zero crossing as is evident from figure 5. Asymptotically

$$R_{o_x} \sim e^{(-c/2 + \sqrt{c^2/4+K})x} \quad \text{as } x \to -\infty$$

and

$$R_{o_x} \sim e^{(-c/2 - \sqrt{c^2/4+K})x} \quad \text{as } x \to \infty$$

thus

$$\delta R \equiv e^{(c/2)x}\,\delta R \sim e^{(c/2)x}R_{o_x} \to 0 \text{ as } x \to \pm\infty$$

and one is again examining localized perturbations to the front R_o. Rewriting (A3a) as

$$(-\partial_{xx} + V)\delta\tilde{R} = -\sigma\delta\tilde{R} \quad \delta\tilde{R} \to 0 \quad \text{as } x \to \pm\infty$$

$$V \equiv c^2/4 - \mu - 2R_o + 3R^2$$

one obtains a Schrodinger equation. The eigenfunction with the lowest energy ($-\sigma = E$, so largest σ) is $\delta\tilde{R} \sim R_{o_x}$ (it has no node), therefore $\sigma \leq 0$ and the front R_o is stable to real perturbations.

DOCUMENT LIBRARY

April 9, 1985

DISTRIBUTION LIST FOR TECHNICAL REPORT EXCHANGE

Institute of Marine Sciences Library
University of Alaska
O'Neill Building
905 Koyukuk Ave., North
Fairbanks, AK

Attn: Stella Sanchez-Wade
Documents Section
Scripps Institution of Oceanography
Library, Mail Code C-075C
La Jolla, CA 92093

Hancock Library of Biology & Oceanography
Alan Hancock Laboratory
University of Southern California
University Park
Los Angeles, CA 90089-0371

Gifts & Exchanges
Library
Bedford Institute of Oceanography
P.O. Box 1006
Dartmouth, NS, B2Y 4A2, CANADA

Office of the International
Ice Patrol
c/o Coast Guard R & D Center
Avery Point
Groton, CT 06340

Library
Physical Oceanographic Laboratory
Nova University
8000 N. Ocean Drive
Dania, FL 33304

NOAA, EDIS Miami Library Center
4301 Rickenbacker Causeway
Miami, FL 33149

Library
Skidaway Institute of Oceanography
P.O. Box 13687
Savannah, GA 31416

Institute of Geophysics
University of Hawaii
Library Room 252
2525 Correa Road
Honolulu, HI 96822

Library
Chesapeake Bay Institute
4800 Atwell Road
Shady Side, MD 20876

MIT Libraries
Serial Journal Room 14E-210
Cambridge, MA 02139

Director, Ralph M. Parsons Laboratory
Room 48-311
MIT
Cambridge, MA 02139

Marine Resources Information Center
Bldg. E38-320
MIT
Cambridge, MA 02139

Library
Lamont-Doherty Geological Observatory
Colombia University
Palisades, NY 10964

Library
Serials Department
Oregon State University
Corvallis, OR 97331

Pell Marine Science Library
University of Rhode Island
Narragansett Bay Campus
Narragansett, RI 02882

Working Collection
Texas A&M University
Dept. of Oceanography
College Station, TX 77843

Library
Virginia Institute of Marine Science
Gloucester Point, VA 23062

Fisheries-Oceanography Library
151 Oceanography Teaching Bldg.
University of Washington
Seattle, WA 98195

Library
R.S.M.A.S.
University of Miami
4600 Rickenbacker Causeway
Miami, FL 33149

ADA 164601

50272-101

REPORT DOCUMENTATION PAGE	1. REPORT NO. WHOI-85-36	2.	3. Recipient's Accession No.

4. Title and Subtitle
Summer Study Program in Geophysical Fluid Dynamics, The Woods Hole Oceanographic Institution, Chaos

5. Report Date
November 1985

6.

7. Author(s)
George Veronis, Director and Linda M. Hudon, Editor

8. Performing Organization Rept. No.
WHOI-85-36

9. Performing Organization Name and Address
Woods Hole Oceanographic Institution
Woods Hole, Massachusetts 02543

10. Project/Task/Work Unit No.

11. Contract(C) or Grant(G) No.
(C) N00014-82-G-0079
(G) MSC-82-00450
DMS-85-04166

12. Sponsoring Organization Name and Address
Office of Naval Research
and
National Science Foundation

13. Type of Report & Period Covered
Technical

14.

15. Supplementary Notes
This report should be cited as: Woods Hole Oceanog. Inst. Tech. Rept., WHOI-85-36.

16. Abstract (Limit: 200 words)

This volume contains the lectures of Edward A. Spiegel (as interpreted and reported by the fellows) which included elementary examples of bifurcation and chaos, symmetry breaking, normal forms and temporal and spatial disorder, as well as pertinent fluid mechanical and astrophysical phenomena. These are followed by extended abstracts of seminars which covered different types of intermittency, phase instability and turbulence and the introduction of new concepts in dynamical systems theory. The final section contains the fellows' reports of their own research activity on the application of dynamical systems to fluid mechanics. These reports are to be treated as unpublished manuscripts. Readers desiring to quote from the material should seek the permission of the author.

17. Document Analysis a. Descriptors
1. Geophysical Fluid Dynamics
2. Dynamical Systems Theory
3. Fluid Chaos

b. Identifiers/Open-Ended Terms

c. COSATI Field/Group

18. Availability Statement:	19. Security Class (This Report)	21. No. of Pages
Approved for publication; distribution unlimited.	UNCLASSIFIED	267
	20. Security Class (This Page)	22. Price

(See ANSI-Z39.18) See Instructions on Reverse OPTIONAL FORM 272 (4-77)
(Formerly NTIS-35)
Department of Commerce

END

FILMED

4-86

DTIC